# ABSTRACT

| | |
|---|---|
| Title of Dissertation: | HIGH-RESOLUTION ANALYSIS OF HIV ENVELOPE-SPECIFIC ANTIBODY RESPONSES TO ACCELERATE RATIONAL IMMUNOGEN DESIGN |
| | Lin Lei, Doctoral of Philosophy, 2020 |
| Dissertation directed by: | Associate Professor, Yuxing Li, Institute for Bioscience and Biotechnology Research, UMCP Department of Microbiology and Immunology, UMB |

The recent isolation of HIV broadly neutralizing antibodies (bNAbs) from HIV infected individuals has reinvigorated efforts to develop B cell-based vaccines. As the sole viral target for bNAbs, HIV envelope glycoprotein (Env) has been engineered as soluble trimers to recapitulate bNAbs responses via vaccination. However, Env-based immunogens thus far primarily induce vaccine-matched neutralizing antibody (nAb) responses. This thesis aims to understand the mechanisms restricting the neutralization breadth and to provide strategies for iterative improvements.

First, we have established an antigen-specific single B cell sorting and monoclonal antibody (mAb) cloning platform for guinea pigs, a small animal model desirable in the field for initial immunogenicity analysis. This method allowed us to dissect the antibody responses at the clonal level with high accuracy and efficiency.

Secondly, we have delineated the specificity of autologous neutralization elicited by the current generation HIV trimer mimicry, BG505 SOSIP.664. Our results reveal a prominent epitope in the C3/V4 region of the Env targeted by one nAb/B cell clonal lineage.

We demonstrate that the nAb responses to this neutralization determinant are prevalent in trimer-vaccinated guinea pigs, rabbits, and non-human primates. In addition, this defined nAb response shares a high degree of similarity with the early nAb response in an HIV-infected pediatric patient, who later developed a bNAb response. This study offers insights into re-designing Env immunogens in the highly immunogenic region to broaden nAb responses.

Lastly, we have engineered novel immunogens based on the Env sequence of a virus strain isolated from bNAb VRC01 donor, which can engage the VRC01 germline precursor in vitro. Sequential prime-boost immunizations in a VRC01-germline immunoglobulin (Ig) encoding genes knock-in mouse model with the designed immunogens induced focused VRC01-like serum antibody responses and clustered VRC01-class somatic mutations in the knock-in VRC01-germline Ig genes. In addition, the mAbs recovered from the immunized mice neutralize selected viruses containing the N276 glycan, a critical roadblock impeding the affinity maturation of VRC01-class bNAbs. Our findings demonstrate that, in the transgenic mouse model, our immunogens effectively activate bNAb precursor B cells and guide their affinity maturations required for bNAb function, which has important implications for HIV vaccine development.

# HIGH-RESOLUTION ANALYSIS OF HIV ENVELOPE-SPECIFIC ANTIBODY RESPONSES TO ACCELERATE RATIONAL IMMUNOGEN DESIGN

by

Lin Lei

Dissertation submitted to the Faculty of the Graduate School of the
University of Maryland, College Park, in partial fulfillment
of the requirements for the degree of
Doctor of Philosophy
2020

Advisory Committee:
Professor Wenxia Song, Chair
Associate Professor Yuxing Li, Co-chair
Professor Roy A. Mariuzza
Assistant Professor Brian G. Pierce
Professor Xiaoping Zhu

# Dedication

I dedicate this dissertation to my family, especially my mom and dad, for their endless love and support.

# Acknowledgments

I would like to first and foremost thank my advisor, Yuxing Li, for her constant advice, patience, compassion, and wisdom. Without her, I would probably have left Maryland or even quit pursuing a Ph.D. in biological sciences. Maryland is now my favorite place in the US, and I will like to be continually working in the area that directly related to my Ph.D. study. I want to express my gratitude for everything she has done for me all these years.

I would also like to thank all my committee members, including Roy Mariuzza, Brian Pierce, Wenxia Song, and Xiaoping Zhu. I will remain forever grateful for their valuable time, knowledge, and guidance along this journey. I am also grateful to Xiaoshun Yuan for recruiting me to the BISI program at the beginning. I would like to thank all the members of the Li lab, including Chi-I Chang, Xuelian Zhao, Yimeng Wang, James Steinhardt, Andrey Galkin, and Xiaoran Shang, for their help over the years. I would also like to acknowledge my collaborators Karen Tran, Renee Yang, Gabriel Ozorowski, Takayuki Ota, Andrew Ward, and Richard Wyatt at Scripps, as well as Sijy O'Dell and Yongli Xiao at NIH. Lastly, I want to thank all the staff in the BISI program and IBBR office for their assistance throughout my training.

On a personal note, I'd like to thank my parents for their unconditional love and support. To the Arsenal FC, my home team, for the good and bad. We move. To my best friends for all their help and company. In particular, to Xuelian Zhao, for being my role model and inspiration as a scientist and a person in life.

# Table of Contents

# List of Tables

# List of Figures

# List of Abbreviations

| | |
|---|---|
| PCP | *pneumocystis carinii pneumonia* |
| KS | Kaposi's Sarcoma |
| AIDS | acquired immune deficiency syndrome |
| LAV | Lymphadenopathy-Associated Virus |
| HTLV-III | human T-lymphotropic virus-III |
| HIV | human immunodeficiency virus |
| ASP | antisense protein |
| Env | envelope glycoprotein |
| PIC | pre-integration complex |
| ART | antiretroviral therapy |
| AZT | antiretroviral medication Zidovudine |
| NRTI | nucleoside reverse-transcriptase inhibitor |
| FDA | Food and Drug Administration |
| PI | protease inhibitor |
| II | integrase inhibitor |
| NNRTI | nucleoside reverse transcriptase inhibitor |
| LRA | latency-reversing agent |
| PrEP | pre-exposure prophylaxis |
| VE | vaccine efficacy |
| Ig | immunoglobulin |
| IGH | Ig heavy |
| IGL | Ig lambda |
| IGK | Ig kappa |
| HC | heavy chain |
| LC | light chain |
| KC | kappa chain |
| V | variable |
| D | diversity |
| J | joining |
| mAb | monoclonal antibody |
| ADCC | antibody-dependent cellular cytotoxicity |
| BCR | B cell receptor |
| GC | germinal center |
| AID | activation-induced deaminase |
| SHM | somatic hypermutation |
| nAb | neutralizing antibody |
| crNAb | cross-reactive nAb |
| bNAb | broadly neutralizing antibody |
| CD4bs | CD4 binding site |
| MPER | membrane-proximal external region |
| NFL | native flexibly linked |
| VLP | virus-like particle |
| glVRC01 | VRC01 germline-reverted antibody |
| CDR | complementarity-determining region |

| | |
|---|---|
| CD4i | CD4-induced |
| NLGS | N-linked glycans |
| PNGS | N-linked glycosylation sites |
| WT | wild type |
| iGL | inferred germline-reverted |
| KI | knock-in |
| AA | amino acid |
| PBMCs | peripheral blood mononuclear cells |
| Ag | antigen |
| BLI | BioLayer Interferometry |
| FACS | fluorescence-activated cell sorting |
| IP | intraperitoneal injection |
| PC | plasmablast cell |
| ER | endoplasmic reticulum |
| CD4bs | CD4 binding site |
| PADRE | pan-DR epitope peptide |

# Chapter 1: Introduction

### *1.1 The Global HIV/AIDS Pandemic*

During the summer of 1981, CDC received a cluster of cases of unusual and rare diseases, such as a lung infection, *pneumocystis carinii pneumonia* (PCP), Kaposi's Sarcoma (KS), and other opportunistic infections, (Centers for Disease Control and Prevention (CDC), 1996; Gottlieb et al., 1981). All the patients displayed similar cell-mediated immune deficiency, predominantly caused by the significantly diminished population of circulating CD4+ T cells (Gottlieb et al., 1981; Masur et al., 1981). In September 1982, the CDC used the term 'AIDS' (acquired immune deficiency syndrome) for the first time to describe the disease with "at least moderately predictive of a defect in cell-mediated immunity, occurring in a person with no known cause for diminished resistance to that disease" (Institute of Medicine (US) Committee on a National Strategy for AIDS., 1986). Despite its large-scale public awareness raised in the 1980s, the disease was later confirmed to start spreading many years before it was spotted in the US (Worobey et al., 2016).

In 1983, investigators finally pinned down the cause of the disease to retroviruses (Barré-Sinoussi et al., 1983; Gallo, 2002; Montagnier, 2002). Experimental data published by a research team in France led by Luc Montagnier suggested the association between Lymphadenopathy-Associated Virus (LAV) and AIDS (Barré-Sinoussi et al., 1983). A year after, a joint conference held by the National Cancer Institute and the French group in the Pasteur Institute announced the virus HTLV-III (human T-lymphotropic virus-III)/LAV was the cause of AIDS (Gallo, 2002; Montagnier, 2002). The HTLV-III/LAV virus was later officially named HIV (human immunodeficiency virus) by the International Committee on the Taxonomy of Viruses in 1986 (Case, 1986). Since its identification, HIV

remains undoubtedly one of the world's leading killers. By 2019, HIV had infected a cumulative total of more than 75 million people globally, and more than 32 million people have died from AIDS-related illnesses (UNAIDS, 2019).

### *1.2 HIV-1 Genome and the Virus Life Cycle*

The HIV RNA genome encodes 10 viral proteins (gag, pol, vif, vpr, vpu, env, tat, rev, nef, and the antisense protein (ASP) ) (**Figure 1.1A)** (Xiao et al., 2019). The four Gag proteins (p6, matrix (p17), capsid (p24), and nucleocapsid (p7)), and the two Env proteins (gp120 and gp41), are the core structural components of the virion (Frankel and Young, 1998; Xiao et al., 2019). The three Pol proteins (integrase (p32), reverse transcriptase (p66), and protease (p22)) are essential enzymes enclosed inside the virus particles (**Figure 1.1A & B**) (Frankel and Young, 1998; Xiao et al., 2019). There are also seven accessory proteins encoded by the HIV genome (ASP, Vpu, Vif, Vpr, Nef, Tat, and Rev) (**Figure 1.1A)**. They are adapter molecules that play important roles in structural integrity, virus assembly, and gene regulation (Affram et al., 2019; Seelamgari, 2004; Xiao et al., 2019). All the HIV proteins identified above are potential targets for antiretroviral drug development. Elucidation of the functions of these proteins paves the way to decipher the complex mechanisms of HIV replication and pathogenesis (Campbell and Hope, 2015; Li and De Clercq, 2016; Swanson and Malim, 2008).

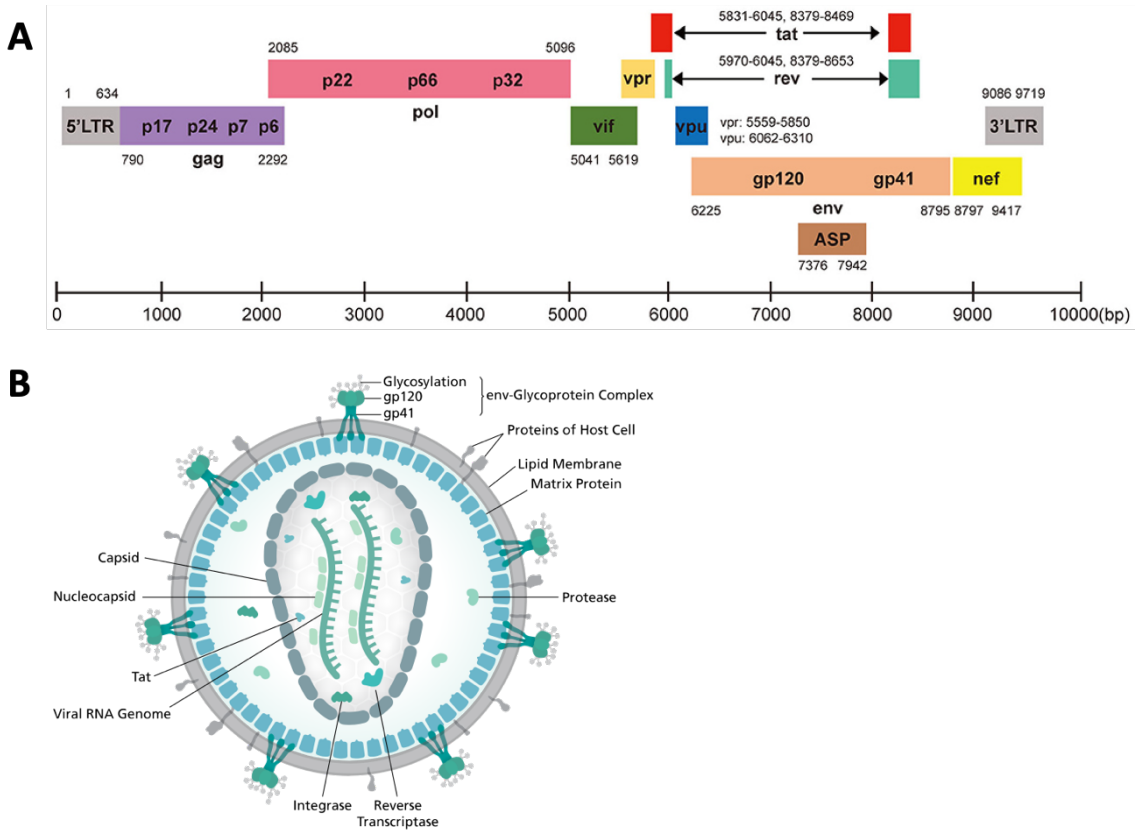


**Figure 1.1 HIV-1 genome and particle structure.** (A) HIV-1 DNA genome map. HIV-1 genome is ~9.8 kb in length with 5′LTR, 3′LTR, and 16 viral protein-encoding genes. DNA positions are based on the reference HIV HXB2 (K03455) (Xiao et al., 2019). (B) Diagram of HIV Particle Structure (Image credit: Dr. Thomas Splettstoesser (www.scistyle.com))

As a typical retrovirus, HIV transcribes its RNA genome into DNA by the reverse transcriptase (p66) enclosed in its capsid. The virus then utilizes the integrase (p32) to insert a copy of the genome into the host cell DNA to replicate. This replication process can be broken down into the following steps (**Figure 1.2**) (Arhel, 2010; Campbell and Hope, 2015; Engelman and Cherepanov, 2012; Freed, 2015; Greene and Peterlin, 2002; Huang et al., 2007; Wilen et al., 2012). The HIV-1 lifecycle starts by the attachment of the envelope glycoprotein (Env) to the CD4 molecule on the cell surface, which further induces a conformational change to expose the co-receptor binding site on CCR5 or CXCR4 (step 1). The Env, which is the core topic of this thesis, initiates the attachment and leads to the

fusion of the viral and cellular membranes (step 2). Uncoated viruses (step 3) release the components in the capsids (**Figure 1.1 & Figure 1.2**), which facilitates reverse transcription of the RNA genome (step 4) to produce a double-stranded viral DNA copy of the HIV genome. The error-prone nature of the reverse transcriptase gives rise to the exceptional diversity of HIV sequences (Lloyd et al., 2014). The double-stranded viral DNA forms the pre-integration complex (PIC) in the host cell cytosol and is then transported into the cell nucleus (step 5). The viral DNA is integrated into the DNA of the host cell (step 6) by integrase carried inside the virus. Viral mRNAs transcribed by host RNA polymerase (step 7) are transported out of the nuclear (step 8) and translated into the regulatory proteins, structural proteins, and Envs (step 9). In the late phase of the HIV-1 life cycle, HIV proteins mentioned above and the genome-length RNA are trafficked and assembled at the host cell plasma membrane (step 10). Packed virus particles bud and are then released from the cell membrane (step 11&12), soon followed by protease-mediated maturation (step 13).

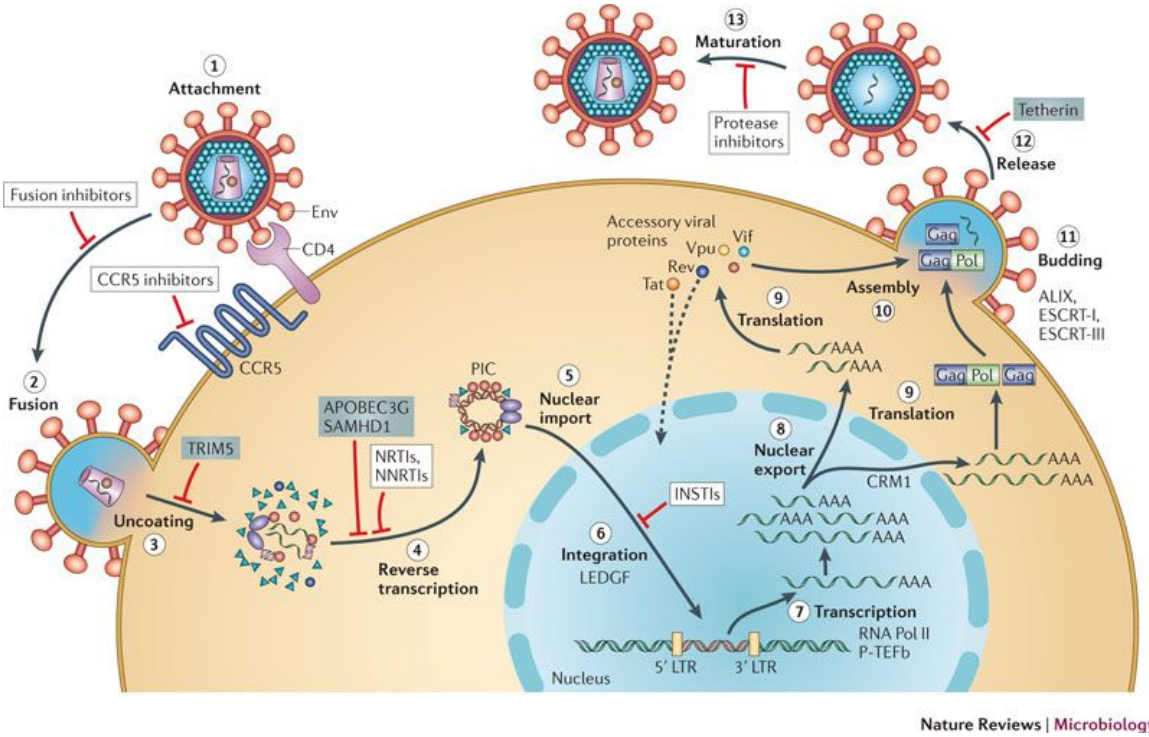


**Figure 1.2 Schematic overview of the HIV-1 replication cycle and targets for antiretroviral therapy** (Engelman and Cherepanov, 2012)**.**

### *1.3 Current Treatment and Prophylaxis for HIV Infection*

#### 1.3.1 HIV Antiretroviral therapy (ART)

In general, each step in the HIV-1 life cycle (**Figure 1.2**) can be potentially targeted by drugs. The first HIV antiretroviral medication Zidovudine (AZT), a nucleoside reverse-transcriptase inhibitor (NRTI), was approved by the Food and Drug Administration (FDA) in 1987. Since then, more than 40 antiretroviral drugs or drug combinations have been approved by the FDA (Food and Drug Administration (FDA), 2018; Kinch and Patridge, 2014; Saag et al., 2018). Antiretroviral therapy (ART) has transformed HIV treatment and is currently the most effective approach for HIV prevention and treatment (Montaner et al., 1999; Saag et al., 2018). The three-drug combination is usually recommended as the standard for care (Montaner et al., 1999; Saag et al., 2018). The cocktail consists of two NRTIs, and one from either a protease inhibitor (PI), an integrase inhibitor (II), or a non-

nucleoside reverse transcriptase inhibitor (NNRTI) (Montaner et al., 1999; Saag et al., 2018). Patients manage to suppress viral loads to undetectable levels by taking pill combinations (Montaner et al., 1999; Saag et al., 2018; Takata et al., 2019). However, the virus rebounds rapidly after the interruption of the treatment (Takata et al., 2019). Besides, drug resistance, the short, and long term side effects of ART cannot be overlooked (Chen et al., 2013). Although improved and newer classes of ART drugs are emerging, they might still be incapable of eradicating the latency established in resting $CD4^+$ T cells and other various cell types (Gulick and Flexner, 2019; Murray et al., 2016). Besides ART, researchers are seeking new approaches such as broadly neutralizing antibodies (bNAbs), stem-cell therapy, latency-reversing agents (LRAs) to target and clear latent reservoirs (Elsheikh et al., 2019; Halper-Stromberg and Nussenzweig, 2016; Takata et al., 2019).

### 1.3.2 HIV Prevention Efforts

As for HIV prevention, pre-exposure prophylaxis (PrEP) by taking the ART drugs is the only option currently available. However, this practice is unlikely to be applicable to everyone considering the cost, side effects, and accessibility (Adamson et al., 2017; Tetteh et al., 2017). A prophylactic or even therapeutic HIV vaccine still holds the best long-term hope to prevent infection and end the pandemic. Historically, effective vaccines have significantly reduced the transmission and spread of many viral diseases (Graham, 2013). HIV vaccine research field, however, had suffered numerous setbacks since the first clinical trial in 1986 (Esparza, 2013). Empirical vaccine design approaches adopted from licensed vaccines, which work well with other viruses, fail to deliver promising results for HIV (Esparza, 2013; Fauci, 2003; Fauci et al., 2014; Johnston and Fauci, 2008). Killed or live attenuated whole-virus were considered unsafe due to the fears of potential proviral

DNA integration and increased risk of HIV acquisition (Fauci, 2003; Zaunders et al., 2011). Subunit vaccines derived from HIV Env were insufficient to confer protection against HIV infection. Antibody responses elicited only neutralized lab-adapted viruses (Tier 1 viruses) but ineffective in neutralizing primary isolates from patients (Tier 2 viruses) (Esparza, 2013; Flynn et al., 2005; Pitisuttithum et al., 2006). T-cell based vaccines designed to induce HIV-specific CD8+ T cell responses to eradicate infected cells had also failed to show efficacy. Instead, clinical trial data even suggested an increased HIV infection risk (Esparza, 2013; Sekaly, 2008).

A milestone in the HIV vaccine field was the 31.2 % vaccine efficacy (VE) achieved by the Thai HIV phase III prime-boost trial (RV144) (Rerks-Ngarm et al., 2009; Tomaras and Haynes, 2013). The regiment consists of a canarypox vector as prime, followed by a recombinant gp120 boost (Tomaras and Haynes, 2013). A similar clinical trial in South African (HVTN 097) also confirms the correlates of protection, which include weak or non-neutralizing V1V2 immunoglobulin G (IgG), HIV Env-specific CD4+ T cell, and antibody-dependent cellular cytotoxicity (ADCC) in vaccinees that have low IgA levels (Gray et al., 2019; Rerks-Ngarm et al., 2009; Tomaras and Haynes, 2013). These results have greatly encouraged rigorous efforts on iteratively optimizing vaccine platforms and immunogens to achieve a higher efficacy. Some new generation HIV vaccine candidates in **1.5 & 1.7** have entered human clinical trials for efficacy examination (Robinson, 2018).

### *1.4 Antigen-Specific B Cell Memory*

Protective B cell responses are the basis of nearly all effective vaccines in the market (Stamatatos et al., 2009). In this regard, to prevent HIV infection, it will most likely require the elicitation of antibody responses that cross-neutralize the highly diverse strains. An effective HIV vaccine should be responsible for driving the antigen-dependent memory response to generate long-lived plasma cells and memory B cells. This process starts from the antigen-binding to the naive B cell receptors (BCRs) (Kurosaki et al., 2015) (**Figure 1.3**). Downstream BCR signaling then initiates the antigen internalization and process, followed by the antigen presentation and activation of antigen-specific T-helper cells. Activated naïve B cells proliferate and form the germinal center (GC), a specialized microstructure within lymph nodes or the spleens for memory B cell development. Some activated B cells differentiate into short-lived plasmas cells. Another subset of B cells in GCs can undergo iterative rounds of antigen-affinity driven B cell proliferation and diversification, which is also referred to as affinity maturation (Klein and Dalla-Favera, 2008). During this process, activation-induced deaminase (AID)-mediated somatic hypermutation (SHM) introduces individual mutations into the germline variable region of BCRs in the dark zone (**Figure 1.3A**). Clonally expanded B cells then relocate to the light zone, where B cells with certain specificities and high affinities with the antigen will be selected (affinity selection) (**Figure 1.3A**). Affinity matured B cells from this process can reenter the dark zone for additional rounds of SHM and clonal expansion. The B cells with substantial affinities to the antigen may exit the cycle and the class-switched GC B cells either differentiate as memory B cells with immunoglobulin (Ig) anchored on the surface or as long-lived plasma cells that continuously secrete Ig (**Figure 1.3A**). The two arms of

B cell memory account for the long-lasting humoral immune response induced by the antigen (Lanzavecchia and Sallusto, 2009).

A typical Ig, also known as an antibody, consists of four chains, two heavy chains and two light chains (**Figure 1.3B**). Each of the four chains contains two elements, a constant region that defines the isotype, and a variable region (Fab) that determines the binding specificity and affinity to the antigens. The variable region is assembled through the V(D)J recombination mechanism (**Figure 1.3C**), which is the hallmark of adaptive immunity (Li et al., 2004). One of the random germline copies from each variable (V), joining (J), and diversity (D) gene segments rearrange and generate a primary BCR repertoire. Although the number of V, D, and J gene segments is limited, random nucleotides insertion at V(D)J junctions further expand sequence diversity (**Figure 1.3C**). Moreover, the primary B cell pool will be heavily mutated in response to different antigens during affinity maturation.

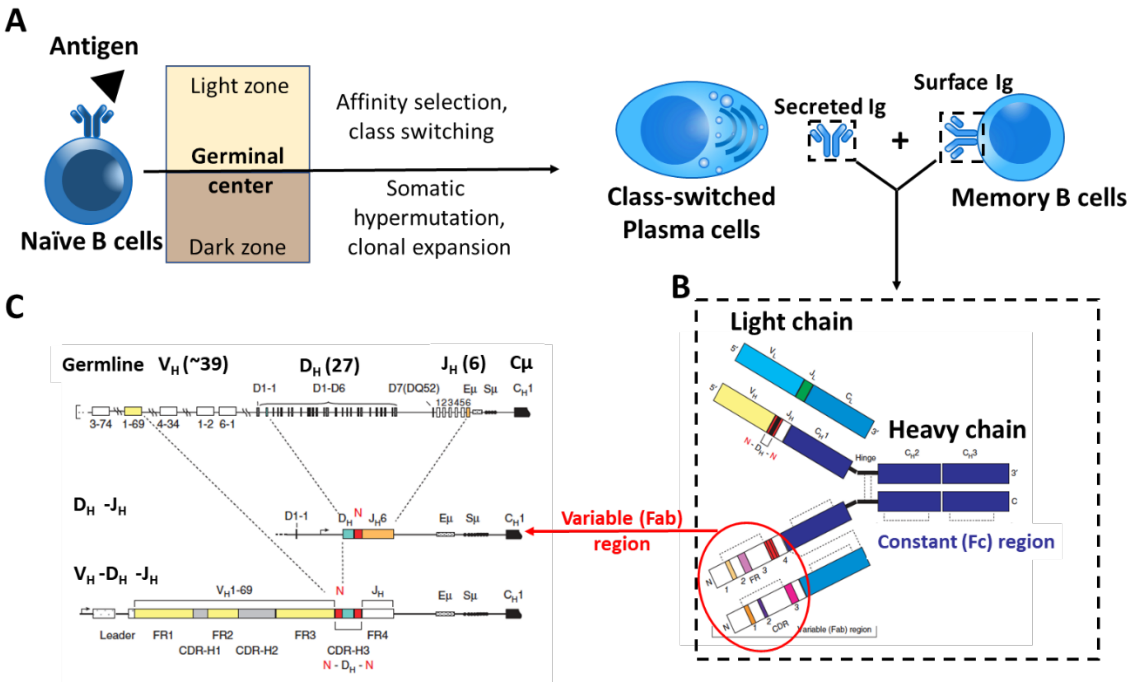

**Figure 1.3 Antigen-induced memory B cell development.** (A) After encountering antigens, naïve B cells recognize certain portions of the antigen via BCRs. The recognition initiates a series of signaling, cytokine synthesis, and clonal expansion of antigen-specific B cells with the assist from other immune cells. Activated B cells then enter the germline center (GC) to proceed with affinity maturation and class switching. The dark zone of the GC is where somatic hypermutation (SHM) and clonal expansion occurs. Mutated B cells migrate to the light zone to undergo affinity-based selection and class switching. The cycles of SHM, clonal expansion, and affinity selection repeats in the GCs. Affinity matured GC B cells further differentiate into long-lived plasma cells and memory B cells. (B) Antibody/surface Ig structure and (C) V(D)J recombination of the antibody variable region are adapted from (Georgiou et al., 2014)

### *1.5 HIV Envelope Glycoprotein (Env) and Broadly Neutralizing Antibodies (bNAbs)*

HIV envelope glycoprotein (Env) mediates virus entry and is the sole target for neutralizing antibodies (nAbs). The Env gene expresses precursor protein gp160 that is cleaved by furin into two subunits, gp120 and gp41 (**Figure 1.1**). Gp120 subunits possess the receptor (CD4) binding and co-receptor binding sites, while gp41 subunits contain transmembrane domains that anchor Envs on the virus membrane. Three gp120-gp41 heterodimers (six protein subunits) further assemble into functional trimeric spikes (Ward and Wilson, 2015).

There are numerous mechanisms for the HIV Env protein to confer immune evasion. For example, Env is the most variable HIV protein. Extremely diverse escape mutations can be generated in Env sequences without affecting viral fitness (Moore, 2018). The protein surface is also heavily covered with N-linked glycans to block antibody response (Stewart-Jones et al., 2016). In addition, functional Env trimers sparsely distributed on the viral membrane together with decoy non-functional Envs (Mascola and Montefiori, 2003). However, in some HIV-infected individuals, the human immune system still manages to produce antibodies attacking relatively conserved regions across diverse HIV strains after extensive affinity maturation process (Kepler and Wiehe, 2017; Sok and Burton, 2018). In consequence, infection-elicited antibodies in these individuals are able to block the virus

particles from entering and infecting target cells. These monoclonal antibodies are so-called broadly neutralizing antibodies (bNAbs), defined by their capability to neutralize a diverse panel of circulating HIV strains with high neutralization potency (low antibody concentrations). A small subset of patients known as elite controllers eventually develop bNAb responses after several years of antibody-virus co-evolution (Landais and Moore, 2018; Sok and Burton, 2018). By studying the bNAb responses in those rare donors, researchers hope to decipher the cellular and molecular determinants that drive the development of the bNAbs, which in turn may better inform vaccine design.

Evolved bNAb isolation methods indisputably play a pivotal role in the new era of B cell-based HIV vaccine design. The first generation of HIV bNAbs (b12, 2G12, 2F5, and 4E10) were isolated by either phage display or hybridoma immortalization (McCoy and Burton, 2017). Those bNAbs are the first proof of concept that antibodies can recognize specific regions of the Env shared by a wide range of strains. Since 2003, flow cytometry-based single B cell technologies have emerged and significantly bolstered the bNAb discovery (McCoy and Burton, 2017). Together with the downstream functional and structural analysis, a large number of bNAbs that bound distinct regions on the Env have been isolated and scrutinized from HIV elite controllers (McCoy, 2018; McCoy and Burton, 2017; Sadanand et al., 2016; Sok and Burton, 2018). Thus far, six different bNAb epitopes on the Env have been defined (**Figure 1.4**). These epitopes include V3 glycan (N332 supersite), V1V2 apex, the CD4 binding site (CD4bs), gp120/gp41 interface, the silent face, and the membrane-proximal external region (MPER) (Sok and Burton, 2018). These characterized vulnerable regions are valuable leads for structure-based and B cell-based HIV vaccine design.

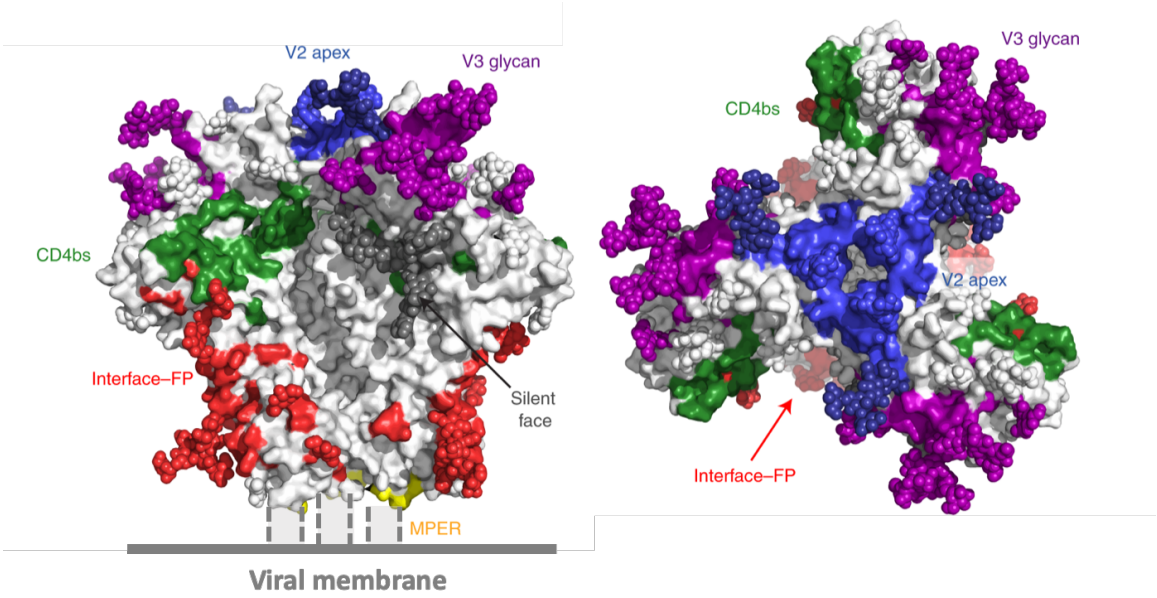


**Figure 1.4 HIV bNAb epitopes identified to date.** Epitopes shown on the HIV Env in a side (left) and top (right) view. Env timer was represented by the native-like trimer mimicry BG505 SOISP.664. Glycans and protein surfaces comprising the bNAb epitopes are indicated in different colors. Purple, V3 glycan; blue, V2 apex region; green, CD4 binding site (CD4bs); grey, silent face; red, gp120/gp41 interface, and fusion peptide (FP); yellow, membrane-proximal external region (MPER) adapted from (Sok and Burton, 2018).

This thesis is mainly focused on CD4bs-directed bNAbs, which target the receptor-binding site on the HIV spike protein (Env). CD4bs is the functional conserved region that the virus cannot afford to mutate substantially. Otherwise, the virus would not be able to infect CD4+ immune cells and replicate. Most of the bNAbs under this category are typified by VRC01 and termed as VRC01-class bNAbs. VRC01-class bNAbs share the same VH1-2 germline gene and mimic the CD4 receptors in terms of angle of approach and footprint via CDRH2 to interact with the viral spike (Bonsignori et al., 2018). Thus far, VRC01-class bNAbs have been isolated from several different donors (Bonsignori et al., 2018), which suggests their potential of being induced via vaccination. On the other hand, VRC01-class bNAbs obtain unusual short CDRL1 loops and relatively high levels of SHM to accommodate dense glycan shield around the CD4bs (Landais and Moore, 2018). These

unique features present roadblocks for rational immunogen design against this epitope. In this thesis, I will summary current efforts and discuss potential strategies towards VRC01-like bNAb elicitation.

## *1.6 HIV Env-Based Immunogen Design*

### 1.6.1 Gp120 immunogens and gp140-foldon trimer design

One strategy to develop an effective HIV vaccine is to teach the immune system to develop bNAb responses to prevent viral acquisition. As the sole target for bNAbs, Env spike serves as a promising template to fulfill this challenge. Continuous endeavors have been taken to design Env-based immunogens to elicit immune responses to the virus sites of vulnerability identified by bNAbs (Bricault et al., 2019; Dubrovskaya et al., 2019; Escolano et al., 2016; Saunders et al., 2017; Xu et al., 2018). The early attempts of Env-based immunogen design started with the gp120 monomers, which are highly immunogenic and share bNAb epitopes with function trimer spikes. (Parren et al., 1997; Sattentau and Moore, 1995). However, the gp120 monomer immunogens tested in clinical trials failed to confer neutralizing and protective responses (Flynn et al., 2005; Gilbert et al., 2010; Pitisuttithum et al., 2006). Compared with gp120 monomers, native Env spikes constrain bNAb epitopes by the quaternary structure and preserve trimer-specific epitopes (Lyumkis et al., 2013; Sanders et al., 2013). Therefore, immunogens mimicking the native trimeric spikes might be more effective in eliciting bNAbs.

Nevertheless, there are many hurdles for Env trimer mimicry design. Similar to other viral fusion proteins, the prefusion state of HIV Env trimer is intrinsically metastable (Torrents de la Peña and Sanders, 2018). Additionally, Env has a transmembrane domain

in the gp41 subunit, which compromises secretion, purification, and solubility of the recombinant protein. Thus, the first bottleneck is how to engineer a soluble and stable Env trimer locked in the prefusion formation. Many approaches have been made to achieve this goal. First, the transmembrane domain and cytoplasmic domains were deleted from the gp41 subunit to increase the solubility (Earl et al., 1991). To prevent the dissociation of the protein, the furin cleavage site (REKR) between the gp120 subunit and the ectodomain of gp41 ($gp41_{ECTO}$) was then inactivated by converting to a (SEKS) sequence. The covalently linked Env (so-called uncleaved gp140) constructs expressed highly heterogenous Env proteins with low trimer yields (Earl et al., 1994; Jeffs et al., 2004; VanCott et al., 1995). To improve trimer formation propensity, the foldon domain, a trimerization motif derived from T4 fibritin protein, was tethered to the C-terminus of the $gp41_{ECTO}$. Env trimers designed based on this strategy are referred to as gp140-foldon trimers (**Figure 1.5A**). In terms of the immunogenicity, gp140-foldon trimers induced non-nAbs, modest tier-1 nAb responses, and rare autologous nAbs against autologous tier-2 viruses (Chakrabarti et al., 2013; Kovacs et al., 2012; Sundling et al., 2012a; Yang et al., 2001). The unsatisfied output was largely due to the imperfect resemblance of functional trimer spikes illustrated by structural analysis and antigenic profiling (Guenaga et al., 2015; Ringe et al., 2013; Tran et al., 2014).

### 1.6.2 SOSIP.664 native-like Env trimers

Inactivation of the proteolytic cleavage and the disulfide bonds within the gp140-foldon constructs are likely to interrupt the Env structure and epitope presentation (Go et al., 2011, 2014, 2016; Ringe et al., 2015; Sanders and Moore, 2017). To address these design problems, an opposite approach had been taken. Instead of preventing the cleavage

of gp120 and gp41, the furin cleavage sequence was optimized to the RRRRRR(R6) motif (Binley et al., 2002) (**Figure 1.5B**). Extra furin gene vector was also co-transfected with gp140 constructs to supplement furin expression. To avoid dissociation between gp120 and $gp41_{ECTO}$ subunits, cysteine substitutions in gp120 and $gp41_{ECTO}$ were screened to form disulfide linkages between the two subunits (Binley et al., 2000). The best double-cysteine pair that gave rise to properly folded gp140 Envs were mutations at residue 501 in gp120, and residue 601 in $gp41_{ECTO}$ (Binley et al., 2000) (**Figure 1.5B**). The cysteine mutations (501C-601C) was also referred to as SOS.

The SOS gp140s tended to undergo the transition towards postfusion conformation. To stabilize the prefusion configuration, an extra point mutation (I559P) was identified and introduced in heptad repeat 1 (HR1) (Sanders et al., 2002). The MPER region was later truncated from the soluble trimer to avoid trimer aggregation. The C-terminus of the new construct ends at residue 664. Combined with all the improvements mentioned above, the final soluble Env trimer construct was designated as SOSIP.664 (**Figure 1.5B**). SOSP.664 Env trimer configuration was applied to different virus strains, among which, the transmitted/founder virus Env gene from a 6-week-old infant (BG505), displayed high native-like trimer yield and trimer thermal stability (Beddows et al., 2006; Guenaga et al., 2015; Iyer et al., 2007; Sanders et al., 2013). Besides, the well-ordered BG505 SOISP.664 trimers had desirable antigenicity properties: bound well with bNAbs but poorly with non-nAbs (Sanders et al., 2013). BG505 SOSIP.664 soon became the benchmark and prototype for next-generation Env immunogens. The trimer structure and bNAb epitopes have been well delineated by both x-ray crystallography and cryo-EM (Julien et al., 2013; Lyumkis et al., 2013; Sanders and Moore, 2017). The abundant available high-resolution structural

data provide a crucial new starting point for structure-based immunogen design (Kulp and Schief, 2013).

The immunogenicity of BG505 SOSIP.664 has also been widely tested in different animal models, such as mice, guinea pigs, rabbits, and macaques (Feng et al., 2016; Hu et al., 2015; Sanders et al., 2015). The partially open trimers expose several non-nAb epitopes such as CD4bs-associated non-nAb epitopes and the immunodominant V3 loop (van Schooten and van Gils, 2018). Nevertheless, the trimers induced consistent high titer of autologous tier-2 neutralizing activities against the BG505 virus in guinea pigs and rabbits (Feng et al., 2016; Sanders et al., 2015). The weaker and inconsistent tier-2 nAb response was observed in macaques, while mice were irresponsive to the immunogen to produce tier-2 nAbs (Hu et al., 2015; Sanders et al., 2015). Obviously, the breadth of the nAb response elicited by BG505 SOSIP.664 was insufficient and needed to be improved. Understanding the mechanisms that restrict the neutralization breadth became the immediate goal. In **Chapter II & III,** we delineated the specificities of nAb response elicited by BG505 SOSIP.664 at the clonal level and provided possible modification strategies on the original trimer.

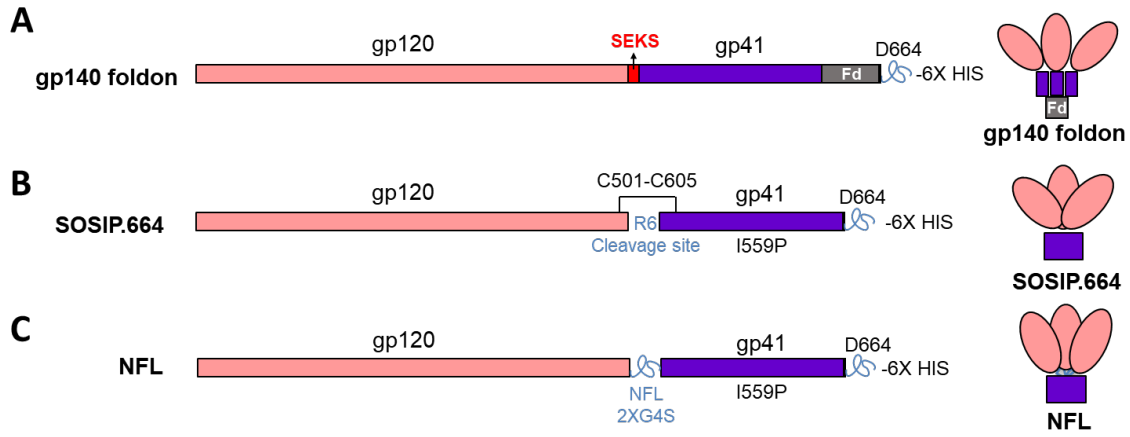


**Figure 1.5 Schematic representations of gp140 foldon pseudotrimer, SOSIP.664, and NFL native-like trimer constructs based on HIV strain BG505.** Gp120s are shown in pink and the gp41$_{ECTO}$s are shown in purple. (A) In the gp140 foldon design, SEKS mutation inactive the furin cleavage site, the foldon trimerization domain is exhibited in grey. (B) I559P mutation and the SOS bond (501C-605C), and RRRRRR(R6) furin cleavage site change are displayed in SOSIP.664. (C) The native flexible linker (NFL) between gp120 and gp41$_{ECTO}$ is depicted in a blue line in the NFL construct. The C-termini of all constructs end at residue 664.

### 1.6.3 NFL native-like Env trimers

An alternative strategy to generate native-like trimers is by adding flexible linkers between gp120 and gp41$_{ECTO}$ subunits. One of the "uncleaved" trimer designs explored in **Chapter IV** is a native flexibly linked (NFL) format developed in Dr. Richard Wyatt's lab (Sharma et al., 2015). The cleavage-independent trimer constructs replaced the furin cleavage site with an optimized linker sequence (GGGGSGGGGS). To allow adequate conformational mobility for proper subunit assembly, at least one I559P prefusion stabilization mutation in SOSIP trimers was required to cooperate with the flexible linker methods (**Figure 1.5C**) (Georgiev et al., 2015; Kong et al., 2016a; Sharma et al., 2015; Yang et al., 2018). Overall, compared to SOSIP trimers, NFL trimers have similar or better yield, antigenicity profiles, structure, and immunogenicity in animal models (Feng et al., 2016; Sarkar et al., 2018; Sharma et al., 2015). Moreover, NFL Env constructs do not need

furin gene co-transfection, which simplifies the process of Env expression in potential applications in vector immunizations.

In summary, both the NFL and SOSIP are well-developed platforms that can be applied for further Env trimer immunogen design. More trimer stabilization mutations are continuously being identified by high throughput screening, mammalian display, and structure-based design to augment trimer formation and immunogenicity (Burton and Hangartner, 2016; Sanders and Moore, 2017). Current native-like trimers consistently induce autologous tier-2 neutralizing responses in various animal models (Haynes and Burton, 2017). However, our final goal is to elicit bNAb responses by immunogens/immunogen combinations. This goal will hopefully be achieved by an iterative process involving the comprehensive analysis of immunogen-induced immune responses and immunogen re-design. In this thesis, especially in **Chapters III & IV**, we characterized the immune responses elicited by immunogens constructed with both SOSIP and NFL forms. We identified the Env immunogenic determinants that restrict the breadth of immunization-elicited nAbs and examined the B cell response induced by bNAb donor-derived Env immunogens. We believe that these efforts will contribute to future immunogen redesign to elicit bNAb response via immunization.

### *1.7 bNAb Elicitation by Sequential Immunization*

Considering the extraordinary diversity of the Env sequences, the existence of bNAbs that target conserved regions on the HIV Env is even more intriguing. bNAbs typically arise from years of fighting and co-evolving with circulating viruses. One indication of the prolonged maturation process is the high levels of somatic hypermutation (SHM) in bNAbs variable sequences (Hwang et al., 2017; Rantalainen et al., 2018; Sanders

et al., 2015). This degree of SHM arises from iterated selection and clonal expansion of B cells in GCs with affinity-enhancing mutations (Doria-Rose and Joyce, 2015). Thus, it might be hard to find a shortcut by just using one immunogen candidate to simulate the extensive affinity maturation.

A more realistic strategy is to use a series of different immunogens to shepherd antibody response toward bNAbs (Burton, 2019) (**Figure 1.6**). The hypothesis is that bNAb response might be achieved if a succession of tailored immunogens can 1) activate rare bNAb precursors in the repertoire, 2) induce high levels of somatic hypermutations in antibody encoding genes in germinal centers where B cells encounter antigens, and 3) successively return B cells to germinal centers to undergo repeated rounds of affinity maturation (Escolano et al., 2016). In other words, this sequential immunization strategy requires specially designed immunogens catering to each step described above.

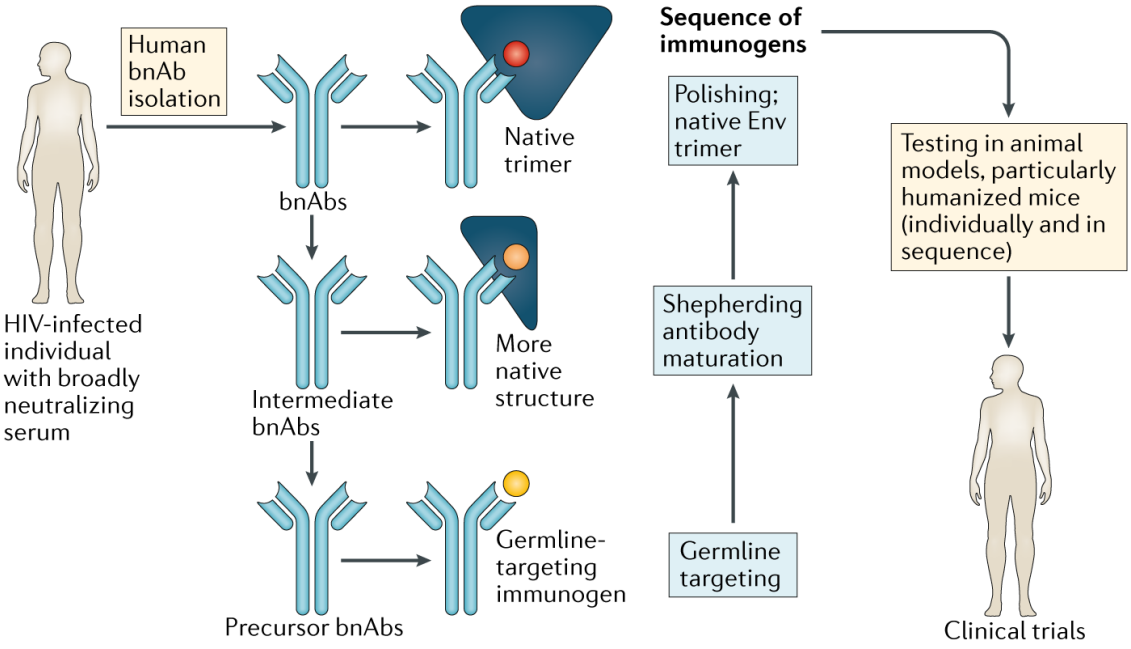


**Figure 1.6 A generalized germline-targeting sequential immunization strategy for HIV.** bNAbs isolated from human donors define vaccine targets (red) on HIV Env, which serve as templates for structure-based vaccine design. The inferred germline-reverted antibodies of bNAbs (precursor bNAbs) usually show undetectable binding to "bait" Env proteins used to isolate bNAb

B cells. Thus, immunogens specially designed to interact with precursor bNAbs (yellow) might be required to initiate bNAb response by vaccination. To guide antibody response towards bNAbs, a succession of immunogens are used to interact with bNAb intermediates identified from donors or computational analysis. Those immunogens may more resemble native-like trimers and should stimulate increased somatic hypermutations in the direction of the bNAb development pathway. Native trimers are likely to be used in final steps to constrain antibody responses to the conserved sites of vulnerability on HIV Env. The efficacy of this immune strategy is first evaluated in animal models with unnaturally high bNAb precursor levels or human-like B cell repertoires (Burton, 2019).

## *1.8 Germline-targeting immunogens*

### 1.8.1 CD4bs-directed germline-targeting immunogens

To activate bNAb precursor B cells, a group of so-called "germline-targeting" immunogens has been designed and continuously expanded to fulfill this purpose. The number of available "germline-targeting" immunogens is still limited (Stamatatos et al., 2017). Most germline-targeting design centers on CD4bs-specific precursor B cells given the balanced breadth and potency shown by CD4bs-directed bNAbs. The VRC01-class bNAbs, in particular, share the same heavy chain variable germline gene segment (VH1-2) and is, therefore, more attainable for immunogens to induce similar bNAb responses. The first of this kind is a self-assembling nanoparticle carrying engineered HIV gp120 outer domains (eOD-GT8) (Jardine et al., 2015). The outer domain gp120 protein was designed through computational modeling and yeast display to interact highly specific to a diverse panel of VRC01-class germline antibodies (glVRC01s) (**Figure 1.7 )** (Jardine et al., 2013, 2015). eOD-GT8 particles have been demonstrated to activate VRC01 precursor B cells in the cell-based assay and VRC01-germline knock-in mouse models (Abbott et al., 2018; Jardine et al., 2015; Sok et al., 2016). The safety and immunogenicity of eOD-GT8 are still under investigation in the clinical trial.

eOD-GT8 has also been used as probes to isolate and determine the frequency of B cells expressing VRC01 germline-like B cell receptors (BCRs) in human donors (Jardine et al., 2016a). Those human VRC01 precursor B cells share VRC01 VH germline (VH1-2*02), while differing in light chains (LCs) (Jardine et al., 2016a). eOD-GT8 binding B cells do not all feature the five-amino-acid-long CDRL3 in the VRC01 LC (Stamatatos et al., 2017). Therefore, eOD-GT8 particles might not specifically stimulate VRC01 precursor B cells in vivo. Immunogenicity studies also demonstrated that a significant portion of antibody responses elicited focused on non-CD4bs (Duan et al., 2018; Tian et al., 2016). Thus, to improve the specificity of eOD-GT8, N-linked glycans have been introduced in eOD-GT8 to block the non-CD4bs epitopes. Glycan-masked eOD-GT mutations displayed more preferred antigenic profiles and reduced off-target immune responses in the humanized mouse model (Duan et al., 2018). Overall, eOD-GT8 and its variants are the first proofs-of-concept that germline-targeting immunization can initiate the affinity maturation of germline precursors.

Other sequence templates have also been explored to design germline-targeting immunogens (McGuire et al., 2013, 2014, 2016). One modification strategy to retain VRC01-class germline antibody binding involves eliminating the glycans around the CD4bs, especially the glycans on loop D (N276) and V5 region (N460 and N463) (Kong et al., 2016b), to avoid the clash with the CDRL1s of germline-reverted VRC01-class antibodies (glVRC01-class Abs). A diverse panel of Env trimers was screened for glVRC01-class Ab binding after glycan modification around the CD4bs. One Env trimer derived from clade C (426c TM) displayed measurable binding to germline-reverted versions of VRC01 and NIH45-46, while remained insensitive to other VRC01-class

germline antibodies (McGuire et al., 2013). Deletion of V1, V2, and V3 regions on 426c TM along with other optimization mutations further improved and expanded the spectrum of glVRC01-class Ab binding (**Figure 1.7)** (McGuire et al., 2016). Following a similar design strategy, a heavily modified BG505 SOSIP.664 variant (BG505 SOSIP.v4.1-GT1) was created (**Figure 1.7)** (Medina-Ramírez et al., 2017). The construct also exhibited improved binding properties to glVRC01-class Abs compared to other BG505-based Env proteins. To sum up, 426c and BG505 SOSIP.v4.1-GT1 are two trimer templates for VRC01 germline-targeting immunogen design.

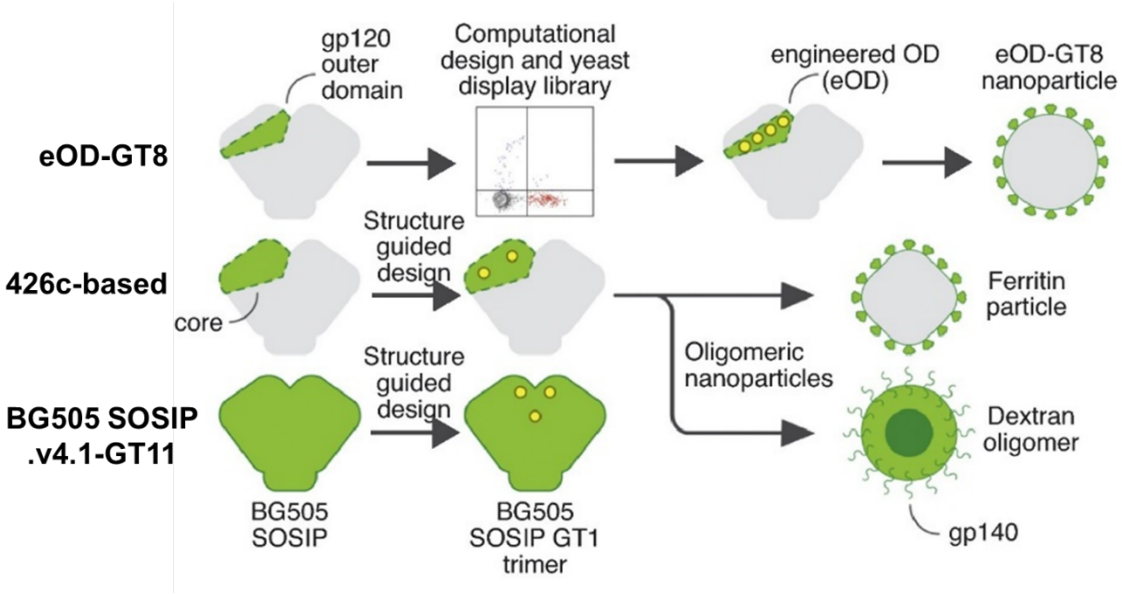


**Figure 1.7 Germline-targeting immunogens against the CD4bs.** Engineered outer domain germline-targeting version 8 (eOD-GT8) is a self-assembled VLP based on the outer domain of the HIV gp120. The protein sequence was designed through computation analysis and yeast display. The 426-based trimer or gp120 immunogen incorporated glycan and variable region deletion to better expose the CD4bs. The multimerized forms on ferritin and dextran display enhanced affinity to VRC01-class germline precursors. BG505 SOSIP.v4.1-GT11 is a CD4bs-targeting variant of the native trimer mimicry, BG505 SOSIP.664. Adapted from (Andrabi et al., 2018).

In **Chapter IV**, we propose two more priming immunogen candidates for VRC0-class bNAb induction. One is a mixture of the modified fusion proteins of gp120 core complexed with CD4-induced (CD4i) antibodies (Core-n5i5-17b and CoreD-n5i5-17b).

Another is a nanoparticle based on a patient-derived Env sequence (dG5 NFL TD_FR). Both prototypical immunogens display augmented VRC01 germline antibody affinity and dampened non-bNAb epitope antigenicity. In the immunogenicity study described in **Chapter IV**, we also observed the VRC01 specific mutations generated in both heavy and light chains by the immunogens. Taken together, there are currently four different templates available for CD4bs-directed germline-targeting immunogen design. In all these cases, modification of N-linked glycans (NLGS) around the CD4bs plays an essential role in the binding of glVRC01-class Abs.

### 1.8.2 N332 supersite-directed germline-targeting immunogens

Similar to CD4bs bNAbs, germline-reverted antibodies of N332 supersite bNAb (PGT121) also lack binding affinities to wild-type (WT) HIV Env recombinant proteins (Stamatatos et al., 2017). A germline-targeting immunogen against N332 supersite was designed by the mammalian cell display platform (Steichen et al., 2016). In brief, BG505 SOSIP whole-gene mutagenesis libraries were transferred to the lentiviral vectors and then transduced to mammalian cells. Cells expressed BG505 SOSIP variants were stained for FACs binding analysis. Germline-targeting mutations on the BG505 gp120 and BG505 SOSIP.664 were screened and identified via evolution-directed affinity testings against the PGT121germline antibody variants (**Figure 1.8A**). The stabilized germline-targeting trimers presented on the liposomes activated PGT121 precursor B cells, which suggested their potential use for PGT121 priming immunogens (Steichen et al., 2016).

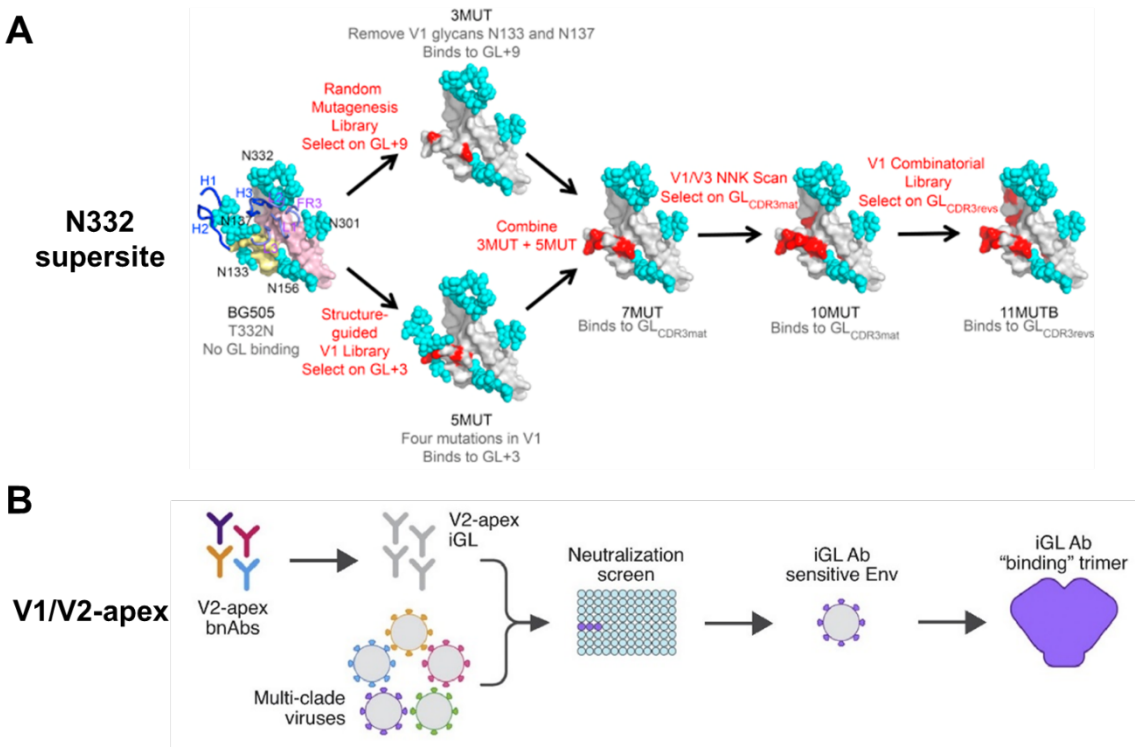


**Figure 1.8 V3 supersite- and V1/V2 apex-directed germline-targeting immunogens.** (A) Germline-targeting immunogen design facilitated by evolutionary screening (Steichen et al., 2016). Glycans are depicted in cyan. Variable loop 1 and 2 are colored in yellow and pink. Germline-targeting mutations introduced are shown in red. GL+9, GL+3, $GL_{CDR3mat}$, and $GL_{CDR3revs}$ are PGT121 germline antibody variants that share VDJ germline gene usage with differences in the CDRL3 region. GL+9 (detectable affinity to BG505 gp120) and GL+3 are more similar to matured PGT121 and used for initial mutation screening. Mutations that displayed binding to either PGT121 germline Abs were then combined for the next screening for $GL_{CDR3mat}$ binding, which leads to more mutations identified in V1 and V3 regions. Mutations based on construct 10MUT were further screened for improved affinity to $GL_{CDR3revs}$, which resemble more to germline-reverted PGT121. The final construct $11MUT_B$ enriched all germline-targeting mutations and displayed the most appreciable binding to the germline variants of the V3 supersite bNAb. **(B)** Screening of V1V2-apex germline-targeting immunogen candidates from neutralization sensitive viruses. Env sequences from viruses sensitive to iGLs of V1V2 bNAbs were selected as templates for epitope grafting (adapted from (Andrabi et al., 2018)).

### 1.8.3 V1/V2 apex-directed germline-targeting immunogens

V1/V2 apex bNAbs are another attract lead for HIV vaccine development. They have exceptionally long (≥ 24 amino acids) CDRH3s to penetrate and interact with strand C of the V1V2 region (Andrabi et al., 2015). Similar to VRC01-class bNAbs, V1/V2 apex-directed bNAb isolated from multiple donors also share commonalities in recognition

(Gorman et al., 2015). However, unlike other bNAb classes, V1V2 targeting bNAbs have lower SHMs and emerge more early and frequently in patients (Doria-Rose et al., 2014; Gorny et al., 2005; Liao et al., 2013a). Another distinct characteristic of V1/V2 apex bNAbs is that specific HIV isolates from patients are highly susceptible to neutralization by inferred germline-reverted (iGL) antibodies (Andrabi et al., 2015; Bonsignori et al., 2011). BG505 DS-SOSIP trimers with swapped V1V2 regions from iGL neutralization sensitive Envs (CRF02_AG_250, ZM233M, BB201.B432, and KER2018) exhibited strong reactivities to two or more iGLs (Andrabi et al., 2015; Liao et al., 2013b; Stamatatos et al., 2017). (**Figure 1.8B**) Additionally, dimerized synthetic V1V2 glycopeptides alone were able to bound to iGLs of PG9 and CH101 bNAbs with apparent nanomolar affinity (Alam et al., 2013; Aussedat et al., 2013). Therefore, the V1V2 chimeric Env trimers and dimeric peptide scaffolds may selectively prime V1V2-directed antibody responses. More investigations are needed to corroborate the immunogenicity of these two germline-targeting immunogens.

### *1.9 Human Immunoglobulin (Ig) Knock-in Mouse Models for Germline-Targeting Immunogen Assessment*

Animal models such as mice, guinea pigs, rabbits, and non-human primates (NHPs) are undeniably crucial for HIV vaccine development (Stamatatos et al., 2017). However, these classic models do not express bNAb germline gene orthologs (Vigdorovich et al., 2016), which is apparently problematic to evaluate the germline-targeting immunogens before clinical assessment. To tackle this issue, genetically engineered bNAb precursor knock-in (KI) mouse models have been generated. These models specifically express either

unrearranged bNAb germline gene segments that can be later developmentally assembled or full-length V(D)J exons of bNAb precursors. Therefore, bNAb KI mice provide an artificial system to accelerate initial germline-targeting immunogen screening and iterative improvement.

Here, we focus on KI mouse models established for VRC01 germline-targeting immunogens/immunization strategies (Stamatatos et al., 2017; Verkoczy, 2017). There are currently four models that have been tested for VRC01 precursor activation (**Figure 1.9A**). One KI mouse model (VH1-2) was developed by replacing the mouse $V_H$81X gene segment at the murine IgH locus with the VH1-2*02 germline gene (**Figure 1.9A**). In this model, around 45% of peripheral B cells encode the VRC01 VH germline, while the CDRH3s vary due to the recombination with mouse D and J segments (Tian et al., 2016). eOD-GT8 was able to elicit VRC01-like antibodies in this model, but the Abs were not matured enough to neutralize tier-2 viruses. However, at least noticeably higher frequency of CD4bs-specific memory B cells with 5-aa CDRL3s was observed in experimental groups than the control group, which indicates selective activation of VRC01-like precursor B cells.

As the number of VRC01 precursors in the VH1-2 KI model is limited, another mouse model that contains higher VRC01-like germline B cells was generated based on the VH1-2 model (**Figure 1.9B**). In this model (VH1-2/LC), the murine $J_k$ segment was further substituted by the VRC01 light chain germline (gl-VRC01LC). Thus, it may provide a more optimal context to test the efficacy of immunogens to facilitate the affinity maturation of VRC01 precursor antibodies. In one study, sequential immunization with eOD-GT8 and 426c-based germline-targeting immunogens described in **1.7** successfully

induced accumulated SHMs in both heavy and light chains of VRC01-like memory B cells. Furthermore, one antibody recovered from these cells displayed autologous 426c virus neutralization (Tian et al., 2016).

The immunogenicity of eOD-GT8 was also tested in a VRC01 KI model (VRC01gH) (**Figure 1.9C**). In this model, the mouse JH locus was replaced by the rearranged VRC01 germline heavy chain (VRC01gH), while the LC repertoire remains of murine origin (**Figure 1.9C**). 85% of B cells express germline VRC01 HC (gl-VRC01HC), and around 0.1% LCs contain the VRC01 signature five-amino-acid (AA) long CDRL3s (Jardine et al., 2015). This model might be more feasible to analyze the effectiveness of selecting VRC01-like LCs by the immunogens. Immunization with eOD-GT8 in this model enriched VRC01 like B memory B cells compared to the control immunogen BG505 SOSIP.664. 92% of CD4bs B cells isolated composed of LCs with 5 AA CDRL3s and carried a partial VRC01 motif QQYXX, suggesting the activation of VRC01 precursor B cells. However, the CD4bs-specific antibodies isolated from the immune mice displayed no neutralizing activity due to the limited SHM level (Jardine et al., 2015).

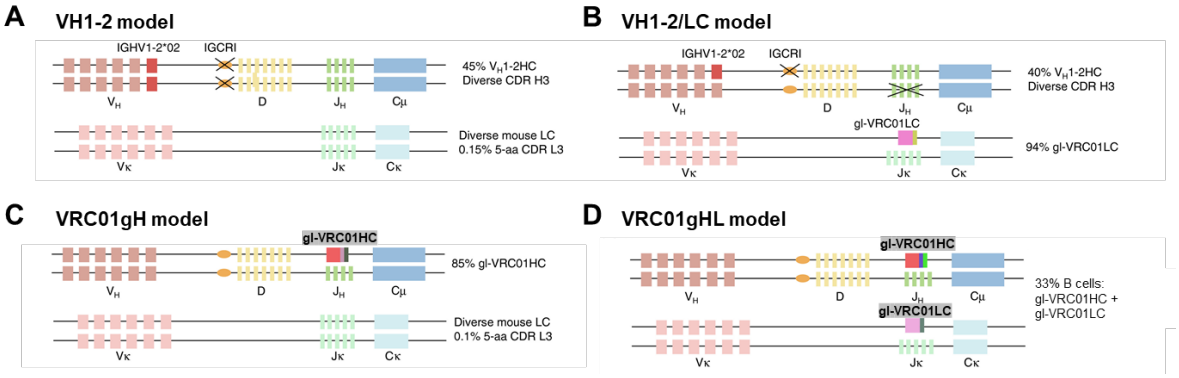


**Figure 1.9 Schematic illustration of human immunoglobulin (Ig) knock-in mouse models for VRC01-class germline targeting immunogen evaluation.** (A) VH1-2 model. In this model, VRC01 germline gene VH1-2*02substitutes for the mouse $V_H$81X segment. The regulatory element IGCRI was also deleted to upregulate the expression of the VH1-2*02 gene. (B) The VH1-2/LC model is generated based on the VH1-2 model with the rearranged gl-VRC01 KC integrated into the $J_K$ locus. Both the VH1-2 model and the VH1-2/LC model express HCs with diverse

CDRH3s. However, almost all B cells in the VH1-2/LC model encode VRC01 germline LC. In contrast, only 0.15% of B cells in the VH1-2 model express the signature 5-aa CDRL3. (C) VRC01gH model where the VDJ replaces JH locus recombined VRC01 germline HC sequence. The mouse LC remains unmodified. (D) VRC01gHL model has an additional rearranged gl-VRC01 HC knocked into the mouse $J_K$ locus of the VRC01gH model. Figures are adapted from (Verkoczy et al., 2017).

In this thesis, we evaluated our newly designed germline-targeting immunogens in a modified version of the VRC01gH model (VRC01gHL), where both VRC01 germline heavy and light chains were knocked into the murine IgH and IgK loci, respectively (**Figure 1.9D**). B cells encoding the germline-reverted VRC01 BCRs develop normally and are responsive to antigen stimulation (Abbott et al., 2018). Although VRC01gL chains and endogenous mouse LCs (lambda chain) are co-expressed, there are still approximately 33% naïve B cells expressing VRC01-class germline BCRs in the heterozygous VRC01gHL mice, which is much higher than the other models mentioned above. Moreover, after preliminary characterization, the frequency of VRC01gHL cells can be altered to more physiologically relevant levels by transferring the B cells to congenic mice (Abbott et al., 2018). In that way, it may introduce B cell lineage competition mimicking the polyclonal system. Thus, VRC01gHL is a more versatile in-vivo system for initial germline-targeting immunogen screening and immunogenicity characterization.

Admittedly, humanized mouse models are the compromise between practicality and physiological relevance. They express enriched germline-like bNAb precursors and may not represent physiological relevant conditions. However, these artificial in vivo systems at least directly reflect whether certain lineages are activated followed by affinity maturation. The trajectories and the pathways induced by the immunogens/immunization strategies can also be examined rapidly and iteratively.

# Chapter 2: Antigen-Specific Single B Cell Sorting and Monoclonal Antibody Cloning in Guinea Pigs

*Adapted from:* Lei, L., Tran, K., Wang, Y., Steinhardt, J. J., Xiao, Y., Chiang, C. I., ... & Li, Y. (2019). Antigen-Specific Single B Cell Sorting and Monoclonal Antibody Cloning in Guinea Pigs. Frontiers in microbiology, 10, 672.

***Synopsis***

In this chapter, we established an antigen-specific single B cell sorting and monoclonal antibody (mAb) cloning platform for analyzing immunization- or viral infection-elicited antibody response at the clonal level in guinea pigs. We stained the peripheral blood mononuclear cells (PBMCs) from a guinea pig immunized with HIV-1 envelope glycoprotein trimer mimic (BG505 SOSIP), using anti-guinea pig IgG and IgM fluorochrome conjugates, along with fluorochrome-conjugated BG505 SOSIP trimer as antigen (Ag) probe to sort for Ag-specific $IgG^{hi}$ $IgM^{lo}$ B cells at single-cell density. We then designed a set of guinea pig immunoglobulin (Ig) gene-specific primers to amplify cDNAs encoding B cell receptor variable regions (V(D)J segments) from the sorted Ag-specific B cells. B cell V(D)J sequences were verified by sequencing and annotated by IgBLAST, followed by cloning into Ig heavy- and light-chain expression vectors containing human IgG1 constant regions and co-transfection into 293F cells to reconstitute full-length antibodies in a guinea pig-human chimeric IgG1 format. Of 88 antigen-specific B cells isolated, we recovered 24 (27%) cells with native-paired heavy and light chains. Furthermore, 85% of the expressed recombinant mAbs bind positively to the antigen probe by enzyme-linked immunosorbent and/or BioLayer Interferometry assays, while 5 mAbs from 4 clonal lineages neutralize the HIV-1 tier 1 virus ZM109. In summary, by coupling Ag-specific single B cell sorting with gene-specific single cell RT-PCR, our method exhibits high efficiency and accuracy, which will facilitate future efforts in isolating mAbs and analyzing B cell responses to infections or immunizations in the guinea pig model.

## *2.1 Introduction*

The guinea pig is considered as the premier model in the study of infectious diseases (Padilla-Carlin et al., 2008). It shares many similarities to humans regarding symptoms and immune responses to infections and therapies (Padilla-Carlin et al., 2008; Tree et al., 2006). Additionally, unlike other small animal models such as the mouse model, the guinea pig model allows sampling significant blood volumes for downstream immunological analysis. Despite these advantages, the immune response of guinea pig model is still relatively understudied, which is largely due to the shortage of guinea pig-specific immune reagents and the lack of basic knowledge about Ig genes (Tree et al., 2006). To delineate the epitope specificity of B cell responses in guinea pigs, we established an antigen-specific single B cell sorting and mAb-cloning platform for the guinea pig model. By using newly designed guinea pig Ig gene-specific primers, we directly cloned and expressed antigen-specific mAbs from B cells isolated from guinea pigs immunized with HIV-1 envelope glycoprotein (Env) vaccine candidate BG505 SOSIP by fluorescence-activated cell sorting (FACS)-based single-cell sorting. This platform allows us to delineate antigen-specific antibody responses in guinea pigs at the clonal level for better understanding the immunogenicity of vaccine candidates and the effect of immunization strategies. Furthermore, this methodology is applicable for isolating/developing essential research reagents and therapeutic mAbs from guinea pigs in the future.

## *2.2 Materials and Methods*

### 2.2.1 Animal immunization and sampling

The guinea pig used in this study, designated as 1567, was immunized in a previous study (Feng et al., 2016). Briefly, along with another five guinea pigs in the same group,

animal 1567 was immunized 4 times at weeks 0, 4, 12, and 24 with HIV-1 Env trimer BG505 SOSIP formulated in ISOMATRIX adjuvant. Blood samples were harvested 2 weeks after each immunization with the terminal bleed on week 46 to prepare for PBMC and sera for downstream analysis (Feng et al., 2016) (**Figure 2.1A, 2.1B**). Four days prior to the termination, an inoculation of 40 μg of Env trimer BG505 SOSIP in the absence of adjuvant was administered by intraperitoneal injection (IP) route. The peripheral blood mononuclear cells (PBMCs) from whole blood were further purified by density gradient centrifugation with Ficoll-Paque PLUS (GE Healthcare). After washing by PBS, cells were resuspended and frozen gradually in Bambanker media (Wako Chemicals) at -80$^{o}$C followed by storage in liquid nitrogen prior to the staining and sorting experiment. The animal study was carried out at Covance with the protocol approved by the Covance Institutional Animal Care and Use Committee (IACUC, protocol #0138-14).

### 2.2.2 Isolation of single guinea pig B cells by fluorescence-activated cell sorting (FACS)

Guinea pig PBMCs were thawed and resuspended in 10 ml of pre-warmed RPMI 1640 medium (Gibco) supplemented with 10% FBS (Gibco) (R10) and 10 μl of DNase I (Roche). The cells were washed and re-suspended with 45 μl of pre-chilled phosphate-buffered saline (PBS). 5 μl of 40-fold water-diluted Live/dead fixable aqua dead stain (Invitrogen) was added to the cells followed by incubation in the dark at 4°C for 10 min. The cells were further stained by adding 50 μl of antibody cocktail in R10 medium containing anti-guinea pig IgM-FITC (100-fold dilution, Antibodies-online, ABIN457754), anti-guinea pig IgG-Alexa Fluor 594 (100-fold dilution, Jackson ImmunoResearch, 116790), and biotin-labeled HIV-1 Env trimer BG505 SOSIP conjugated with streptavidin-PE (Invitrogen) and streptavidin-APC (Invitrogen), respectively at 4 μg/ml as described

previously (Wu et al., 2010). The cell and antibody cocktail mixture was incubated in the dark at 4°C for 1 hour. After staining, the cells were washed and re-suspended in 0.5 ml of pre-chilled R10 medium and passed through a 70 µm cell strainer (BD Biosciences) prior to cell sorting. 3 ul of Dynalbeads™ Protein G (Invitrogen) stained with the same volume of anti-guinea pig IgM-FITC and anti-guinea pig IgG-Alexa Fluor 594, respectively, as well as 20 µl of biotin bead (Spherotech, TP-30-5) stained with 0.1 µl of streptavidin-PE and streptavidin-APC, respectively in a total volume of 100 µl at room temperature for 20 min, were used for compensation.

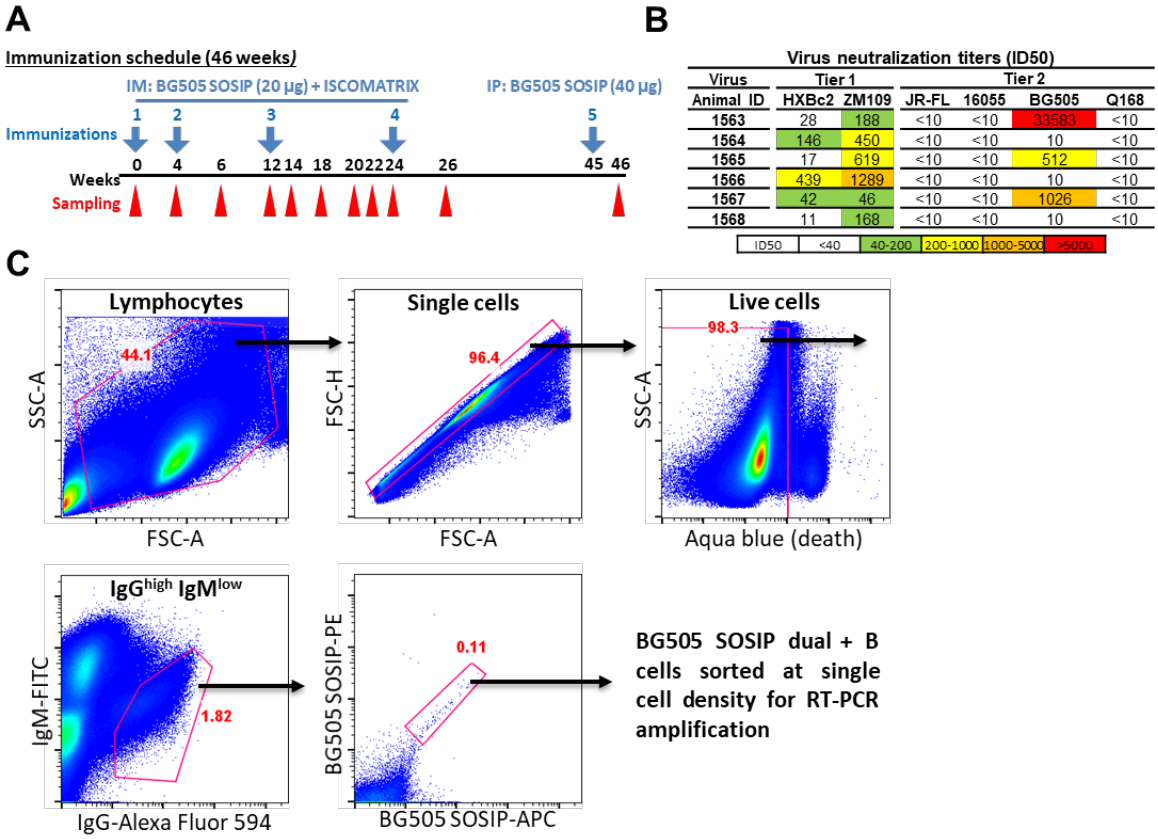


**Figure 2.1. Isolation of vaccine-induced antigen-specific guinea pig B cells.** (A) Guinea pigs (n=6) were immunized at week 0, 4, 12, and 24 with BG505 SOSIP formulated in ISCOMATRIX adjuvant via intramuscular (IM) route. Serum sampling was performed at weeks indicated in the scheme. On week 45, BG505 SOSIP was injected by intraperitoneal (IP) route followed by termination bleed on week 46 and collection of spleens for splenocytes. (B) Neutralization $ID_{50}$ titers (reciprocal serum dilution factor) of plasma collected at week 26 from guinea pigs against a panel of tier 1 and tier 2 viruses using the TZM-bl pseudovirus assay. The data are representative of at least two independent experiments. (C) Single B cell isolation was performed in an antigen-

selective manner by multicolor fluorescence-activated cell sorting (FACS). Peripheral blood mononuclear cells (PBMCs) from guinea pig 1567 on week 46 were stained by a cocktail of fluorochrome-conjugated antibodies and antigens for identifying $IgG^{hi}$ $IgM^{lo}$ B cell subpopulations with dual positive binding to BG505 SOSIP trimers to minimize non-specific antigen probe binding.

Antigen-specific single B cells were identified and sorted by a FACS Aria III cell sorter (BD Biosciences) at single-cell density into 96-well PCR plates containing 20 µl of lysis buffer as previously described (Sundling et al., 2012a). A representative example of the FACS gating strategy used for identifying HIV Ag BG505 SOSIP-dual positive single B cells is shown in **Figure 2.1C.** In brief, after the gating of lymphocytes (SSC-A vs. FSC-A) and singlets (FSC-H vs. FSC-A), live cells were identified by the negative aqua blue staining phenotype. Antigen-specific $IgG^{hi}$ B cells were then determined as $IgG^{hi}$ $IgM^{lo}$ and dual positive ($PE^{+}$ $APC^{+}$) for BG505 SOSIP probes. The percentage of gated cells in their parental cell population is shown in red **(Figure 2.1C)**.

### 2.2.3 Guinea pig Ig gene-specific single cell RT-PCR

We first performed reverse transcription (RT) to convert mRNA to cDNA with the sorted single B cells. We thawed the cells in lysis buffer followed by the addition of 450 ng random hexamers (Gene Link), 2 µl 10 mM dNTP (Sigma), 200 U Superscript III (Invitrogen) to a 26 µl final reaction volume. The RT program was set as the following: 10 min at 42°C, 10 min at 25°C, 60 min at 50°C, 5 min at 94°C, followed by held at 4ºC.

To amplify immunoglobulin (Ig) encoding genes from the cDNA, we designed primers for semi-nested PCR reactions based on the guinea pig Ig gene segments recently identified (Guo et al., 2012) **(Figure 2.2, Tables 2.2, 2.3, & 2.4)**. The 5' forward primers were designed to anneal to the 5' end of the framework 1 (FR1) regions in V-gene segments. The 3' reverse primers are situated in the constant region, with the 3' inner primers for the 2nd PCR closer to J genes than the 3' outer primers for the 1st PCR reactions **(Figure**

**2.2C)**. The 1st PCR reaction was performed in a 50 µl reaction mixture consisting of 5 µl of cDNA, 5 µl of 10X PCR Buffer (Qiagen), 1 µl of 25 mM $MgCl_2$ (Qiagen), 1 µl of 10 mM dNTPs (Sigma), 2 Unites of HotStar Taq Plus (Qiagen), 5 µl of 25 µM 5' primer mixtures, and 1 µl of 25 µM 3' outer primers. The 2nd PCR reaction mixture consisted of 2.5 µl of the same 5' forward primer mixtures (25 µM) as in the 1st PCR with 0.5 µl of 25 µM 3' inner primers as reverse primers (**Figure 2.2C**), and 5 µl 5X Q-solution without $MgCl_2$ in 25 µl of volume. All the 5' primers used for each heavy (VH), lambda (VL), and kappa (VK) chain amplification were stored at 25 µM and mixed in equal volume prior to the PCR reactions. All semi-nested PCRs were incubated at 94 °C for 5 min followed by 50 cycles of 94 °C for 30 s, 50 °C for 45 s, and 72 °C for 1 min with a final elongation at 72 °C for 10 min before cooling to 4 °C. The PCR products were evaluated on 2% 96-well E Gels (Life Technologies). Wells with expected sizes approximately 500 bp for heavy and kappa chains and 420 bp for lambda chain, respectively, were identified followed by PCR product purification and sequencing using downstream 3' inner primers. The PCR primers for heavy, lambda and kappa chains are described in **Tables 2.2, 2.3, and 2.4,** respectively.

### 2.2.4 Single B cell Ig gene sequence analysis

Sequences of the semi-nested PCR products were initially analyzed by IMGT / High V-Quest (Alamyar et al., 2012) to define Ig gene structure, particularly the framework and CDR boundaries, using human Ig sequences as reference. The V(D)J sequences identified were further annotated by the stand-alone software IgBLAST (Ye et al., 2013) using previously annotated guinea pig germline sequences (Guo et al., 2012) as reference, which were annotated from guinea pig genome database (http://www.ensembl.org).

Somatic hypermutation (SHM) level (Mut %) was calculated as the divergence of antibody VH/VL/VK sequences from the assigned germline sequences at the nucleotide level. Clonal lineages were defined by the usage of V and J segments, and complementarity-determining region (CDR3) homology (90% homology).

### 2.2.5 Cloning and expression of guinea pig monoclonal antibodies in a guinea pig-human chimeric form

After sequence annotation, the VH/VK/VL amplicons from single cell RT-PCR were inserted into human IgG1 expression vectors (Tiller et al., 2008) by seamless cloning as described next to form guinea pig-human chimeric mAbs. Amplicons were subjected to another round of PCR amplification (cloning PCR) using seamless cloning primers, which contain VH/VK/VL gene-specific regions and additional overhangs identical to the sequences in the expression vectors **(Figure 2.2C**). The products of cloning PCR reactions were purified and inserted into expression vectors by seamless cloning. Seamless cloning primers designed for VH, VK and VL amplification and cloning are summarized in **Figure 2.2C, Tables 2.5, 2.6 & 2.7**. The primers for each cloning PCR were selected based on germline V and J gene segment usage derived from the Ig gene sequence analysis. The cloning PCR reaction was performed in a total volume of 50 µl with high-fidelity DNA polymerase (Roche). The PCR reaction mixture consisted of 1 µl of template using the 2$^{nd}$ PCR product from the single cell RT-PCR reaction, 5 µl of 10X reaction buffer, 1 µl of 10 mM dNTPs, 1 µl of 25 µM of 5' and 3' cloning primers, 1 µl of high-fidelity DNA polymerase (3.5 Unit/µl, Roche) and nuclease-free water. The PCR program had an initial denaturation at 95°C for 3 min, followed by 20 cycles of 95°C for 30 s, 50°C for 30s, and 68°C for 2 min. There was a final elongation step at 68°C for 8 min. The products were

evaluated on 1% agarose gels before being assembled into their respective expression vectors containing human Igγ1H, Igκ1L, or Igλ2L constant regions described previously (Tiller et al., 2008). The assembly (insertion) reactions were performed with GeneArt assembly enzyme mix (Invitrogen) per manufacturer's instructions.

For antibody expression, an equal amount of heavy and light chain expression vectors containing the paired VH/VK/VL amplicons were transfected into 293F cells with 293fectin transfection reagent (Life Technologies) as previously described (Wang et al., 2016). For a typical transfection reaction, 12.5 μg of each of the VH/VK/VL expression vectors, prepared from 50 ml *E.coli* DH5α cultures, were used to transfect 50 million 293F cells in 50 ml volume. Supernatants were harvested 4 days post-transfection, followed by antibody purification with Protein A Sepharose columns (GE Healthcare). Thus, each guinea pig mAb was expressed as a chimeric mAb with the variable regions (VH/VK or VL) derived from guinea pig and the constant regions from human.

For antibody expression, equal amount of heavy and light chain expression vectors containing the paired VH/VK/VL amplicons were transfected into 293F cells with 293fectin transfection reagent (Life Technologies) as previously described (Wang et al., 2016). For a typical transfection reaction, 12.5 μg of each of the VH/VK/VL expression vectors, prepared from 50 ml *E.coli* DH5α cultures, were used to transfect 50 million 293F cells in 50 ml volume. Supernatants were harvested 4 days post-transfection, followed by antibody purification with Protein A Sepharose columns (GE Healthcare). Thus, each guinea pig mAb was expressed as a chimeric mAb with the variable regions (VH/VK or VL) derived from guinea pig and the constant regions from human.

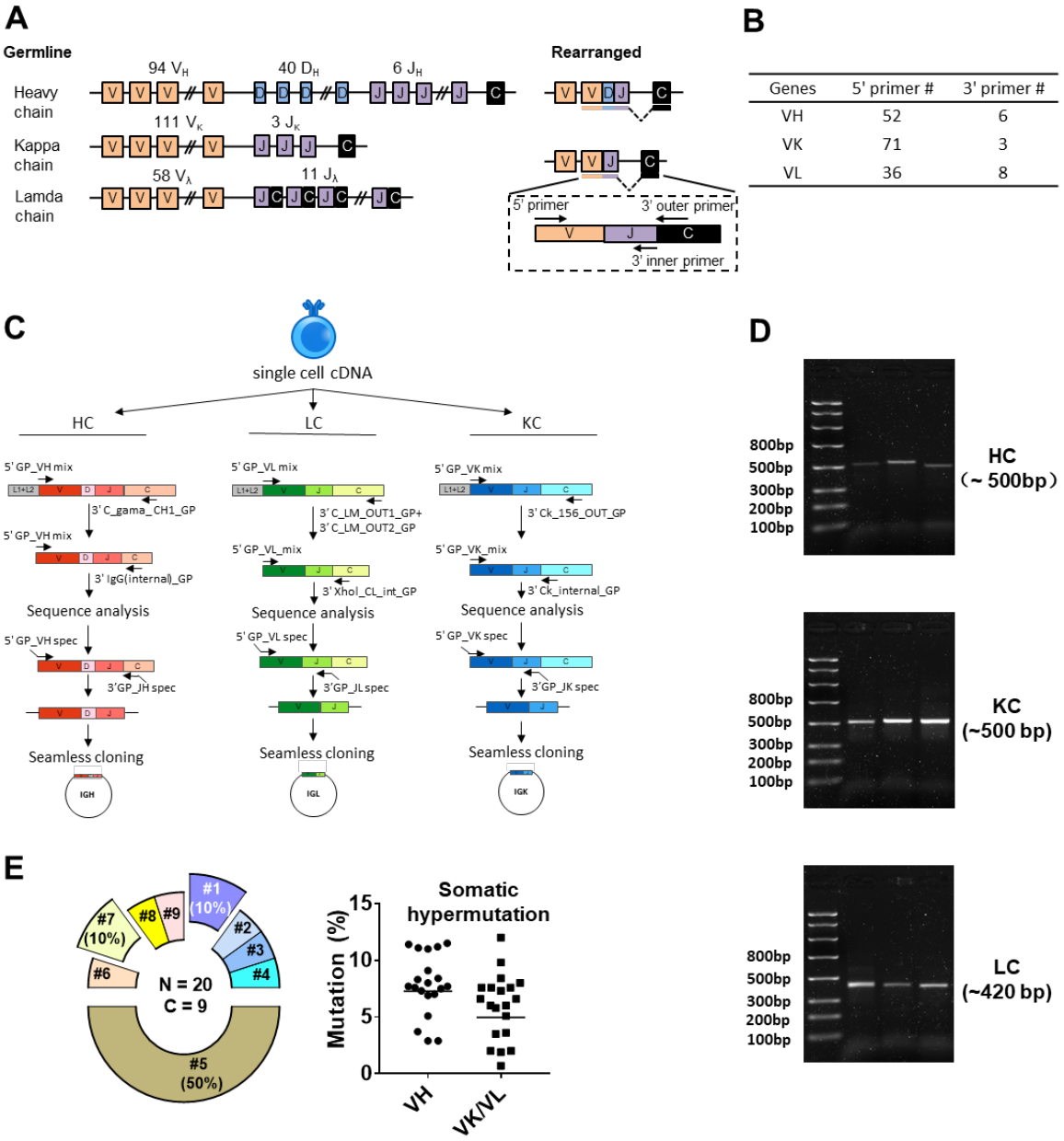


**Figure 2.2. Single cell RT-PCR to amplify antigen-specific guinea pig B cell IGH, IGL, and IGK transcripts.** (A) Guinea pig heavy and light chain gene organization and primer design. Antibody repertoire diversity is primarily determined by the somatic recombination of variable (V), diversity (D) and joining (J) gene segments, followed by the random non-templated nucleotides insertions in the V-D-J or V-J hotspots. Numbers of functional V, D, and J gene segments identified for heavy and light chains are indicated. (B) Numbers of primers designed for VH, VK and VL amplification. (C) Immunoglobulin gene amplification by semi-nested PCR from single cell cDNA resulted from random-hexamer primed reverse transcription. The 1st PCRs were performed with 5' forward primer mixtures and 3' reverse primers specific for the heavy- or light-chain constant regions. The 2nd PCRs were performed with the same set of 5' primers and 3' reverse primers specific for the constant regions more adjacent to the J gene segments. The 2nd PCR products were sequenced to determine the V and J primers for seamless cloning PCR. Cloning PCR products were assembled with antibody heavy and light chain expression vectors. (D). Representative 2% gel

electrophoresis patterns of the 2nd PCR products of heavy chain (HC, ~500 bp), kappa chain (KC, ~500 bp), and lambda chain (LC. ~450 bp). (E) Genetic analysis of the sorted Ag-specific B cells with paired heavy- and light-chains. (Left) Clonal lineage analysis of the sorted putative Ag-specific mAb variable sequences. N, total number of sorted cells; C, total number of clonal lineages, which is determined by the following criteria: B cell clones with the same Ig V, J gene usage and identical CDR3 length with CDR3 nucleotide sequence homology > 90% belong to the same clonal lineage and are likely derived from one naïve B cell precursor. Each slice of the pie chart represents one clonal lineage. Clonal lineages (#1, #5 & #7) with multiple members are displayed as exploded slices. (Right) Somatic hypermutation levels of the Ag-specific B cell Ig variable regions (VH and VK/VL) were calculated as percentage of nucleotide sequence divergence from germline V gene sequences.

### 2.2.6 MAb binding analysis by enzyme-linked immunosorbent assay (ELISA)

The binding specificity of the guinea pig mAbs recovered from single B cells was initially tested with the sorting probe, BG505 SOSIP trimer, and V3 peptides derived from BG505 V3 region (CTRPNNNTRKSIRIGPGQAFYATGDIIGDIRQAHC) and JR-FL (CTRPNNNTRKSIHIGPGRAFYTTGEIIGDIRQAHC) V3 region by ELISA assay. MaxiSorp 96-well plates (Nunc, Thermo Scientific) were coated with a mouse anti-His tag mAb (R&D Systems, MAB050) at 2 μg/ml in 100 μl of phosphate buffered saline (PBS) at 4°C overnight. After incubating with blocking buffer (PBS containing 5% FBS/2% non-fat milk) for 1 hr at 37°C, 2 μg/ml of BG505 SOSIP trimers were added into each well and incubated for 1 hr at room temperature. Subsequently, guinea pig mAbs were added in 5-fold serial dilutions starting at 50 μg/ml and incubated for 1 hr at room temperature. After wash, secondary HRP-conjugated anti-human IgG (Jackson ImmunoResearch) diluted at 1:10,000 in PBS/0.05% Tween 20 was added and incubated for 1 hr at room temperature. The signal was developed by adding 100 μl of TMB substrate (Life Technologies) and incubation for 5 min followed by the addition of 100 ul of 1 N sulfuric acid to stop the reactions. The optical density (OD) of each well was measured at 450 nm to quantify binding activity. Between each incubation step, the plates were washed extensively with

PBS supplemented with 0.05% Tween 20. The V3 peptides were coated at 2 μg/ml in 100 ul PBS at 4°C overnight, followed by the blocking, binding, washing, and detection procedures as stated above.

### 2.2.7 MAb binding analysis by BioLayer Interferometry (BLI) assay

The binding activity and kinetics of selected mAbs to BG505 SOSIP trimer were further assessed by BioLayer Interferometry (BLI) assay via an Octet RED96 system (ForteBio) following the manufacturer's instruction as previously described (Wang et al., 2016). Octet Analysis version 9.0 software was used for data anlaysis. The guinea pig mAbs bearing the human IgG constant regions were initially captured by anti-human IgG Fc biosensors, followed by immersing into: 1) analyte wells containing BG505 SOSIP trimer in 2-fold dilution series in binding buffer (PBS/0.05% Tween 20/0.1% BSA) starting from 1000 nM to 250 nM to assess association rate (on-rate, $k_{on}$), and subsequently 2) wells containing binding buffer to assess dissociation rate (off-rate, $k_{off}$). Binding affinity constants (dissociation constant, $K_D$) were determined as $k_{off}/k_{on}$.

### 2.2.8 HIV-1 neutralization assays

Antibody/serum neutralization assays were performed in a single round of infection using HIV-1 Env-pseudoviruses and TZM-bl target cells, as previously described (Li et al., 2005). Antibodies (starting at 50 μg/ml) and serum (starting at 10-fold dilution) were diluted in 5-fold series to assess neutralization activity. Neutralization curves were fitted by nonlinear regression using a five-parameter hill slope equation. The $IC_{50}$ (or $ID_{50}$) values of each antibody (or serum) were determined as the concentration (or dilution) of antibody (or serum) required to inhibit infection by 50%.

## *2.3 Results*

### 2.3.1 Guinea pig Ag-specific B cell sorting

To analyze B cell response in guinea pigs at the clonal level, we developed this antigen-specific single B cell sorting and mAb isolation method (**Figures 2.1 & 2.2**). To evaluate the feasibility of this method, we first sorted HIV-1 Env-specific single B cells by FACS from PBMCs of animal 1567, which displayed potent serum neutralization against the autologous tier 2 virus BG505 and tier 1 isolate ZM109 (**Figure 2.1A & B**). We selected animal 1567 for this study as its serum represents the overall virus neutralization profiles of this group, although this serum did not display the highest BG505 neutralization titer within the same group. Class-switched B cells with high level of surface IgG expression profile ($IgG^{hi}$) were distinguished by sequential gating for lymphocytes, single cells, live cells (Aqua $blue^{-}$), and cells with high/low signal for IgG and IgM, respectively ($IgG^{hi}$ $IgM^{lo}$) (**Figure 2.1C**). Statistically, from 10 million PBMCs, 4.4 million cells were identified as lymphocytes, and 4.3 million lymphocytes were gated as singlet cells (**Figure 2.1C**). Live cells, accounting for 98.3% of the singlet cells were identified with the negative Aqua Blue binding phenotype. 76,545 $IgG^{hi}$ $IgM^{lo}$ B cells were further determined among the live cells at the frequency of 1.82%, based on the fluorescent signals of anti-guinea pig IgM-FITC and anti-guinea pig IgG-Alexa Fluor 594 (**Figure 2.1C**). Subsequently, we identified 88 Env-specific B cells (0.11% of $IgG^{hi}$ $IgM^{lo}$ B cells) with the phenotype of $IgG^{hi}$ $IgM^{lo}$ /BG505 SOSIP $dual^{+}$ ($PE^{+}APC^{+}$) (**Figure 2.1C**), which were gated and sorted at single cell density into a 96-well PCR plate for downstream single cell IgG RT-PCR reactions (**Table 2.1**).

### 2.3.2 Guinea pig Ig heavy/light chain amplification

We performed RT-PCR to recover the variable region of heavy/light chain (VH/VK/VL) encoding genes of the sorted Ag-specific guinea pig B cells (**Figure 2.2**). The cDNA of each single cell was synthesized by reverse transcription primed by random hexamers. To efficiently amplify Ig genes from cDNA, we developed a semi-nested PCR strategy. All the primers were designed based on the recently annotated guinea pig Ig loci (Guo et al., 2012). From the guinea pig genome sequence annotation study (Guo et al., 2012), 94 VH, 40 DH, and 6 JH gene segments were identified as functional heavy chain genes (**Figure 2.2A**). In the Igκ locus, 111 potentially functional Vκ and 3 J κ genes were determined (**Figure 2.2A**). For Igλ, 58 Vλ and 11 Jλ genes were categorized as potentially functional (**Figure 2.2A**). By analyzing the functional gene segment sequences, we designed 5' forward primers spanning the first 21-25 nt of the framework 1 (FR1) regions in V-gene segments. In total, based on sequence homology, 52, 71, and 36 5' primers were synthesized for heavy, kappa and lambda chain amplification, respectively (**Figure 2.2B, Tables 2.2, 2.3 & 2.4**). Two sets of 3' reverse primers were sequentially used to anneal to the Ig constant regions during PCR reactions (**Figure 2.2C, Tables 2.2, 2.3 & 2.4**). After two rounds of PCR, products were checked on 96-well E Gels. 45/88 (51%) positive wells were observed for the heavy chain amplification, while 36/88 (41%) and 16/88 (18%) positive wells for the lambda and kappa chain amplifications, respectively. From the 88 cells sorted, we successfully recovered 24 paired heavy- and light-chain variable domain genes (**Table 2.1**). All of the amplicons from the second PCR reactions with the expected sizes (**Figure 2.2D**) were sequenced and annotated initially by V-Quest through IMGT with the human Ig germline database as reference to delineate CDR boundary.

Subsequently, we used IgBLAST to determine the closest functional V, D, and J segments using in-house guinea pig germline database derived from the work of Guo et al (Guo et al., 2012).

### 2.3.3 Guinea pig mAb cloning and expression

Based on the V and J segments assigned with IgBLAST, the corresponding cloning PCR primers for each mAb were chosen from the seamless cloning primer sets shown in **Tables 2.5, 2.6 & 2.7**. Cloning PCR products were further inserted into expression vectors by GeneArt seamless cloning and assembly kit, followed by sequencing verification. By co-transfection of heavy- and light-chain expression vectors into 293F cells, 20 out of 24 (83%) chimeric mAbs were efficiently expressed and purified from cell culture supernatants. Genetic analysis grouped them into 9 clonal lineages, with most lineages consisting single member while three lineages (#1, #5 & #7) containing multiple clonal members (**Figure 2.2E, Table 2.8**). Clonal dominance is notable: one clonal lineage #5 (**Figure 2.2E, Table 2.8**) consisting of 10 clonal members predominantly accounts for 50% of the total sorted B cells. Somatic hypermutation (SHM) levels (Mut %) of the sorted B cells were calculated as the percentage of nucleotide sequence divergence from the germline V gene sequences (**Table 2.8**). We found moderate level of SHM for the VH and VK/VL of the sorted B cells, ranging from 2.9-11.5%, and 0.7-12%, respectively (**Figure 2.2E**, **Table 2.8**), consistent with the SHM level of Env-specific mAbs elicited by immunization in rhesus monkeys reported previously (Wang et al., 2016).

### 2.3.4 Guinea pig mAb characterization

Since we sorted HIV-1 Env-specific B cells for Ig encoding gene analysis and mAb cloning, we further verified the mAb binding specificity by ELISA binding assays, with

BG505 SOSIP pre-coated on ELISA plates and mAbs serving as analytes. We found that 16/20 (80%) of the guinea pig mAbs recognized the antigen probe, BG505 SOSIP trimer by ELISA assay (**Figure 2.3A, Tables 2.1 & 2.8**). The predominant clonal lineage #5, consists 7 members that bind BG505 SOSIP well (**Figure 2.3A, Table 2.8**) and 3 members (CP61, 62 & 91) showing negligible BG505 SOSIP binding assayed by ELISA (**Figure 2.3A, Table 2.8**). This observation demonstrates the heterogeneity of affinity for antigen between clonal members within the same clonal lineage.

We subsequently used BioLayer Interferometry (BLI) assay to characterize the antigen-binding activity of selected guinea pig mAbs (**Figure 2.3B**). In this BLI assay, the mAbs bearing the human Fc portion was initially captured to the anti-human IgG Fc biosensors followed by the association reaction with BG505 SOSIP analytes, which assesses the binding reaction in an orientation different from that in the ELISA assay. Thus, the BLI assay result would complement the ELISA measurement, especially for epitopes sensitive to antigen pre-coating. We selected a few members (**Table 2.8**) from the clonal lineage #5 with different ELISA binding profiles, including CP3 (high binding), CP53 (weak binding), and CP61, 62 & 91 (no binding), as well as CP58 (no ELISA binding) in clonal lineage #7 for BLI assay. We found that consistent with the ELISA assay, CP3 and CP53 showed decent binding signals for BG505 SOSIP (**Figure 2.3B**), while no binding signal was observed for CP61, 62 & 91. Interestingly, CP53 showed affinity (dissociation constant $K_D$ approximately 2 nM) for BG505 SOIP equivalent to CP3 in this BLI assay, while its binding to BG505 SOSIP was weaker than CP3 in ELISA assay (**Figure 2.3A**). CP58 displayed moderate binding affinity for BG505 SOSIP ($K_D$ =26 nM) (**Figure 2.3B**) assessed by BLI, whereas it had no ELISA binding to BG505 SOSIP. Our results suggest

that the results of ELISA and BLI binding assays corroborate with each other, while the sensitivity of BLI assay is often higher than ELISA. Based on BLI assay, 85% (17 /20) of the guinea pig mAbs recognized the antigen probe, BG505 SOSIP trimer (**Figure 2.3C**, **Tables 2.1 & 2.8**). Therefore, BLI assay could be used as complementary method of ELISA to assess Ab-Antigen binding (**Figure 2.3C**).

**Table 2.1 Statistic properties of the BG505-specific B cell sorting and Ig cloning**

| Animal | Guinea Pig #1567 |
|---|---|
| Total PBMCs | 10,050,000 |
| Total Lymphocytes | 4,429,926 |
| Total Lymphocytes % | 44.1 |
| Total single cells | 4,272,286 |
| Total single cells % | 96.4 |
| Total live cells | 4,199,193 |
| Total live cells % | 98.3 |
| Total IgG+IgM- memory B cell | 76,545 |
| Total IgG+IgM- memory B cell % | 1.82 |
| Total IgG+IgM- BG505 SOSIP dual + memory B cell | 81 |
| Total IgG+IgM- BG505 SOSIP dual + memory B cell % | 0.11 |
| Sorted cells | 88 |
| Sorted cells with paired VH or VL | 35 |
| Expressed mAbs | 20 |
| BG505 SOSIP + mAbs | 16 |
| Sorting precision ((GP+mAbs/Expressed mAbs)*100) | 80% |

We then estimated the precision of our Ag-specific class-switched B cell sorting and Ig cloning method by consolidating the results of Ag-binding assays (ELISA and BLI) and genetic analysis. Since B cells derived from the same clonal lineage share similar Ag recognition determinants, we used clonal lineage information of the sorted mAbs to infer the Ag-binding specificity of mAbs with inappreciable Ag ELISA/BLI binding phenotypes. For example, CP61, 62, & 91 from clonal lineage #5 barely bound BG505 SOSIP (**Figures**

**2.3A & 2.3B**). However, their related mAb clones such as CP3 & CP92 from lineage #5 showed strong binding with BG505 SOSIP trimer by ELISA and/or BLI (**Figures 2.3A & 2.3B**). Thus, we inferred the Ag specificity of CP61, 62, & 91 to be the same with CP3 & CP92 (**Table 2.8**). Such mAbs showing negative antigen-binding phenotypes in ELISA/BLI assays possess low affinity for BG505 SOSIP (**Figure 2.3B**). However, in the FACS sorting procedure, streptavidin-PE or -APC conjugates were premixed with the biotin-labeled BG505 SOSIP trimers to form high-order sorting probe complex with elevated binding valence, which could presumably facilitate the binding and isolation of B cells with low affinity B cell receptors encoding the above stated mAbs. Thus, in addition to functional antigen-binding assays, clonal lineage analysis is informative for determining the antigen-binding specificity of low affinity mAbs. To the end, we concluded that all the 20 mAbs derived from the Ag-selection based sorting/cloning study were Ag-specific (**Tables 2.1 & 2.8**), with various affinities for the cognate Ag (**Figure 2.3B**), belonging to 9 clonal lineages (**Figure 2.2E, Table 2.8**). Thus, the sorting and cloning method is feasible for guinea pig Ag-specific B cell analysis, with virtually 100% precision (**Table 2.1**).

To map the binding epitopes of the mAbs, we tested their reactivity against V3 peptides derived from the Envs of BG505 and JR-FL, since the V3 region is one of the immunodominant epitopes of HIV Env shown by previous studies (Phad et al., 2015; Wang et al., 2017). We found that five mAbs including CP2, CP6, CP10, CP67, and CP94 bound the autologous BG505 V3 peptide well (**Figure 2.3D & E**), while three of them (CP2 & CP94 from clonal lineage #1, and CP10 from clonal lineage #3) bound V3 peptide derived from isolate JR-FL with high binding activity (**Figure 2.3E**), suggesting the prominent immunogenicity of the BG505 SOSIP V3 region in this study. The substantial frequency

of V3-reactive mAbs resulted from this immunization is consistent with the notion that V3 region is still a prominent immunogenic element of the current generation of HIV-1 Env trimer immunogen such as BG505 SOSIP.

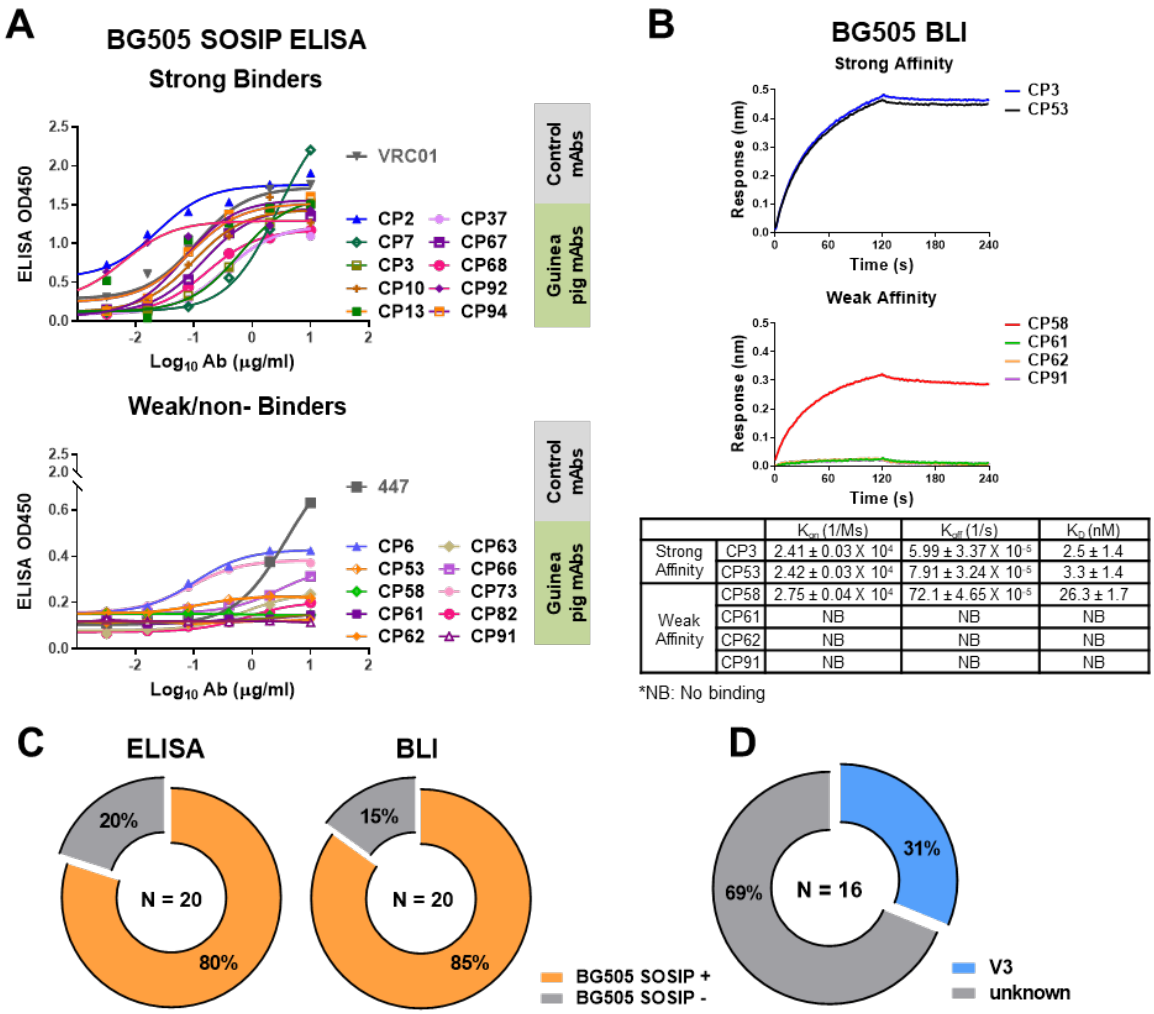


| | | $K_{on}$ (1/Ms) | $K_{off}$ (1/s) | $K_D$ (nM) |
|---|---|---|---|---|
| Strong Affinity | CP3 | 2.41 ± 0.03 X $10^4$ | 5.99 ± 3.37 X $10^{-5}$ | 2.5 ± 1.4 |
| | CP53 | 2.42 ± 0.03 X $10^4$ | 7.91 ± 3.24 X $10^{-5}$ | 3.3 ± 1.4 |
| Weak Affinity | CP58 | 2.75 ± 0.04 X $10^4$ | 72.1 ± 4.65 X $10^{-5}$ | 26.3 ± 1.7 |
| | CP61 | NB | NB | NB |
| | CP62 | NB | NB | NB |
| | CP91 | NB | NB | NB |

**Figure 2.3. Binding specificity and neutralization profile of guinea pig mAbs isolated from PBMCs.** (A) Reactivity of guinea pig mAbs to BG505 SOSIP trimer by ELISA assay. Strong binding (OD450 > 0.5); weak/no binding (weak-binding, 0.2<OD450 <0.5; no binding, OD450 <0.2). Data were duplicated, with the mean of OD450 shown. (B) Reactivity of selected guinea pig mAbs to BG505 SOSIP trimer by BLI assay. (Upper) BLI binding curves of mAbs from clonal lineages #5 & 7. mAbs were captured by anti-human IgG Fc biosensors, followed by interaction with BG505 SOSIP trimer in 2-fold dilution series starting from 1000 nM to 250 nM, with the curves of 1000 nM shown. (Lower) mAb-BG505 SOSIP trimer binding kinetic parameters, shown as measured value ± error. $k_{on}$, on-rate or association rate; $k_{off}$, off-rate or dissociation rate; $K_D$, binding affinity constants (dissociation constant) is determined as $k_{off}/k_{on}$. (C) Summary of BG505 SOSIP trimer reactivity by ELISA and BLI (right). Of 20 mAbs expressed, (left) 16 (80%), and (right) 17 (85%) show detectable binding activity to BG505 SOSIP trimers by ELISA and BLI assay, respectively. (D) Pie chart showing the binding specificity of the 16 BG505 SOSIP-reactive mAbs isolated from guinea pig 1567. V3-reacivity was assessed by positive reactivity (OD450 >0.2)

with peptides derived from V3 regions of HIV isolates BG505 or JR-FL by ELISA. (E) Neutralization potency ($IC_{50}$, μg/mL) of isolated mAbs against Env-pseudotyped viruses. mAbs are color-coded to differentiate corresponding clonal lineage. Animal 1567 plasma neutralization titers ($ID_{50}$) against HXBc2, ZM109, BG505 N332 (autologous virus corresponding to the immunogen, BG505 SOSIP, which contains N332 glycan), and JR-FL pseudoviruses were shown for comparison. $ID_{50}$ are values of the plasma reciprocal dilution factors at which 50% inhibition of infection are achieved in the assay. The background neutralization $ID_{50}$ titer threshold is set as <10. ND, not determined. ELISA binding to BG505 SOSIP trimer, BG505 gp120 monomer, BG505 V3 and JR-FL V3 peptide are also shown. Broadly neutralizing mAb, VRC01 (CD4bs epitope specific) is shown as control. Data are duplicated with the mean of $IC_{50}$ /$ID_{50}$ shown.

To characterize the function of the isolated mAbs further, we analyzed their neutralization capacity via the TZM-bl assay utilizing a panel of pseudotyped HIV-1 viruses. Five mAbs from four clonal lineages neutralized the tier 1 virus ZM109, which is consistent with the polyclonal plasma neutralization capacity against the same virus (**Figure 2.3E**). All the tier 1 virus neutralizing antibodies recognize the V3 region (**Figure 2.3E**). It is notable that none of the cloned mAbs from this study neutralizes the autologous virus BG505 N332 as the plasma does (**Figure 2.3E**). BG505 SOSIP trimer contains the conserved V3 glycan N332 (Sanders et al., 2013). Therefore, virus BG505 N332 is used as the virus for assessing mAb and plasma autologous neutralization activities.

### *2.4 Discussion*

Small animal models are typically utilized for initial preclinical evaluation of vaccine candidates in vivo. The guinea pig model, compared to the mouse model, is more immunologically similar to human and has an adequate amount of blood volume for initial immunological analysis (Padilla-Carlin et al., 2008). Some recent studies have used the guinea pig model to evaluate the immunogenicity of HIV Env-based immunogen candidates and immunization strategies (Feng et al., 2016; Nkolola et al., 2010; Zhou et al., 2017). However, the characterization of B cell response in these studies is still limited to the polyclonal level. Besides serum neutralization assay and epitope mapping, a high-

resolution strategy to delineate B cell response is desirable, as it will substantially aid vaccine evaluation and vaccine design.

There are two major technique hurdles obstructing single B cell analysis in guinea pigs: i) the lack of sophisticated B cell surface marker antibody panels for identifying guinea pig memory B cells, in contrast to mouse, macaque, and human (Sundling et al., 2012a; Tiller et al., 2008, 2009), and ii) the unavailability of primer sets for amplifying guinea pig Ig heavy- and light-chain encoding genes. In this study, we took advantage of the expression of B cell receptors (BCR) on the surface of $IgG^{hi}$ $IgM^{lo}$ B cells, which renders the corresponding B cells recognizable by antigens and anti-IgG secondary antibodies. Using FACS sorting technique with fluorochrome-conjugated antigen and anti-guinea pig IgG secondary antibody cocktails, we successfully isolated antigen-specific guinea pig class-switched $IgG^{hi}$ B cells for further analysis. The combination of antigen and anti-guinea pig IgG secondary antibody is sufficient to capture antigen-specific B cells, as demonstrated that >85% mAbs cloned from the sorted B cells are specifically reactive to the sorting antigen probe. In addition, we designed a set of guinea pig Ig gene-specific primers based on recently annotated guinea pig Ig gene cluster mapping (Guo et al., 2012), by using a pool of 5' forward primers derived from the framework 1 of guinea pig heavy- and light-chain variable domains, and 3' reverse primers annealing to the constant regions of guinea pig heavy/light chains. We recovered guinea pig Ig sequences by a semi-nested PCR strategy similar to the strategies proposed for mouse (Tiller et al., 2009), rabbit (Starkie et al., 2016), macaque (Sundling et al., 2012a), and human (Tiller et al., 2008). Approximately 50-60% heavy and light chain recovery efficiency was observed, while 27% of sorted cells have paired heavy and light chain amplicons for further functional analysis.

Of note, none of the mAbs isolated from this study displayed neutralization against the autologous tier 2 virus, BG505, suggesting that a more selective sorting strategy may be required to specifically isolate the antibodies recapitulating the autologous serum neutralization capacity against the BG505 virus with this cloning platform (Lei et al., 2019b). Sampling lymphoid tissues including spleen and lymph nodes where B cell germinal center activation primarily occurs (Victora and Nussenzweig, 2012) may lead to capturing the antigen-specific $IgG^{hi}$ B cells at a higher frequency. Consistent with this notion, in a related study (Lei et al., 2019b) using similar BG505 SOSIP sorting probes, we found that about 3% of class-switched $IgG^{hi}$ B cells are antigen-specific in splenocytes, which is 30-fold higher than that in PBMCs (**Figure 2.1C**). Nevertheless, we isolated five mAbs from four clonal lineages encoding tier 1 virus neutralizing antibodies targeting the V3 crown of the HIV-1 Env (**Figure 2.3E**, **Table 2.8**). The failure of these V3-specific mAbs to neutralize tier 2 viruses (**Figure 2.3E**) is consistent with the notion that the V3 crown is mostly occluded by other structural elements such as the V1V2 loops and glycans on the static (closed) HIV Env trimers of primary isolates (e.g. tier 2 viruses such as BG505) (Julien et al., 2013; Do Kwon et al., 2015; Lyumkis et al., 2013). However, these V3-specific mAbs are able to access the V3 crown on the tier 1 virus Env spikes, which sample more opened configurations than tier 2 viruses (Wang et al., 2017; Zolla-Pazner et al., 2016), to mediate tier 1 virus neutralization. In addition, we found that these V3-specific mAbs all use VH3-197/JH4 and mostly VL3-41 segments (**Table 2.8**). Moreover, we identified a predominant clonal lineage consisting of 10 clonal members (Lineage #5, **Table 2.8**) with the usage of VH3-183_D15_JH4 & VL4-82_JL1 gene segments (**Table 2.8**), which accounts for 50% of the well-expressed mAbs derived from the Ag-specific

$IgG^{hi}$ $IgM^{lo}$ B cells with paired heavy/light chains. The observed skewed Ig gene segment usage highlights the immunodominance of certain B cell lineages in the Env-specific B cell repertoire following BG505 SOSIP trimer immunization.

This method enables us sampling 27% Ag-specific B cells with paired heavy- and light-chain from 88 Ag-reactive single $IgG^{hi}$ $IgM^{lo}$ B cells (out of 10 million PBMCs) for functionality analysis, defining clonal lineage relationship between sorted B cells, and delineating epitope binding specificity of selected mAb clones (**Figure 2.3, Table 2.8**). Our result demonstrates the essential efficiency and feasibility of this platform for guinea pig single B cell analysis. The relatively low frequency of sorted cells with paired heavy and light chain amplicons may be caused by Ig gene polymorphisms (Corcoran et al., 2016). We anticipate that with the improvement in guinea pig Ig primer set design in the future, by primer optimization informed by individualized V gene sequencing (Corcoran et al., 2016), this platform can be more efficient and comparable to previous methods developed for mouse, macaque, and human (Tiller et al., 2009; Wu et al., 2010; Zhao et al., 2017). With the method developed herein, specific antibody lineages responsible for neutralization activity can be identified and characterized from vaccinated animals. In complement to previous elegant study focused on enriching plasmablast cells (PCs) containing abundant endoplasmic reticulum (ER) with fluorescent dye specific for the ER to recover Ig encoding genes (Kurosawa et al., 2012), our platform is applicable to analyze various class-switched B cell populations including memory B cells and a subset of PCs, which remain expression of cell surface-bound IgGs. In addition, the primers designed for guinea pig single cell RT-PCR can be applied for next-generation Ig sequencing library preparation to interrogate B cell clonal lineage evolution during immunization. All the

information gleaned from these analyses will contribute to a better understanding of immune response quality and detailed specificities to inform future vaccine design. Furthermore, this method enables the isolation of Ag-specific mAbs for developing therapeutic reagents in the guinea pig model. Thus, the platform described here will clearly benefit future B cell response analyses at both the clonal and repertoire levels, which helps to facilitate future efforts in immune response characterization as well as genetic and functional interpretation of the guinea pig model for applicable infectious diseases, including but not limited to HIV-1.

## Table 2.2 Ig heavy chain PCR primers.

IGH PCR primers

| PCR | Primer | Sequence (5' - 3') | V gene segment |
|---|---|---|---|
| Heavy Chain | 5'GP_VH#1 | GAGGAGCAACTGGTGGAGTCC | VH3-157, VH3-139 |
| Forward primers | 5'GP_VH#2 | CAGTTGCAGCTGCAGGAGTCA | VH1-14 |
| | 5'GP_VH#3 | CAGGTGCAGCTGCAGGAGTCG | VH1-120, VH1-115, VH1-58 |
| | 5'GP_VH#4 | CAGGTGCAGCTGCAGGAGTTG | VH1-56 |
| | 5'GP_VH#5 | GAAGTACAGCTCACACAATCT | VH3-184 |
| | 5'GP_VH#6 | GAGGTGCAGCTCGTGGAGTCT | VH3-170, VH3-167 |
| | 5'GP_VH#7 | CAGGTTCAGCTGCAGGAGTCG | VH1-66, VH1-75 |
| | 5'GP_VH#8 | CAGGTTCAGCTGCAGGAGTCA | VH1-1 |
| | 5'GP_VH#9 | GAGGAGCAGCTGGTAGAGTCC | VH3-63, VH3-3 |
| | 5'GP_VH#10 | GAGGTGCAGCTGGTGGAGTCT | VH3-35 |
| | 5'GP_VH#11 | GAGGTGCAGCTGATGGAGTCC | VH3-230 |
| | 5'GP_VH#12 | CAGGTGCAGCTACAGGAGTCG | VH1-95 |
| | 5'GP_VH#13 | GAAGAGCAGCTGGTGGAGTCT | VH3-80 |
| | 5'GP_VH#14 | GAGCCGCAGCTGGTGGAGTCA | VH3-194 |
| | 5'GP_VH#15 | GAAGTACAGCTCACACAGTCT | VH3-201 |
| | 5'GP_VH#16 | GAAGTGCAGCTCGTGGAGTCC | VH3-262 |
| | 5'GP_VH#17 | GAAGTGCAACTCGTGGAGTCC | VH3-126 |
| | 5'GP_VH#18 | GGTGCAGCTGGTGGAGTCCGG | VH3-98 |
| | 5'GP_VH#19 | GAGGTACAGCTCGTGGAATCT | VH3-282 |
| | 5'GP_VH#20 | GACGTACAGCTCGTGGAGTCT | VH3-265 |
| | 5'GP_VH#21 | GAGGAGCAACTGGTAGAGTCT | VH3-74 |
| | 5'GP_VH#22 | GAGCCGCAGCTGGTAGAATCC | VH3-204 |
| | 5'GP_VH#23 | GCGGAGCAGCTGGTGGAGTCC | VH3-189 |
| | 5'GP_VH#24 | GAGGTGCAGCTGGTAGAGTCT | VH3-42, VH3-23, VH3-2 |
| | 5'GP_VH#25 | GAGGTGCAGTTGGTAGAGTCT | VH3-9 |
| | 5'GP_VH#26 | GATGAGCAACTGGTAGAGTCC | VH3-20 |
| | 5'GP_VH#27 | GAGGTGCAGCTCATGGAGTCT | VH3-166 |
| | 5'GP_VH#28 | CAGGTGCAGCTACAGGAGTCA | VH1-68, VH1-59 |
| | 5'GP_VH#29 | GAGTTGCAGCTGGTGGAGTAC | VH3-222 |
| | 5'GP_VH#30 | GAGGAGCAGGTGGTGGAGCCC | VH3-36, VH3-8 |
| | 5'GP_VH#31 | GAGGTACAGCTCGTGGAGTCT | VH3-194 |
| | 5'GP_VH#32 | CAGGTGAAGCTGCAGGAGTCA | VH2-67 |
| | 5'GP_VH#33 | GAGCAGCAACTCGTGGAGTCC | VH3-255 |
| | 5'GP_VH#34 | CAGCTGCAGCTGAAGGAGTCA | VH1-4 |
| | 5'GP_VH#35 | CAAATGCAGCTGCAAGAGTCA | VH2-145 |
| | 5'GP_VH#36 | CAGGTGCAGCTGCAGGAGTCC | VH1-215, VH1-209, VH1-84 |
| | 5'GP_VH#37 | GAGGTGCTGCTGGTGGAGTCT | VH3-48 |
| | 5'GP_VH#38 | CAGGTGCAGAAGCAGGAGTCA | VH2-70 |
| | 5'GP_VH#39 | GAGGTGCAGCTGGTGGAGTCC | VH3-114 |
| | 5'GP_VH#40 | GAGGTACAGCTCGTGGAGGCT | VH3-211 |
| | 5'GP_VH#41 | CAAATGCAGCTGCAGGAGTCA | VH2-216 |
| | 5'GP_VH#42 | AAGGTACGGCTGGTGGAGTCC | VH3-190 |
| | 5'GP_VH#43 | CAGGTGCAGCTGCAAGAGTCG | VH1-140 |
| | 5'GP_VH#44 | CAGGTTCAGCTGCAAGAGTCA | VH1-151 |
| | 5'GP_VH#45 | CAGGTGCAGCTGCAGGAGTCA | VH2-239, VH1-171, VH1-156, VH1-101, VH1-77, VH2-160, VH2-94, VH2-86, VH2-54, VH2-43, VH2-35, VH2-28, VH2-27, VH2-17, VH2-7 |
| | 5'GP_VH#46 | CAGGGGCAGCTGCAGGAGTCA | VH2-121, VH2-109 |
| | 5'GP_VH#47 | GAGGAGCAGCTGGTGGAGTCC | VH3-229, VH3-186, VH3-185, VH3-183, VH3-51, VH3-24 |
| | 5'GP_VH#48 | CAGATGCAGCTGCAGGAGTCA | VH1-91 |
| | 5'GP_VH#49 | GAGGAGCAACTGGTAGAGTCC | VH3-150, VH3-102, VH3-89, VH3-46, VH3-37, VH3-30, VH3-176, VH3-135, VH3-80 |
| | 5'GP_VH#50 | GAGGCGCAGCTGGTGGAATCC | VH3-197 |
| | 5'GP_VH#51 | GAGGAGAAGCTGGTGGAGTCT | VH3-137 |
| | 5'GP_VH#52 | GAGGAGCAGCTGGTGGAGTCT | VH3-287, VH3-271, VH3-104 |
| Reverse primers | 3' C_gama_CH1_GP | GGTAGGTGTGCACTCCACTGGTC | Cγ (1st PCR) |
| | 3'IgG(Internal)_GP | GCTCAGGGAAGTAGCCCTTGAC | Cγ (2nd PCR) |

## Table 2.3 Ig lambda chain PCR primers.

IGL PCR primers

| PCR | Primer | Sequence (5' - 3') | V gene segment |
|---|---|---|---|
| Lambda Chain Forward primers | 5'GP_VL#1 | CAGCTTGTGCTGACTCAGTCACCCT | VL4-92 |
| | 5'GP_VL#2 | TCCTATGTGCTGACACAGCCGTCTT | VL3-39 |
| | 5'GP_VL#3 | TCCTATGTGCTCAAACAGCCACCTT | VL3-30 |
| | 5'GP_VL#4 | CAGCCGGTGCTCACTCAACCACCCT | VL3-134 |
| | 5'GP_VL#5 | CAGCCTGTGCTGACTCAGCTTCCCT | VL8-87 |
| | 5'GP_VL#6 | TCCTATGTACTGACACAGCCATCTT | VL3-27 |
| | 5'GP_VL#7 | CAGGAACTGGTGACTCAGGAACCCT | VL5-74 |
| | 5'GP_VL#8 | TCTTACACCCTCACTCAACCTCCCT | VL3-55, VL3-31, VL3-47, VL3-41, VL3-9 |
| | 5'GP_VL#9 | TCCTATGTATTCACACAGCCACCTT | VL3-6 |
| | 5'GP_VL#10 | CAGCCTGTGCTGAAACAGTCACCCT | VL4-138, VL4-84, VL4-82 |
| | 5'GP_VL#11 | CAGGTTGTGCTGACTCAGTCACCCT | VL4-80 |
| | 5'GP_VL#12 | CAGACTTCAGTCACCCAGGAGCCAT | VL7-129 |
| | 5'GP_VL#13 | CAGCCTGTGCTGACTCAGCTGCCCT | VL8-104, VL8-85 |
| | 5'GP_VL#14 | CAGGCAGTGCTGAGTCAGCCGCCCT | VL1-125 |
| | 5'GP_VL#15 | CAGGATCTGGTGACTCAGGAACCCT | VL5-79, VL5-78 |
| | 5'GP_VL#16 | CTGGCTGTGGTAACTCAGGAATCTT | VL6-102 |
| | 5'GP_VL#17 | TCGTATGTGCTGACGCAGCCATCTT | VL3-21 |
| | 5'GP_VL#18 | TCCTATGTGCTGACACAGCCATCTT | VL3-4 |
| | 5'GP_VL#19 | CAGTCTGGCCTAAGTCAGGAAGCTT | VL1-96 |
| | 5'GP_VL#20 | TCCTATGTACTCACACAGCCACCCT | VL3-53 |
| | 5'GP_VL#21 | AAGGCTGTGGTGACTCAGGAATCTT | VL6-115 |
| | 5'GP_VL#22 | TCCTATGTACTCACACAGTCACCTT | VL3-24 |
| | 5'GP_VL#23 | TCCTATGTGCTGACGCAGCCATCTT | VL3-50, VL3-34, VL3-32, VL3-16, VL3-48, VL3-45, VL3-42, VL3-13, VL3-10 |
| | 5'GP_VL#24 | TCCTATGTACTCACACAGCCACCTT | VL3-52, VL3-29 |
| | 5'GP_VL#25 | CAGGCTGTGGTGACTCAGGAACCTT | VL6-71 |
| | 5'GP_VL#26 | CAGCTTGTGCTGACTCAGTCACCTT | VL4-121 |
| | 5'GP_VL#27 | CAGAATGTAGCGACCCAGGTATCCT | VL5-106 |
| | 5'GP_VL#28 | CAGACTGTGGTGACCCAGGTATTCT | VL5-122 |
| | 5'GP_VL#29 | CAGGCAGTGCTGACTCAGCTGCCCT | VL1-95 |
| | 5'GP_VL#30 | CAGGCAGTGCTGACTCAGCCGCCCT | VL1-109 |
| | 5'GP_VL#31 | TCTTATATCTTGACACAGCCACCCT | VL3-19 |
| | 5'GP_VL#32 | TCTTACATCTTGACACAGCCTCCCT | VL3-43_VL3-35 |
| | 5'GP_VL#33 | CAGGCTGTGGTGACTCAGGAATCTT | VL6-132, VL6-98, VL6-69, VL6-68, VL6-116 |
| | 5'GP_VL#34 | CAGGATCTGGTAACTCAGGAACCTT | VL5-99 |
| | 5'GP_VL#35 | TCCTATGTGCTCACACAGCCACCTT | VL3-8 |
| | 5'GP_VL#36 | CAGCCTGTAGTGACTCAACCACCCT | VL5-139 |
| Reverse primers | 3'_C_LM_OUT1_GP | CACCACTGTGGCCTTGTTKTCCTGG | Cλ (1st PCR) |
| | 3'_C_LM_OUT2_GP | CACCACTGTGGCCTTGTTTTCGTTG | Cλ (1st PCR) |
| | 3' XhoI_CL_Int_GP | CTCCTCACTCGAGGGYGGGAAYAGGCTG | Cλ (2nd PCR) |

## Table 2.4 Ig kappa chain PCR primers.

IGK PCR primers

| PCR | Primer | Sequence (5' - 3') | V gene segment |
|---|---|---|---|
| Kappa Chain | 5'GP_VK#1 | GACATCCAGATGACCCAGTCTCCAT | Vk1-142 |
| Forward primers | 5'GP_VK#2 | GACATTGTTATGACCCAGTCTACAG | Vk4-36 |
| | 5'GP_VK#3 | GCATCCAGTTGACACAGCCTCCATC | Vk1-178 |
| | 5'GP_VK#4 | GTCATCCAGATGATGCAGTATTCAT | Vk3-108 |
| | 5'GP_VK#5 | GATATCCAGTTGACACAGCCTGCAT | Vk1-147, Vk1-58 |
| | 5'GP_VK#6 | GACATTTTGATGACCCAGTCTCCAG | Vk4-37 |
| | 5'GP_VK#7 | GAAATTCAGATGACACAAACTTCCT | Vk1-99 |
| | 5'GP_VK#8 | GAAGTTGTGCTGACCCAGACTCCAC | Vk2-124 |
| | 5'GP_VK#9 | GACATCCAGATGATCCAGTCACCAG | Vk1-133 |
| | 5'GP_VK#10 | GACATCCAGATTACTCAGACTCCAT | Vk1-174 |
| | 5'GP_VK#11 | GACATCCAGATGACTCAGACTCCAT | Vk1-280, Vk1-226, Vk1-55, Vk1-51, Vk1-47, Vk1-40, Vk1-15 |
| | 5'GP_VK#12 | GACATCCAGATGACTCAGACTCCGT | Vk1-272 |
| | 5'GP_VK#13 | GAAACCCTGCTGACTGAGACTCCAG | Vk3-25 |
| | 5'GP_VK#14 | GACATCCAGTTGACGCAGCCTCCAT | Vk1-201 |
| | 5'GP_VK#15 | GATGTTCTGATGACCCAGACCCCAC | Vk2-15 |
| | 5'GP_VK#16 | GATGTAGTGATGACCCAGACTCCAC | Vk2-16 |
| | 5'GP_VK#17 | GATACTCAGATGACTCAGTCTCCAT | Vk1-247 |
| | 5'GP_VK#18 | GAAACCCTTCTGACACAGACCCCAG | Vk3-155 |
| | 5'GP_VK#19 | GATGTTGTGGTGACCCAGACCCCAC | Vk2-51, Vk2-11 |
| | 5'GP_VK#20 | GATATCCAGATGACTCAGGCTCCTT | Vk1-230 |
| | 5'GP_VK#21 | GACATCCAGATGATTCAGACTCCAT | Vk1-21 |
| | 5'GP_VK#22 | GACATTGTGATGACTCAGTCTCCAG | Vk4-28 |
| | 5'GP_VK#23 | GACATCCAGTTAACACAGCCTCCAT | Vk1-211, Vk1-159 |
| | 5'GP_VK#24 | GACATCCAGTTGACCCAGTCTCCAT | Vk1-246 |
| | 5'GP_VK#25 | GACATTAGGATGACCCAGACCCCAC | Vk2-85 |
| | 5'GP_VK#26 | GATGTTGTATTGACCCAAACCCCAC | Vk2-14 |
| | 5'GP_VK#27 | GACATCCAGATGACCCAGTCACCAT | Vk1-190 |
| | 5'GP_VK#28 | GACATTGTGATGACCCAGTCTCCAG | Vk4-70, Vk4-95, Vk4-45, Vk4-41, Vk4-39, Vk4-32, Vk4-29, Vk4-90, Vk4-83, Vk4-81 |
| | 5'GP_VK#29 | GAAACCCTGTTGACCCAGACTCCAG | Vk3-170 |
| | 5'GP_VK#30 | GATATCCAGTTGACACAGCCTCCAT | Vk1-152 |
| | 5'GP_VK#31 | GACATTGTGATGACCCAGTCACCAG | Vk4-74 |
| | 5'GP_VK#32 | GAAATTGTGATGACCCAGTCTCCAG | Vk4-77 |
| | 5'GP_VK#33 | GACATCCCGATGACTCAGATTCCAT | Vk1-36 |
| | 5'GP_VK#34 | GACATTCAGATGACCCAGTCTCCAT | Vk1-140, Vk1-65, Vk1-254 |
| | 5'GP_VK#35 | GACATACAGATGACCCAGTGTCCAT | Vk1-234 |
| | 5'GP_VK#36 | GACAATGTGGTGATCCAGTCTCCAG | Vk4-69 |
| | 5'GP_VK#37 | GACATCCAGTTGACACAGCCTCCTT | Vk1-214 |
| | 5'GP_VK#38 | GACATCCAGATGACCCAGTCTCAAT | Vk1-144 |
| | 5'GP_VK#39 | GACACCCAGATGACCCAGTCTCCAT | Vk1-145 |
| | 5'GP_VK#40 | GACATCCAGATGACTCAGACTGCAT | Vk1-59 |
| | 5'GP_VK#41 | GACTTCCAGATGACCCAGTCACCAT | Vk1-219 |
| | 5'GP_VK#42 | GACATCCAGTTGACACAGCCTCCAT | Vk1-242, Vk1-239 |
| | 5'GP_VK#43 | GACATAGTGATGACCCAGACCCCAC | Vk2-10 |
| | 5'GP_VK#44 | GATGTTGTGATGACCCAGACCGCAC | Vk2-7 |
| | 5'GP_VK#45 | GACATCCGGATGACTCAGACTCCAT | Vk1-179 |
| | 5'GP_VK#46 | GAAAAATTACTGACTAAGACTCCAG | Vk3-263 |
| | 5'GP_VK#47 | GATATCCAGATGACTCAGGCTCCCT | Vk1-267 |
| | 5'GP_VK#48 | GACATCCAATTGACACAGCCTGCAT | Vk1-279, Vk1-266, Vk1-29, Vk1-18, Vk1-1 |
| | 5'GP_VK#49 | GAAACCCAGCTGACTCAGACTCCAG | Vk3-281, Vk3-60, Vk3-42 |
| | 5'GP_VK#50 | GATATTGTGATGACACAGACCCCAC | Vk2-20 |
| | 5'GP_VK#51 | GACATCCAGTTGACCCAGACTCCAG | Vk1-126 |
| | 5'GP_VK#52 | GACATCCTATTAACCCAGCCTCCCT | Vk1-101 |
| | 5'GP_VK#53 | CAAATTGTGCTCACCCAGACTCCAG | Vk5-57 |
| | 5'GP_VK#54 | GATGTTTTGATGACCCAGACCCCAC | Vk2-22 |
| | 5'GP_VK#55 | GAAATTGTGCTTACCCAGTCTCCAG | Vk5-105 |
| | 5'GP_VK#56 | GATATCCAGTTGACCCAGTCTTCCT | Vk1-117 |
| | 5'GP_VK#57 | GACATCAAATTGACTCAGCCAGCAT | Vk1-233 |
| | 5'GP_VK#58 | GTGTAGGAAAAAACATCACTATTAC | Vk1-245 |
| | 5'GP_VK#59 | GACATCCAGATGACTCAGACTCTCT | Vk1-153 |
| | 5'GP_VK#60 | GACATCCAGTTGACCCAGTCTCCCT | Vk1-131, Vk1-115, Vk1-65 |
| | 5'GP_VK#61 | GACCTTGTTATGACACAGTCTCCAG | Vk4-76 |
| | 5'GP_VK#62 | GACATTCAGATGAGCCAGTCTCCAT | Vk1-184 |
| | 5'GP_VK#63 | GACATCCAGTTGATGCAGCCTCCAT | Vk1-253 |
| | 5'GP_VK#64 | GATGTTGTGATGACCCAGACCCCAC | Vk2-3 |
| | 5'GP_VK#65 | GACATCCAACTGACACAACCTGCAT | Vk1-261, Vk1-203 |
| | 5'GP_VK#66 | GACATCCAGATGACTCAGTCTCCCT | Vk1-130, Vk1-128 |
| | 5'GP_VK#67 | GACATCCAAATGACTCAGGTTCCAT | Vk1-166 |
| | 5'GP_VK#68 | GATGTTTTGTTGTCCCAGACCCCAC | Vk2-2 |
| | 5'GP_VK#69 | GACATCCAGTTGACACAGCCTGCAT | Vk1-275, Vk1-271, Vk1-225, Vk1-54, Vk1-50, Vk1-46, Vk1-45, Vk1-39, Vk1-35, Vk1-24, Vk1-20, Vk1-14, Vk1-8 |
| | 5'GP_VK#70 | GACATCCAGCTGACACAGCTTGCAT | Vk1-11 |
| | 5'GP_VK#71 | GCGTTGCCCTGACACAGTCCCCAGC | Vk6-164 |
| Reverse primers | 3' Ck 156_OUT_GP | GTGTTGTCCTTGCTGTCCTGATC | Cκ (1st PCR) |
| | 3'Ck_internal_GP | GTTCAGAGCCATCCACCTTCCAC | Cκ (2nd PCR) |

## Table 2.5 Ig heavy chain cloning primers.

IGH cloning primers

| Cloning PCR | Primer | Sequence (5' - 3') | V gene segment |
|---|---|---|---|
| Heavy Chain | SL_5'GP_VH#1 | tttctagtagcaactgcaaccggtgtacattctGAGGAGCAACTGGTGGAGTCC | VH3-157, VH3-139 |
| Forward primers | SL_5'GP_VH#2 | tttctagtagcaactgcaaccggtgtacattctCAGTTGCAGCTGCAGGAGTCA | VH1-14 |
| | SL_5'GP_VH#3 | tttctagtagcaactgcaaccggtgtacattctCAGGTGCAGCTGCAGGAGTCG | VH1-120, VH1-115, VH1-58 |
| | SL_5'GP_VH#4 | tttctagtagcaactgcaaccggtgtacattctCAGGTGCAGCTGCAGGAGTTG | VH1-56 |
| | SL_5'GP_VH#5 | tttctagtagcaactgcaaccggtgtacattctGAAGTACAGCTCACACAATCT | VH3-184 |
| | SL_5'GP_VH#6 | tttctagtagcaactgcaaccggtgtacattctGAGGTGCAGCTCGTGGAGTCT | VH3-170, VH3-167 |
| | SL_5'GP_VH#7 | tttctagtagcaactgcaaccggtgtacattctCAGGTTCAGCTGCAGGAGTCG | VH1-66, VH1-75 |
| | SL_5'GP_VH#8 | tttctagtagcaactgcaaccggtgtacattctCAGGTTCAGCTGCAGGAGTCA | VH1-1 |
| | SL_5'GP_VH#9 | tttctagtagcaactgcaaccggtgtacattctGAGGAGCAGCTGGTAGAGTCC | VH3-63, VH3-3 |
| | SL_5'GP_VH#10 | tttctagtagcaactgcaaccggtgtacattctGAGGTGCAGCTGGTGGAGTCT | VH3-35 |
| | SL_5'GP_VH#11 | tttctagtagcaactgcaaccggtgtacattctGAGGTGCAGCTGATGGAGTCC | VH3-230 |
| | SL_5'GP_VH#12 | tttctagtagcaactgcaaccggtgtacattctCAGGTGCAGCTACAGGAGTCG | VH1-95 |
| | SL_5'GP_VH#13 | tttctagtagcaactgcaaccggtgtacattctGAAGAGCAGCTGGTGGAGTCT | VH3-80 |
| | SL_5'GP_VH#14 | tttctagtagcaactgcaaccggtgtacattctGAGCCGCAGCTGGTGGAGTCA | VH3-194 |
| | SL_5'GP_VH#15 | tttctagtagcaactgcaaccggtgtacattctGAAGTACAGCTCACACAGTCT | VH3-201 |
| | SL_5'GP_VH#16 | tttctagtagcaactgcaaccggtgtacattctGAAGTGCAGCTCGTGGAGTCC | VH3-262 |
| | SL_5'GP_VH#17 | tttctagtagcaactgcaaccggtgtacattctGAAGTGCAACTCGTGGAGTCC | VH3-126 |
| | SL_5'GP_VH#18 | tttctagtagcaactgcaaccggtgtacattctGGTGCAGCTGGTGGAGTCCGG | VH3-98 |
| | SL_5'GP_VH#19 | tttctagtagcaactgcaaccggtgtacattctGAGGTACAGCTCGTGGAATCT | VH3-282 |
| | SL_5'GP_VH#20 | tttctagtagcaactgcaaccggtgtacattctGACGTACAGCTCGTGGAGTCT | VH3-265 |
| | SL_5'GP_VH#21 | tttctagtagcaactgcaaccggtgtacattctGAGGAGCAACTGGTAGAGTCT | VH3-74 |
| | SL_5'GP_VH#22 | tttctagtagcaactgcaaccggtgtacattctGAGCCGCAGCTGGTAGAATCC | VH3-204 |
| | SL_5'GP_VH#23 | tttctagtagcaactgcaaccggtgtacattctGCGGAGCAGCTGGTGGAGTCC | VH3-189 |
| | SL_5'GP_VH#24 | tttctagtagcaactgcaaccggtgtacattctGAGGTGCAGCTGGTAGAGTCT | VH3-42, VH3-23, VH3-2 |
| | SL_5'GP_VH#25 | tttctagtagcaactgcaaccggtgtacattctGAGGTGCAGTTGGTAGAGTCT | VH3-9 |
| | SL_5'GP_VH#26 | tttctagtagcaactgcaaccggtgtacattctGATGAGCAACTGGTAGAGTCC | VH3-20 |
| | SL_5'GP_VH#27 | tttctagtagcaactgcaaccggtgtacattctGAGGTGCAGCTCATGGAGTCT | VH3-166 |
| | SL_5'GP_VH#28 | tttctagtagcaactgcaaccggtgtacattctCAGGTGCAGCTACAGGAGTCA | VH1-68, VH1-59 |
| | SL_5'GP_VH#29 | tttctagtagcaactgcaaccggtgtacattctGAGTTGCAGCTGGTGGAGTAC | VH3-222 |
| | SL_5'GP_VH#30 | tttctagtagcaactgcaaccggtgtacattctGAGGAGCAGGTGGTGGAGCCC | VH3-36, VH3-8 |
| | SL_5'GP_VH#31 | tttctagtagcaactgcaaccggtgtacattctGAGGTACAGCTCGTGGAGTCT | VH3-194 |
| | SL_5'GP_VH#32 | tttctagtagcaactgcaaccggtgtacattctCAGGTGAAGCTGCAGGAGTCA | VH2-67 |
| | SL_5'GP_VH#33 | tttctagtagcaactgcaaccggtgtacattctGAGCAGCAACTCGTGGAGTCC | VH3-255 |
| | SL_5'GP_VH#34 | tttctagtagcaactgcaaccggtgtacattctCAGCTGCAGCTGAAGGAGTCA | VH1-4 |
| | SL_5'GP_VH#35 | tttctagtagcaactgcaaccggtgtacattctCAAATGCAGCTGCAAGAGTCA | VH2-145 |
| | SL_5'GP_VH#36 | tttctagtagcaactgcaaccggtgtacattctCAGGTGCAGCTGCAGGAGTCC | VH1-215, VH1-209, VH1-84 |
| | SL_5'GP_VH#37 | tttctagtagcaactgcaaccggtgtacattctGAGGTGCTGCTGGTGGAGTCT | VH3-48 |
| | SL_5'GP_VH#38 | tttctagtagcaactgcaaccggtgtacattctCAGGTGCAGAAGCAGGAGTCA | VH2-70 |
| | SL_5'GP_VH#39 | tttctagtagcaactgcaaccggtgtacattctGAGGTGCAGCTGGTGGAGTCC | VH3-114 |
| | SL_5'GP_VH#40 | tttctagtagcaactgcaaccggtgtacattctGAGGTACAGCTCGTGGAGGCT | VH3-211 |
| | SL_5'GP_VH#41 | tttctagtagcaactgcaaccggtgtacattctCAAATGCAGCTGCAGGAGTCA | VH2-216 |
| | SL_5'GP_VH#42 | tttctagtagcaactgcaaccggtgtacattctAAGGTACGGCTGGTGGAGTCC | VH3-190 |
| | SL_5'GP_VH#43 | tttctagtagcaactgcaaccggtgtacattctCAGGTGCAGCTGCAAGAGTCG | VH1-140 |
| | SL_5'GP_VH#44 | tttctagtagcaactgcaaccggtgtacattctCAGGTTCAGCTGCAAGAGTCA | VH1-151 |
| | SL_5'GP_VH#45 | tttctagtagcaactgcaaccggtgtacattctCAGGTGCAGCTGCAGGAGTCA | VH2-239, VH1-171, VH1-156, VH1-101, VH1-77, VH2-160, VH2-94, VH2-86, VH2-54, VH2-43, VH2-35, VH2-28, VH2-27, VH2-17, VH2-7 |
| | SL_5'GP_VH#46 | tttctagtagcaactgcaaccggtgtacattctCAGGGGCAGCTGCAGGAGTCA | VH2-121, VH2-109 |
| | SL_5'GP_VH#47 | tttctagtagcaactgcaaccggtgtacattctGAGGAGCAGCTGGTGGAGTCC | VH3-229, VH3-186, VH3-185, VH3-183, VH3-51, VH3-24 |
| | SL_5'GP_VH#48 | tttctagtagcaactgcaaccggtgtacattctCAGATGCAGCTGCAGGAGTCA | VH1-91 |
| | SL_5'GP_VH#49 | tttctagtagcaactgcaaccggtgtacattctGAGGAGCAACTGGTAGAGTCC | VH3-150, VH3-102, VH3-89, VH3-46, VH3-37, VH3-30, VH3-176, VH3-135, VH3-80 |
| | SL_5'GP_VH#50 | tttctagtagcaactgcaaccggtgtacattctGAGGCGCAGCTGGTGGAATCC | VH3-197 |
| | SL_5'GP_VH#51 | tttctagtagcaactgcaaccggtgtacattctGAGGAGAAGCTGGTGGAGTCT | VH3-137 |
| | SL_5'GP_VH#52 | tttctagtagcaactgcaaccggtgtacattctGAGGAGCAGCTGGTGGAGTCT | VH3-287, VH3-271, VH3-104 |
| Reverse primers | 3' SalI JH 1_GP | agaccgatgggcccttggtcgacGCTGACGTGACGGTGACTGAG | JH 1 |
| | 3' SalI JH 2_4_6_GP | agaccgatgggcccttggtcgacGCTGAGGAGACGGTGACCAG | JH 2, JH 4, JH6 |
| | 3' SalI JH 3_GP | agaccgatgggcccttggtcgacGCTGAGGAGATAGTGACCAG | JH 3 |
| | 3' SalI JH 5_GP | agaccgatgggcccttggtcgacGCTGAGGAGACGGTGACCGA | JH 5 |

## Table 2.6 Ig lambda cloning primers.

IGL cloning primers

| Cloning PCR | Primer | Sequence (5' - 3') | V gene segment |
|---|---|---|---|
| Lambda Chain Forward primers | SL_5'GP_VL#1 | tttctagtagcaactgcaaccggttctctctcgCAGCTTGTGCTGACTCAGTCACCCT | VL4-92 |
| | SL_5'GP_VL#2 | tttctagtagcaactgcaaccggttctctctcgTCCTATGTGCTGACACAGCCGTCTT | VL3-39 |
| | SL_5'GP_VL#3 | tttctagtagcaactgcaaccggttctctctcgTCCTATGTGCTCAAACAGCCACCTT | VL3-30 |
| | SL_5'GP_VL#4 | tttctagtagcaactgcaaccggttctctctcgCAGCCGGTGCTCACTCAACCACCCT | VL3-134 |
| | SL_5'GP_VL#5 | tttctagtagcaactgcaaccggttctctctcgCAGCCTGTGCTGACTCAGCTTCCCT | VL8-87 |
| | SL_5'GP_VL#6 | tttctagtagcaactgcaaccggttctctctcgTCCTATGTACTGACACAGCCATCTT | VL3-27 |
| | SL_5'GP_VL#7 | tttctagtagcaactgcaaccggttctctctcgCAGGAACTGGTGACTCAGGAACCCT | VL5-74 |
| | SL_5'GP_VL#8 | tttctagtagcaactgcaaccggttctctctcgTCTTACACCCTCACTCAACCTCCCT | VL3-55, VL3-31, VL3-47, VL3-41, VL3-9 |
| | SL_5'GP_VL#9 | tttctagtagcaactgcaaccggttctctctcgTCCTATGTATTCACACAGCCACCTT | VL3-6 |
| | SL_5'GP_VL#10 | tttctagtagcaactgcaaccggttctctctcgCAGCCTGTGCTGAAACAGTCACCCT | VL4-138, VL4-84, VL4-82 |
| | SL_5'GP_VL#11 | tttctagtagcaactgcaaccggttctctctcgCAGGTTGTGCTGACTCAGTCACCCT | VL4-80 |
| | SL_5'GP_VL#12 | tttctagtagcaactgcaaccggttctctctcgCAGACTTCAGTCACCCAGGAGCCAT | VL7-129 |
| | SL_5'GP_VL#13 | tttctagtagcaactgcaaccggttctctctcgCAGCCTGTGCTGACTCAGCTGCCCT | VL8-104, VL8-85 |
| | SL_5'GP_VL#14 | tttctagtagcaactgcaaccggttctctctcgCAGGCAGTGCTGAGTCAGCCGCCCT | VL1-125 |
| | SL_5'GP_VL#15 | tttctagtagcaactgcaaccggttctctctcgCAGGATCTGGTGACTCAGGAACCCT | VL5-79, VL5-78 |
| | SL_5'GP_VL#16 | tttctagtagcaactgcaaccggttctctctcgCTGGCTGTGGTAACTCAGGAATCTT | VL6-102 |
| | SL_5'GP_VL#17 | tttctagtagcaactgcaaccggttctctctcgTCGTATGTGCTGACGCAGCCATCTT | VL3-21 |
| | SL_5'GP_VL#18 | tttctagtagcaactgcaaccggttctctctcgTCCTATGTGCTGACACAGCCATCTT | VL3-4 |
| | SL_5'GP_VL#19 | tttctagtagcaactgcaaccggttctctctcgCAGTCTGGCCTAAGTCAGGAAGCTT | VL1-96 |
| | SL_5'GP_VL#20 | tttctagtagcaactgcaaccggttctctctcgTCCTATGTACTCACACAGCCACCCT | VL3-53 |
| | SL_5'GP_VL#21 | tttctagtagcaactgcaaccggttctctctcgAAGGCTGTGGTGACTCAGGAATCTT | VL6-115 |
| | SL_5'GP_VL#22 | tttctagtagcaactgcaaccggttctctctcgTCCTATGTACTCACACAGTCACCTT | VL3-24 |
| | SL_5'GP_VL#23 | tttctagtagcaactgcaaccggttctctctcgTCCTATGTGCTGACGCAGCCATCTT | VL3-50, VL3-34, VL3-32, VL3-16, VL3-48, VL3-45, VL3-42, VL3-13, VL3-10 |
| | SL_5'GP_VL#24 | tttctagtagcaactgcaaccggttctctctcgTCCTATGTACTCACACAGCCACCTT | VL3-52, VL3-29 |
| | SL_5'GP_VL#25 | tttctagtagcaactgcaaccggttctctctcgCAGGCTGTGGTGACTCAGGAACCTT | VL6-71 |
| | SL_5'GP_VL#26 | tttctagtagcaactgcaaccggttctctctcgCAGCTTGTGCTGACTCAGTCACCTT | VL4-121 |
| | SL_5'GP_VL#27 | tttctagtagcaactgcaaccggttctctctcgCAGAATGTAGCGACCCAGGTATCCT | VL5-106 |
| | SL_5'GP_VL#28 | tttctagtagcaactgcaaccggttctctctcgCAGACTGTGGTGACCCAGGTATTCT | VL5-122 |
| | SL_5'GP_VL#29 | tttctagtagcaactgcaaccggttctctctcgCAGGCAGTGCTGACTCAGCTGCCCT | VL1-95 |
| | SL_5'GP_VL#30 | tttctagtagcaactgcaaccggttctctctcgCAGGCAGTGCTGACTCAGCCGCCCT | VL1-109 |
| | SL_5'GP_VL#31 | tttctagtagcaactgcaaccggttctctctcgTCTTATATCTTGACACAGCCACCCT | VL3-19 |
| | SL_5'GP_VL#32 | tttctagtagcaactgcaaccggttctctctcgTCTTACATCTTGACACAGCCTCCCT | VL3-43_VL3-35 |
| | SL_5'GP_VL#33 | tttctagtagcaactgcaaccggttctctctcgCAGGCTGTGGTGACTCAGGAATCTT | VL6-132, VL6-98, VL6-69, VL6-68, VL6-116 |
| | SL_5'GP_VL#34 | tttctagtagcaactgcaaccggttctctctcgCAGGATCTGGTAACTCAGGAACCTT | VL5-99 |
| | SL_5'GP_VL#35 | tttctagtagcaactgcaaccggttctctctcgTCCTATGTGCTCACACAGCCACCTT | VL3-8 |
| | SL_5'GP_VL#36 | tttctagtagcaactgcaaccggttctctctcgCAGCCTGTAGTGACTCAACCACCCT | VL5-139 |
| Reverse primers | 3_GP_XhoI_JL_1_4_7 | ggcttgaagctcctcactcgagggcgggaacagagtgaccaaggggaagccttgggctgaccgAGGACGGTCAGCTTGGTG | JL 1, JL 4, JL 7 |
| | 3_GP_XhoI_JL_2_5_9 | ggcttgaagctcctcactcgagggcgggaacagagtgaccaaggggaagccttgggctgaccgAGGACCGTCAGCCTGGTT | JL 2, JL 5, JL 6 |
| | 3_GP_XhoI_JL3_6_10 | ggcttgaagctcctcactcgagggcgggaacagagtgaccaaggggaagccttgggctgaccgAGGACGGTCAGCTTGGTT | JL 3, JL 6, JL 10 |
| | 3_GP_XhoI_JL8 | ggcttgaagctcctcactcgagggcgggaacagagtgaccaaggggaagccttgggctgaccgAGGACTGTCAGGTCGGTT | JL 8 |
| | 3_GP_XhoI_JL11 | ggcttgaagctcctcactcgagggcgggaacagagtgaccaaggggaagccttgggctgaccgAGGACGGTCACCTTGGTC | JL 11 |

## Table 2.7 Ig kappa cloning primers.

IGK cloning primers

| Cloning PCR | Primer | Sequence (5' - 3') | V gene segment |
|---|---|---|---|
| Kappa Chain | SL_5'GP_VK#1 | tttctagtagcaactgcaaccggtgtacattctGACATCCAGATGACCCAGTCTCCAT | Vk1-142 |
| Forward primers | SL_5'GP_VK#2 | tttctagtagcaactgcaaccggtgtacattctGACATTGTTATGACCCAGTCTACAG | Vk4-36 |
| | SL_5'GP_VK#3 | tttctagtagcaactgcaaccggtgtacattctGCATCCAGTTGACACAGCCTCCATC | Vk1-178 |
| | SL_5'GP_VK#4 | tttctagtagcaactgcaaccggtgtacattctGTCATCCAGATGATGCAGTATTCAT | Vk3-108 |
| | SL_5'GP_VK#5 | tttctagtagcaactgcaaccggtgtacattctGATATCCAGTTGACACAGCCTGCAT | Vk1-147, Vk1-58 |
| | SL_5'GP_VK#6 | tttctagtagcaactgcaaccggtgtacattctGACATTTTGATGACCCAGTCTCCAG | Vk4-37 |
| | SL_5'GP_VK#7 | tttctagtagcaactgcaaccggtgtacattctGAAATTCAGATGACACAAACTTCCT | Vk1-99 |
| | SL_5'GP_VK#8 | tttctagtagcaactgcaaccggtgtacattctGAAGTTGTGCTGACCCAGACTCCAC | Vk2-124 |
| | SL_5'GP_VK#9 | tttctagtagcaactgcaaccggtgtacattctGACATCCAGATGATCCAGTCACCAG | Vk1-133 |
| | SL_5'GP_VK#10 | tttctagtagcaactgcaaccggtgtacattctGACATCCAGATTACTCAGACTCCAT | Vk1-174 |
| | SL_5'GP_VK#11 | tttctagtagcaactgcaaccggtgtacattctGACATCCAGATGACTCAGACTCCAT | Vk1-280, Vk1-226, Vk1-55, Vk1-51, Vk1-47, Vk1-40, Vk1-15 |
| | SL_5'GP_VK#12 | tttctagtagcaactgcaaccggtgtacattctGACATCCAGATGACTCAGACTCCGT | Vk1-272 |
| | SL_5'GP_VK#13 | tttctagtagcaactgcaaccggtgtacattctGAAACCCTGCTGACTGAGACTCCAG | Vk3-25 |
| | SL_5'GP_VK#14 | tttctagtagcaactgcaaccggtgtacattctGACATCCAGTTGACGCAGCCTCCAT | Vk1-201 |
| | SL_5'GP_VK#15 | tttctagtagcaactgcaaccggtgtacattctGATGTTCTGATGACCCAGACCCCAC | Vk2-15 |
| | SL_5'GP_VK#16 | tttctagtagcaactgcaaccggtgtacattctGATGTAGTGATGACCCAGACTCCAC | Vk2-16 |
| | SL_5'GP_VK#17 | tttctagtagcaactgcaaccggtgtacattctGATACTCAGATGACTCAGTCTCCAT | Vk1-247 |
| | SL_5'GP_VK#18 | tttctagtagcaactgcaaccggtgtacattctGAAACCCTTCTGACACAGACCCCAG | Vk3-155 |
| | SL_5'GP_VK#19 | tttctagtagcaactgcaaccggtgtacattctGATGTTGTGGTGACCCAGACCCCAC | Vk2-51, Vk2-11 |
| | SL_5'GP_VK#20 | tttctagtagcaactgcaaccggtgtacattctGATATCCAGATGACTCAGGCTCCTT | Vk1-230 |
| | SL_5'GP_VK#21 | tttctagtagcaactgcaaccggtgtacattctGACATCCAGATGATTCAGACTCCAT | Vk1-21 |
| | SL_5'GP_VK#22 | tttctagtagcaactgcaaccggtgtacattctGACATTGTGATGACTCAGTCTCCAG | Vk4-28 |
| | SL_5'GP_VK#23 | tttctagtagcaactgcaaccggtgtacattctGACATCCAGTTAACACAGCCTCCAT | Vk1-211, Vk1-159 |
| | SL_5'GP_VK#24 | tttctagtagcaactgcaaccggtgtacattctGACATCCAGTTGACCCAGTCTCCAT | Vk1-246 |
| | SL_5'GP_VK#25 | tttctagtagcaactgcaaccggtgtacattctGACATTAGGATGACCCAGACCCCAC | Vk2-85 |
| | SL_5'GP_VK#26 | tttctagtagcaactgcaaccggtgtacattctGATGTTGTATTGACCCAAACCCCAC | Vk2-14 |
| | SL_5'GP_VK#27 | tttctagtagcaactgcaaccggtgtacattctGACATCCAGATGACCCAGTCACCAT | Vk1-190 |
| | SL_5'GP_VK#28 | tttctagtagcaactgcaaccggtgtacattctGACATTGTGATGACCCAGTCTCCAG | Vk4-70, Vk4-95, Vk4-45, Vk4-41, Vk4-39, Vk4-32, Vk4-29, Vk4-90, Vk4-83, Vk4-81 |
| | SL_5'GP_VK#29 | tttctagtagcaactgcaaccggtgtacattctGAAACCCTGTTGACCCAGACTCCAG | Vk3-170 |
| | SL_5'GP_VK#30 | tttctagtagcaactgcaaccggtgtacattctGATATCCAGTTGACACAGCCTCCAT | Vk1-152 |
| | SL_5'GP_VK#31 | tttctagtagcaactgcaaccggtgtacattctGACATTGTGATGACCCAGTCACCAG | Vk4-74 |
| | SL_5'GP_VK#32 | tttctagtagcaactgcaaccggtgtacattctGAAATTGTGATGACCCAGTCTCCAG | Vk4-77 |
| | SL_5'GP_VK#33 | tttctagtagcaactgcaaccggtgtacattctGACATCCCGATGACTCAGATTCCAT | Vk1-36 |
| | SL_5'GP_VK#34 | tttctagtagcaactgcaaccggtgtacattctGACATTCAGATGACCCAGTCTCCAT | Vk1-140, Vk1-65, Vk1-254 |
| | SL_5'GP_VK#35 | tttctagtagcaactgcaaccggtgtacattctGACATACAGATGACCCAGTGTCCAT | Vk1-234 |
| | SL_5'GP_VK#36 | tttctagtagcaactgcaaccggtgtacattctGACAATGTGGTGATCCAGTCTCCAG | Vk4-69 |
| | SL_5'GP_VK#37 | tttctagtagcaactgcaaccggtgtacattctGACATCCAGTTGACACAGCCTCCTT | Vk1-214 |
| | SL_5'GP_VK#38 | tttctagtagcaactgcaaccggtgtacattctGACATCCAGATGACCCAGTCTCAAT | Vk1-144 |
| | SL_5'GP_VK#39 | tttctagtagcaactgcaaccggtgtacattctGACACCCAGATGACCCAGTCTCCAT | Vk1-145 |
| | SL_5'GP_VK#40 | tttctagtagcaactgcaaccggtgtacattctGACATCCAGATGACTCAGACTGCAT | Vk1-59 |
| | SL_5'GP_VK#41 | tttctagtagcaactgcaaccggtgtacattctGACTTCCAGATGACCCAGTCACCAT | Vk1-219 |
| | SL_5'GP_VK#42 | tttctagtagcaactgcaaccggtgtacattctGACATCCAGTTGACACAGCCTCCAT | Vk1-242, Vk1-239 |
| | SL_5'GP_VK#43 | tttctagtagcaactgcaaccggtgtacattctGACATAGTGATGACCCAGACCCCAC | Vk2-10 |
| | SL_5'GP_VK#44 | tttctagtagcaactgcaaccggtgtacattctGATGTTGTGATGACCCAGACCGCAC | Vk2-7 |
| | SL_5'GP_VK#45 | tttctagtagcaactgcaaccggtgtacattctGACATCCGGATGACTCAGACTCCAT | Vk1-179 |
| | SL_5'GP_VK#46 | tttctagtagcaactgcaaccggtgtacattctGAAAAATTACTGACTAAGACTCCAG | Vk3-263 |
| | SL_5'GP_VK#47 | tttctagtagcaactgcaaccggtgtacattctGATATCCAGATGACTCAGGCTCCCT | Vk1-267 |
| | SL_5'GP_VK#48 | tttctagtagcaactgcaaccggtgtacattctGACATCCAATTGACACAGCCTGCAT | Vk1-279, Vk1-266, Vk1-29, Vk1-18, Vk1-1 |
| | SL_5'GP_VK#49 | tttctagtagcaactgcaaccggtgtacattctGAAACCCAGCTGACTCAGACTCCAG | Vk3-281_Vk3-60_Vk3-42 |
| | SL_5'GP_VK#50 | tttctagtagcaactgcaaccggtgtacattctGATATTGTGATGACACAGACCCCAC | Vk2-20 |
| | SL_5'GP_VK#51 | tttctagtagcaactgcaaccggtgtacattctGACATCCAGTTGACCCAGACTCCAG | Vk1-126 |
| | SL_5'GP_VK#52 | tttctagtagcaactgcaaccggtgtacattctGACATCCTATTAACCCAGCCTCCCT | Vk1-101 |
| | SL_5'GP_VK#53 | tttctagtagcaactgcaaccggtgtacattctCAAATTGTGCTCACCCAGACTCCAG | Vk5-57 |
| | SL_5'GP_VK#54 | tttctagtagcaactgcaaccggtgtacattctGATGTTTTGATGACCCAGACCCCAC | Vk2-22 |
| | SL_5'GP_VK#55 | tttctagtagcaactgcaaccggtgtacattctGAAATTGTGCTTACCCAGTCTCCAG | Vk5-105 |
| | SL_5'GP_VK#56 | tttctagtagcaactgcaaccggtgtacattctGATATCCAGTTGACCCAGTCTTCCT | Vk1-117 |
| | SL_5'GP_VK#57 | tttctagtagcaactgcaaccggtgtacattctGACATCAAATTGACTCAGCCAGCAT | Vk1-233 |
| | SL_5'GP_VK#58 | tttctagtagcaactgcaaccggtgtacattctGTGTAGGAAAAAACATCACTATTAC | Vk1-245 |
| | SL_5'GP_VK#59 | tttctagtagcaactgcaaccggtgtacattctGACATCCAGATGACTCAGACTCTCT | Vk1-153 |
| | SL_5'GP_VK#60 | tttctagtagcaactgcaaccggtgtacattctGACATCCAGTTGACCCAGTCTCCCT | Vk1-131, Vk1-115, Vk1-65 |
| | SL_5'GP_VK#61 | tttctagtagcaactgcaaccggtgtacattctGACCTTGTTATGACACAGTCTCCAG | Vk4-76 |
| | SL_5'GP_VK#62 | tttctagtagcaactgcaaccggtgtacattctGACATTCAGATGAGCCAGTCTCCAT | Vk1-184 |
| | SL_5'GP_VK#63 | tttctagtagcaactgcaaccggtgtacattctGACATCCAGTTGATGCAGCCTCCAT | Vk1-253 |
| | SL_5'GP_VK#64 | tttctagtagcaactgcaaccggtgtacattctGATGTTGTGATGACCCAGACCCCAC | Vk2-3 |
| | SL_5'GP_VK#65 | tttctagtagcaactgcaaccggtgtacattctGACATCCAACTGACACAACCTGCAT | Vk1-261, Vk1-203 |
| | SL_5'GP_VK#66 | tttctagtagcaactgcaaccggtgtacattctGACATCCAGATGACTCAGTCTCCCT | Vk1-130, Vk1-128 |
| | SL_5'GP_VK#67 | tttctagtagcaactgcaaccggtgtacattctGACATCCAAATGACTCAGGTTCCAT | Vk1-166 |
| | SL_5'GP_VK#68 | tttctagtagcaactgcaaccggtgtacattctGATGTTTTGTTGTCCCAGACCCCAC | Vk2-2 |
| | SL_5'GP_VK#69 | tttctagtagcaactgcaaccggtgtacattctGACATCCAGTTGACACAGCCTGCAT | Vk1-275, Vk1-271, Vk1-225, Vk1-54, Vk1-50, Vk1-46, Vk1-45, Vk1-39, Vk1-35, Vk1-24, Vk1-20, Vk1-14, Vk1-8 |
| | SL_5'GP_VK#70 | tttctagtagcaactgcaaccggtgtacattctGACATCCAGCTGACACAGCTTGCAT | Vk1-11 |
| | SL_5'GP_VK#71 | tttctagtagcaactgcaaccggtgtacattctGCGTTGCCCTGACACAGTCCCCAGC | Vk6-164 |
| Reverse primers | 3' BsiWI Jk 1 2 3 GP | cagatggtgcagccaccgtacgTTTGATTTCCAGCTTGGTC | JK 1, JK 2, JK 3 |

**Table 2.8 Genetic and binding specificity analysis of guinea pig mAb variable region sequences.**

| | mAb | Lineage # | VDJ segments_CDRH3 length (AA) | VH Mut (%) | CDRH3 AA seq | VJ segments_CDRL3 length (AA) | VL Mut (%) | CDRL3 AA seq | Binding specificity (ELISA/BLI) |
|---|---|---|---|---|---|---|---|---|---|
| nAbs | CP2 | 1 | VH3-197_D6_JH4_CDR3_17 | 7.5 | TRNLLLSGVESTGAFDV | VL3-41_JL_3_CDR3_13 | 2.0 | AITLGSGSIFQSV | Env (V3) |
| | CP94 | 1 | VH3-197_D6_JH4_CDR3_17 | 8.4 | TRNLLLSGVESTGAFDV | VL3-41_JL_3_CDR3_13 | 2.0 | AITLGSGSIFQSV | Env (V3) |
| | CP6 | 2 | VH3-197_D18_JH4_CDR3_12 | 11.0 | AKNKGETASFDV | VL3-41_JL_1_CDR3_13 | 6.0 | SIARVSGNNIQWV | Env (V3) |
| | CP10 | 3 | VH3-197_D3_JH4_CDR3_15 | 9.1 | AKNGDTSNGETTPDV | VL3-41_JL_1_CDR3_13 | 6.0 | TVAHVSGNAFQWV | Env (V3) |
| | CP67 | 4 | VH3-197_D17_JH4_CDR3_17 | 7.3 | AKNLLLSEATSTGAFDV | VL4-82_JL_1_CDR3_9 | 12.0 | AVGHSAGWV | Env (V3) |
| Non- nAbs | CP3 | 5 | VH3-183_D15_JH4_CDR3_18 | 8.0 | TRGPYYRWGTWSLYYFDI | VL4-82_JL_1_CDR3_9 | 6.6 | AVGYNTGWV | Env, unknown |
| | CP7 | 5 | VH3-183_D15_JH4_CDR3_18 | 11.2 | ARAPYYKWGTWSLYYFDI | VL4-82_JL_1_CDR3_9 | 8.4 | AVGHSAGWV | Env, unknown |
| | CP13 | 5 | VH3-183_D15_JH4_CDR3_18 | 6.9 | ARGAYYRWGTWSLYYFDV | VL4-82_JL_1_CDR3_9 | 5.1 | AVGYSAGWV | Env, unknown |
| | CP37 | 5 | VH3-183_D15_JH4_CDR3_18 | 7.7 | ARGAYYKWGTWTLYYFDL | VL4-82_JL_1_CDR3_9 | 7.6 | AVGHSAGWV | Env (unknown) |
| | CP53 | 5 | VH3-183_D15_JH4_CDR3_18 | 11.4 | ARAPYYKWGTWSLYYFDI | VL4-82_JL_1_CDR3_9 | 7.6 | AVGHSAGWV | Env (unknown) |
| | CP61 | 5 | VH3-183_D15_JH4_CDR3_18 | 7.7 | ARGPYYRWGTWSLYYFDI | VL4-82_JL_1_CDR3_9 | 5.8 | AVGYSAGWV | *Env (unknown) |
| | CP62 | 5 | VH3-183_D15_JH4_CDR3_18 | 11.5 | ARAPYYKWGTWSLYYFDI | VL4-82_JL_1_CDR3_9 | 9.8 | AVGHSAGWV | *Env (unknown) |
| | CP73 | 5 | VH3-183_D15_JH4_CDR3_18 | 11.1 | ARGPYYRWGTWSLYYFDI | VL4-82_JL_1_CDR3_9 | 7.6 | AVGYSAGWV | Env (unknown) |
| | CP91 | 5 | VH3-183_D15_JH4_CDR3_18 | 7.6 | ARGPYYKWGTWSLYYFDI | VL4-82_JL_1_CDR3_9 | 7.3 | AVGYSAGWV | *Env (unknown) |
| | CP92 | 5 | VH3-183_D15_JH4_CDR3_18 | 7.0 | ARGAYYKWGTWTLYYFDL | VL4-82_JL_1_CDR3_9 | 8.0 | AVGYSAGWI | Env (unknown) |
| | CP68 | 6 | VH3-183_D15_JH2_CDR3_18 | 8.3 | QEGSYYKWGMGMTSNHHA | VL4-82_JL_1_CDR3_9 | 6.6 | AVGYSAGWV | Env (unknown) |
| | CP58 | 7 | VH3-230_D31_JH2_CDR3_7 | 5.1 | TTTGLTY | Vk1-201_JK2_CDR3_9 | 3.6 | WQYDKLPLT | Env (unknown) |
| | CP63 | 7 | VH3-230_D17_JH2_CDR3_7 | 2.9 | TTTGLGY | Vk1-201_JK2_CDR3_9 | 3.5 | WQYDKLPLT | Env (unknown) |
| | CP66 | 8 | VH3-139_D27_JH4_CDR3_7 | 2.9 | ARMWVDV | Vk4-83_JK2_CDR3_9 | 0.7 | MQDYNPPYT | Env (unknown) |
| | CP82 | 9 | VH3-80_D31_JH4_CDR3_17 | 3.7 | ARDGWEEYMWGGSFLDL | Vk4-28_JK3_CDR3_11 | 1.9 | LQYYDFPNT | Env (unknown) |

‡*Heavy- and light-chain sequences of mAbs cloned were analyzed by IgBLAST and assigned to the closest V, D, and J germline genes. Clonal lineage criteria are shown in* ***Figure 2****. Somatic hypermutation level (Mut %) were calculated as percentage of nucleotide sequence divergence from germline V gene sequences. *ELISA/BLI negative. Specificity inferred by clonal lineage analysis, e.g., belonging to the same lineage with BG505 SOSIP binding clones.*

# Chapter 3: The HIV-1 Envelope Glycoprotein C3/V4 Region Defines a Prevalent Neutralization Epitope following Immunization

*Adapted from* Lei, L., Yang, Y.R., Tran, K., Wang, Y., Chiang, C.I., Ozorowski, G., Xiao, Y., Ward, A.B., Wyatt, R.T. and Li, Y., 2019. The HIV-1 envelope glycoprotein C3/V4 region defines a prevalent neutralization epitope following immunization. *Cell reports*, *27*(2), pp.586-598.

***Synopsis***

Despite recent progress in engineering native trimeric HIV-1 envelope glycoprotein (Env) mimics as vaccine candidates, Env trimers often induce vaccine-matched neutralizing antibody (nAb) responses. Understanding the specificities of autologous nAb responses and the underlying molecular mechanisms restricting the neutralization breadth is therefore informative to improve vaccine efficacy. Here, we delineate the response specificity by the single B cell sorting platform established in **Chapter 2** and the serum analysis of guinea pigs immunized with BG505 SOSIP.664 Env trimers. Our results reveal a prominent immune target containing both conserved and strain-specific residues in the C3/V4 region of Env in trimer-vaccinated animals. The defined nAb response shares a high degree of similarity with the early nAb response developed by a naturally infected infant from whom the HIV virus strain BG505 was isolated and later developed broadly nAb response. The study in this chapter informs on strain-specific responses and their possible evolution pathways, thereby highlighting the potential to broaden nAb responses by immunogen re-design.

***3.1 Introduction***

Recently, considerable efforts have been made to design HIV-1 native trimer mimics to induce broadly neutralizing antibody (bNAb) responses in vivo (Sanders and Moore, 2017). Well-ordered trimeric Envs have been engineered with enhanced thermostability, improved bNAb epitope presentation, and dampened non-neutralizing epitopes (Feng et al., 2016; Kulp et al., 2017; Martinez-Murillo et al., 2017; Sanders et al., 2013; Sharma et al., 2015). The desirable antigenicity profiles of engineered Env trimer immunogens, however, largely do not translate into the desired immunogenic outcome of

eliciting bNAbs (Klasse, 2014; Ward and Wilson, 2017). Conserved neutralizing epitopes are often recessed and occluded on the Env native trimer. Such conserved epitopes are recognized by bNAbs in vitro but weakly immunogenic in vivo in general (Feng et al., 2012; Kelsoe et al., 2013), except in some unique experimental animals, such as cows, that can readily generate antibodies with ultralong heavy chain complementary determining regions (HCDR3) to access these hard-to-reach determinants (Sok et al., 2017). In contrast, Env variable elements or non-neutralizing epitopes are immunodominant (Havenar-Daughton et al., 2017; Saunders et al., 2017; Wiehe et al., 2017). Despite the undesirable immunodominance and the elicitation of limited neutralization breadth, recent immunization studies have at least achieved consistent induction of vaccine-matched tier 2 virus (primary virus isolate) neutralizing antibody (nAb) responses (Feng et al., 2016; Hessell et al., 2016; Martinez-Murillo et al., 2017; Sanders et al., 2015; Saunders et al., 2017). In HIV-1 infected individuals, such strain-specific nAb responses often appear several months post-infection, which may reflect the initial antibody responses following natural infection (Klasse et al., 2018). These autologous nAbs apply selection pressure on the Env and drive neutralization escape of circulating viruses, which lead to the development of heterologous or bNAb responses (Anthony et al., 2017; van Haaren et al., 2017; Sather et al., 2014). Thus, studying trimer-induced tier 2 nAb responses in animal models provides an opportunity to characterize the strain-restricted specificities, and to compare with the initial nAb responses in natural infection. In conjunction, such parallel efforts could inform future vaccine design or vaccination strategies to expand neutralization breadth.

In this study, we characterized the specificities mediating autologous tier 2 neutralization induced by BG505 SOSIP.664, which represents the current generation of cleaved and well-ordered native-like Env trimer immunogens in guinea pigs. BG505 SOSIP.664, derived from a clade A primary virus isolate BG505, consists of a genetically engineering disulfide bond linkage at the interface of gp120-gp41, an I559P mutation to maintain the gp41 subunits in their pre-fusion form, and truncation at residue 664 to improve trimer solubility (Sanders et al., 2013). Besides conventional serum neutralization and epitope mapping analysis at the polyclonal level, we interrogated nAb responses at the clonal level by our recently established single B cell RT-PCR method in the guinea pig model (Lei et al., 2019). We have isolated three BG505-specific nAbs derived from a single clonal lineage that target the C3 region flanking the Env CD4 binding loop, and V4 region, an important part of the Env "silent face" (Wyatt and Sodroski, 1998). Interestingly, the critical Env C3/V4 residues recognized by the nAbs elicited by immunization substantially overlap with the Env residues under autologous nAb selection pressure located in the same Env region during early infection (Sanders et al., 2015). In addition, given the similar serological responses in other animal models induced by BG505 SOSIP.664 (Klasse et al., 2018; McCoy et al., 2016; Sanders et al., 2015), the strain-specific epitope defined here is likely a prominent immunogenic target on BG505 SOSIP.664 trimer. Furthermore, BG505 SOSIP.664 is derived from a clade A HIV-1 primary virus strain isolated from a 6-week old infant, who later on developed a broaden nAb response targeting undefined epitope(s) within 2 years of infection (Goo et al., 2014). Therefore, understanding the mechanism of the prevalent strain-specific nAb response elicitation and the evolution of the responses would provide insight into future immunogen design.

## *3.2 Materials and Methods*

### 3.2.1 Animal Immunization and Sampling

The animals (N=6/group) were immunized 4 times with 20 μg of BG505 SOSIP.664 formulated in ISOMATRIX adjuvant on weeks 0, 4, 12, and 24 via intramuscular route as previously described (Feng et al., 2016), followed by an intraperitoneal injection of 40 μg of BG505 SOSIP.664 four days prior to the termination of the animal (**Figure 3.1A**). The size of the animal group (N=6) was determined based on results from previous study in which antibody response difference between different immunization regimens could be significantly observed by non-parametric statistical analysis such as Mann-Whitney test (Feng et al., 2012). Randomization of animal group assignment was performed arbitrarily, without blinding.

Animal 1567 was selected for isolating Env-specific antibodies as its serum represents the overall virus neutralization profiles of this group (**Figure 3.1A**), with a median BG505 neutralization $ID_{50}$ titer of this group (**Figure 3.1A**). The splenocytes were further released from spleen and purified by density gradient centrifugation with Ficoll-Paque PLUS (GE Healthcare). After washing by PBS, cells were frozen in Bambanker (Wako Chemicals).

Plasma from animals 1563, 1565, and 1567 were used to screen neutralization capacity against BG505 Env C3/V4 mutant virus panel subsequently, since plasma from these animals displayed positive BG505 neutralization titers ($ID_{50}$ >10).

### 3.2.2 Soluble Env Protein Production

BG505 SOSIP.664 trimers (Sanders et al., 2013), BG505 gp120 monomers (Sok et al., 2014), and YU2 gp140-F with a D368R mutation (Yang et al., 2002) were used in this

study to generate corresponding Avi-tagged sorting probes. BG505 SOSIP.664 His-Avi contains additional sequences (GSGSGGSG*HHHHHHHH***GLNDIFEAQKIEWHE**) following the C-terminus of BG505 SOSIP.664, with linker underlined, 8XHis tag in italic font, and Avi-tag in bold font.

The BG505 gp120 (Sok et al., 2014) has a sequence similar to the gp120 components of the BG505 SOSIP.664 trimer with a deletion (AENLWVTVYYGVP) at the N-terminus (Hoffenberg et al., 2013). A linker (GSTGS) and an Avi-Tag (GLNDIFEAQKIEWHE) were introduced at the N-terminus following the signal peptide (METDTLLLWVLLLWVP) to facilitate biotinylating the protein (Sok et al., 2014). Avi- and 6xHis-tagged YU2 gp140-F_D368R (Sundling et al., 2012b) was constructed by appending additional sequences (GGSG*HHHHHH***GLNDIFEAQKIEWHE**) to the C-terminus of YU2 gp140-F as described previously (Doria-Rose et al., 2009), with linker underlined, 6XHis tag in italic font, and Avi-tag in bold font.

Env proteins were expressed by co-transfection of expression vectors and furin (except for BG505 gp120 and YU2 gp140-F_D368R) in FreeStyle 293F cells with 293fectin transfection reagent (Life Technologies) as described previously (Guenaga et al., 2015). Cell culture supernatants were collected 5 days post transfection and purified with *Galanthus nivalis* lectin-agarose (Vector Laboratories) columns followed by size exclusion chromatography (SEC) on Hiload 16/60 Superdex 200 pg column (GE Healthcare). Fractions containing the trimers or monomers were pooled and concentrated for further analysis. Antigen probes used for single B cell sorting were biotinylated by BirA biotin-protein ligase standard reaction kit (Avidity) per manufacturer's instructions. Excess biotin was removed by five times of buffer exchange in Amicon ultra 10K concentrators.

Antigenicity of the biotinylated proteins was assessed by ELISA analysis with well-characterized mAbs as described previously (Doria-Rose et al., 2009).

### 3.2.3 Guinea Pig Env-Specific Single B Cell Sorting

Cryopreserved splenocytes were thawed and resuspended in RPMI1640 medium (Gibco) supplemented with 10% FBS (Gibco) and 1 µl/ml of DNase (Roche). Cell staining was performed as described by a recent study **(Lei et al, 2019)**. Briefly, the cells were washed and incubated with diluted Live/Dead Fixable Aqua Cell Dead Stain (Invitrogen) in the dark at 4°C for 10 min. A cocktail of antibodies consisting of anti-guinea pig IgM-FITC (antibodies-online, ABIN457754), anti-guinea pig IgG-Alexa Fluor 594 (Jackson ImmunoResearch, 116790) was mixed with biotinylated BG505 SOSIP.664 trimers conjugated with PE (Invitrogen, S21388), BG505 gp120 conjugated with APC (Invitrogen, S32362), and YU2 gp140-F_D368R conjugated with Qdot655 (Invitrogen, Q10121MP). The cells were stained by the antibody/antigen cocktail, and class-switched $IgG^+$ single B cells with the desirable phenotype (Aqua $blue^-$/$IgG^+IgM^-$/BG505 $SOSIP^+$/BG505 $gp120^+$/YU2 gp140-F_$D368R^-$) were isolated by a FACS Aria III cell sorter (BD Biosciences).

### 3.2.4 Guinea Pig Single B Cell RT-PCR

mRNA from sorted single B cells were converted to cDNA by reverse transcription with random hexamers (Gene Link). IgG variable region sequences were then amplified by a semi-nested PCR strategy as described previously (**Lei et al, 2019**). The 1st PCR reaction was performed in a 50 µl reaction mixture consisting of 5 µl of cDNA, 5 µl of 10X PCR Buffer (Qiagen), 1 µl of 25 mM $MgCl_2$ (Qiagen), 1 µl of 10 mM dNTPs (Sigma), 2 Unites of HotStar Taq Plus (Qiagen), 5 µl of 25 µM 5’ primer mixtures, and 1 µl of 25 µM

3’ outer primers. The 2nd PCR reaction mixture consisted of the same 5’ forward primer mixtures as in the 1st PCR with 3’ inner primers as reverse primers, and 5 µl 5XQ-solution without $MgCl_2$ in 25 µl of volume. All semi-nested PCRs were incubated at 94 °C for 5 min followed by 50 cycles of 94°C for 30 s, 50°C for 45 s, and 72°C for 1 min with a final elongation at 72°C for 10 min before cooling to 4°C. After two rounds of PCR, positive PCR products were sequenced and genetic properties analyzed by IgBlast (Ye et al., 2013), including V(D)J segment usage, CDR3 boundary and length, somatic hypermutation level of VH (VH Mut%) and VL (VL Mut%), which is defined as divergence of the VH and VL of each mAb from the inferred VH and VL germline sequence at the nucleotide sequence level. The sequences of the PCR primers are described in (Lei et al., 2019a) **& Supplementary Table3**).

### 3.2.5 Guinea Pig Monoclonal Antibody Expression

The products of single cell RT-PCR reactions were purified, amplified by cloning PCR, and inserted into expression vectors by seamless cloning. The primers for each cloning PCR were described in (**Lei et al, 2019; & Supplementary Table 3**) and chosen based on germline V and J gene segments usage derived in Ig gene sequence analysis. The cloning PCR reaction was performed in a total volume of 50 µl with high-fidelity DNA polymerase (Roche). The PCR reaction mixture consisted of 1 µl of template using the 2nd PCR product from the single cell RT-PCR reaction, 5 µl of 10X reaction buffer, 1 µl of 10 mM dNTPs, 1 µl of 25 µM of 5’ and 3’ cloning primers, 1 µl of high-fidelity DNA polymerase (Roche) and nuclease-free water. The PCR program had an initial denaturation at 95°C for 3 min, followed by 20 cycles of 95°C for 30 s, 50°C for 30s, and 68°C for 2 min. There was a final elongation step at 68°C for 8 min. Positive cloning PCR products

were purified, and the assembly reactions were then performed with GeneArt assembly enzyme mix (Invitrogen) per manufacturer's instructions.

Equal amount of heavy- and light-chain expression vectors were transfected into 293F cells with 293fectin transfection reagent (Life Technologies) to produce monoclonal antibodies as previously described (Wang et al., 2016). Supernatants were harvested 4 days post-transfection followed by purification with Protein A Sepharose columns (GE Healthecare). Fabs described in this paper were transfected in a similar fashion with heavy chain variable regions inserted into Fab heavy chain expression vectors (Tran et al., 2014). Fabs were further purified by complete His-tag purification resin (Sigma-Aldrich).

### 3.2.6 ELISA Binding Assays

The binding specificity of the guinea pig mAbs was tested against BG505 SOSIP.664 trimer, BG505 gp120 monomer, and YU2 gp140-F_D368R by ELISA as described previously (Wang et al., 2016). MaxiSorp 96-well plates (Nunc, Thermo Scientific) were directly coated with BG505 gp120 monomer and YU2 gp140-F_D368R, respectively at 2 μg/ml in 100 μl of phosphate buffered saline (PBS) at 4°C overnight, followed by blocking with blocking buffer (PBS containing 5% FBS/2% non-fat milk). For BG505 SOSIP.664 ELISA, mouse anti-His tag mAb (R&D Systems, MAB050) at 2 μg/ml in 100 μl of phosphate buffered saline (PBS) was coated at 4°C overnight. After incubating with blocking buffer for 1 hr at 37°C, 2 μg/ml of BG505 SOSIP.664 Env proteins were added into each well and incubated for 1 hr at room temperature.

Subsequently, guinea pig mAbs were added in 5-fold serial dilutions starting at 50 μg/ml and incubated for 1 hr at room temperature. After wash, secondary HRP-conjugated anti-human IgG (Jackson ImmunoResearch) diluted at 1:10,000 in PBS/0.05% Tween 20

was added and incubated for 1 hr at room temperature. The signal was developed by adding 100 µl of TMB substrate (Life Technologies) and incubation for 5 min followed by the addition of 100 ul of 1 N sulfuric acid to stop the reactions. The optical density (OD) of each well was measured at 450 nm to quantify binding avidity. Between each incubation step, the plates were washed extensively with PBS supplemented with 0.05% Tween 20.

For cross competition ELISA, antibodies were biotinylated using EZ-Link NHS-Biotin (Pierce Biotechnology, Thermo Scientific). BG505 SOSIP.664 trimers were captured by anti-His tag mAbs (R&D Systems, MAB050) pre-coated on the ELISA plates. Serum/Ab competitors in serial dilutions were incubated with the captured trimers at room temperature for 30 min, followed by the addition of biotinylated mAbs diluted at concentrations pre-determined to give ~75% of the maximum binding signal. The optical density (OD) at 450 nm was measured and binding data were analyzed with Prism V7 Software (GraphPad Prism Software, Inc.). The degree of competition is calculated by the percentage of biotin binding signal reduction in the absence and presence of a given competitor mAb, respectively.

### 3.2.7 Negative-Stain EM

CP506 Fab/BG505 SOSIP.664 complexes were generated by incubating 6X molar Fab with BG505 SOSIP.664 overnight at 4°C. Grid preparation, image processing, and raw data analysis followed a similar protocol described in (Zhao et al., 2017). Briefly, three µl of sample was applied to a 400 mesh copper grid coated with carbon, then stained with 2% (w/v) uranyl formate. After the grid was completely dry (using blotting paper), the grids were imaged on a 120 keV FEI Tecnai Spirit electron microscope using a normal magnification of 52000x, resulting in 2.05 Å/px at the image plane. 107 micrographs were

collected with a TVIPS TemCam-F416 (4k x 4k) camera using the Leginon interface (Carragher et al., 2000). 19,669 particles were selected using Appion DoGPicker (Lander et al., 2009) from these 107 micrographs. Data were then processed using Relion 2.1 (Scheres, 2012). 14,022 particles were selected from 119 classes after 2D classification. A final number of 12,100 particles went into 3D refinement. The EM reconstruction has been deposited to the Electron Microscopy Data Bank (EMD-9003).

### 3.2.8 HIV-1 Neutralization Assays

HIV-1 pseudoviruses were produced by co-transfecting *env* plasmids with an env-deficient backbone plasmid (pSG3 Δ*env*) in HEK293T cells in a 1:2 ratio, using FuGENE® 6 Transfection Reagent (Promega). Cell supernatants were harvested and sterile-filtered (0.45 μm) after 48hr incubation and stored at -80°C. Neutralization assays were performed in a single round of infection using pre-titrated HIV-1 Env-pseudoviruses and TZM-bl target cells as the following: 40 μL of titrated pseudoviruses were incubated with 10 μL of serially diluted antibodies/sera or complete DMEM for 30 min at 37°C in 96-well cell culture plates (Thermo Fisher), and 20 μL of resuspended TZM-bl cells at 0.5 million/mL were transferred into each well and incubated overnight, followed by the addition of 130 μL of fresh complete DMEM to each well on the following day and a continued incubation for another 16-24 hours until cells reaching > 90% confluency. After the removal of supernatant, the cells were lysed with 5X lysis buffer (Promega) for 15 min at RT before the addition of the Luciferase Activation Reagent (Promega). The luminescence signal was acquired immediately on a Biotek Plate reader. The percentage of neutralization was calculated using signals from wells containing viruses only as 100% infection reference and neutralization curves were fitted by nonlinear regression using a five-parameter hill

slope equation. The $IC_{50}$ values of each antibody were determined as the concentration of antibody required to inhibit infection by 50%. The 50% inhibitory dilutions ($ID_{50}$) for plasma neutralization were calculated in the same way.

### *3.3 Results*

#### 3.3.1 Three BG505-specific mAbs from one clonal lineage recapitulate serum autologous tier 2 virus neutralization capacity

In a previous study designed to investigate the immunogenicity of well-ordered trimers displaying different levels of thermostability, guinea pigs were immunized with BG505 SOSIP.664 Env trimers formulated in ISCOMATRIX adjuvant (**Figure 3.1A**). These trimers elicited potent BG505 "autologous tier 2" virus neutralizing antibodies in several animals (**Figure 3.1B**) (Feng et al., 2016), consistent with previous reports in rabbits and NHPs (Bale et al., 2018; Pauthner et al., 2017; Sanders et al., 2015). To delineate the autologous tier 2 virus neutralization specificity in the sera, we employed a FACS-based single B cell sorting and cloning method that we recently developed to isolate antigen-specific monoclonal antibodies (mAbs) from immunized guinea pigs (Lei et al., 2019a). In that initial study (chapter 2), we used the autologous BG505 SOSIP.664 trimer as the antigen probe to sort antigen-specific class-switched B cells from a single guinea pig (#1567) and cloned 16 mAbs recognizing BG505 SOSIP.664 from 10 million PBMCs. However, none of these 16 mAbs neutralizes the autologous tier 2 virus BG505 while only five of them neutralize tier 1 virus ZM109, recognizing the V3 crown, an immunodominant element of HIV-1 Env, especially on monomeric gp120, disordered trimers, or ordered trimers that expose this determinant *in vivo*.

A

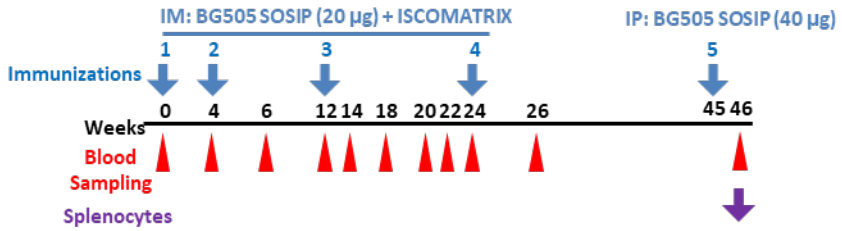


B

Sera Virus Neutralization Titers ($ID_{50}$)

| Virus | Tier 1 | | Tier 2 | | | |
|---|---|---|---|---|---|---|
| Animal ID | HXBc2 | ZM109 | JR-FL | 16055 | BG505 T332N | Q168 |
| 1563 | 28 | 188 | <10 | <10 | 33583 | <10 |
| 1564 | 146 | 450 | <10 | <10 | 10 | <10 |
| 1565 | 17 | 619 | <10 | <10 | 512 | <10 |
| 1566 | 439 | 1289 | <10 | <10 | 10 | <10 |
| 1567 | 42 | 46 | <10 | <10 | 1026 | <10 |
| 1568 | 11 | 168 | <10 | <10 | 10 | <10 |

| $ID_{50}$ | <40 | 40-200 | 200-1000 | 1000-5000 | >5000 |
|---|---|---|---|---|---|

C

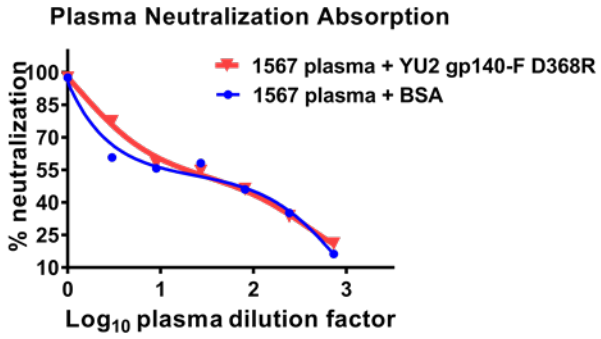


**Figure 3.1. BG505 SOSIP.664 trimers induced potent autologous tier 2 virus neutralizing antibody response in guinea pigs.** (A) Guinea pigs (n=6) were immunized on weeks 0, 4, 12, and 24 with BG505 SOSIP.664 formulated in ISCOMATRIX adjuvant, via intramuscular (IM) route. Blood sampling was performed at weeks indicated by red arrows in the scheme. Splenocytes were harvested on week 46, with intraperitoneal (IP) injection of BG505 SOSIP.664 (40 µg) four days (on week 45) prior to the termination of the animal on week 46. (B) Neutralization ID50 titers (reciprocal dilution factor) of sera collected on week 26 from guinea pigs determined with a panel of tier 1 and tier 2 viruses using the TZM-bl pseudovirus assay. The data are duplicated with the mean of ID50 titer shown. (C) Guinea pig 1567 plasma neutralization capacity depletion by YU2gp140-F_D368R probe against BG505 T332N pseudovirus. YU2 gp140-F_D368R was pre-incubated with serially diluted plasma (week 46) prior to the standard neutralization assays. Bovine serum albumin (BSA) was used as negative control. YU2 gp140-F_D368R shows no effect on plasma neutralization capacity. The data are duplicated.

The initial failure to obtain the BG505 neutralizing clones in our previous attempt suggests that a more selective sorting strategy is needed to capture the relatively rare class-switched B cells accounting for the autologous neutralization capacity. We hypothesized that the autologous neutralizing antibodies should recognize BG505 Env but not react with Envs of heterologous isolates such as YU2. Thus, it is possible to use Env antigen derived from heterologous virus YU2 as a negative selection probe to enrich the B cells encoding the BG505 nAbs. To test this hypothesis, we assessed the guinea pig serum neutralizing activity against BG505 virus after neutralization activity depletion by YU2 gp140-F_D368R trimer absorption. The YU2 gp140-F_D368R trimer is a CD4 binding site (CD4bs) knockout mutant of the early generation of uncleaved gp140 trimer derived from isolate YU2 and characterized as a disordered trimer (Tran et al., 2014). We observed that the serum BG505 neutralization activity was not decreased after incubation with YU2 gp140-F_D368R, confirming that antibodies with no reactivity to the YU2-derived Env probe mediate the serum BG505 neutralization (**Figure 3.1C**). Furthermore, in a previous study the serum autologous tier 2 neutralization activity was shown to be largely absorbed by monomeric BG505 gp120 (Feng et al., 2016). Therefore, it might be feasible to isolate the class-switched B cells encoding the BG505 nAbs by capturing the B cells with a BG505 SOSIP.664$^{+}$/BG505 gp120$^{+}$/YU2 gp140-F_D368R$^{-}$ phenotype.

We performed guinea pig single B cell sorting by using the splenocytes from animal #1567 with the differential Env probe sorting scheme stated above (**Figure 3.2A**). We sorted antigen-specific class-switched B cells for single B cell IgG gene amplification (**Figure 3.2A**). Eight out of ten of the sorted cells with matched heavy and light chains were subsequently expressed well as soluble full-length mAbs in IgG1 form (**Table 3.1**).

Four of these mAbs displayed the desirable Env-binding phenotype: BG505 SOSIP.664$^{+}$/BG505 gp120$^{+}$/YU2 gp140-F_D368R$^{-}$ (**Figure 3.2B; Table 3.1**). Three of these BG505-specific mAbs (CP503, CP506, and CP507) (**Figure 3.2B**) showed potent neutralization against the BG505 virus (**Figure 3.2C**). In addition, we characterized the genetic properties of the BG505-specific mAbs, including the V(D)J gene segment usage, complementary determining region 3 (CDR3) length, and levels of SHM (**Figure 3.2D**). Interestingly, these three BG505 virus nAbs that share high sequence homology with the same V(D)J gene segment usage and virtually identical CDR3s (>80% nucleotide sequence homology) (**Figure 3.2D; Figure 3.3**), along with two additional mAbs (CP460 & 493, cloned from the same sorting experiment but expressed too little for functional characterization) (**Figure 3.2D; Figure 3.3)**, were assigned to the same clonal lineage. This clonal lineage is distinct from the other five expressed mAbs (none-neutralizing or binding) in this study (**Figure 3.2C; Table 3.2; Figure 3.3)** and previously isolated mAbs (Lei et al., 2019a). Therefore, we set to focus on characterizing the three clonally related nAbs (somatic variants of each other) including CP503, CP506, and CP507 that mediate the autologous BG505 virus serum neutralization.

**Table 3.1 Statistic properties of the Env-specific single B cell sorting and IgG cloning**

| | |
|---|---|
| Total splenocytes | 3,203,760 |
| Total Lymphocytes | 2,726,418 |
| Total Lymphocytes % | 85.6 |
| Total single cells | 2,672,228 |
| Total single cells % | 98.0 |
| Total live cells | 1,811,871 |
| Total live cells % | 67.8 |
| Total IgG+IgM- class-switched B cell | 185,624 |
| Total IgG+IgM- class-switched B cell % | 10.2 |
| BG505 SOSIP + BG505 gp120 + class-switched B cell | 5640 |
| BG505 SOSIP + BG505 gp120 + class-switched B cell % | 3.0 |
| BG505 SOSIP + BG505 gp120 + YU2 gp140-F D368R- class-switched B cell | 61 |
| BG505 SOSIP + BG505 gp120 + YU2 gp140-F D368R- class-switched B cell % | 1.1 |
| Sorted cells | 88 |
| Sorted cells with paired VH or VL | 10 |
| Expressed mAbs | 8 |
| BG505 SOSIP + mAbs (Assessed by ELISA) | 4 |
| Sorting precision ((GP+mAbs/Expressed mAbs)*100) | 50% |

**Table 3.2 Genetic and binding specificity analysis of guinea pig mAbs cloned in this study. Related to Figure 3.2**

| | mAb | VDJ segments_CDRH3 length (AA) | VH Mut (%) | CDRH3 AA seq | VJ segments_CDRL3 length (AA) | VL Mut (%) | CDRL3 AA seq |
|---|---|---|---|---|---|---|---|
| Non-binder | **CP445** | VH3-262_D19_JH6_CDR3_5 | 4.9 | EALDI | Vk1-147_Jk3_CDR3_9 | 12.6 | QQCGDFPFT |
| | **CP451** | VH3-255_D25_JH4_CDR3_9 | 5.6 | GSSWNSFDV | Vk2-16_Jk3_CDR3_9 | 5.0 | LQTSHDPFT |
| | **CP452** | VH3-183_D15_JH4_CDR3_6 | 10.0 | ARHWGT | Vk2-3_Jk1_CDR3_9 | 3.2 | FQNTQPPQT |
| | **CP500** | VH3-167_D6_JH4_CDR3_17 | 6.7 | ATGPYIWSSYYVYYFEA | Vk1-226_Jk2_CDR3_9 | 5.3 | QQCYNSPYT |
| BG505 binders | **CP482** | VH3-282_D28_JH4_CDR3_15 | 2.8 | TAEVLTSDGYSTGDV | Vk1-174_Jk1_CDR3_9 | 3.0 | QQGYHSPWT |
| | **CP503** | VH1-140_D23_JH4_CDR3_10 | 10.6 | ATLLWLRFDI | Vk1-54_Jk2_CDR3_9 | 11.1 | QQFEGWPLT |
| | **CP506** | VH1-140_D23_JH4_CDR3_10 | 9.4 | ATLLWLRLDI | Vk1-54_Jk2_CDR3_9 | 8.1 | QQFQNWPLT |
| | **CP507** | VH1-140_D23_JH4_CDR3_10 | 8.4 | ASLLWLRFDF | Vk1-54_Jk2_CDR3_9 | 10.7 | QQFEGWPLT |
| No expression | **CP460*** | VH1-140_D23_JH4_CDR3_10 | 9.1 | ATLLWLRFDV | Vk1-54_Jk2_CDR3_9 | 11.5 | QQFNYWPLT |
| | **CP493*** | VH1-140_D23_JH4_CDR3_10 | 8.7 | ATLLWLRFEI | Vk1-54_Jk2_CDR3_9 | 11.1 | QQFEGWPLT |

* mAbs belong to CP506 clonal lineage which were not characterized due to low expression level

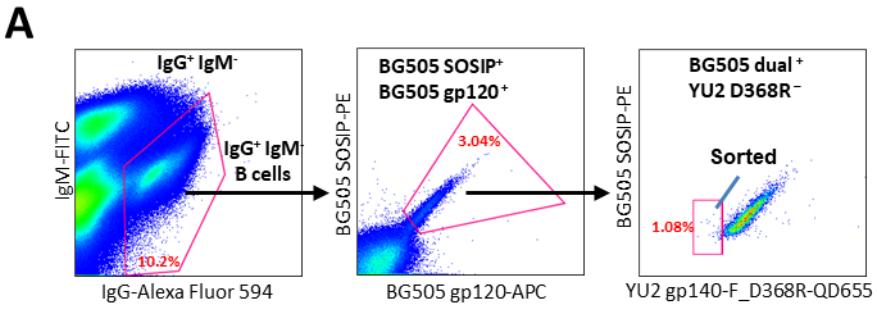


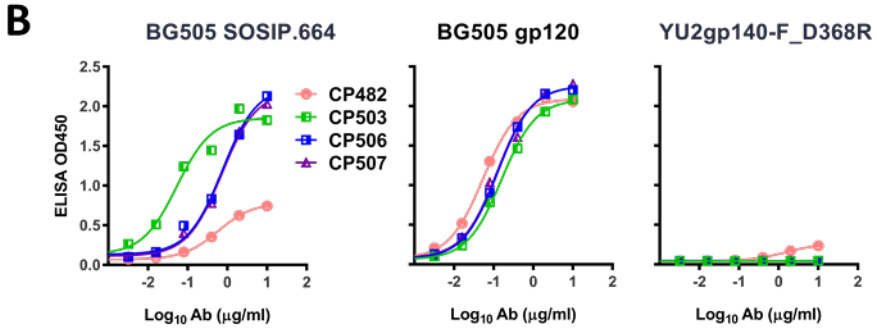


C

| Neutralization (mAb $IC_{50}$, µg/ml; serum $ID_{50}$) | | | | | |
|---|---|---|---|---|---|
| | Tier 1 | | Tier 2 | | |
| mAb | HXBc2 | ZM109 | BG505 T332N | BG505 WT | JR-FL |
| CP482 | >50 | >50 | >50 | >50 | >50 |
| CP503 | >50 | >50 | 0.67 | 2.1 | >50 |
| CP506 | >50 | >50 | 0.1 | 0.68 | >50 |
| CP507 | >50 | >50 | 0.42 | 1.19 | >50 |
| **Serum** | **42** | **46** | **1026** | **ND** | **<10** |
| VRC01 | 0.03 | 0.07 | 0.07 | 0.07 | 0.02 |

D

| mAb | VDJ segments_CDRH3 length (AA) | VH Mut (%) | CDRH3 AA seq | VJ segments_CDRL3 length (AA) | VL Mut (%) | CDRL3 AA seq |
|---|---|---|---|---|---|---|
| CP482 | VH3-282_D28_JH4_CDR3_15 | 2.8 | TAEVLTSDGYSTGDV | Vk1-174_Jk1_CDR3_9 | 3 | QQGYHSPWT |
| CP503 | VH1-140_D23_JH4_CDR3_10 | 10.6 | ATLLWLRFDI | Vk1-54_Jk2_CDR3_9 | 11.1 | QQFEGWPLT |
| CP506 | VH1-140_D23_JH4_CDR3_10 | 9.4 | ATLLWLRLDI | Vk1-54_Jk2_CDR3_9 | 8.1 | QQFQNWPLT |
| CP507 | VH1-140_D23_JH4_CDR3_10 | 8.4 | ASLLWLRFDF | Vk1-54_Jk2_CDR3_9 | 10.7 | QQFEGWPLT |
| CP460* | VH1-140_D23_JH4_CDR3_10 | 9.1 | ATLLWLRFDV | Vk1-54_Jk2_CDR3_9 | 11.5 | QQFNYWPLT |
| CP493* | VH1-140_D23_JH4_CDR3_10 | 8.7 | ATLLWLRFEI | Vk1-54_Jk2_CDR3_9 | 11.1 | QQFEGWPLT |

**Figure 3.2 Isolation and characterization of BG505-specific guinea pig mAbs from animal 1567 that recapitulate serum autologous tier 2 virus neutralization.** (A) Single B cell sorting to isolate BG505-specific guinea pig mAbs by flow cytometry sorting of splenocytes. The frequency (percentage) of the gated cell population in parent population is indicated in red. Antigen-specific class-switched B cells (Aqua blue$^-$IgG$^+$IgM$^-$BG505 SOSIP$^+$BG505 gp120$^+$YU2 gp140-F_D368R$^-$) were sorted for Ig gene amplification. Approximately 3 million of splenocytes from one animal (#1567) were analyzed. A single sorting experiment was performed. (B) Binding specificity of four guinea pig mAbs to the sorting probes assessed by ELISA. Data were generated in duplication, with the mean of OD450 nm shown. (C) Neutralization potency ($IC_{50}$ titer, µg/mL) of four BG505 SOSIP.664 binding mAbs against Env-pseudotyped viruses. The background neutralization $IC_{50}$ (mAb) and $ID_{50}$ (serum) titer threshold is set as >50 µg/mL and <10, respectively.

ND, not determined. Data were generated in duplication with the mean of $ID_{50}$ titer reported. (D) Genetic analysis of four guinea pig mAb variable region sequences. * indicating mAbs related to CP506 clonal lineage which were not characterized due to low expression level.


**Figure 3.3 Genetic features of heavy and light chains of cloned guinea pig mAbs in this study. Related to Figure 3.2.** Alignment of heavy and light chains of **(A)** CP506 clonal lineage mAbs that mediate BG505 virus neutralization. VH1-140 and Vk1-54 are the inferred guinea pig heavy- and light- chain germline V gene segments for CP506 lineage mAbs, respectively. N, the region that serves as the junction between VH-DH and DH-JH, or VK-JK segments. Somatic hypermutations are highlighted in red. CP460 & 493 mAbs are related clonal members, which were not characterized due to low expression level; **(B)** non-neutralizing mAbs isolated in this study, with diversified residues highlighted in red. The framework and complementarity-determining regions (CDRs) are annotated based on the IMGT numbering system.

### 3.3.2 Autologous nAbs target the C3 and V4 regions on BG505 SOSIP.664

To determine the binding epitope of the three BG505 nAbs, we first performed cross-competition analysis using a panel of well-defined bNAbs. The selected bNAbs were grouped into four distinct epitope clusters: CD4bs, V3-glycan, V1/V2-glycan, and gp120/gp41 interface. The CP506 lineage nAbs showed complete self-competition (75%-

100%) for binding to BG505 SOSIP.664 (**Figure 3.4A**). In addition, we observed strong binding competition of the CP506 lineage nAbs with the CD4bs-directed bNAb VRC01 (50%-75%), and gp120/gp41 interface bNAbs 35O22, 8ANC195, and 3BC315 (75% - 100%) (**Figure 3.4A**). The binding inhibition between the three CP506 lineage nAbs and VRC01 or 3BC315 was reciprocal, regardless of the order of competitors and analytes in the assay (**Figure 3.4A**), suggesting that the epitope of the CP506 lineage nAbs is very close to that of VRC01 and 3BC315. Thus, the cross-competition data indicate that the footprint of CP506 clonal lineage members on BG505 Env trimer may be proximal to both the CD4bs and the gp120/gp41 interface.

To better understand how these nAbs interact with BG505 SOSIP trimer, we pursued a structural visualization by negative-stain electron microscopy (EM). We generated the antigen-binding fragment (Fab) version of CP506 and incubated it with BG505 SOISP.664 trimer to form a Fab-trimer complex followed by single-particle EM analysis (**Figure 3.5A**). The complex 3D reconstruction showed that the major species of the complex are Env trimers bound with three CP506 Fabs per particle, with Fabs approaching the Env with a nearly perpendicular angle relative to the trimer center axis (**Figure 3.4B**). By fitting the crystal structure coordinate data of BG505 SOSIP.664 (PDB: 4TVP) into the EM trimer electron density, we determined that the Fab interacts with gp120 C3 region, including the periphery of the CD4 binding loop, and the V4 region (**Figure 3.4B)**. It is notable that there are several N-linked glycans including N339, N355 in C3 region, N363 in the periphery of CD4bs and in close contact with VRC01 (Stewart-Jones et al., 2016), N392 and N398 in V4 region of Env at the interface with CP506 Fab (**Figure 3.4B**).

Docking of VRC01 Fab into the EM complex indicated that CP506 and VRC01 contact the trimer from different angles with slightly overlapped density (**Figure 3.4C**), which is consistent with the observed reciprocal cross-competition between these two mAbs (**Figure 3.4A**) and potential overlap around N363 glycan (**Figure 3.4B**). The epitope overlap was further confirmed by strong competition between CP506 Fab and VRC01 IgG/Fab, of which the Fab excludes the influence of the respective IgG constant regions (**Figure 3.4D**). Additionally, we docked gp120/gp41 interface bNAbs including 3BC315, 8ANC195, and 35O22 into the trimer EM complex, which displayed cross-competition with the CP506 lineage mAbs (**Figure 3.4A**) for Env trimer binding. The docking result demonstrated that both 8ANC195 and 35O22 had no footprint overlapping with CP506 lineage mAbs (**Figure 3.5B**), consistent with the observed non-reciprocal cross-competition pattern (**Figure 3.4A**) that may result from unilaterally allosteric inhibition. The EM/docking analysis showed that the Fabs of CP506 and 3BC315 have no steric clash with each other (**Figure 3.4C**), despite that both CP506 Fab and IgG cross-compete with IgG and Fab versions of 3BC315 in a reciprocal manner (**Figure 3.4A, 3.4D).** This observation may be explained by conformational change or glycan reorientation on BG505 trimer upon 3BC315 binding (Derking et al., 2015). In summary, the EM data suggest potential contact between CP506 and the gp120 C3/V4 region that partially overlaps with the CD4 binding site and is close to the gp120/gp41 interface, corroborating the observed reciprocal binding inhibition between CD4bs bNAb (VRC01), gp120/gp41 interface bNAb (3BC315), and CP506 (**Figure 3.4A, 3.4D**).

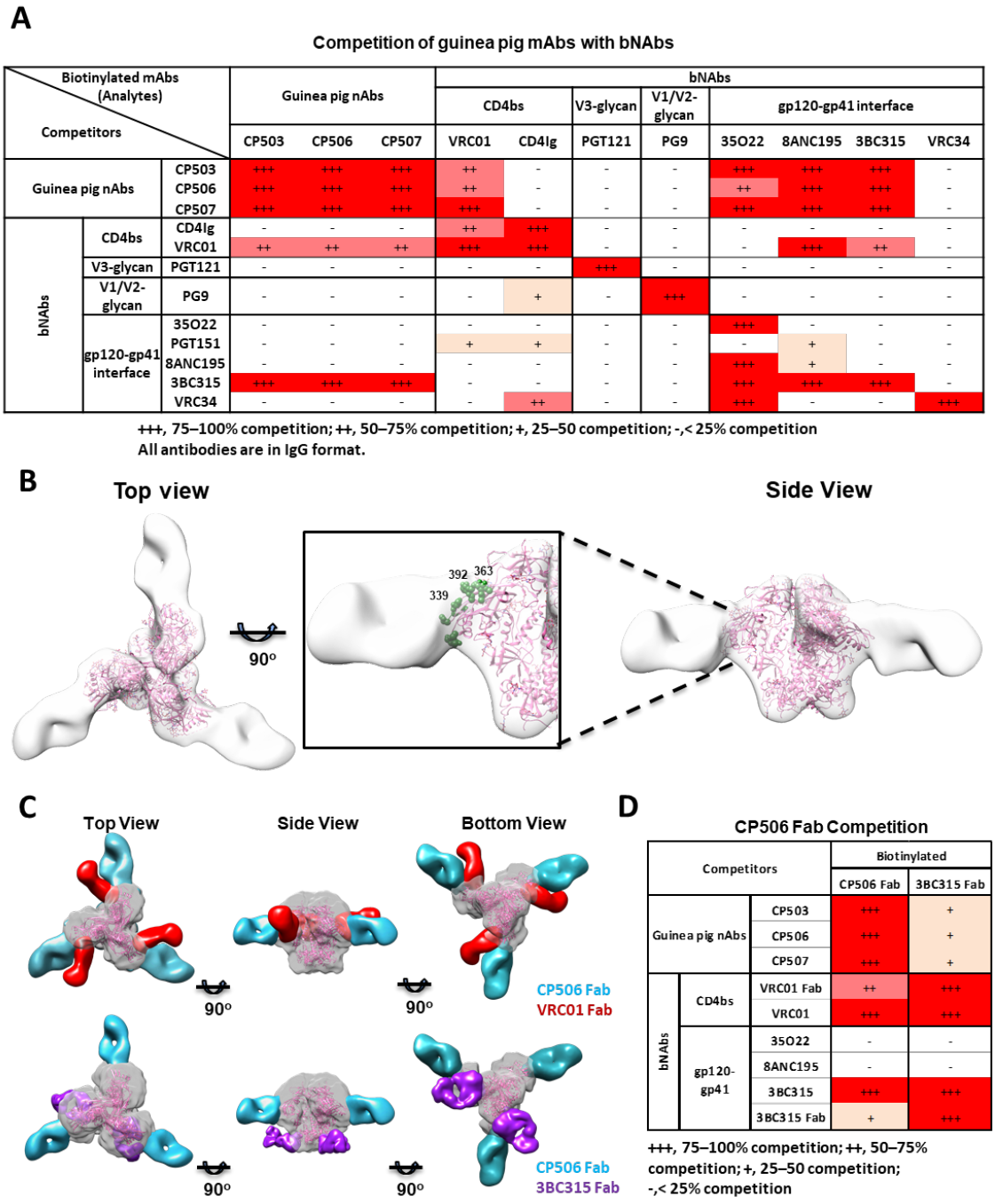


**Figure 3.4 Guinea pig nAbs target the C3 and V4 region on BG505 SOSIP.664.** (A) Cross-competition of guinea pig nAbs with epitope well-defined bNAbs for binding to BG505 SOSIP.664 trimer. Data were generated in duplication with selected reactions repeated at least twice. (B) 3D EM reconstruction of CP506 Fab/BG505 SOSIP.664 complex. The crystal structure of BG505 SOSIP.664 trimer (PDB: 4TVP), displayed in pink ribbons, is docked into the trimer EM density. Five N-linked glycans at the contact interface are highlighted in green, labeled with respective residue numbers. (C) Comparison of the mode of CP506 binding to BG505 SOSIP.664 Env trimer with bNAbs VRC01 (upper) (EMD-6193) and 3BC315 (lower) (EMD-3067), which recognizes the

CD4bs and gp120/gp41 interface of Env, respectively. (D) Competition ELISA assay using biotin-labeled CP506 Fab and 3BC315 Fab as analytes confirms competition between CP506 lineage nAbs and bNAbs including VRC01 and 3BC315. Data were generated in duplication with reactions of 3BC315 Fab repeated twice.

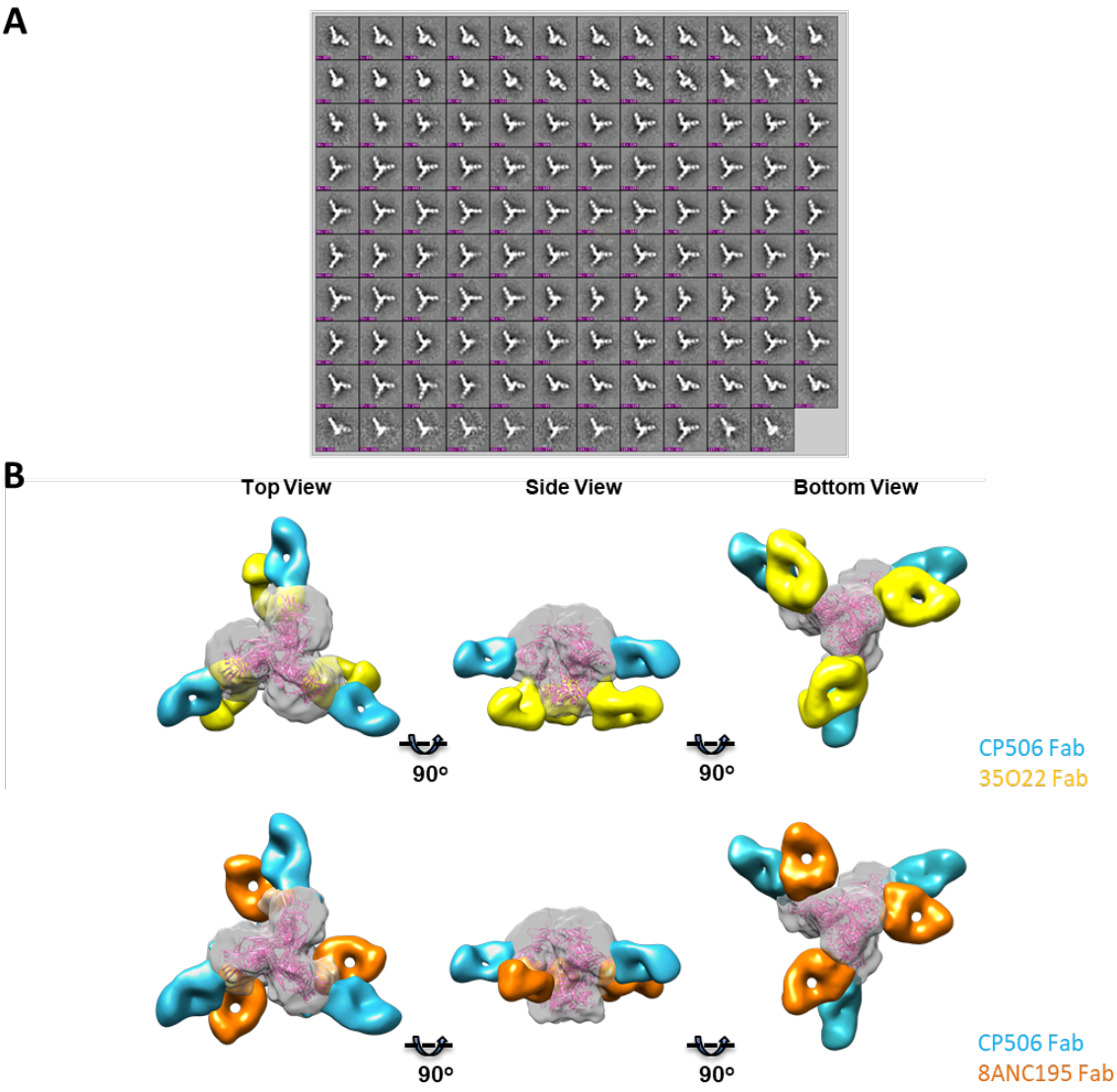


**Figure 3.5 Single-particle electron microscopy analysis. Related to Figure 2.** (A) EM 2D class averages of CP506 Fab:BG505 SOSIP.664 trimer complexes. 14,022 particles with 119 classes were identified. (B) The Fab of 35O22 (upper) (EMDB: EMD-2672) and 8ANC195 (lower) (EMDB: EMD-8693) showing no competition with CP506 linage nAbs in competition ELISA assay, is docked into CP506 Fab:BG505 SOSIP.664 trimer 3D EM complex reconstruction, respectively.

### 3.3.3 Molecular basis for strain-specific neutralization mediated by CP506 lineage mAbs

We next focused on delineating the specific residues critical for the neutralizing activity of the CP506 clonal lineage. By studying the EM 3D reconstruction of the CP506 Fab:BG505 Env complex, we identified several potential N-linked glycosylation sites (PNGS) with the N(X)S/T motif within the Env C3/V4 regions displaying potential contacts with CP506 Fab, which may be critical for CP506 recognition. These PNGS include N339, N355, and N363 from the C3 region as well as N392 and N398 on the V4 loop (**Figure 3.4B**). To examine the effect of these glycans on CP506 recognition, we genetically eliminated the glycan sites individually (**Figure 3.6A**) on the Env gp160 of BG505 T332N pseudovirus. We mutated the corresponding asparagine residues in the N(X)S/T PNGS motif to alanine (N→A) or the threonine or serine residues to alanine in the N(X)S/T motif (S/T→A) at positions 341, 365, and 394, respectively, and tested the neutralization sensitivity of these BG505 glycan-deleted variants to the CP506 lineage mAbs. The BG505 variant strains, N339A or T341A, N363A or S365A, and N392A or T394A with the glycan knock-out at residues N339, N363, and N392, respectively, displayed complete ablation in neutralization sensitivity to all three CP506 clonal lineage members (**Figure 3.6B**), suggesting that these glycans are likely critical for CP506 lineage mAb recognition. Glycosylation sites at 339 and 392 are highly conserved in HIV Env, since 64.2% and 80.9% of HIV-1 isolates contain glycans at residues 339 and 392 (**Figure 3.6C**), respectively (McCoy et al., 2016). On the contrary, glycan at 363 is very rare, with frequency as low as 8.7% (**Figure 3.6C**). Of note, right adjacent to the CD4 binding loop (**Figure 3.6A, 3.6C**), glycan N363 is directly involved in the epitope of CD4bs bNAb

VRC01 (Stewart-Jones et al., 2016). Therefore, the antigen-binding sites of CP506 overlap with that of VRC01 on N363 as revealed by structural analysis, which is consistent with the observation that the CP506 lineage mAbs compete strongly with VRC01 (**Figure 3.4A**). Collectively, we identified three PNGS in the Env C3 and V4 regions that are essential for the CP506 lineage antibody recognition (**Figure 3.6A, 3.6C**), with one glycan site (N363) close to the CD4 binding loop conferring strain-specific recognition and neutralization.

We further investigated other Env elements involved in the CP506 lineage nAb epitope. We compared the amino acid sequences of the Envs from BG505 and its maternal virus MG505.A2 (McCoy et al., 2016), which have different sensitivities to CP506 neutralization. We identified five mutations within the C3 and V4 regions on MG505.A2 Env (**Figure 3.6A**) compared to BG505, which may confer CP506 neutralization resistance. We then introduced corresponding point mutations to the residues in BG505 T332N Env, designated as G343E, $^{357}$TIIR$^{360}$→$^{357}$KTII$^{360}$, and I396N (**Figure 3.6B**), respectively. We observed that BG505 T332N virus neutralization by CP506 mAbs was abolished by mutations $^{357}$TIIR$^{360}$→$^{357}$KTII$^{360}$, and I396N on two anti-parallel β strands (**Figure 3.6B, 3.6C**), suggesting that these residues are important for CP506 mAb recognition. However, the $^{357}$TIIR$^{360}$ motif only appears at the frequency of 0.06% in 8,472 unique Env sequences recovered from the Los Alamos National Laboratory database (http://www.lanl.gov) (**Figure 3.6C**), while most Envs have the $^{357}$KTII$^{360}$ motif as the counterpart. Additionally, I396 in the V4 region only occurs in 4% of these Env sequences (**Figure 3.6C**). Therefore, besides the rare glycan at residue N363 on BG505 Env, the $^{357}$TIIR$^{360}$ and I396 motifs in the context of BG505 Env, which present at low frequencies in Envs of other virus isolates, contribute to the strain-specific neutralization by CP506 lineage mAbs (**Figure 3.6C**).

Taken together, the data suggest that the CP506 lineage mAbs possess an epitope consisting of three potential N-glycosylation sites (N339, N392, and N363) and residues on two β-strands in the C3/V4 region of BG505 Env. The BG505 strain-specific neutralization mediated by CP506 lineage nAbs is attributed to certain contact residues on BG505 Env, which are not common for Envs from other virus isolates.

A

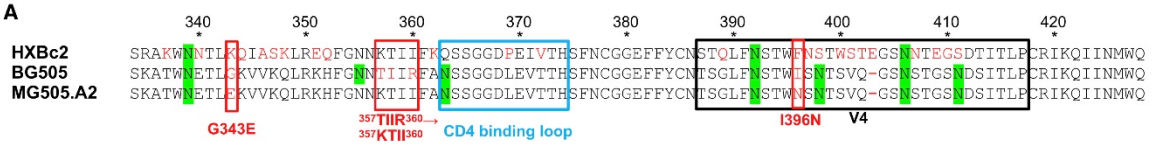


B

| Virus strains | | Guinea pig mAbs $IC_{50}$ (μg/ml) | | | bNAb |
|---|---|---|---|---|---|
| | | CP503 | CP506 | CP507 | VRC01 |
| Env region | WT | 1.77 | 1.04 | 0.45 | 0.04 |
| C3 | N339A | >50 | >50 | >50 | 0.07 |
| | T341A | >50 | >50 | >50 | 0.07 |
| | G343E | 2.66 | 0.65 | 0.5 | 0.07 |
| | N355A | 0.09 | 0.07 | 0.12 | 0.05 |
| | 357TIIR360→ 357KTII360 | >50 | >50 | >50 | 0.01 |
| | N363A | >50 | >50 | >50 | 0.07 |
| | S365A | >50 | >50 | >50 | 0.04 |
| V4 | N392A | >50 | >50 | >50 | 0.07 |
| | T394A | >50 | >50 | >50 | 0.06 |
| | I396N | >50 | >50 | >50 | 0.05 |
| | N398A | 0.16 | 0.09 | 0.06 | 0.04 |
| | N406A | 0.66 | 0.5 | 0.46 | 0.04 |
| | N411A | 1 | 1.03 | 0.82 | 0.06 |

C

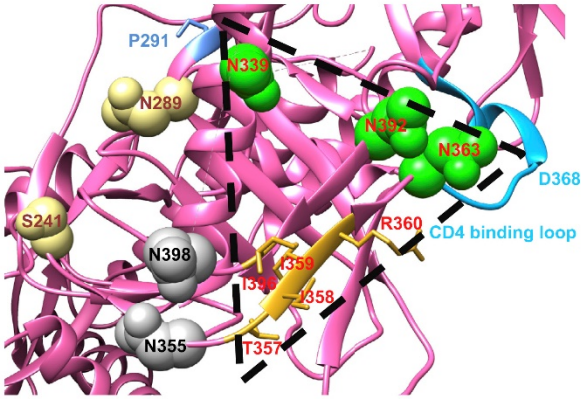


| Critical residues | N339 glycan | N363 glycan | N392 glycan | 357TIIR360 | I396 |
|---|---|---|---|---|---|
| Frequency in Env variants (%) | 64.2 | 8.7 | 80.9 | 0.06 | 4 |

**Figure 3.6 Epitope mapping of CP506 lineage mAbs.** (A) Sequence alignment of gp120s of HXBc2 (resistant to CP506 neutralization), BG505.W6M.C2 (sensitive to CP506 neutralization), and MG505.W0M.A2 (resistant to CP506 neutralization). Residues that differ between BG505.C2 and MG505.A2 on the C3 and V4 region are denoted in red boxes. CD4 binding loop is depicted by the blue box. PNGS are highlighted in green. (B) Neutralization (IC50, μg/mL) of guinea pig NAbs against BG505 T332N Env-pseudotyped viruses bearing mutations in the C3 and V4 region. Critical and non-critical glycans are listed in green and gray, respectively. Other residues critical to neutralization sensitivity are listed in red. Data were generated in duplication, with the mean of IC50 shown. (C) CP506 footprint determined by mutagenesis analysis in (B). (Top) Mutated residues for CP506 lineage mAb epitope mapping are shown on the crystal structure of BG505 SOSIP.664 (PDB: 4TVP). Critical and non-critical glycans are labeled in green and gray spheres, respectively. The 357TIIR360 strand and I396 are highlighted in gold. Residues 241 and 289, the centers of the 241/289 glycan hole, are labeled in yellow. The minimal footprint of CP506 lineage mAbs mapped here is outlined by a triangle. (Bottom) The frequency of CP506 binding critical residues in Env sequences retrieved from the Los Alamos National Laboratory database (https://www.lanl.gov/).

### 3.3.4 CP506 lineage autologous nAbs target an epitope on BG505 Env trimer that is distinct from the 241/289 glycan hole

Previous studies revealed two relatively conserved glycosylation sites at the gp120/gp41 interface, residues 241 and 289, on Envs of most HIV virus isolates. The absence of these two glycans on the BG505 Env thus results in a glycan hole on the Env surface. This glycan hole was reported as an immunodominant region associated with the autologous nAb responses evidenced by the isolation of several 241/289-dependent BG505 strain-specific mAbs (Klasse et al., 2018; McCoy et al., 2016)**,** and polyclonal serum neutralization specificity analysis (Klasse et al., 2018; McCoy et al., 2016; Pauthner et al., 2017).

To examine whether the epitope of the CP506 lineage nAbs overlaps with the 241/289 glycan hole, we superimposed the 241/289-dependent BG505 strain-specific mAbs, 10A and 11A (McCoy et al., 2016) onto the 3D reconstruction of CP506/BG505 SOSIP.664 complex as shown in **Figure 3.7A**. We found that the footprints of the 241/289-dependent rabbit mAbs on BG505 SOSP.664 trimer are distinct from the CP506 lineage nAbs (**Figure 3.7A**). This was further supported by the competition ELISA analysis in which no competition was observed between the competitor 10A Fab or 11A Fab and the biotin-labeled CP506 Fab for BG505 SOSIP.664 trimer binding (**Figure 3.7B**). However, non-reciprocal competition was observed when the CP506 lineage nAbs served as competitors and the signal of the biotin-labeled 241/289-dependent IgG or Fab bindings to Env were used as the readout (**Figure 3.7B**), suggesting that CP506 and 241/289 glycan hole targeting nAbs may bind Env with different conformations.

Furthermore, we constructed a BG505 Env glycan 241 knock-in (KI) mutant virus, S241N, which is resistant to 241/289 glycan hole antibodies (McCoy et al., 2016), and tested its neutralization sensitivity to CP506 lineage nAbs. Virtually the knockin glycan 241 has no effect on virus neutralization sensitivity to the CP06 lineage nAbs, as mutant virus S241N displayed neutralization sensitivity similar to the WT BG505 T332N virus (**Figure 3.7C**), strengthening the notion that the epitope of CP506 lineage nAbs is distinct from those of the 241/289-dependent nAbs.

It is notable that the edge of the 241/289 glycan hole, including residues N289 and P291, is close to the "3 glycan & 2 strands" epitope of the CP506 lineage nAbs (**Figure 3.6C**). Moreover, a 289-glycan knock-in mutant BG505 virus P291S showed completely ablated neutralization sensitivity to CP506 lineage nAbs (**Figure 3.7C**), indicating that either the knock-in glycan at 289 directly blocks the cognate contact residues, or the proline moiety on residue 291 is critical for CP506 recognition (**Figure 3.7C**). Thus, the 241/289 glycan hole on BG505 SOSIP.664 trimer is spatially and functionally relevant to the footprints of CP506 lineage nAbs (**Figure 3.6C**). However, the CP506 lineage mAb epitope still appears distinct from the 241/289 glycan hole dependent mAbs. As shown in **Figure 3.7A,** there is no steric clash between CP506 and the previously described glycan-hole dependent nAbs 10A and 11A (Klasse et al., 2018; McCoy et al., 2016) in the superimposed 3D reconstruction of BG505 SOSIP.664.

Furthermore, we assessed the neutralization sensitivities of five CP506-lineage neutralization resistant viral mutants (**Figure 3.6B)** to the 241/289-dependent nAbs (10A, 11A, & 11B), which readily neutralize the majority of the CP506-lineage resistant virus mutants with potency similar to the wildtype BG505 T332N virus, in contrast to CP506

(**Figure 3.8**). Therefore, both structural and functional analyses confirmed that CP506 lineage nAbs target an epitope on BG505 Env trimer distinctive from those previously described mAbs focused on the 241/289 glycan hole (**Figure 3.9A, 3.9B**).

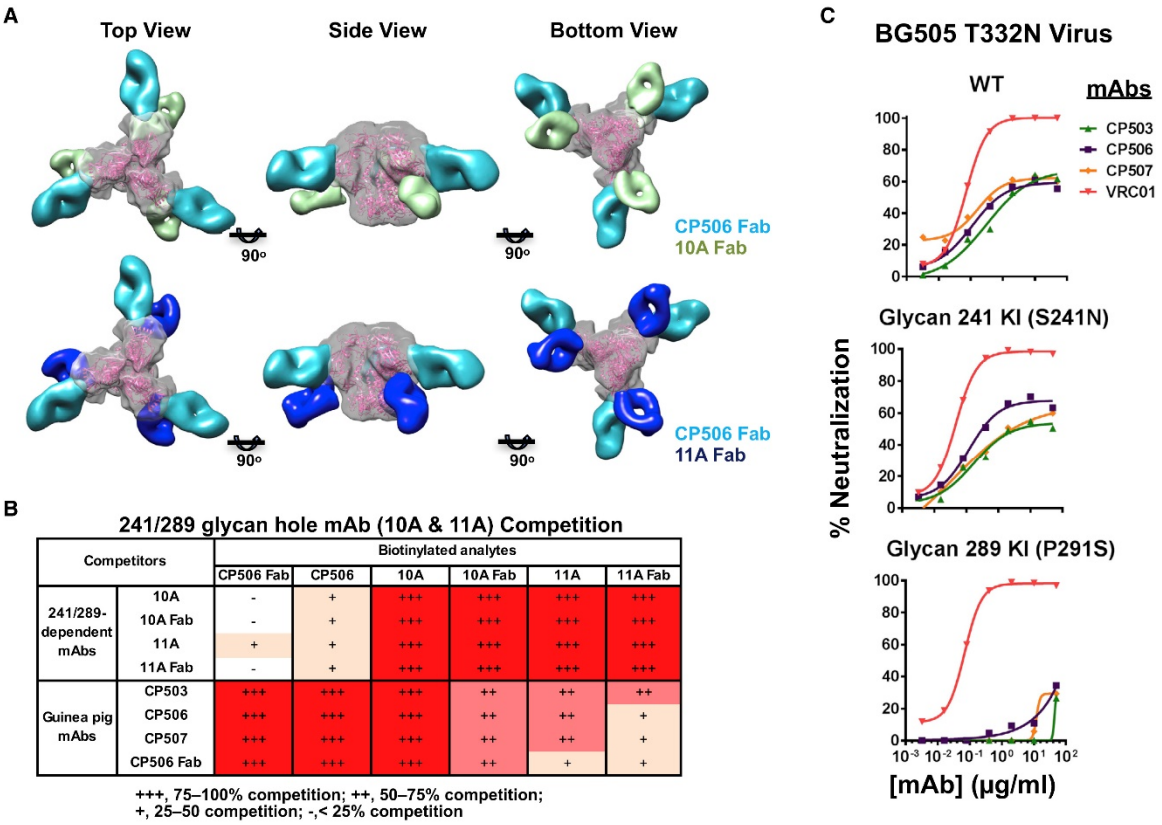


**Figure 3.7 CP506 epitope is different from the glycan-hole recognizing nAbs identified previously.** (A) Comparison of the mode of CP506 binding to BG505 SOSIP.664 trimer with rabbit antibodies 10A (EMD-8312) and 11A (EMD-8311), which recognize the 241/289 glycan hole. (B) Non-reciprocal competition between CP506 Fab and 10A or 11A Fab shown by competition ELISA. Data were generated in duplication with reactions of CP506Fab repeated at least twice. (C) The BG505 241 glycan knock-in (KI) mutation, S241N, has no effect on virus neutralization sensitivity to CP506 lineage nAbs, while the 289 glycan knock-in mutation P291S abolishes neutralization sensitivity. Viruses with BG505 T332N background were tested. WT, wildtype. VRC01 is used as a control antibody. Data were generated in duplication, with the mean of % Neutralization shown.

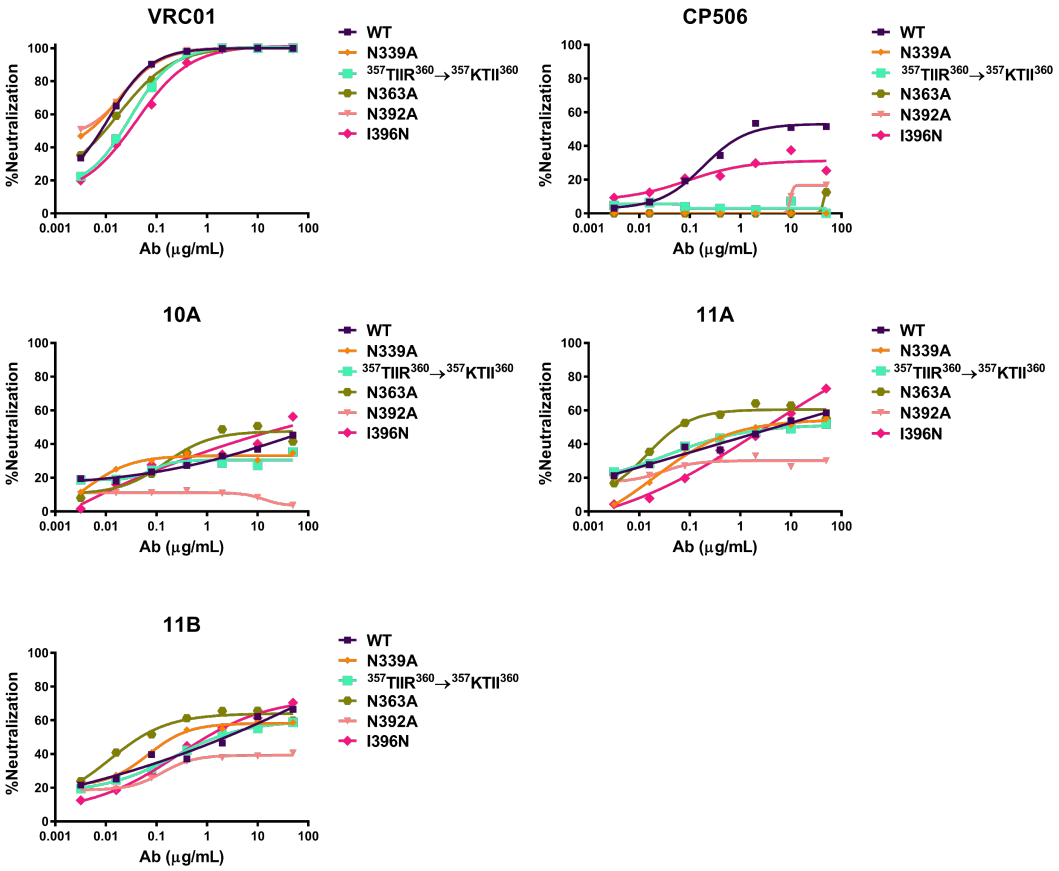


**Figure 3.8 Comparison of neutralization profiles between glycan-hole nAbs (10A, 11A, and 11B) and CP506 against five BG505 T332N Env-pseudotyped viruses bearing mutations on Env residues critical for the neutralization of CP506 lineage nAbs shown in Figure 3B. Related to Figures 3.6 & 3.7.** WT, BG505 T332N. CD4bs bNAb VRC01 served as positive control. Data shown as means of % neutralization were generated in duplication. Note that majority of the mutant viruses remain sensitive to neutralization mediated by glycan-hole nAbs, with the exception of N392A.

### 3.3.5 C3/V4 Region of Env trimer as a prominent immunogenic determinant

While the CP506 lineage nAbs were isolated from one guinea pig immunized with BG505 SOSIP.664 trimer (guinea pig 1567), we wanted to determine the prevalence of this strain-specific neutralizing response in other animals immunized with BG505 SOSIP.664 from the same study. Since plasma from animals 1563 and 1565 also displayed positive BG505 neutralization titers ($ID_{50}$ >10) along with that from animal 1567, they were screened against the BG505 Env mutant panel which was used for delineating the epitope

of CP506 lineage nAbs earlier in **Figure 3.6**. We measured the neutralization titers of plasma samples to each mutant virus ($ID_{50}$ mut) and compared with those to the BG505 T332N virus ($ID_{50}$ wt), which are reported as relative neutralization activity using the following formula: Relative Neutralization Activity = ($ID_{50}$ mut/ $ID_{50}$ wt)*100 (**Figure 3.10**). We found that the neutralization specificity of guinea pig plasma is largely represented by CP506 lineage nAbs. Similar to the CP506 lineage nAbs, all three plasma in this study showed substantially decreased neutralization titers against mutant viruses containing mutations on critical contact residues for CP506 nAbs, including the glycan N339 (N339A) and V4 loop β-strand mutants ($^{357}$TIIR$^{360}$→$^{357}$KTII$^{360}$; **Figure 3.10**). Besides that, N392A and I396N virus mutants showed reduced neutralization sensitivities to certain guinea pig plasma, especially in guinea pig 1567 from which CP506 nAbs were isolated (**Figure 3.10**). Moreover, like the CP506 lineage nAbs, all three guinea pig plasma displayed decreased neutralization activity to the 289-glycan KI mutant P291S (**Figure 3.10**). Two guinea pig plasma showed abolished neutralization to the 241-glycan KI mutant S241N, which is not sensitive to the neutralization of CP506 lineage nAbs (**Figure 3.10**), suggesting the co-existence of nAb responses to 241/289 glycan hole and CP506-like epitope. Furthermore, like the CP506 lineage nAbs, two animal plasma (1565 and 1567) were not able to neutralize wildtype virus MG505.A2 (**Figure 3.10**), whereas the MG505.A2 variant with the triple-mutation (E343G_$^{357}$TIIR$^{360}$→$^{357}$KTII$^{360}$_N396I) was sensitive to the neutralization of CP506 nAbs and plasma from these two guinea pigs (**Figure 3.10**). Likewise, plasma from animal 1563 showed >20-fold increased neutralization titer against the MG505.A2 virus bearing the triple-mutation compared to

the wildtype virus MG505.A2 (**Figure 3.10**). These observations highlight the prevalence of CP506-like nAb responses in different animals in the same study.

In addition to the virus neutralization assay stated above, to assess the prevalence of CP506-like antibody responses in this study, we performed antibody competition ELISA using plasma antibodies from three immunized animals (1563, 1565, and 1567) and one naïve animal (1749) as competitor to compete against biotin-labeled CP506 Fab, CP506 IgG, or 10A Fab, respectively, for BG505 SOSIP.664 binding. Plasma from all three animals immunized with BG505 SOSIP.664 trimer showed strong competition with CP506 Fab and IgG, while that from naïve animal displayed no binding inhibition (**Figure 3.11A**), which further confirmed the CP506-like antibody responses are prominent in these trimer-immunized animals.

Therefore, the epitope residues of CP506 clonal lineage in the BG505 Env C3/V4 region define a prevalent target of BG505-elicited nAb responses for different vaccinated guinea pigs in the same study. In addition, this pattern of specificity exists, regardless of the 241-dependent nAb responses (**Figure 3.10**).

In order to weigh the prevalence of the C3/V4 neutralizing responses observed here, we further compared the autologous neutralizing responses described in other immunogenicity studies (Klasse et al., 2018; Sanders et al., 2015) using BG505 SOSIP.664 trimer as the immunogen. In one study (Sanders et al., 2015), sera from more than 50% of animals immunized with BG505 SOSIP.664 trimer inhibited the binding of bNAbs such as VRC01, 3BC315, and 35O22 to BG505 Env trimer, respectively, which resembles the binding specificity of the guinea pig CP506 lineage nAbs isolated herein. Moreover, sera from more than 50% of the immunized rabbits displayed neutralization responses directed

to the C3 region of Env, evidenced by the substantially diminished serum neutralization activity after adsorption by BG505 gp120 carrying C3 region mutations (Sanders et al., 2015). Comparable neutralization profiles were found against a panel of alanine substituted viruses on the C3 and V4 regions among rabbits ((Sanders et al., 2015), **Figure 3.11B**). In particular, sera from rabbits 1410 and 1274, albeit with varied reactivity to the 241 glycan hole, showed sensitivities to viruses bearing mutations in the $^{357}$TIIR$^{360}$ motif (T357A, I358A, & R360A), N363A, and N392A, which are the common epitope residues for the CP506 clonal lineage (**Figure 3.11B**). In another study, all sera from the macaques immunized by BG505 SOSIP.664 trimer displayed reduced neutralization against mutant viruses with mutations in the C3 and V4 region (Klasse et al., 2018). These similarities in immune responses from different studies including ours further support the prevalence of the CP506-like nAb responses elicited by BG505 Env trimer in B cell repertoires from different species including small animals, macaques, and humans. Taken together, in addition to the 241/289-glycan hole, glycans and strain-specific residues on the C3 and V4 regions surrounding the CD4 binding loop of HIV-1 Env are prominent immunogenic determinants (**Figure 3.9A; Figure 3.9B**), as presented in the context of prototypical trimer immunogen BG505 SOSIP.664.

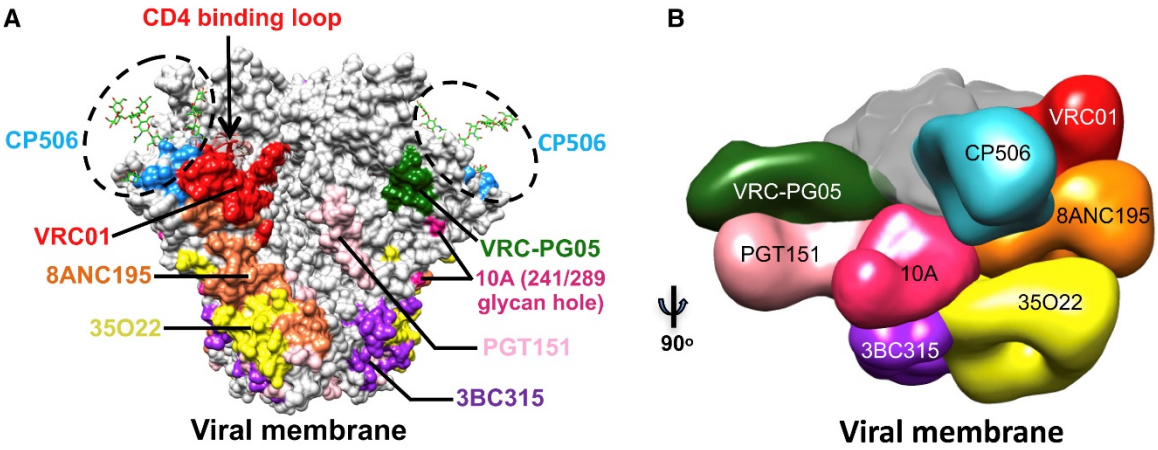

**Figure 3.9 CP506 lineage antibody epitopes on the Env trimer.** (A) Epitopes of the CP506-lineage antibodies, representative bNAbs, & 241/289 glycan hole targeting mAb 10A on the BG505 SOSIP.664 trimer surface (PDB: 4TVP), with side view of two protomers shown. (B) Binding site comparison of CP506 to selected bNAbs and 241/289 glycan hole targeting mAb 10A on 3D EM reconstruction in complex with the BG505 SOSIP.664 trimer. To simplify the view, only antibodies bound with one protomer are depicted.

| Virus strains | | | Guinea pig plasma neutralization (relative to BG505 T332N virus %) | | | $IC_{50}$ (μg/ml) | | | |
|---|---|---|---|---|---|---|---|---|---|
| | | | | | | mAbs from guinea pig 1567 | | | bNAb |
| | | | 1563 | 1565 | 1567 | CP503 | CP506 | CP507 | VRC01 |
| BG505 T332N | Env region | WT | 100 | 100 | 100 | 1.77 | 1.04 | 0.45 | 0.04 |
| | C3 | N339A | 18 | 31 | 35 | >50 | >50 | >50 | 0.06 |
| | | G343E | 13 | 34 | 49 | 2.66 | 0.65 | 0.5 | 0.06 |
| | | N355A | 26 | 37 | 36 | 0.09 | 0.07 | 0.12 | 0.06 |
| | | $^{357}$TIIR$^{360}$→ $^{357}$KTII$^{360}$ | 29 | 26 | 33 | >50 | >50 | >50 | 0.07 |
| | | N363A | 103 | 73 | 92 | >50 | >50 | >50 | 0.06 |
| | V4 | N392A | 92 | 58 | 46 | >50 | >50 | >50 | 0.05 |
| | | I396N | 23 | 451 | 41 | >50 | >50 | >50 | 0.04 |
| | | N398A | 1551 | 649 | 127 | 0.16 | 0.09 | 0.06 | 0.02 |
| | | N406A | 173 | 966 | 161 | 0.66 | 0.5 | 0.46 | 0.02 |
| | | N411A | 437 | 34 | 36 | 1 | 1.03 | 0.82 | 0.02 |
| | Glycan hole | S241N | 82 | NN | NN | 1.14 | 0.35 | 0.71 | 0.06 |
| | | P291S | NN | NN | NN | >50 | >50 | >50 | 0.07 |
| MG505 A2 | Env region | WT | 100 | NN | NN | >50 | >50 | >50 | 0.05 |
| | Glycan hole | K241S | 123 | NN | NN | >50 | >50 | >50 | 0.03 |
| | C3 | E343G | 133 | NN | NN | >50 | >50 | >50 | 0.03 |
| | C3 | $^{357}$KTII$^{360}$→ $^{357}$TIIR$^{360}$ | 168 | NN | NN | >50 | >50 | >50 | 0.05 |
| | V4 | N396I | 130 | NN | NN | >50 | >50 | >50 | 0.04 |
| | C3/V4 | Triple mutations* | 2889 | *756 ($ID_{50}$)* | *734 ($ID_{50}$)* | 0.94 | 0.42 | 0.52 | 0.03 |

*Triple mutations: E343G_$^{357}$TIIR$^{360}$→ $^{357}$KTII$^{360}$_N396I

**Figure 3.10 Prevalence of CP506-like nAb responses in all three guinea pigs whose polyclonal plasma possess BG505 neutralization capacity in the same study.** Guinea pig NAbs (from one animal) and week 46 plasma (from three animals) were tested against a panel of BG505 and MG505 mutant viruses. Plasma neutralization profiles are shown as relative titer (percentage) for mutant viruses compared to BG505 T332N WT virus using the following formula: relative neutralization activity = (ID50 mut/ID50 wt) × 100. Relative neutralization titers <50% of the WT virus are highlighted in blue. The acquisition of neutralization sensitivity to MG505 mutant is highlighted in green. NN, no neutralization. Data were generated in duplication, with the mean of relative neutralization activity (plasma) or IC50 titers (mAbs) shown.

**A**

**nAbs competition with animal plasma**

| Competitors | | Biotinylated analytes | | |
|---|---|---|---|---|
| | | CP506 Fab | CP506 | 10A Fab |
| Guinea pig plasma | 1563 | +++ | +++ | ++ |
| | 1565 | +++ | +++ | +++ |
| | 1567 | ++ | ++ | ++ |
| | 1748 (Naïve) | - | - | - |

+++, 75–100% competition; ++, 50–75% competition;
+, 25–50 competition; -,< 25% competition

**B**

| Env Region | Mutation | Rabbit sera neutralization reduced >2-fold to mutant virus (Sanders *et al*., 2015) | | | | | | | | |
|---|---|---|---|---|---|---|---|---|---|---|
| | | #1256 | #1257 | #1274 | #1279 | #1284 | #1409 | #1410 | #1411 | #1412 |
| C3 | N339A | | | | | | ND | ND | ND | ND |
| | T357A | | | + | | | | + | | |
| | I358A | + | | + | | | + | | | + |
| | R360A | + | + | | | | + | + | | + |
| | N363A | | | + | | | | + | | |
| V4 | N392A | | + | + | | + | | + | | |
| | I396A | + | | + | + | | | + | | + |
| | N398A | | | | | | + | + | | + |

**Figure 3.11 Autologous nAb responses targeting the C3 and V4 region of BG505 SOSIP.664 trimer in vaccinated animals. Related to Figure 3.10. (A)** Antibody competition ELISA using plasma from three BG505 SOSIP.664-immunized animals (guinea pigs 1563. 1565, and 1567) and one naïve guinea pig (1749) as competitors against biotin-labeled CP506 Fab, CP506 IgG, and 10A Fab. The degree of competition is calculated by biotin binding signal reduction (in percentage) in the absence and presence of a given competitor sample. Data were generated in duplication. **(B)** Sera from rabbits immunized with BG505 SOSIP.664 with autologous neutralization capacity were tested for neutralization against a panel of mutant viruses (with BG505 T332N background) bearing mutations in the C3/V4 region (generated in the previous study, Sanders et al., 2015). BG505 T332N is used as the control (wildtype, WT). Serum neutralization titers reduced >2-fold to mutant viruses compared to the WT virus are marked with "+". Rabbit sera containing nAb response directed to residues 354-363 on the C3 region described in Sanders *et al*., 2015 are listed in green font. Rabbits 1410 and 1411 are the animals from which 241/289 glycan hole dependent nAbs, 10A and 11A, were isolated. ND: not determined. CP506 critical contact residues are listed in red font.

### *3.4 Discussion*

The prototypical current generation of native-like HIV-1 Env trimer immunogens frequently elicit nAb responses to primary virus isolates with Env matched with the immunogen (autologous responses), while bNAb responses remain elusive. In this study, to inform immunogen design aiming at improving the elicitation of cross-nAb responses, we delineated the autologous tier 2 neutralization specificity induced by BG505 SOSIP.664

in guinea pigs by our recently established antigen-specific single B cell sorting and RT-PCR cloning method (Lei et al., 2019a). From one immunized guinea pig, we identified a clonal lineage of BG505-specific nAbs, namely CP506 lineage that target the C3 and V4 region flanking the CD4 binding loop on HIV-1 Env and largely recapitulate the concurrent guinea pig immune sera neutralization capacity described previously (Feng et al., 2016). Moreover, we found that the CP506-like nAb responses are prevalent in all of the sera from guinea pigs displaying BG505 autologous neutralization capacity in the same study. Thus, BG505 SOSIP.664 trimer consistently elicits prominent autologous neutralization responses in guinea pigs focusing on an epitope consisting of several potential N-glycosylation sites (N339, N392, and N363) and residues on two β-strands within the C3 and V4 regions of BG505 Env trimer at the periphery of CD4 binding site. Our findings are consistent with the previous observations in which the C3/V4 region of BG505 Env is prominent neutralization epitope during natural infection (Sanders et al., 2015; Wu et al., 2006) and immunization (Klasse et al., 2018; Sanders et al., 2015).

Current HIV immunogen design strategies have successfully induced potent strain-matched tier 2 nAb responses in animal models (Bradley et al., 2016; Crooks et al., 2015; Hessell et al., 2016; Martinez-Murillo et al., 2017; McCoy et al., 2016; Sanders et al., 2015). In these studies, a few HIV-1 tier-2 nAbs have been isolated and characterized from vaccinated rabbits and macaques. The neutralizing epitopes identified vary depending on the corresponding immunogens, which include the V2 loop of clade C virus isolate 16055 (Martinez-Murillo et al., 2017), loop E, the V5 loop around the CD4bs of Env derived from a transmitted/founder virus variant (Bradley et al., 2016), and the 241/289 glycan hole of BG505 Env (McCoy et al., 2016). BG505-based immunogens naturally lack two conserved

glycan sites at 241 and 289, which forms an immunogenic target for neutralizing antibodies (McCoy et al., 2016). A large subset of BG505 SOSIP.664 immunized animals have shown neutralization specificity to the 241/289 glycan hole (Klasse et al., 2018; McCoy et al., 2016). Nevertheless, it only partially recapitulates the sera neutralization responses observed in the studies stated above, while there is another prominent neutralization specificity targeting the C3/V4 region, as represented by the CP506-like nAbs identified in this study. Therefore, there are two prominent autologous neutralizing epitopes on BG505 SOSIP.664 trimer: the 241/289 glycan hole identified in previous studies and the epitope of "3 glycans & 2 strands" targeted by CP506-like nAbs revealed in this study, with the epitope of the CP506-like nAbs adjacent to the 289 glycan hole (**Figure 3.9A, 3.9B**).

As a member of the CP506 clonal lineage, CP506 Fab competes strongly with CD4bs bNAb VRC01 (**Figure 3.4A**), consistent with the notion that the epitope of CP506-like mAbs is at the periphery of CD4 binding loop (**Figure 3.6A, 3.6C**). It was reported that sera from animals immunized with BG505 or JR-FL Env trimers inhibit VRC01 binding, which suggests that the sera contain antibodies with epitopes in the vicinity of the CD4bs (Crooks et al., 2015; Sanders et al., 2015). In our study, negative EM analysis clearly presents a horizontal angle of approach of CP506 Fab to the C3 and V4 region on HIV-1 gp120 subunits. Superimposition of this EM 3D reconstruction data with the crystal structure of the VRC01-BG505 SOSIP.664 complex reveals that CP506-like mAbs interact with the viral spike on a similar axial plane, however, with a shifted footprint near the CD4bs (**Figures 3.4 & 3.6**). Although CD4bs-directed bNAbs can be generated in natural infection (Huang et al., 2016; Li et al., 2007; Wu et al., 2010), the CD4bs is partially occluded by V1/V2 loops and flanking N-linked glycans (Burton and Parren, 2000;

Stewart-Jones et al., 2016). Autologous nAbs that contain epitopes overlapping with the CD4bs often make contact with variable residues on the Env to achieve strain-specific Env binding and neutralization (Bradley et al., 2016; Wibmer et al., 2016). Here, we note that BG505 glycan N363, a residue critical for CP506 recognition, is right adjacent to the CD4 binding loop and directly in contact with CD4bs bNAb VRC01 (Stewart-Jones et al., 2016). Thus, the notion that autologous nAbs hitting the periphery of the HIV-1 receptor binding site is consistent with our findings.

The epitope of CP506-like nAbs contains two conserved glycans (N339 and N392), along with other Env surface residues more specific for BG505 strain, which accounts for the limited neutralization breadth. Interestingly, the BG505 virus strain was isolated from a 6-week old infant, who developed broadly nAb response against an uncharacterized epitope within 2 years of infection (Goo et al., 2014; Wu et al., 2006). The template sequence of BG505 SOSIP.664 was isolated from week 6 post-infection. The sera of this infant at subsequent time points contained virus escape variants with Env sequences highly divergent from BG505 (Goo et al., 2014; Wu et al., 2006). The C3 and V4 were the exact regions under extensive selection pressure. At week 14, of three mutated residues, two residues at 358 and 396 (**Figure 3.6A**) are part of the epitope of CP506 clonal lineage (Goo et al., 2014; Sanders et al., 2015). At month-27, there were seven primary changes in the C3 region from residues 354 to 363 (**Figure 3.6A**), which include four mutations (T357K, I358T, R360I, and N363K) (**Figure 3.6C**) largely overlapping with critical contact residues for CP506-like nAbs (Sanders et al., 2015). Thus, CP506-like nAb response may be elicited in this infant, which imposed pressure on BG505 infant viruses leading to viral escape, a hypothesis that merits further investigations. Accordingly, the BG505 mutant virus panel

shown in **Figure 3.6A** will be useful to delineate CP506-like neutralization specificity of sera from HIV-1 infected individuals.

Nevertheless, the similarities between the nAb responses targeting the C3/V4 region of BG505 Env during natural infection as well as immunization in animal models suggests that the C3 region is quite immunogenic. Moreover, at least in early subtype C infection described previously, the C3 region is reported as a predominant nAb target due to its increased exposure caused by selection pressures from nAb responses (Moore et al., 2008, 2009). From the perspective of immunogen design, considering the prominent immunogenicity of the C3/V4 region, further modifications in this region may lead to the elicitation of nAb responses with improved breadth. For example, the strain-specific residues in the BG505 SOSIP.664 C3/V4 region (e.g., $^{357}$TIIR$^{360}$ & I396, **Figure 3.6C**) could be replaced by more conserved residues derived from representative HIV-1 virus Envs, which may result in chimeric BG505 SOSIP.664 trimer to elicit cross-reactive nAb responses at high titers. In addition, since CP506-like nAbs compete with a number of bNAbs including VRC01 (CD4bs) and 3BC315 (gp120/gp41 interface), the prevalence of such strain-specific antibody responses in immunization may impede the elicitation of bNAb responses. Thus, modifications based on the CP506 epitope could also help mask or dampen these strain-specific immune responses.

In summary, we report here a prominent strain-specific neutralizing epitope on the Env of HIV-1 primary isolate BG505 encompassing the C3 (periphery of CD4bs) and V4 (silent face) region, as revealed by three autologous tier 2 nAbs isolated from a guinea pig immunized with BG505 SOSIP.664. This type of Env epitopes consisting of both conserved and variable structural elements have frequently been targeted during natural

infection in humans and immunization in guinea pigs, rabbits, and non-human primates. Our finding highlights the challenge and opportunity to the efforts of immunogen design for the elicitation of bNAb responses, an important component of HIV vaccine development.

# Chapter 4: HIV-1 Broadly Neutralizing Antibody VRC01 Donor-Derived Germline-Targeting Env Immunogens Activate and Drive Affinity Maturation of VRC01 Precursors in Transgenic Mice

***Synopsis***

In this chapter, we engineered novel immunogens based on an HIV-1 Env (45_01dG5) isolated from the donor of broadly neutralizing antibody (bNAb) VRC01. We observed improved binding affinity of the VRC01 germline antibody to our designed immunogens, suggesting their potential to activate the germline precursor B cells in vivo. To recapitulate the naturally occurring VRC01 response, we proposed sequential immunization strategies in the VRC01-germline heavy and light chain knock-in mouse model (VRC01gHL). The successive prime-boost immunogens elicited focused VRC01-like serum antibody responses. We further interrogated Env-specific single B cells and observed clustered VRC01/VRC01-class somatic mutations in the antibody variable region sequences. Moreover, VRC01 lineage mAbs from the transgenic mice neutralized selected viruses with the N276 glycan, a critical roadblock for VRC01 maturation. Overall, the results demonstrate that our specifically designed immunogens and immunization strategies shepherd affinity maturation toward VRC01-like bNAbs. The patient-derived immunogens in the study may serve as prototypes for future modification to address the restricted neutralization breadth and potency.

***4.1 Introduction***

VRC01-class broadly neutralizing antibodies (bNAbs) target the functional conserved CD4 binding site (CD4bs) and potently neutralize up to 90% of HIV-1 primary strains (Huang et al., 2016). The functions, sequence signatures, structures, and ontogenies of this bNAb class have been well elucidated (Bonsignori et al., 2016, 2018; Gristick et al., 2016; Huang et al., 2016; Hwang et al., 2017; Klein et al., 2012; Kong et al., 2016b; Li et al., 2011; Scheid et al., 2011; Torres et al., 2015; West et al., 2012; Wu et al., 2010, 2015;

Zhou et al., 2010, 2013, 2015; Zhu et al., 2013). VRC01-class bNAbs exhibit many characteristics as attractive leads for HIV immunogen design (Wibmer et al., 2015). For example, multiple donors developed the bNAbs through similar maturation pathways, which suggests reproducible vaccine elicitation (Zhou et al., 2013). The VH1-2 germline alleles, which are exclusively used by VRC01 bNAbs, exist in ~96% of humans and are frequently employed by all human antibodies (~3%) (Briney et al., 2016; Jardine et al., 2015; Sok et al., 2016). Besides, several different light chain germline genes are compatible with the VH1-2-derived heavy chains (Zhou et al., 2013). The heavy chain complementarity-determining region 3 (CDRH3) in VRC01-class bNAbs is also much shorter than those of most other bNAb classes (Bonsignori et al., 2018; Wu et al., 2010, 2015; Zhou et al., 2010, 2013, 2015; Zhu et al., 2013), which might be more feasible to achieve via vaccination. All these features favor the VRC01-class bNAbs as a vaccine template.

Nevertheless, VRC01-class bNAbs also display unique features that pose roadblocks for vaccine development. VRC01-class bNAbs typically require years to develop and thus often accumulate high levels of somatic hypermutation (up to 42% in nucleotide sequence) (Umotoy et al., 2019). The signature 5-aa short light chain CDR3s are unusual in naive human B cell repertoires. Therefore, the natural frequency of the VRC01-like naïve B cells is extremely low (1 in 2.4 million) (Abbott et al., 2018; Havenar-Daughton et al., 2018; Jardine et al., 2016a; Silva et al., 2017). Another significant roadblock that hinders the elicitation of VRC01-like bNAbs is the glycans surrounding the CD4 binding site (CD4bs). N-linked glycans (NLGS) at position 276 in loop D as well as glycans 460 and 463 in the V5 region, in particular, occlude the CD4 binding loop (Borst

et al., 2018; Diskin et al., 2011; Kong et al., 2016b; Li et al., 2011; McGuire et al., 2016; Umotoy et al., 2019; Wibmer et al., 2016). Matured VRC01-class bNAbs eventually overcome these glycans through extensive affinity maturation, which generate deletions or glycine substitutions in light chain CDR1 (CDRL1) to avoid clashes with the glycans around the CD4bs (Gristick et al., 2016; Scharf et al., 2016). However, these glycans prevent activation and maturation of VRC01-class antibodies due to their unfavorable interactions with the CDRL1 (Borst et al., 2018; Diskin et al., 2011; Kong et al., 2016b; Li et al., 2011; McGuire et al., 2016; Umotoy et al., 2019; Wibmer et al., 2016). Native Env trimer reconstructs on the background of different clade sequences failed to engage inferred germline precursors of VRC01-class bNAbs without further modification (Bonsignori et al., 2018; Hoot et al., 2013; Jardine et al., 2013; Kong et al., 2016b; McGuire et al., 2013; Scheid et al., 2011; Zhou et al., 2015). Therefore, a specific group of immunogens has been engineered to initiate the activation of VRC01 precursor B cells (Havenar-Daughton et al., 2018; van Schooten and van Gils, 2018; Stamatatos et al., 2017). The modification strategies usually involve the elimination of the glycans mentioned above to expose the CD4bs and retrieve the reactivity of Env mimics against VRC01-class bNAb precursors (McGuire et al., 2013, 2016; Stamatatos et al., 2017). The immunogens capable of binding VRC01-class germline precursor antibodies are termed as “VRC01-class germline-targeting immunogens”.

As genetically unmodified animal models have no human VH1-2*02 allele orthologs (Parks et al., 2019; Stamatatos et al., 2017), they are impractical for initial germline-targeting immunogen evaluation and selection before clinical assessment. Humanized immunoglobulin mice developed recently, on the other hand, carry abundant

bNAb precursor B cells and provide more effective platforms to assess and iteratively refine HIV immunogens (Verkoczy et al., 2017). Immunization studies in knock-in mouse models have successfully enriched antibody responses to the bNAb epitopes and obtained sequence features in resemblance to affinity matured bNAbs (Abbott et al., 2018; Dosenovic et al., 2015; Escolano et al., 2016; Jardine et al., 2015; McGuire et al., 2016; Parks et al., 2019; Saunders et al., 2019; Sok et al., 2016; Verkoczy et al., 2017). In particular, sequential immunization with PGT121 germline-targeting and native trimer immunogens elicited V3-directed bNAb responses in the mouse models contain either the germline-reverted version of PGT121 (glPGT121) B cells or PGT121 intermediate (mature PGT121 pair with glPGT121 LC) B cells (Escolano et al., 2016). With regards to initial germline-targeting immunogen screening for VRC01-like bNAbs, four different knock-in (KI) mouse models have been generated (Verkoczy et al., 2017). One KI mouse model (VH1-2) was developed by replacing the mouse VH81X gene segment at the murine IgH locus with the VH1-2*02 germline gene. In this model, around 45% of peripheral B cells encode the VRC01 VH germline, while the CDRH3s vary due to the recombination with mouse D and J segments (Tian et al., 2016). As the number of VRC01 precursors in the VH1-2 KI model is limited, another mouse model that contains higher VRC01-like germline B cells was developed based on the VH1-2 model generated (Verkoczy et al., 2017). In this model (VH1-2/LC), the murine Jk segment was further substituted by the full-length V(D)J exons of the germline VRC01 light chain (gl-VRC01LC). KI mice expressing the rearranged VRC01 germline heavy chain (gl-VRC01HC) were also generated. In this model (VRC01gH), the mouse JH locus was replaced by the glVRC01HC, while the LC repertoire remains naïve (Jardine et al., 2015; Verkoczy et al., 2017). 85% of

B cells express gl-VRC01HC, and around 0.1% LCs contain the VRC01 signature five-amino-acid (AA) long CDRL3s (Jardine et al., 2015). This model might be more feasible to analyze the effectiveness of selecting VRC01-like LCs by the immunogens. Immunization with eOD-GT8 in this model enriched VRC01 like B memory B cells. 92% of CD4bs B cells isolated composed of LCs with 5 AA CDRL3s and carried a partial VRC01 motif QQYXX, suggesting the activation of VRC01 precursor B cells. However, CD4bs-specific antibodies displayed no neutralizing activity due to limited SHM levels (Jardine et al., 2015)

In this study, to evaluate the immunogenicity of patient-derived immunogens, we utilized a heterozygous VRC01 germline knock-in mouse model (VRC01gHL), where both VRC01 germline heavy and light chains were knocked into the murine IgH and IgK loci. B cells encoding the germline-reverted VRC01 BCRs develop normally and are responsive to antigen stimulation (Abbott et al., 2018). In addition, the mouse model expresses an exceptionally high level of germline-reverted VRC01 (glVRC01) B cells ( ~33% of B cells bind to VRC01-specific immunogen eOD-GT8) in the periphery (Abbott et al., 2018). We hypothesized that the CD4bs neutralizing antibody responses could be enriched explicitly by vaccination in the VRC01gHL model with Env immunogens derived from HIV-1 infected individuals displaying substantial CD4bs-specific neutralization breadth. We engineered Env trimers based on an HIV-1 Env isolated from patient 45 (45_01dG5), from whom CD4bs bNAb VRC01 was isolated (Lynch et al., 2015; Wu et al., 2010). These immunogens obtain detectable binding affinities for glVRC01, a germline-reverted version of the mature bNAb VRC01, thus may stimulate CD4bs-specific antibody response superior to prototypical immunogens, for example, BG505 SOSIP.664. We then

immunized the VRC01gHL mice with designed immunogens in a sequential format and examined the quality of the elicited immune response at both the repertoire and clonal levels. We show that the VRC01-like B cell precursors have been activated during vaccination with our novel immunogens. Moreover, the germline-targeting sequential immunization strategy guided further affinity maturation toward bNAb VRC01, and clustered VRC01/VRC01-class antibodies mutations were generated in both heavy and light chains of antibody sequences. Therefore, dG5-based Env immunogens in this study provide alternative templates for future refinement to elicit CD4bs-focused bNAb responses.

## *4.2 Materials and Methods*

### 4.2.1 HIV Env-based Protein Production

45_01dG5 Env sequence was extracted from Genbank (GenBank: JQ609687.1). dG5-based soluble Env trimers were engineered in SOSIP (Sanders et al., 2013) and NFL formats (Sharma et al., 2015) with sequence modifications, respectively. BG505 trimer-derived (TD) mutations were introduced into dG5 NFL sequences to increase trimer pre-fusion stability and propensity (**Figure 4.2**). K278T mutation was introduced into dG5 NFL TD construct to restore the glycan N276. To generate dG5-based ferritin constructs, dG5 Env fragments were fused to *Helicobacter pylori*-bullfrog hybrid ferritin sequences (Kanekiyo et al., 2015) with a G4S linker, an HA tag (YPYDVPDYA), a G4S linker, a His tag (HHHHHH), and a GSG linker.

Env proteins were expressed by co-transfection of expression vectors with furin (for Env trimers in SOSIP format) or without furin (for constructs in NFL format) in FreeStyle 293F cells with 293fectin transfection reagent (Life Technologies) as described

previously (Guenaga et al., 2015). Cell culture supernatants were collected 5 days post-transfection for native trimers or 6 days post-transfection for Env-based ferritin particles. Proteins were then purified with *Galanthus nivalis* lectin-agarose (Vector Laboratories) columns followed by size exclusion chromatography (SEC) on Hiload 16/60 Superdex 200 pg column (GE Healthcare) or superdex 200 increase 10/300 GL (GE Healthcare).

Antigen probes used for single B cell sorting (eOD-GT8, eOD-GT8 D279K_D368R) were biotinylated by BirA biotin-protein ligase standard reaction kit (Avidity) per manufacturer's instructions. Excess biotin was removed by five times of buffer exchange in Amicon ultra 10K concentrators. Antigenicity of the Emv-based proteins was assessed by ELISA analysis with well-characterized mAbs as described previously (Doria-Rose et al., 2009).

### 4.2.2 Mouse Immunization and Sampling

The animals (N = 5/group) were immunized four times, with 10 ug of immunogens formulated in the Ribi adjuvant, as illustrated in **Figure 4.4A**. Three experimental groups (Group A, Group B, and Group C) were primed two times with different immunogens on weeks 0 and 2, and then boosted by dG5 NFL TD_PADRE trimer with 276 glycan on week 5, and 9, all via the intraperitoneal route. During the sequential immunization, two random animals from each group were sacrificed at week 5 to evaluate the VRC01-class B cell activation after priming. Splenocytes for the rest of the animals were isolated and purified by density gradient centrifugation with Ficoll-Paque PLUS (GE Healthcare) on week 13. Blood samples were collected at weeks 0, 3, 4, 5 10, and 13. All mouse experiments were done with the approval of the IACUC committees of TSRI.

### 4.2.3 Heterozygous VRC01$^{gHL}$ Mice Antigen-Specific Single B Cell Sorting

VRC01$^{gHL}$ KI mouse splenocytes were thawed and resuspended in 10 ml of pre-warmed RPMI 1640 medium (Gibco) supplemented with 10% FBS (Gibco) (R10) and 10 µl of DNase I (Roche). The cells were washed and re-suspended with 45 µl of pre-chilled phosphate-buffered saline (PBS). Cell staining was performed as described in (Lei et al., 2019a). Briefly, 5 µl of 40-fold water-diluted pacific blue or Live/dead fixable aqua dead stain (Invitrogen) was added to the cells followed by incubation in the dark at 4°C for 10 min. The cells were further stained by adding 50 µl of cell marker antibody/antigen cocktails in R10 medium at 4 °C for 1 hour. Cells were passed through a 70 µm cell strainer (BD Biosciences) before cell sorting. The class-switched IgG+ single B cells with the desirable phenotype (pacific blue +/ H57-597_PerCP-Cy.5 -/ IgM & IgD_APC -/ IgG1,2a,2b_FITC +/ eOD-GT8_PE +) for week 5 splenocytes and the phenotype (Aqua blue -/ CD19_APC-Cy7 +/ CD3 & F4/80 & Gr1_PerCP-Cy.5 -/ IgM_PE-Cy7 +/ IgD_PB -/ B220_APC-Cy5.5 +/ IgG1,2a,2b_Alexa 594 +/ eOD-GT8_PE +/ CD4bs KO_APC -) for week 13 splenocytes were then isolated by a FACS Aria III cell sorter (BD Biosciences).

### 4.2.4 VRC01-KI Mouse Single B Cell RT-PCR

Single B cells were sorted into Cells-to-cDNA™ cell lysis buffer (Thermo Fisher) followed by an inactivation step (75°C for 10 minutes). cDNA synthesis and the first of the nested PCR reaction were carried out by OneStep *Ahead* RT-PCR Kit (Qiagen) according to manufacturer's instructions. In brief, 1 µl of primer mixture for both VRC01-class heavy and kappa chains was added into 5 µl cell lysis along with the master mix and buffer in the kit to a 20 µl final reaction volume. Two primers were designed to amplify kappa chains:

KF and KR (**Figure 4.1**). Four primers were used for 1st heavy chain amplification: H4, IgGR1, IgGR2a, and IgGR2b (**Figure 4.1**). IgGR1, IgGR2a, and IgGR2b are three reverse primers specific to the constant region of IgG and were pooled evenly into a mixture (IgGRs) at the concentration of 25 µM. IgGRs were then combined with the rest three primers (H3, KF, and KR) in an equal molar amount (25 µM) as the final primer pool for 1st PCR. The RT-PCR program was set as the following: 10 min at 50°C, 5 min incubation at 95°C, followed by 45 cycles of 10 sec at 95°C, 10 sec at 57°C, and 10 sec at 72°C with a final elongation at 72°C for 2 min before cooling to 4°C.

The PCR products of the 1st reaction were then diluted 5 times with nuclease-free water and 12 µl was used as the template for heavy or kappa chain 2nd nested PCR reaction. The 2nd nested PCR reaction was performed in a 25 µl mixture consisting of 12 µl template, 2.5 µl of 10X PCR Buffer (Qiagen), 0.5 µl of 10 mM dNTPs (Sigma), 1 Unit of HotStar Taq Plus (Qiagen), 0.5 µl of 25 µM 5' primer (Nterm2_inner or T3_KF), 0.5 µl of 25 µM 3' primer(Cterm2_inner or T7_KR) (**Figure 4.1**), and 5 µl 5X Q-solution without $MgCl_2$ in 25 µl of volume. All 2nd nested PCR reactions were incubated at 94 °C for 5 min followed by 50 cycles of 94 °C for 30 s, 57 °C for 30 s, and 72 °C for 1 min with a final extension at 72 °C for 7 min before held at 4 °C. The 2nd PCR products were evaluated on 2% 96-well E Gels (Life Technologies). Positive wells were identified followed by PCR product purification and sequencing using T7 for kappa chains and both Cterm2_inner and Nterm2_inner for heavy chains.

### 4.2.5 Antibody Sequence Data Analysis

Sequence data was initially annotated by V-Quest through IMGT with the human Ig germline database as the reference to delineate CDR boundary. Subsequently, IgBLAST

was used to determine the closest functional V, D, and J segments using an in-house guinea pig germline database derived from the work of Guo et al (Guo et al., 2012). For the phylogenetic analysis, the sequences were aligned by vectorNTI Advance 11.5 (ThermoFisher). The tree files were configured and drawn in iTOL v5 (https://itol.embl.de/).

### 4.2.6 VRC01-KI Mouse Ab Cloning and Expression

Purified heavy and kappa chain PCR products were subjected to cloning PCR amplification as described in (Lei et al., 2019b) by corresponding seamless cloning primer sets (**Figure 4.1**), which contain glVRC01 heavy or kappa chain gene-specific sequences and additional overhangs identical to the sequences in the human IgG1 expression vectors (Tiller et al., 2008). The cloning PCR reaction was performed in a total volume of 50 µl with high-fidelity DNA polymerase (Roche). The PCR reaction mixture consisted of 1 µl of DNA template, 5 µl of 10X reaction buffer, 1 µl of 10 mM dNTPs, 1 µl of 25 µM of 5' and 3' cloning primers, 1 µl of high-fidelity DNA polymerase (Roche) and nuclease-free water. The PCR program had an initial denaturation at 95°C for 3 min, followed by 20 cycles of 95°C for 30 s, 50°C for 30 s, and 68°C for 2 min. There was a final extension step at 68°C for 8 min. Positive cloning PCR products were then purified and assembled into expression vectors with GeneArt assembly enzyme mix kit (Invitrogen) per manufacturer's instructions. For monoclonal antibodies production, an equal amount of heavy- and light-chain expression vectors were transfected into 293F cells with 293fectin transfection reagent (Life Technologies). Supernatants were harvested 4 days post-transfection followed by purification with Protein A Sepharose columns (GE Healthcare).

**RT and 1st nested PCR primers:**
**Heavy chain**
H4: TGCAGTCTGGGGCTGAGGTGAA
IgGR1: CAGATGGGGGTGTCGTTTTGGCTGA
IgGR2a: CTGATGGGGGTGTTGTTTTGGCTGA
IgGR2b: CCGATGGGGCTGTTGTTTTGGCTGA

**Kappa chain**
KF: GTCATATTGTCCAGTGGAGAAATTGTGTTGAC
KR: ACTGCTCACTGGATGGTGGGAAGATGG

**2nd nested PCR primers:**
**Heavy chain**
Nterm2_inner: GGGGCTGAGGTGAAGAAGCC
Cterm2_inner: GGAGACGGTGACCAGGGTGCCC

**Kappa chain**
T3_KF: ATTAACCCTCACTAAAGGGAtGTCATATTGTCCAGTGGAGAAATTGTGTTGAC
T7_KR: TAATACGACTCACTATAGGGtTGCTCACTGGATGGTGGGAAGAT

**Seamless cloning primers:**
**Heavy chain**
SL_VH_VRC01GL_for:
TTTCTAGTAGCAACTGCAACCGGTGTACATTCTCAGGTGCAGCTGGTGCAGTCTGGGGCTGAGG
TGAAGAAGCCTGG
SL_VH_VRC01GL_rev:
AGACCGATGGGCCCTTGGTCGACGCTGAGGAGACGGTGACCAGGGTGCCCTGG

**Kappa chain**
SL_VK_VRC01GL_for:
TTTCTAGTAGCAACTGCAACCGGTGTACATTCTGAAATTGTGTTGACACAGTCTCCAGCCACCC
SL_VK_VRC01GL_rev:
CAGATGGTGCAGCCACCGTACGTTTGATCTCCAGCTTGGTGCCC

**Figure 4.1 Primers designed for KI mice single B cell RT-PCR and antibody cloning.**

### 4.2.7 ELISA Binding Assays

The binding specificity of the VRC01-class mAbs isolated from KI mice was tested against HIV Env proteins (dG5 NFL TD, CoreD-n5i5-17b, dH5 SOSIP, BG505 SOSIP T278A, CoreD, dG5 NFL TD K278T, 426c SOSIP, BG505 SOSIP, and Core) by ELISA as described previously (Lei et al., 2019b). MaxiSorp 96-well plates (Nunc, Thermo Scientific) were directly coated with HIV Env gp120-based proteins (Core, CoreD, and), at 2 μg/ml in 100 μl of phosphate-buffered saline (PBS) at 4°C overnight, followed by blocking with blocking buffer (PBS containing 5% FBS/2% non-fat milk). For HIV-1 Env

trimer-based proteins (dG5 NFL TD, dH5 SOSIP, BG505 SOSIP, BG505 SOSIP T278A, dG5 NFL TD K278T, and 426c SOSIP), mouse anti-His tag mAb (R&D Systems, MAB050) at 2 μg/ml in 100 μl of phosphate-buffered saline (PBS) was coated at 4°C overnight. After incubating with blocking buffer for 1 hr at 37°C, 2 μg/ml of Env proteins were added into each well and incubated for 1 hr at room temperature. Subsequently, humanized mouse mAbs were added in 5-fold serial dilutions starting at 50 μg/ml and incubated for 1 hr at room temperature. After wash, secondary HRP-conjugated anti-human IgG (Jackson ImmunoResearch) diluted at 1:10,000 in PBS/0.05% Tween 20 was added and incubated for 1 hr at room temperature. The signal was developed by adding 100 μl of TMB substrate (Life Technologies) and incubation for 5 min followed by the addition of 100 ul of 1 N sulfuric acid to stop the reactions. The optical density (OD) of each well was measured at 450 nm to quantify binding avidity. Between each incubation step, the plates were washed extensively with PBS supplemented with 0.05% Tween 20.

For serum binding analysis, streptavidin (SA)-precoated 96-well plates (Pierce™, Thermo Scientific) were first incubated with biotin-labeled Env trimers dG5 NFL TD K278T_PADRE or eOD-GT8 particles at 2 μg/ml in 100 μl of phosphate-buffered saline (PBS) for 1 hour. Serum samples (starting at 100-fold dilution) collected and combined within each immunization group were then diluted in 5-fold series to assess binding activity. Serially diluted sera were added into the plates and incubated for 1 hour at room temperature. After wash, secondary HRP-conjugated anti-mouse IgG (Jackson ImmunoResearch) diluted at 1:10,000 in PBS/0.05% Tween 20 was added and incubated for 1 hr at room temperature. Signal development and reading are the same as described above.

Regarding the absorption binding assay in **Figure 4.4D**, dG5 NFL TD K278T PADRE was first added into the streptavidin (SA)-precoated 96-well plates (Pierce™, Thermo Scientific). Diluted sera were then incubated with eOD GT8 WT or the CD4bs KO variant (D279K/D368R) at a final concentration of 15 μg/mL for 30 mins at 37°C, 100 μl plasma/protein mixture per well was transferred back to the SA plates coated to test the binding with the dG5 N276+ trimers. Secondary HRP-conjugated anti-mouse IgG (Jackson ImmunoResearch) and TMB substrate (Life Technologies) were used for signal development and reading, similar to the protocol for the mAb binding test described above.

### 4.2.8 Immunogen Binding Characterization by BioLayer Interferometry (BLI)

Besides ELISA binding assays, the binding activity and kinetics of selected mAbs (VRC01, glVRC01, F105, PGT121, and PGT151) to designed immunogens were further assessed by BioLayer Interferometry (BLI) assay via an Octet RED96 system (ForteBio) following the manufacturer's instruction as previously described (Lei et al., 2019a). Octet Analysis version 9.0 software was used for data analysis. The mAbs bearing the human IgG constant regions were initially captured by anti-human IgG Fc biosensors, followed by immersing into 1) analyte wells containing trimer-based in 2-fold or 3-fold dilution series in binding buffer (PBS/0.05% Tween 20/0.1% BSA) to assess association rate (on-rate, $k_{on}$), and subsequently 2) wells containing binding buffer to assess dissociation rate (off-rate, $k_{off}$).

### 4.2.9 HIV-1 Neutralization Assays

Antibody neutralization assays were performed in a single round of infection using HIV-1 Env-pseudoviruses and TZM-bl target cells, as previously described (Li et al., 2005). Antibodies (starting at 50 μg/ml) were diluted in 5-fold series to assess neutralization

activity. Neutralization curves were fitted by nonlinear regression using a five-parameter hill slope equation. The $IC_{50}$ values of each antibody were determined as the concentration of antibody required to inhibit infection by 50%.

### *4.3 Results*

#### 4.3.1 Native Env trimer design based on VRC01-sensitive virus 45_01dG5

As one of the early proviral VRC01-sensitive viruses isolated from donor 45, 45_01dG5 naturally lacks the glycans at residues 276 (loop D) and 460 (V5 region) (Lynch et al., 2015). Glycan 276 on HIV-1 is extremely conserved (>95%), and along with the V5 loop glycans, they represent a major hurdle for VRC01-class antibodies to acquire neutralization breadth (Kong et al., 2016b; Umotoy et al., 2019). One explanation for the existence of the unusual glycan 276 and V5 glycan-lacking viruses in the VRC01 donor is that these viruses might be involved in the initial engagement with the naïve VRC01 BCR. Once the VRC01 germline-like B cells recognized the viruses lacking the glycans at position 276 and in the V5 loop, the first burst of antibody response exerted selection pressure on the viruses and caused virus escape. The subsequent emergence of glycan 276-containing viruses further induced the premature VRC01 lineage to undergo affinity maturation to avoid clashes with the glycans at N276 and in the V5 loop region, which leads to the induction of VRC01-like bNAbs. Based on this hypothesis, in this paper, we explore the feasibility of mimicking this VRC01-like antibody response in vivo by sequential immunization with a series of Env-based immunogens, including the 45_01dG5 Env.

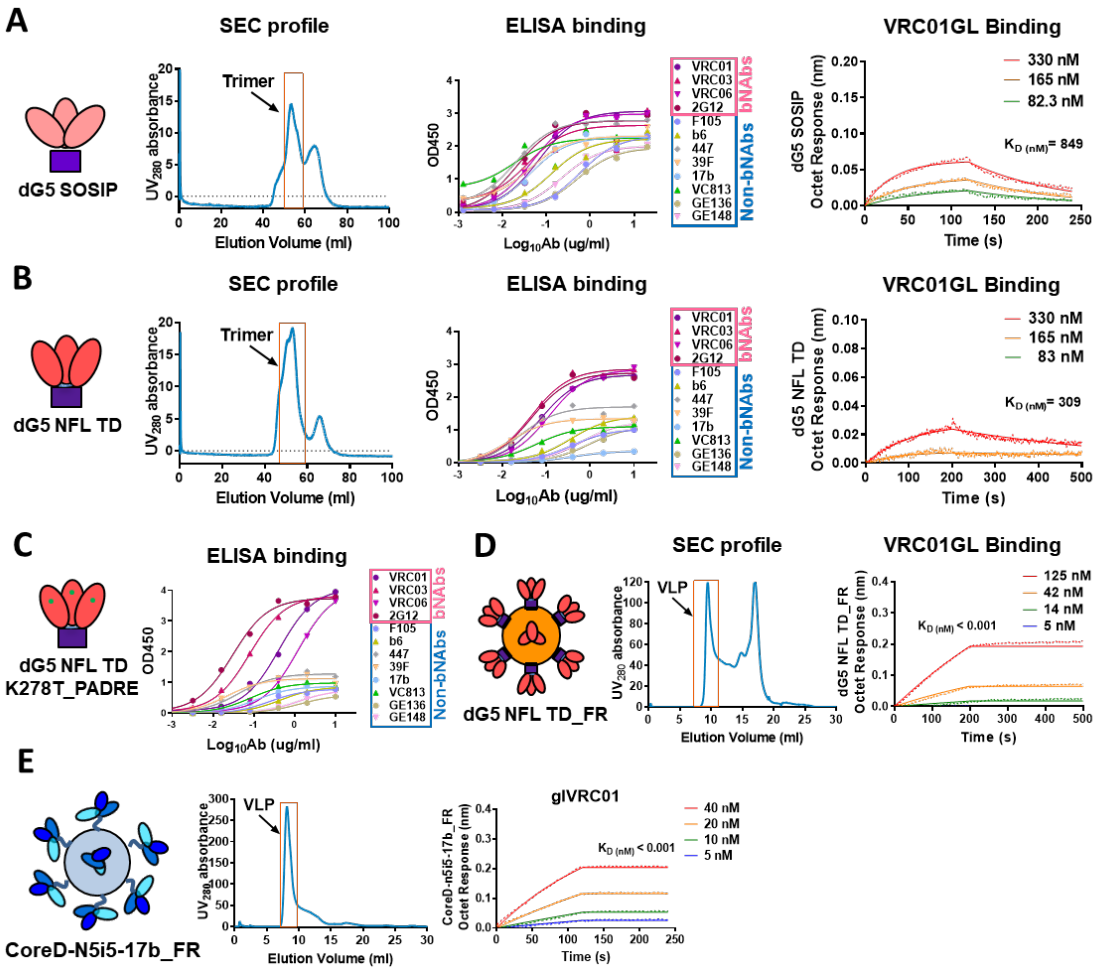


**Figure 4.2 Characterization of VRC01 germline-targeting soluble Env-based immunogens**. (A) From left to right: Size exclusion chromatography (SEC) profile of Galanthus nivalis lectin (GNL)-purified dG5 SOSIP expression in 293F cells; ELISA binding against selected bNAbs and non-bNAbs; Bio-layer interferometry (BLI) Biding of VRC01GL to the dG5 SOSIP trimers. (B) From left to right: Size exclusion chromatography (SEC) profile of Galanthus nivalis lectin (GNL)-purified dG5 NFL TD expression in 293F cells; ELISA binding against selected bNAbs and non-bNAbs; Bio-layer interferometry (BLI) Biding of VRC01GL to the dG5 NFL TD trimers. (C) ELISA binding profile of dG5 NFL TD K278T_PADRE variant after 447 negative selection. (D) SEC profile of dG5 NFL TD_FR VLPs and BLI binding to VRC01GL. (E) SEC profile and BLI binding of germline-targeting immunogen CoreD-n5i5-17b to VRC01GL. (C) BLI binding of HIV bNAbs and CD4bs nAb F105 to dG5 NFL TD_FR. (D) "Trimer-derived" mutations introduced into dG5 Env sequences. (E) Trimer formation propensity and yield of dG5-based trimeric Env variants.

We first engineered 45_01dG5 Env in the format of SOSIP (Sanders et al., 2013) (**Figure 4.2A**). The soluble trimer showed detectable binding to VRC01GL by biolayer

interferometry (BLI) (**Figure 4.2A**), which suggested that the lack of N276 and N460 glycans in the context of 45_01dG5 exposes the trimer surface for VRC01 precursors to engage. However, the antigenicity profile by ELISA exhibited indiscriminate binding activities of dG5 SOSIP to both bNAbs and non-bNAbs (**Figure 4.2A**), and negative selection by 447 eliminated all the trimer portion (data not shown). To optimize the formation of dG5 spike mimicry, we applied the native, flexibly linked (NFL) design strategy (Sharma et al., 2015) and generated a trimer variant, dG5 NFL. In brief, a glycine-serine (G4S) based flexible peptide linker was adopted to replace the furin cleavage site between the two Env subunits, gp120 and gp41, rendering the trimers both covalently linked and cleavage independent (Sharma et al., 2015). To further improve the propensity of homogenous native-like trimers, a series of mutations derived from the BG505 SOSIP sequence, termed "trimer-derived" (TD) (Guenaga et al., 2016), was introduced into the 45_01dG5 Env sequence (**Figure 4.3B**). This variant, namely, dG5 NFL TD, possessed a much higher level of homogeneity in terms of trimer assembly (**Figure 4.3A**), maintained the VRC01GL binding reactivity, and favored bNAb binding over non-bNAb binding after negative selection by 447 (**Figure 4.2B**). Additionally, we further presented the dG5 NFL TD trimers on the ferritin particles reported previously (Sliepen et al., 2015). The multimeric Env-based protein (dG5 NFL TD_FR) properly presented well-ordered trimers, indicated by the Galanthus binding of trimer specific bNAb PGT151 (**Figure 4.3C)**. Moreover, the dG5 NFL TD_FR virus-like particles (VLPs) showed significantly increased affinity to VRC01GL compared to parental soluble trimer dG5 NFL TD (**Figure 4.2A & 4.3C**). Considering the high avidity and potentially improved immunogenicity by this multivalent display platform (He et al., 2018; Sliepen et al., 2015), we proposed to prime

with dG5 NFL TD_FR as a germline-targeting immunogen to seek activation of VRC01-class precursors in vivo. In addition to dG5 NFL TD_FR, we have recently designed a dual CD4i mAbs-gp120 fusion complex (CoreD-n5i5-17b) that showed selective binding to CD4bs-targeting bNAbs and high affinity to VRC01 germline-reverted version (VRC01gl). We also incorporated this construct into the ferritin presentation platform (CoreD-n5i5-17b_FR) and observed an enhanced affinity to VRC01gl (**Figure 4.2E**). Thus, both particles could serve as priming immunogen candidates for VRC01 precursor activation.

**A**

| dG5 variants | Trimer (%) | Trimer yield ( ug/L) | Trimer yield to WT (%) |
|---|---|---|---|
| SOSIP (WT) | 7.4 | 226 | 100 |
| SOSIP TD | 18.1 | 210 | 93 |
| SOSIP DS | 5.1 | 126 | 56 |
| SOSIP TD/DS | 7.4 | 870 | 38 |
| NFL TD | 40.0 | 1401 | 619 |
| NFL TD/DS | 31.1 | 1138 | 500 |

**B**

**dG5 NFL TD**

| Residue | Trimer Derived (TD) (n=14) |
|---|---|
| E47 | D |
| T49 | E |
| V65 | K |
| E106 | T |
| S164 | E |
| M165 | L |
| E172 | V |
| P308 | R |
| E429 | R |
| K432 | Q |
| L543 | N |
| N553 | S |
| K588 | R |
| E662 | A |

**C**

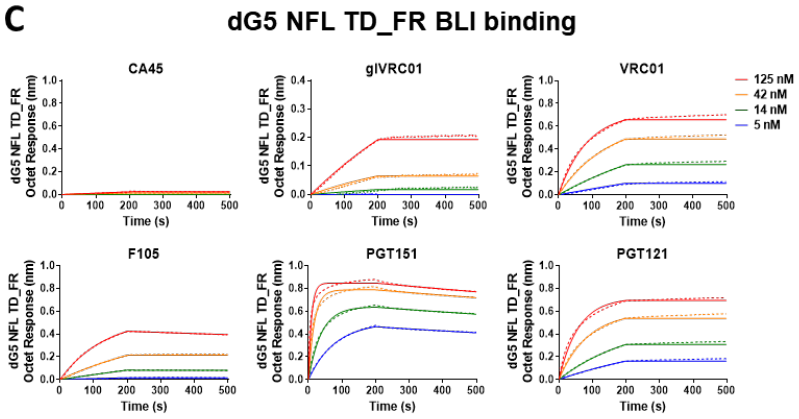


**Figure 4.3 Native-like trimer immunogen design based on the 45_01 dG5 Env.** (A) Trimer formation propensity and yield of dG5-based trimeric Env variants. (B) "Trimer-derived" mutations introduced into dG5 Env sequences. (C) BLI binding of HIV bNAbs and CD4bs nAb F105 to dG5 NFL TD_FR.

### 4.3.2 Sequential immunization elicited focused CD4bs targeting antibody responses in VRC01$^{gHL}$ mice

To determine whether our Env based immunogens can induce affinity maturation of VRC01gl B cell precursors in vivo, we conducted a priming-boosting immunization in the heterozygous VRC01gHL knock-in mouse model developed recently (Abbott et al., 2018). In this animal model, ~ 33% of B cells are eOD-GT8-binding cells, which ensures abundant VRC01-class precursors to be potentially activated (Abbott et al., 2018). Under this circumstance, we evaluated whether our designed immunogens initiated and led the precursor B cells towards a similar pathway of VRC01 maturation. We first immunized three groups of experimental animals twice at week 0 and week 2 with germline-targeting particles eOD GT8, CoreD-n5i5-15b_FR, and dG5 NFL TD_FR, respectively, to seek to activate low-affinity germline-like B cells (**Figure 4.4A**). After priming, K278T mutation was then introduced in the dG5 NFL TD as the boosting immunogen for all three groups to select and potentially mature the VRC01-class B cells that can bind or have circumvented N276 glycan. A pan-DR epitope peptide (PADRE) was added to the dG5 NFL TD K278T sequence to serve as a conserved T-help epitope. (**Figure 4.2C & 4.4A**).

To examine the enrichment of the VRC01-like antibody response, we first assessed serum antibody responses. Serum samples from week 4 (after primings) were tested against eOD GT8 WT and the CD4bs knock-out (KO) version (eOD GT8 D279K_D368R) to determine the binding specificity. We observed that the serum binding of all three immunization groups to the CDbs KO protein was mostly abolished (**Figure 4.4B**), which suggests the elicitation of CD4bs targeting antibodies prior to boosting. After boosting (week 13), sera from all three groups showed increased binding activities against the

boosting immunogen dG5 NFL TD_K278T (dG5 N276+) comparing with samples right after two primings (week 4) (**Figure 4.4C**). Group C, in particular, exhibited the highest binding titer and the most substantial fold of increase (**Figure 4.4C**). We then tested the binding specificity of the post-boosting sera. Similar to the samples from boosting (week 4), the dramatic reduction in binding to CD4bs KO was observed (**Figure 4.4D**), which indicates focused CD4bs targeting antibodies exist in the sera of all three experimental groups. We further confirmed the CD4bs-directed reactivity of week 13 samples by the absorption binding assay (**Figure 4.4E**). Serum antibodies were first depleted with eOD GT8 WT or the CD4bs KO variant, then were tested for binding to dG5 N276+ trimer. All three groups displayed higher binding when absorbed first by CD4bs KO compared with WT, which confirms the existence of CD4bs targeting antibodies in each group.

Moreover, we also calculated the difference of dG5 N276+ binding reactivity of each group after serum absorption by eOD GT8 WT and CD4bs KO. We observed that group B and group C sera retained more than half of their binding activities after absorbed by CD4bs KO proteins compared with samples depleted by eOD GT8 WT (**Figure 4.4E**). The considerably high value of disparity suggests that a significant portion of antibodies in Group B and Group C animal week 13 plasma are not reactive to CD4bs KO protein, which affirms that the majority of induced antibodies are sensitive to CD4bs KO mutations. Overall, the proposed immunization strategy elicited CD4bs epitope-specific antibody responses in all experimental groups; Group B and Group C exhibited much higher reactivities to the boosting immunogen. Therefore, sera from Group B and Group C may contain more VRC01-like antibodies that accommodate well with the glycan N276.

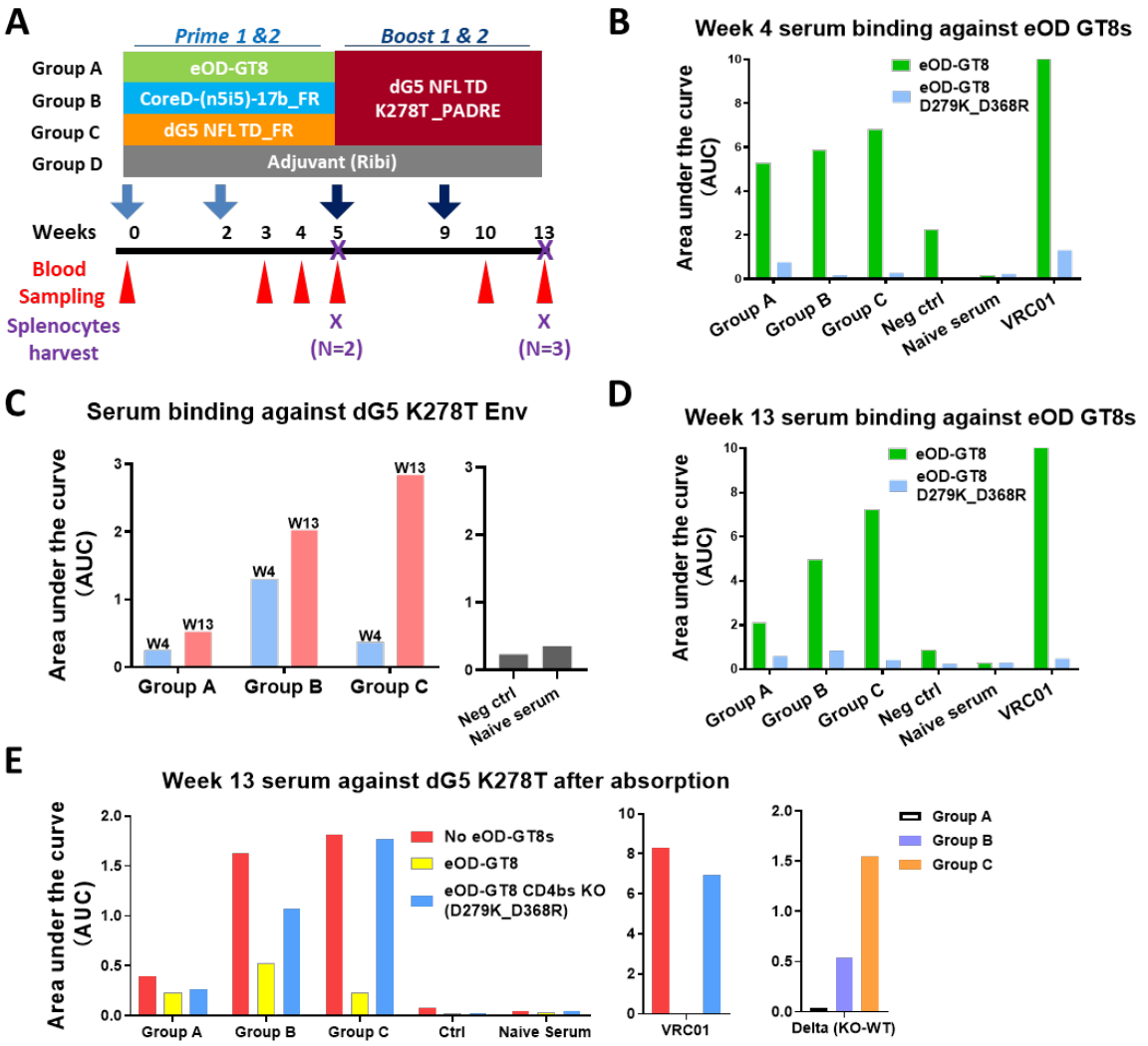


**Figure 4.4 Enriched CD4bs-directed antibody responses in VRC01gHL mice.** (A) Immunization scheme for heterozygous VRC01$^{gHL}$ mice. Group A, B, and C were primed at week 0 and week 2 with germline-targeting immunogens eOD-GT8, CoreD-n5i5-17b_FR, and dG5 NFL TD_FR, respectively. After priming, the animals were boosted twice at week 5 and week 9 with dG5 NFL TD K278T_PADRE. Splenocytes were harvested at week 5 and week 13. (B) Week 4 serum binding against eOD-GT8 WT particles and the CD4 binding site (CD4bs) KO variant eOD-GT8 D279K_D368R. (C) Reactivities of week 4 & week 13 mouse sera with HIV Env trimer dG5 NFL TD K278T. (D) Week 13 serum binding against eOD-GT8 WT particles and the CD4 binding site (CD4bs) KO variant eOD-GT8 D279K_D368R. (E) Week 13 serum binding against dG5 NFL TD K278T after absorbed by eOD-GT8 WT or the CD4bs KO variant.

### 4.3.3 VRC01-like mutations accumulated in antigen-specific B cells

To investigate the CD4bs-specific antibody responses at the clonal level, we first isolated the antigen-specific single memory B cells from the heterozygous VRC01gHL mice. eOD GT8, a germline targeting VLP designed to attain superior affinity to VRC01-class mAbs (Jardine et al., 2015), was used as the antigen probe to identify the VRC01-class B cells from KI mice splenocytes after two primes. Antigen-specific class-switched B cells (H57-597$^{-}$ B220$^{+}$ IgM$^{-}$ IgD$^{-}$ IgG$^{+}$ eOD-GT8$^{+}$) were sorted for antibody variable region PCR amplification. For single B cell isolation from boosting samples, we employed a modified sorting strategy with more cell markers to increase precision and one more CD4bs KO antigen probe (eOD GT8 D279K_D368R) for negative gating of CD4

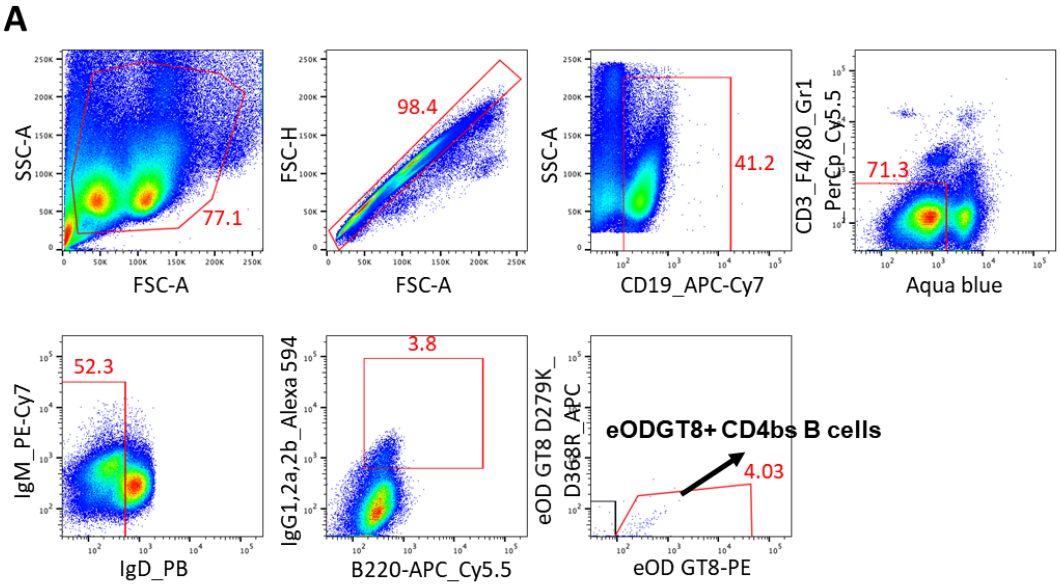


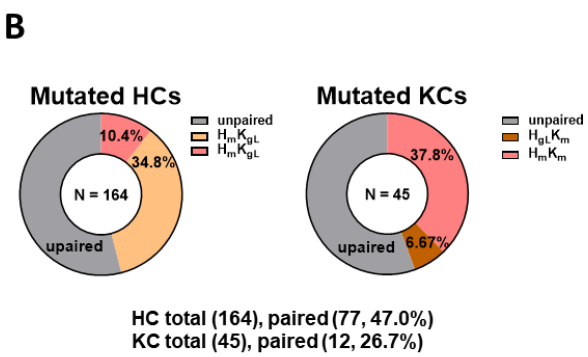


C

| Mutated sequences isolated | | | | mAb expressed | | |
|---|---|---|---|---|---|---|
| mutated sequence # | | Total | paired | HmKm | HmKgL | HgLKm |
| GrpA_W5 | HC | 2 | 1 | 0 | 1 | 0 |
| | KC | 4 | 0 | | | |
| GrpA_W13 | HC | 16 | 6 | 0 | 6 | 0 |
| | KC | 14 | 0 | | | |
| GrpB_W5 | HC | 11 | 8 | 0 | 8 | 0 |
| | KC | 2 | 0 | | | |
| GrpB_W13 | HC | 27 | 20 | 1 | 19 | 0 |
| | KC | 12 | 1 | | | |
| GrpC_W5 | HC | 53 | 17 | 9 | 7 | 1 |
| | KC | 13 | 10 | | | |
| GrpC_W13 | HC | 55 | 25 | 7 | 16 | 2 |
| | KC | 17 | 9 | | | |

**Figure 4.5 Summary of VRC01gHL mouse single B cell sorting and mAb cloning.** (A) VRC01-like B cells were isolated from splenocytes of VRC01$^{gHL}$ mouse by multicolor fluorescence-activated cell sorting (FACS). The frequencies (percentages) of the gated cell population in the parent population are indicated in red. Class-switched VRC01-class B cells (Aqua blue-/ CD19+/ CD3-/ F4/80-/ Gr1-/ IgM+/ IgD-/ B220+/ IgG1,2a,2b+/ eOD-GT8+/ CD4bs KO-) from week 13 splenocytes were sorted for antibody variable region PCR amplification.Summary of all the sequences isolated from antigen-specific single B cells. (B) Pie chart of the percentage of heavy and kappa chain mutated sequences in all sequences recovered. Paring information and percentage are also specified. (C) The number of mutated heavy and light sequences recovered from each immunization group and the pairing information of all mAbs tested.

binding site positive cells (**Figure 4.5A**). The variable regions of antibody sequences were sequenced from each positive wells after single-cell RT-PCR. Both mutated and unmutated antibody sequences were identified in the antigen-specific single B cells (**Figure 4.6B**). For week 5, lower than 30% of the B cells contain somatic mutations. However, much higher percentages of B cells with mutations were observed in week 13 samples, especially for group B and group C, more than 50% of cells accumulated mutations in either heavy- or light-chains. (**Figure 4.6B**). Naturally paired heavy and kappa chains were then cloned into expression vectors for mAb expression (**Figure 4.5B & 4.5C**). Around 77% of mutated HCs had paired KCs from single cells and in total 77 mAbs were successfully expressed for downstream analysis (**Figure 4.5B & 4.5C**).

To study the molecular process of VRC01 germline activation and affinity maturation toward the development of matured VRC01, we first examined mutations in all sequences isolated from single B cells. After priming, eOD-GT8 60mer elicited very rare HC (2% mutated) and KC (4% mutated) mutations; Group B showed more HC (11% VH amplicons are mutated) mutations than group A, but very rare KC mutations (2% mutated); Group C showed the highest mutation rates in VH (63% amplicon mutated) and VK (14% amplicons mutated) (**Figure 4.6B & 4.7B**). This suggests that CoreD-CD4i fusion proteins are able to drive affinity maturation of VH but not VK, while trimer imposes selection on both

chains and eOD-GT8 imposes minor selection pressure on both chains. After booster immunizations, more mutations were observed for both heavy and light chains in each group (**Figure 4.6B & 4.7B**). 32% HCs and 16% KCs were mutated in Group A week 13 samples. 24% HCs and 7% KCs in Group B accumulated somatic mutations. Group C still showed the highest mutation rates in HCs (41%), and KCs (20%), however, the overall mutation rates dropped compared from antigen-specific B cells from week 5 (**Figure 4.6B & 4.7B**).

In general, most mutations occurred within the CDR1 and CDR2 regions of heavy (HCs) and kappa chains (KCs) at both time points (**Figure 4.6D & 4.7D**). Amino acid (AA) mutations identified were further grouped into four different categories: all mutations (total mutations identified from the variable region of antibody sequences), VRC01 class mutations (the mutations that share the same amino acids with any of the VRC01 class mAbs in the 9 lineages (Tian et al., 2016), VRC01 converging mutations (non-VRC01 mutations reside at the same positions of VRC01 mutations), and VRC01 identical mutations (the mutations that are identical to VRC01 at the same positions). HCs inspected at both time points (week 5 & week 13) displayed much higher mutation rates than KCs within the same groups under all four categories (**Figure 4.6 & 4.7**). We also compared mutation rates among different immunization groups. In general, group C obtained consistently more mutations in the four categories during the immunizations (**Figure Figure 4.6 & 4.7**). Thus, the immunogen combination in group C stimulated more somatic mutations overall. However, there is no significant difference in mutation rates of HCs and KCs between week 5 (after priming) and week 13 (after boosting) for all three experimental groups, except for the VRC01-class and VRC01 converging mutations in the group C HCs

(**Figure 4.6A & 4.7A**). In sum, all three immunization regimes and strategies induced VRC01-like mutations with different magnitude, while group C accumulated more mutations under the four categories defined above.

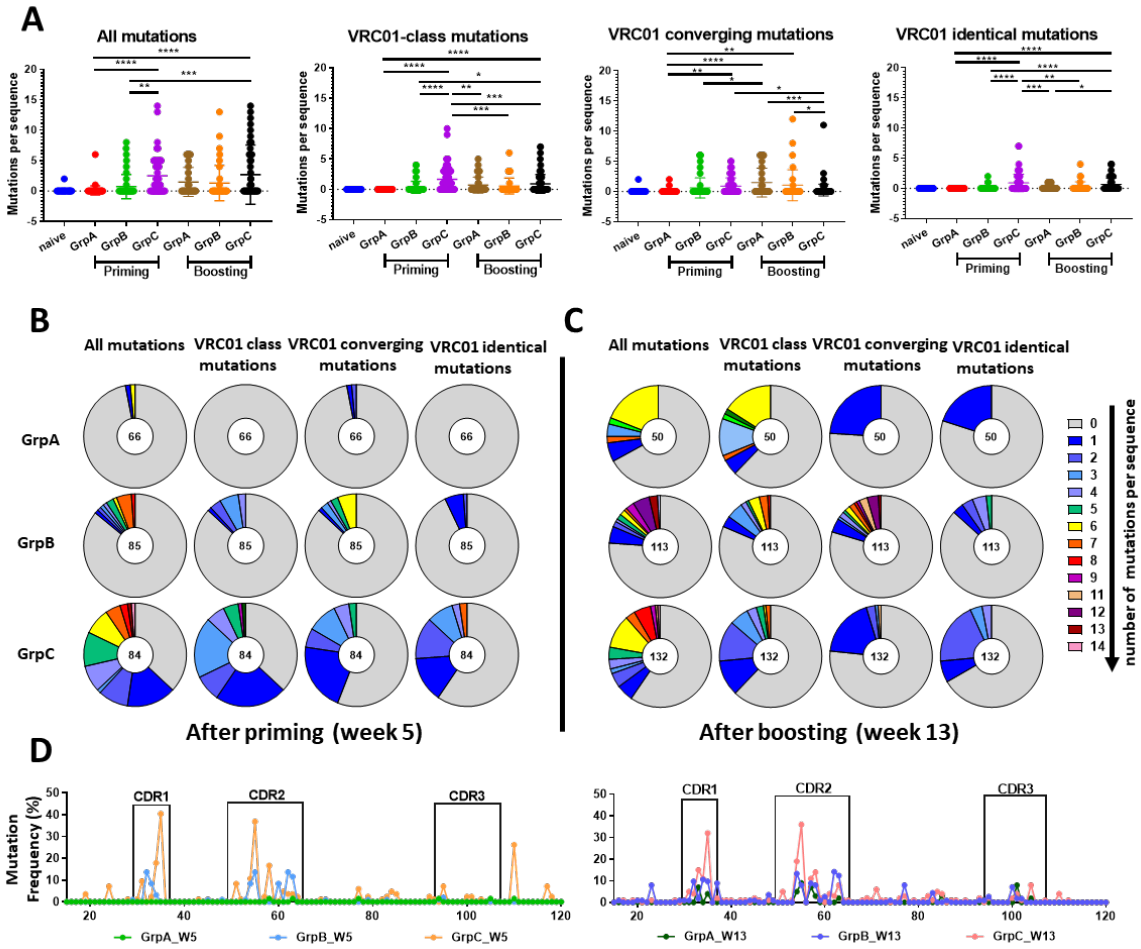


**Figure 4.6 Characterization of heavy chain (HC) mutation rates in the Env-specific single B cells.** (A) The amino acid (AA) mutation rates of all heavy chain (HC) sequences isolated from priming and boosting samples under four different categories. (B) and (C) Summary of the number of the AA mutations identified per HC sequence under four different categories from week 5 (after priming) and week 13 (after boosting) samples. The numbers in the circle indicate the total sequences identified for each immunization group. (D) Frequencies of HC AA mutations per residue position at week 6 or week 13 for three immunization groups. CDR regions are highlighted.

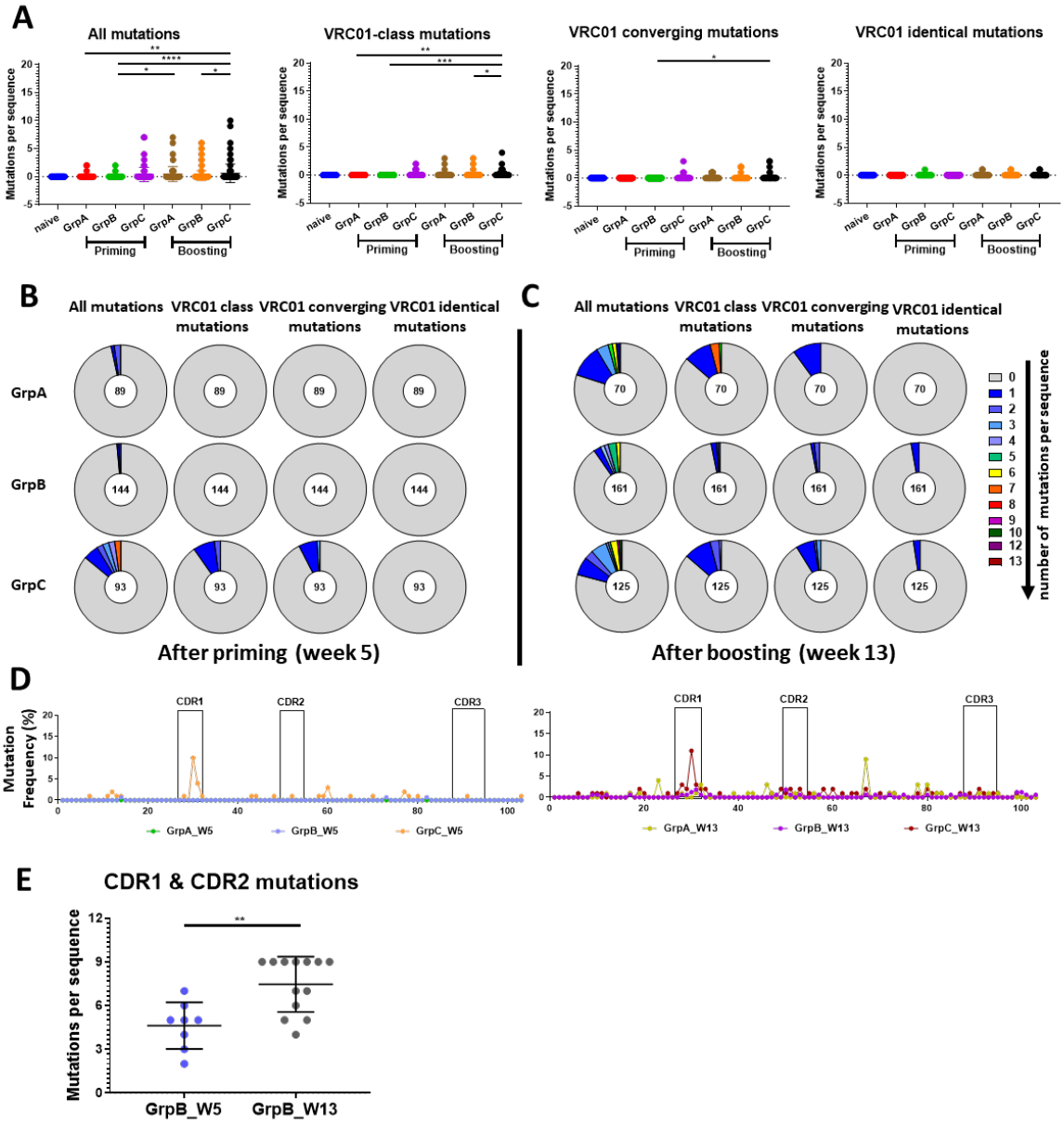


**Figure 4.7 Characterization of kappa chain (KC) mutation rates in the Env-specific single B cells.** (A) The amino acid (AA) mutation rates of all kappa chain (KC) sequences isolated from priming and boosting samples under four different categories. (B) and (C) Summary of the number of the AA mutations identified per KC sequence under four different categories from week 5 (after priming) and week 13 (after boosting) samples. The numbers in the circle indicate the total sequences identified for each immunization group. (D) Frequencies of KC AA mutations per residue position at week 6 or week 13 for three immunization groups. CDR regions are highlighted. (E) Comparison of the total mutations in the heavy chain CDR1 and CDR2 regions between mAb isolated from group B week 5 and week 13.

### 4.3.4 mAbs recovered from VRC01 knock-in mice displayed cross-binding and cross-neutralization activities

For the naturally paired heavy and kappa chain sequences recovered from single-cell RT-PCR, we cloned them into expression vectors for mAb expression (**Figure 4.5B & 4.5C**). Around 77% of mutated HCs had paired KCs recovered from single cells and 77 mAbs in total were successfully expressed for downstream analysis (**Figure 4.5C**). We first characterized the binding specificities of the reconstituted mAbs against a panel of HIV-1 Envs by ELISA (**Figure 4.8C**). We compared the area under the curve (AUC) of each antibody with the AUC of positive control (VRC01). To better define the binding intensity, we calculated relative AUC (rAUC) for all the antibodies we isolated. The relative AUC (rAUC) was defined as: rAUC = ($AUC_{KImice\_mAb}/AUC_{VRC01}$).

For group A, only one VRC01-class antibody was recovered after priming (week5), and 6 were recovered from the boosting sample (**Figure 4.5C**). Most of them (5/7) bind to Env-based proteins that lack the glycan N276 (dG5 NFL TD, dH5 SOSIP, CoreD, CoreD-n5i5-17b, and BG505 SOSIP T278A) in the panel (**Figure 4.8A & 4.8C**). Nevertheless, they exhibited minimal binding activities against Envs with the glycan N276 (dG5 NFL TD PARDE K278T, 426c SOSIP, BG505 SOSIP, and YU2 core) (**Figure 4.8A & 4.8C**). As for group B, all mAbs from week 5 and the majority (16/20) of mAbs from week 13 showed strong binding to the immunogen CoreD-n5i5-17b and its related Env gp120-based protein CoreD (**Figure 4.8A & 4.8C**), which indicates a responsive and sustained priming effect. In terms of boosting, binding of week 13 mAbs to dG5, dH5, and BG505 K278T

native-like trimers and YU2 Core were considerably improved in contrast to the mAbs from week 5 (**Figure 4.8A & 4.8C**).

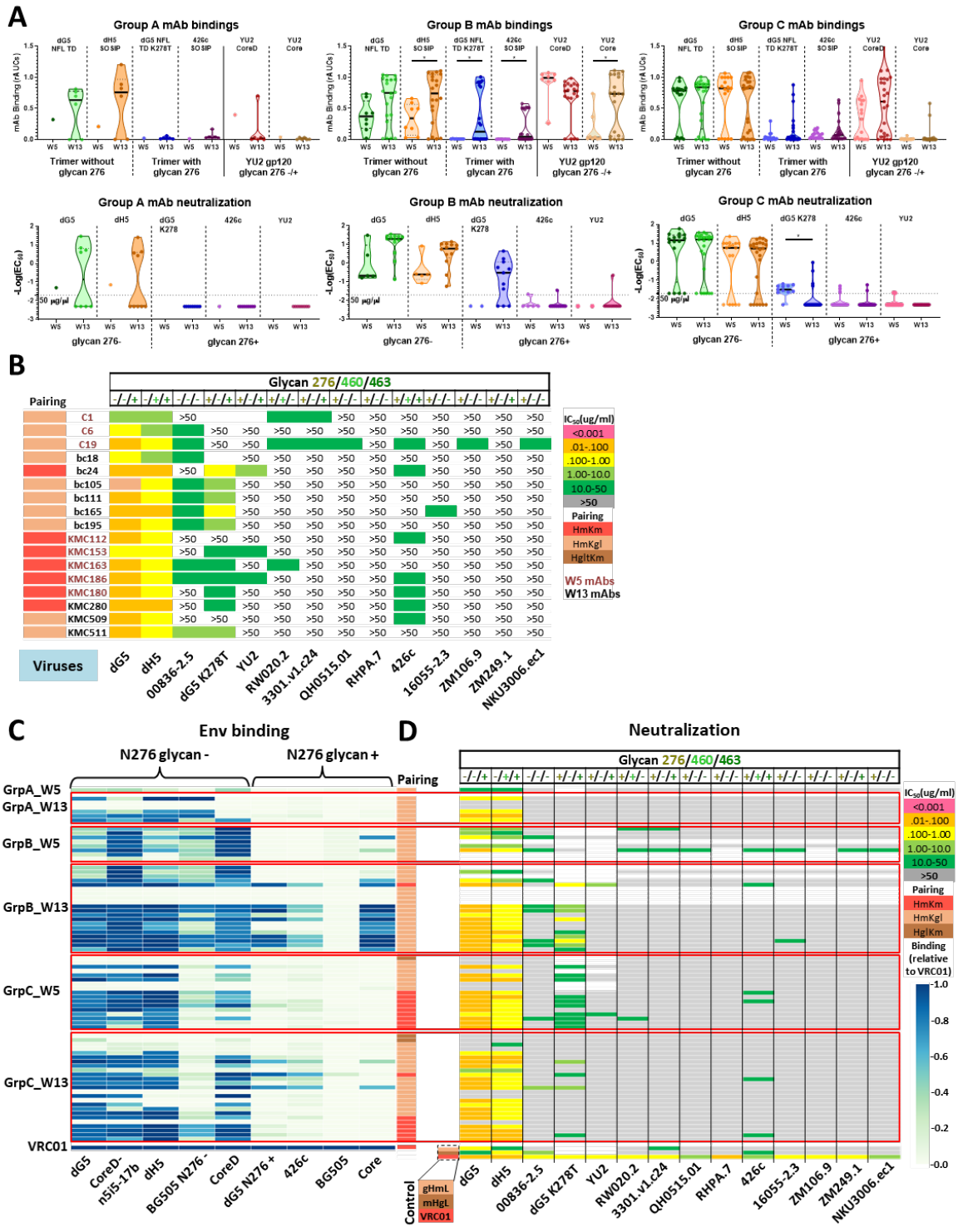

**Figure 4.8 Characterization of the binding and neutralizing activities of monoclonal antibodies (mAbs) isolated from VRC01-class B cells.** (A) Binding and neutralization of mAbs from the three immunization groups against selected Envs and viruses. The binding intensity was determined by the ratio of area under the curve (AUC) of the ELISA binding curve of each antibody to the AUC of positive control (VRC01). (B) mAbs displayed cross-reactive neutralizing activities against a panel of representative CD4bs sentinel viruses. Antibody heavy and light chain pairing (HmKm, HmKgl, and HglKm) was indicated in three different colors. The presence of glycans at position 276, 460. and 463 in the virus Env sequences were also annotated on the top of the figure. (C) Binding of mAbs against a panel of HIV Env glycoproteins with/without the glycan N276. (D) Neutralization of all mAbs recovered against the panel of representative CD4bs sentinel viruses.

Moreover, a large portion of week 13 mAbs (13/20) displayed strong binding to glycan N276 containing trimer 426c SOSIP and boosting immunogen dG5 NFL TD K278T, whereas none of the mAbs from group B priming was sensitive to any of the Envs carrying glycan N276 (**Figure 4.8A & 4.8C**). We also detected augmented binding against all the Envs in the panel from group C week 13 mAbs compared with week 5 mAbs (**Figure 4.8A & 4.8C**). However, the frequency and intensity were generally lower than the mAbs from group B, week 13. Only 4 out of 25 exhibited similar reactivity to Envs with glycan N276 (**Figure 4.8C**). In summary, all experimental groups responded well to both priming and boosting immunogens in respect of binding reactivity. After priming with VRC01 germline-targeting immunogens, dG5 NFL TD PADRE K278T bolstered cross-reactivity to all Env proteins in the panel regardless of the presence of glycan N276, suggesting that prime-boost immunizations with our novel germline-targeting immunogens are able to drive the affinity maturation of VRC01 lineage B cells to accommodate the N276 glycan surrounding the cognate CD4bs epitope.

We further examined the neutralizing activity of the VRC01 GL KI mice mAbs to a virus panel, namely "CD4bs sentinel virus panel" along with two autologous virus strains, 45_01 dG5 and 45_01 dH5, which were isolated from donor 45 (the VRC01 donor), and 45_01 dG5 K278T, the N276 glycan knockin variant of 45_01 dG5 (**Figure 4.8D**). CD4bs

mAbs of both group A and group B showed increased neutralizing activities against 45_01 dG5 and 45_01 dH5 after boosting (**Figure 4.8A & 4.8D**).

However, consistent with the minimal binding activities against Envs bearing the N276 glycan, none of the group A mAbs showed neutralization against viruses carrying N276 glycan. Furthermore, group B week 13 mAbs displayed potent neutralization against 45_01 dG5 K278T virus; in contrast, none of the group B week 5 mAbs showed binding activity to the dG5 K278T trimers assessed by ELISA (**Figure 4.8A, 4.8B & 4.8D**). A few mAbs isolated from the two immunization time points cross-neutralized other viruses in the panel, 00836-2.5.SG3 and 426c.SG3 in particular (**Figure 4.8B & 4.8D**). Of note, 00836-2.5 misses glycans at position 276, 460, and 463, while 426c obtains all of them. Therefore, the combination of CoreD-n5i5-17b_FR and dG5 NFL TD PADRE K278T in this group successfully induced mAbs that overcome the N276 glycan and interact favorably with heterologous viruses, similar to the mature bNAb VRC01. One mAb especially, from group B week 5 (C19), displayed the most broader neutralizing activity (**Figure 4.8B**). However, the potencies of the observed virus neutralization are moderate in general, as the mAb $IC_{50}$s for more than half of the neutralization-sensitive viruses were close to 50 μg/ml (**Figure 4.8B**), which needs to be improved in future studies. For group C, most of the mAbs at both week 5 and week 13 maintained potent neutralizing activities against autologous 45_01 dG5 and 45_01 dH5. Some of them also showed cross-neutralization to 45_01 dG5 K278T, 00836-2.5.SG3, and 426c.SG3 viruses (**Figure 4.8B & 4.8D**). Even though the frequency of 45_01 dG5 K278T neutralizers dropped from 10/17 (58.8%) at week 5 to 3/25 (12%) at week 13, the neutralizers after boosting were more potent (**Figure 4.8B & 4.8D**). To sum up, the tolerance of the glycan N276 displayed by

the VRC01 lineage mAbs results from the affinity maturation elicited by the prime-boost immunizations with our novel germline-targeting immunogens, which leads to restricted cross-neutralization of heterologous viruses (**Figure 4.8B & 4.8D**).

### 4.3.5 Glyan N276-tolerant mAbs share the genetic signatures of VRC01-class bNAbs

To better assess the contribution of mutations induced by our immunization strategies to N276 glycan accommodation, we analyzed amino acid (AA) mutations that garnered in each mAb recovered (**Figure 4.9A**). We first compared the heavy chain (HC) AA mutations of dG5 NFL TD K278T binders (rAUC > 0.2) and the non-binders (rAUC < 0.2). We noticed that dG5 K278T binders achieved significantly higher mutations than non-binders (**Figure 4.9C**). We also observed that the VRC01 identical mutation and VRC01 class mutation rates for dG5 K278T binders were notably higher (**Figure 4.10C**). Taken together, a higher level of mutations that resemble matured VRC01 were accomplished by the immunizations to tolerate the glycan N276 better. Besides, VRC01 identical and class mutations largely accumulated in the CDRH1 and CDRH2 regions (**Figure 4.10A & 4.10B**). Among these mutations, H35N in CDRH1, which is reported to interact with N100a in HCDR3 and required to achieve breadth (Abbott et al., 2018; Jardine et al., 2016b), was acquired by all dG5 K278T binders (**Figure 4.10A & 4. 10B**). VRC01 class mutations were also abundantly generated at the positions of Y32H (73%) and M34I/L (80%), which were revealed to be critical for VRC01 structure and neutralization (Jardine et al., 2016b) (**Figure 4.10A & 4.10B**). In CDRH2, VRC01 mutations (G57A, T58V) and VRC01 class mutations (N54T, S55R) accumulated in most of the K278T binder HCs (**Figure 4.10A & 4.10B**). Moreover, 60% of dG5 K278T binders have all four mutations (G57A, T58V, N54T, and S55R) in the HCs (**Figure 4.10A & 4.10B**). All these

dG5 K278T binders also have the VRC01 Q61R mutation in the heavy chains (**Figure 4.10A & 4.10B**). R61 inserts in the cavity formed by gp120 V5 and β24 to stable the V5 region on HIV Env (Zhou et al., 2010). Overall, the mutations in the CDRH1 and CDRH2 regions of dG5 K278T binders strongly mirror the genetic features achieved by VRC01.

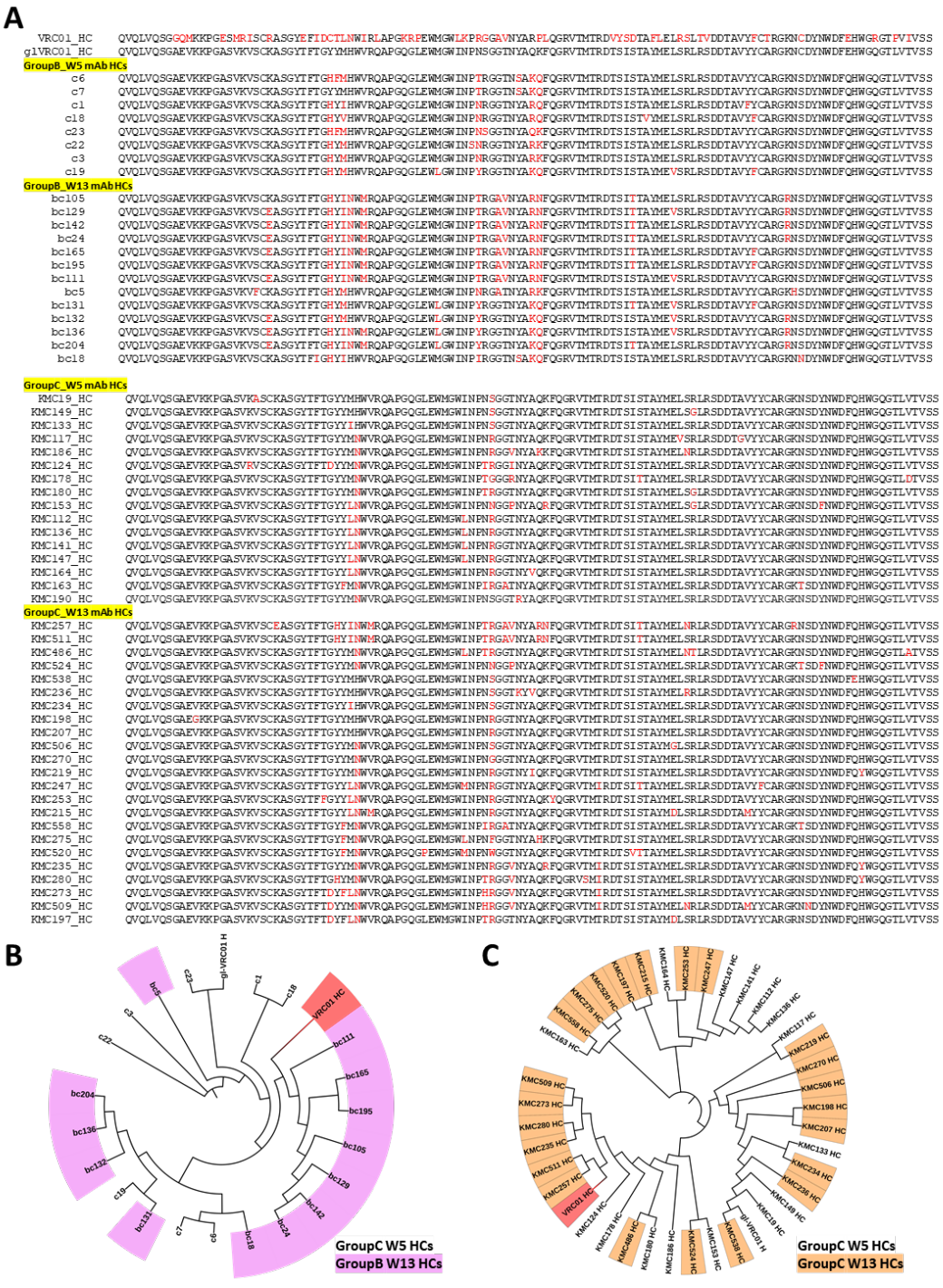

**Figure 4.9 Summary of all mAb heavy chain (HC) sequences recovered from antigen-specific single B cells.** (A) Sequence alignment of all mutated mAb heavy chains recovered from three immunization groups. (B) Phylogenetic analysis of mAb heavy chain sequences isolated from group B. (C) Phylogenetic analysis of mAb heavy chain sequences isolated from group C.

Additionally, for group B, the mutation rates in CDRH1 and CDRH2 regions is significantly higher than the mAb HCs from the same group at week 5 (**Figure 4.7E**). VRC01 mutations H35N, G57A, and T58V only appear in the HCs from week 13 mAbs (**Figure 4.10A**). The phylogenetic analysis also reveals that the branches from week 13 are derived from the branches of week 5 mAbs **(Figure 4.9B)**. Regarding the group C, although phylogenetic analysis displayed mixed week 5 and week 13 HC branches in the tree, 6 HCs from week 13 can be grouped into one clade with VRC01 HC and they are closer to VRC01 HC than the HCs from week 5 (**Figure 4.9C**). In addition, VRC01-class mutation Y32H was only spotted after boosting. Therefore, in both groups, the antigen-specific B cells from boosting potentially affinity matured from the mAbs activated in priming. Besides, Nearly identical mutations accumulated on HC sequences were observed in the HCs from group B week 13. For example, KMC257H from group C week 13 almost has the same mutations with bc142H isolated from group B week 13, with one AA mutation difference (**Figure 4.10A**). Collectively, the comparable antibody response across the two immunization groups suggests that both immunogen combinations effectively activated VRC01gl B cells and introduced mutations converging toward the matured VRC01.

As some of the dG5 K278T non-binders showed weak neutralizing activities against the 45_01 dG5 K278T virus, we also grouped the total mAb HCs isolated to dG5 K278T neutralizers and dG5 K278T non-neutralizers (**Figure 4.11**). We observed the consistent significant difference of mutation levels in terms of total mutations, VRC01

identical mutations, and VRC01-class mutations between dG5 K278T neutralizers and non-neutralizers (**Figure 4.11C**). The VRC01/VRC01-class mutations clustered in the CDRH1 and CDRH2 in dG5 K278T neutralizers, while in dG5 K278T non-neutralizers, the two regions largely remain unchanged (**Figure 4.11A**). We also performed the same analysis for all mAb KC chain AA sequences isolated (n=14). Similar to the conclusion drawn from the HC analysis, KCs of dG5 K278T neutralizers obtained substantially higher mutation levels than the KCs from dG5 K278T non-neutralizers (**Figure 4.10F**). Moreover, clustered VRC01/VRC01-class mutations were generated in the CDRK1 region, suggesting affinity maturation efforts driven by the immunization (**Figure 4.10D & 4.10E**). However, no deletions similar to VRC01 KC in the CDRK1 were generated during the immunizations (**Figure 4.10D & 4.10E**). Thus, the steric clash between the glycan N276 and the CDRK1 might still retain, which corroborates the limited the binding and neutralization activities of mAbs against virus variants with the glycan N276 (**Figure 4.8**).

In conclusion, our designed immunogens and immunization strategy affinity matured VRC01 germline B cells towards the development pathway of VRC01/VRC01-class bNAbs, and the mutations induced were beneficial to interact with the glycan N276. Of note, additional somatic hypermutations are required to achieve a broader and more potent CD4bs-directed antibody neutralization.

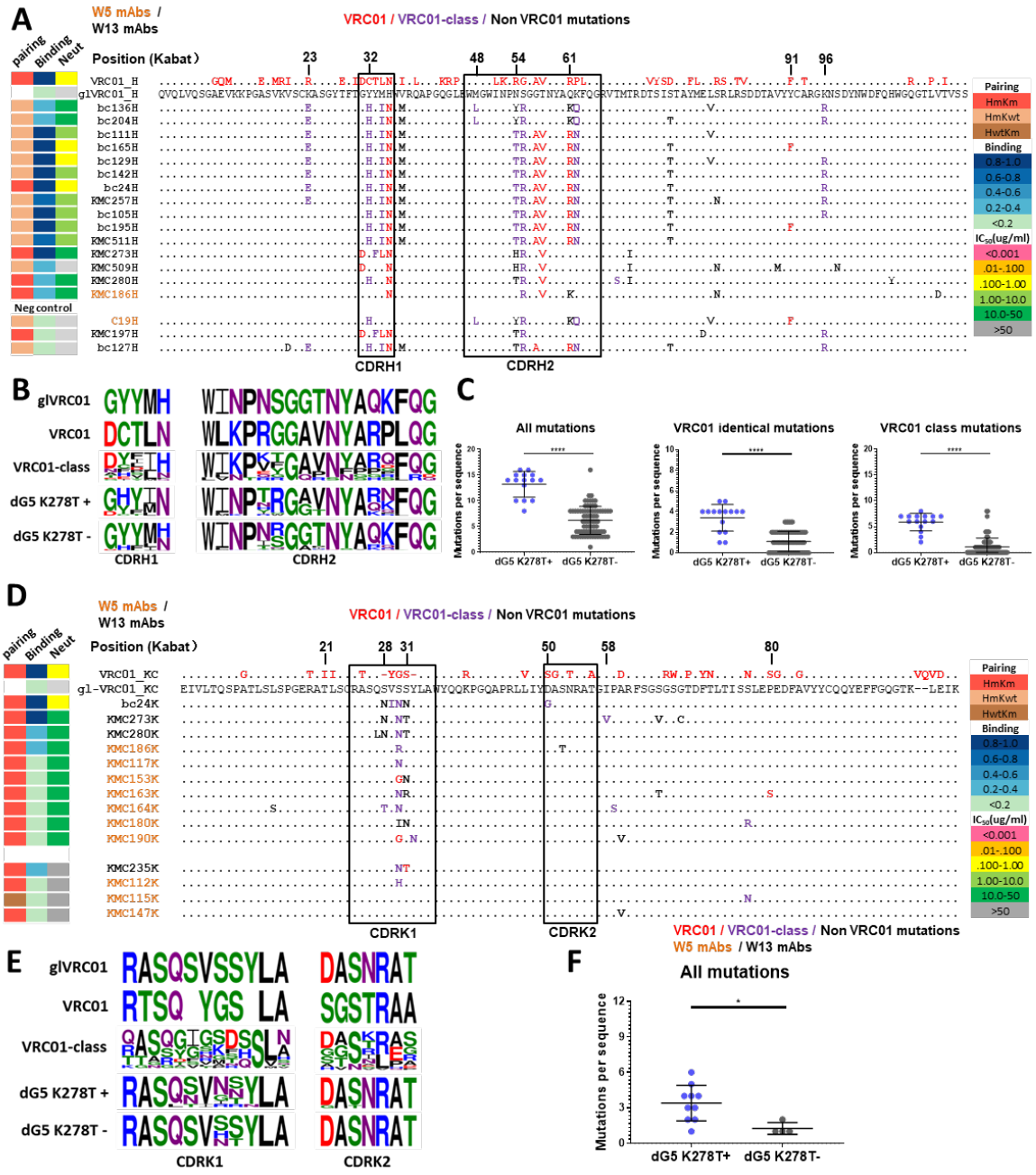


**Figure 4.10 Sequence analysis of the heavy and light chains of mAbs that bind to the boosting immunogen (dG5 NFL TD K278T_PADRE).** (A) Heavy chain AA sequence alignment. VRC01 mutations are colored in red, VRC01-class mutations are shown in purple, non-VRC01 mutations are in black. Kabat-defined CDRH1 and CDRH2 regions are highlighted. (B) Sequence logos of CDRH1s and CDRH2s of glVRC01, VRC01, VRC01-class antibodies, all dG5 NFL TD K278T binders, and all non-dG5 K278T NFL TD K278T binders. (C) Comparison of the AA mutations per HC sequence between dG5 K278T binders and non-dG5 K278T binders isolated from all three immunized groups under three categories (all mutations, VRC01 identical mutations, and VRC01 class mutations). (D) Kappa chain AA sequence alignment. VRC01 mutations are colored in red, VRC01-class mutations are shown in purple, non-VRC01 mutations are in black. Kabat-defined CDRK1 and CDRK2 regions are highlighted. (E) Sequence

logos of CDRK1s and CDRK2s of glVRC01, VRC01, VRC01-class antibodies, all dG5 K278T neutralizers, and all non- dG5 K278T neutralizers. (F) Comparison of the all AA mutations per KC sequence between dG5 K278T neutralizers and non-dG5 K278T neutralizers isolated from all three immunized groups.

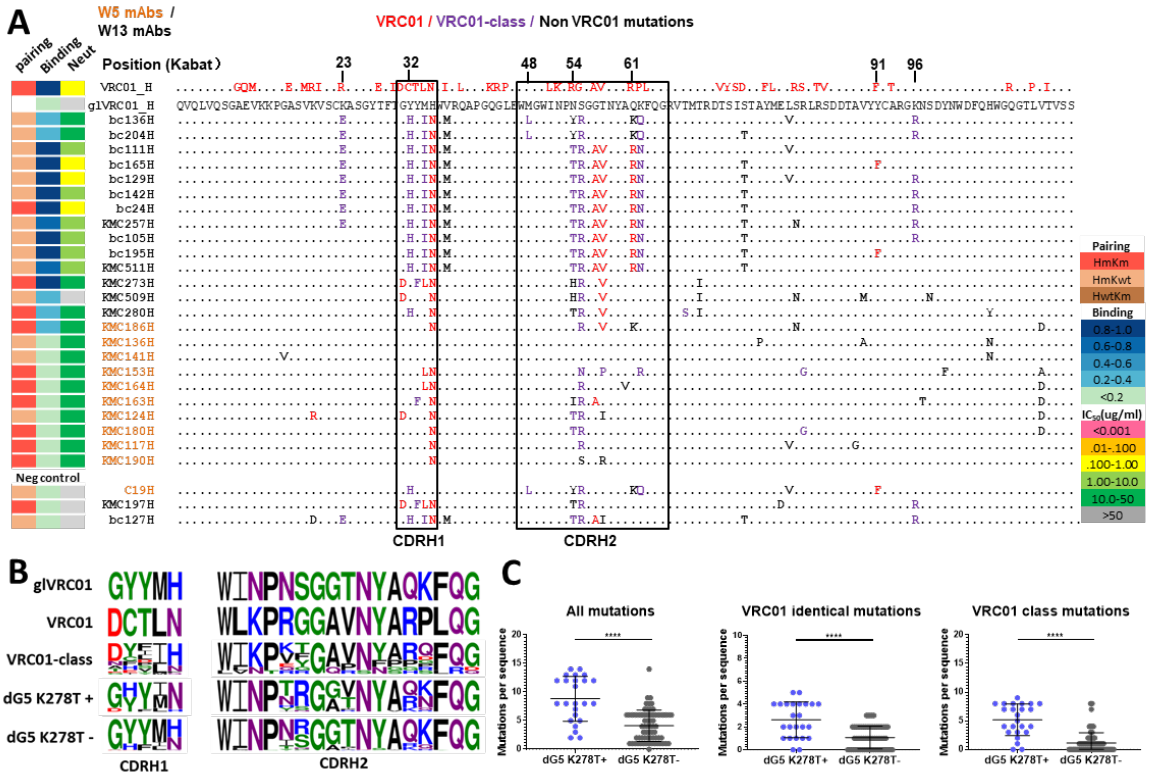


**Figure 4.11 Sequence analysis of the mAbs that neutralize 45_01dG5 K278T virus.** (A) Heavy chain AA sequence alignment. VRC01 mutations are colored in red, VRC01-class mutations are shown in purple, non VRC01 mutations are in black. Kabat-defined CDRH1 and CDRH2 regions are highlighted. (B) Sequence logos of CDRH1s and CDRH2s of glVRC01, VRC01, VRC01-class antibodies, all dG5 K278T neutralizers, and all non- dG5 K278T neutralizers. (C) Comparison of the AA mutations per HC sequence between dG5 K278T neutralizers and non- dG5 K278T neutralizers isolated from all three immunized groups under three categories (all mutations, VRC01 identical mutations, and VRC01 class mutations).

### *4.4 Discussion*

For VRC01 germline-targeting immunogen design, removal of the glycans obstructing the CD4bs, especially all the glycans at position 276, 460, and 463, seems to be indispensable to engage VRC01-class mAb precursors. (Jardine et al., 2013; LaBranche et al., 2018; McGuire et al., 2016; Medina-Ramírez et al., 2017; Stamatatos et al., 2017).

Interestingly, glycans N276 and N460 are naturally missing in the 45_01dG5 Env sequence. Trimer-based immunogens on the background of dG5 even confer binding to VRC01gl without any adjustment in the CD4bs epitope (**Figure 4.2**). To evaluate the immunogenicity of these immunogens, we utilized a transgenic mouse model (VRC01$^{gHL}$ mice) that expresses unnaturally high VRC01 precursors (Abbott et al., 2018). This VRC01GL knock-in mouse model is an excellent in vivo platform to evaluate initial naïve VRC01 B cell activation and directional maturation by vaccination. Our immunogens and immunization strategies tested in this system successfully induced epitope-specific antibody responses and mixed VRC01 and VRC01-class mutations within the same BCR sequences (**Figure 4.3, 4.6, 4.7, 4.10 & 4.11**). In particular, priming and boosting with trimer-based immunogens in group C stimulated consistently more mutations in both heavy and light chains, suggesting the trimer context imposes more stringent selections on affinity maturation on both chains, especially the light chain, compared to the monomeric context in eOD-GT8 and CoreD-(n5i5)-17 complexes (**Figure 4.3, 4.6, 4.7, 4.10 & 4.11**). Furthermore, our immunizations induced somatic mutations critical for the function of VRC01-class bNAbs, and a fraction of mAbs isolated from this study tolerated well with the N276 glycan (**Figure 4.10 & 4.11**). However, they still displayed limited neutralization breadth and potency against tier-2 viruses, which needs to be addressed by future immunogen modification.

Admittedly, BCR affinity maturation in the germinal centers is driven by multiple factors (B cell precursor frequency, BCR affinity, competition for Tfh cells, etc.), not just the absolute affinity (Dal Porto et al., 1998; Havenar-Daughton et al., 2017; Schwickert et al., 2011; Shih et al., 2002; Tas et al., 2016). Thus, the affinity maturation process observed

in the germinal center environment with the super-high frequency of VRC01-class precursor B cells may not fully speak for the immune responses induced by our designed immunogens in the polyclonal repertoires. To precisely control the frequency of VRC01 precursors, we will also test the immunogenicity of dG5-based immunogens in a B cell transfer model, in which VRC01$^{gHL}$ precursor B cells are transferred from VRC01gHL mice to congenic parental mice at various frequencies mimicking the physiologically relevant conditions (Abbott et al., 2018). In addition, mouse models genetically engineered to carry entire human immunoglobulin (Ig) genes are also practical platforms to study our designed immunogens to guide further refinement (Lee et al., 2014; Ma et al., 2013; Murphy et al., 2014).

Cross-reactive nAbs (crNAbs) with the broad breadth but suboptimal potency have been successfully isolated from animals subsequently vaccinated with heterologous HIV Env-based immunogens (Dubrovskaya et al., 2019; Xu et al., 2018). Despite the quality, robustness, and frequency of the serum neutralization in these studies still need to be improved, it is encouraging to achieve nAb responses mirroring the bNAbs in the animals with polyclonal repertoires (Dubrovskaya et al., 2019; Xu et al., 2018). These results are proof of principles that bNAbs targeting different epitopes can be recapitulated through exquisite immunogen design and immunization strategy optimization. Accordingly, dG5-based immunogens described in this study might also be applicable for future heterologous cocktail sequential immunizations to induce CD4bs bNAb responses. However, further sequence modifications around the CD4bs in the dG5 sequence might be beneficial to better expose the CD4bs for initial interaction with naïve VRC01 precursor B cells (Dubrovskaya et al., 2019; Zhou et al., 2017; Zhu et al., 2019). Moreover, to constrain the

approaching angle of selected B cells and augment their tolerance of critical glycans during directional affinity maturation, graduate restoration of the N-linked glycosylation sites (PNGS) and mutations back to wild type or even more glycosylated versions of dG5 trimers surrounding the CD4bs might be essential in the subsequent boosts (Borst et al., 2018; Dubrovskaya et al., 2019). Another feasible immunogen design strategy to explore in the context of dG5 is to repair or graft strain-specific residues/regions around and in the CD4bs with more prevalent ones (Rutten et al., 2018; Sliepen et al., 2019). However, further investigations are still ongoing to determine the components and combinations of immunization regimens.

In summary, bNAb VRC01 intermediates have been successfully elicited by our immunogens and immunization strategies, and the dG5-based immunogens proposed here might serve as prototypes to induce cross-reactive CD4bs nAb responses in future experiments.

# Chapter 5: Conclusions and Future Directions

bNAbs isolated from HIV elite controllers have reinvigorated the HIV vaccine research field after years of frustrating setbacks from traditional vaccine design approaches. The essential goal in the field now is to design protein molecules as antigens to elicit similar bNAb-like responses via tailored immunization strategies. Engineered Env-based immunogens thus far induce robust and consistent autologous tier-2 serum neutralizing antibody responses (Montefiori et al., 2018; Moore, 2018; Sanders and Moore, 2017). A few sporadic studies have even successfully induced cross-reactive neutralizing antibodies from vaccinated animals (Dubrovskaya et al., 2019; Wang et al., 2017; Xu et al., 2018). However, in general, the antibody responses induced by current immunogens and immunization strategies are still way inferior to the bNAb responses from natural infections.

The primary focus of the studies in this thesis is to provide immunogen modification strategies and potential templates for bNAb induction. We first developed and validated a new guinea pig single B cell analysis platform for immunogen evaluation. As an alternative to the mouse model, the guinea pig model offers abundant raw samples for B cell response analysis. The work described in **Chapter II** was undertaken specifically to address the lack of single B cell sorting and antibody cloning protocols for guinea pigs. The workflow introduced in the study can also be applied to generate guinea pig-specific mAbs for other cell markers not available in the market yet. An expanded the reagent panel will enhance the sorting resolution to differentiate the subsets of the immune cells more precisely. The primers designed in the study can also be used for NGS library preparation of bulk guinea pig antigen-specific B cells. The cloning primer set itself could be iteratively tweaked with the sequencing data of naive B cell repertoires. Future efforts on these applications may facilitate immunogen screening and refinement.

In **Chapter III**, we revealed a strain-specific immunodominant epitope on the BG505 SOSIP.664, the benchmark native-like Env trimer immunogen. Our study showed that a large portion of induced neutralizing antibodies only targets the non-conserved Env sequences around the CD4bs (C3/V4) and incompetent to recognize the same region of other virus strains. Therefore, to improve the immunogenicity of the BG505 SOSIP, antibody responses to the C3/V4 region need to be dampened and shifted towards more conserved regions (CD4bs, etc.). This requires tweaking the BG505-specific sequences and filling the glycan holes missing at the conserved positions on the trimer. However, the exact sequence that will be grafted into the C3/V4 region might be determined by the combination of rational exploitation, computational aid, and experimental screening. The overall aim is to alter the immunodominant regions to more conserved epitopes without losing the immunogenicity of the BG505 SOSIP trimer.

In addition to the chimeric BG505 variants, we proposed another HIV immunogen template in **Chapter IV**. The Env sequence of the patient-derived virus (45_01dG5) naturally lacks key glycans impeding the maturation of VRC01 B cell lineage (Lynch et al., 2015). The dG5-based immunogens designed in the study engaged with the VRC01 germline precursors and induced VRC01 mutations in a humanized mouse model. We have confirmed the dG5-based immunogens initiated the activation of VRC01 precursor B cells. However, the germline-targeting immunogens alone are not enough to generate bNAbs responses against HIV-1. In addition, the germline-targeting sequential immunization strategy remains to be tested in genetically unmodified animal models. The challenge to pursue is how to drive and accumulate critical SHM and broaden the spectrum of neutralizing antibody response for various HIV-1 virus strains. The Env template is likely

required to go through rounds of sequence modifications to explore the proper combination and permutation of dG5 variants as priming/boosting immunogens. Glycan manipulation around the CD4bs might be a feasible starting point for inspection. Detailed insights distilled from structural and sequence analysis of VRC01-like antibodies and Envs may also yield sequence revision tactics in the background of dG5.

FACS-based single-cell sorting is one of the core technologies that transformed the HIV vaccine research over recent decades. This well-developed technology lays the groundwork for the isolation and characterization of numerous HIV bNAbs. In this thesis, the same strategy was applied to dissect the vaccine-induced polyclonal antibody responses and identify rare B cells with desired specificities from large heterogeneous populations. The multi-parametric analysis platform unquestionably empowers HIV mAb isolation and immunological studies. However, like any technology, it has its limitations. For users, the cell sorter has a relatively steep learning curve. Highly skilled specialists are required to handle the complex instrument. As for the machine itself, the sorter demands frequent maintenance. It has a delicate microfluidics system that prone to blockages. The lasers also require regular calibration and warm-up before the experiments. In regards to single B cell analysis, although the relatively high throughput workflow is achievable, the cell sorting rate is slow for rare populations. The downstream single-cell sequencing and antibody screening could also be cost-ineffective and labor-intensive.

More seamless and higher throughput approaches that emerged in the market may better complement or ultimately replace the FACs cell sorting in analyzing B cell repertories at single-cell resolution. The burst of lab-on-a-chip devices based on microfluidic chips (Berkeley Lights NanOblast, Takara ICELL8, etc.), gel bead emulsion

(GEM) droplets (10X Genomics, Illumina ddSEQ, etc.), and micro-well plates (BD Rhapsody, CellRaft AIR, etc.) provide alternative single B cell manipulation and sequencing approaches (Jorgolli et al., 2019; Valihrach et al., 2018; Winters et al., 2019; Wyatt Shields IV et al., 2015). However, these miniaturized devices still require an additional process for antigen-specific B cell enrichment, which is likely to be carried out by either FACS or magnetic-activated cell sorting (MACS). Beacon Opotofludic devices from Berkley Lights offer another more integrated option to select, manipulate, analyze, and culture thousands of antigen-specific single B cells (Jorgolli et al., 2019). Overall, FACs-based single B cell analysis is still the benchmark. However, at least from the trend, we can envision the next-generation single-cell sorting devices with lower fluidic running pressure to avoid potential biohazard aerosols, equivalent or faster sorting rates, high single-cell capturing accuracy and purity, and more automated processing workflow. Along with the computational power for large dataset analysis and high-resolution cryo-EM structural analysis, the technological advances will inevitably empower and transform scientific discoveries that eventually lead to significant progress in HIV vaccine development.

***Concluding Remarks***

The development of a preventive HIV vaccine remains a formidable challenge, the filed just experienced another setback in the clinical trial HVTN 702 early this year. However, looking back at the milestones in recent HIV vaccine research, we have reason to believe the efficacy of future vaccine candidates will continue to be improved. Admittedly, there is no guarantee that a subunit HIV vaccine can be protective. I am still confident that the researchers might eventually find a solution to provide sterile immunity

and eliminate the acquired infection. Ending the HIV pandemic represents the aspirations of the whole community. The journey of a thousand miles begins with a single step. The quest for an HIV vaccine has already started since the beginning of the pandemic. It will not stop until completed.

# Publication Information

**Peer-reviewed articles related to the dissertation:**

1. **Lei, L.**, Tran, K., Wang, Y., Steinhardt, J.J., Xiao, Y., Chiang, C.-I., Wyatt, R.T., and Li, Y. (2019). Antigen-Specific Single B Cell Sorting and Monoclonal Antibody Cloning in Guinea Pigs. Front. Microbiol. *10*, 672.
2. **Lei, L.**, Yang, Y.R., Tran, K., Wang, Y., Chiang, C.-I., Ozorowski, G., Xiao, Y., Ward, A.B., Wyatt, R.T., and Li, Y. (2019). The HIV-1 Envelope Glycoprotein C3/V4 Region Defines a Prevalent Neutralization Epitope following Immunization. Cell Rep. *27*, 586-598.e6.

**Other peer-reviewed publications:**

3. Wang, Y., O'Dell, S., Turner, H.L., Chiang, C.-I., **Lei, L.**, Guenaga, J., Wilson, R., Martinez-Murillo, P., Doria-Rose, N., Ward, A.B., et al. (2017). HIV-1 Cross-Reactive Primary Virus Neutralizing Antibody Response Elicited by Immunization in Nonhuman Primates. J. Virol. *91*.
4. hao, X., Howell, K.A., He, S., Brannan, J.M., Wec, A.Z., Davidson, E., Turner, H.L., Chiang, C.I., **Lei, L.**, Fels, J.M., et al. (2017). Immunization-Elicited Broadly Protective Antibody Reveals Ebolavirus Fusion Loop as a Site of Vulnerability. Cell *169*, 891-904.e15.
5. Steinhardt, J.J., Guenaga, J., Turner, H.L., McKee, K., Louder, M.K., O'Dell, S., Chiang, C.-I., **Lei, L.**, Galkin, A., Andrianov, A.K., et al. (2018). Rational design of a trispecific antibody targeting the HIV-1 Env with elevated anti-viral activity. Nat. Commun. *9*, 877.

# Bibliography


Abbott, R.K., Lee, J.H., Menis, S., Skog, P., Rossi, M., Ota, T., Kulp, D.W., Bhullar, D., Kalyuzhniy, O., Havenar-Daughton, C., et al. (2018). Precursor Frequency and Affinity Determine B Cell Competitive Fitness in Germinal Centers, Tested with Germline-Targeting HIV Vaccine Immunogens. Immunity *48*, 133-146.e6.

Adamson, B.J.S., Carlson, J.J., Kublin, J.G., and Garrison, L.P. (2017). The Potential Cost-Effectiveness of Pre-Exposure Prophylaxis Combined with HIV Vaccines in the United States. Vaccines *5*, 13.

Affram, Y., Zapata, J.C., Gholizadeh, Z., Tolbert, W.D., Zhou, W., Iglesias-Ussel, M.D., Pazgier, M., Ray, K., Latinovic, O.S., and Romerio, F. (2019). The HIV-1 Antisense Protein ASP Is a Transmembrane Protein of the Cell Surface and an Integral Protein of the Viral Envelope. J. Virol. *93*, e00574-19.

Alam, S.M., Dennison, S.M., Aussedat, B., Vohra, Y., Park, P.K., Fernandez-Tejada, A., Stewart, S., Jaeger, F.H., Anasti, K., Blinn, J.H., et al. (2013). Recognition of synthetic glycopeptides by HIV-1 broadly neutralizing antibodies and their unmutated ancestors. Proc. Natl. Acad. Sci. *110*, 18214–18219.

Alamyar, E., Duroux, P., Lefranc, M.-P., and Giudicelli, V. (2012). IMGT(®) tools for the nucleotide analysis of immunoglobulin (IG) and T cell receptor (TR) V-(D)-J repertoires, polymorphisms, and IG mutations: IMGT/V-QUEST and IMGT/HighV-QUEST for NGS. Methods Mol. Biol. *882*, 569–604.

Andrabi, R., Voss, J.E., Liang, C.-H., Briney, B., McCoy, L.E., Wu, C.-Y., Wong, C.-H., Poignard, P., and Burton, D.R. (2015). Identification of Common Features in Prototype Broadly Neutralizing Antibodies to HIV Envelope V2 Apex to Facilitate Vaccine Design. Immunity *43*, 959–973.

Andrabi, R., Bhiman, J.N., and Burton, D.R. (2018). Strategies for a multi-stage neutralizing antibody-based HIV vaccine. Curr. Opin. Immunol. *53*, 143–151.

Anthony, C., York, T., Bekker, V., Matten, D., Selhorst, P., Ferreria, R.-C., Garrett, N.J., Karim, S.S.A., Morris, L., Wood, N.T., et al. (2017). Cooperation between Strain-Specific and Broadly Neutralizing Responses Limited Viral Escape and Prolonged the Exposure of the Broadly Neutralizing Epitope. J. Virol. *91*, e00828-17.

Arhel, N. (2010). Revisiting HIV-1 uncoating. Retrovirology *7*, 96.

Aussedat, B., Vohra, Y., Park, P.K., Fernández-Tejada, A., Alam, S.M., Dennison, S.M., Jaeger, F.H., Anasti, K., Stewart, S., Blinn, J.H., et al. (2013). Chemical Synthesis of Highly Congested gp120 V1V2 N -Glycopeptide Antigens for Potential HIV-1-Directed Vaccines. J. Am. Chem. Soc. *135*, 13113–13120.

Bale, S., Martiné, A., Wilson, R., Behrens, A.-J., Le Fourn, V., de Val, N., Sharma, S.K., Tran, K., Torres, J.L., Girod, P.-A., et al. (2018). Cleavage-Independent HIV-1 Trimers From CHO Cell Lines Elicit Robust Autologous Tier 2 Neutralizing Antibodies. Front. Immunol. *9*, 1116.

Barré-Sinoussi, F., Chermann, J.C., Rey, F., Nugeyre, M.T., Chamaret, S., Gruest, J., Dauguet, C., Axler-Blin, C., Vézinet-Brun, F., Rouzioux, C., et al. (1983). Isolation of a T-lymphotropic retrovirus from a patient at risk for acquired immune deficiency syndrome (AIDS). Science *220*, 868–871.

Beddows, S., Kirschner, M., Campbell-Gardener, L., Franti, M., Dey, A.K., Iyer, S.P.N., Maddon, P.J., Paluch, M., Master, A., Overbaugh, J., et al. (2006). Construction and Characterization of Soluble, Cleaved, and Stabilized Trimeric Env Proteins Based on HIV Type 1 Env Subtype A. AIDS Res. Hum. Retroviruses *22*, 569–579.

Binley, J.M., Sanders, R.W., Clas, B., Schuelke, N., Master, A., Guo, Y., Kajumo, F., Anselma, D.J., Maddon, P.J., Olson, W.C., et al. (2000). A Recombinant Human Immunodeficiency Virus Type 1 Envelope Glycoprotein Complex Stabilized by an Intermolecular Disulfide Bond between the gp120 and gp41 Subunits Is an Antigenic Mimic of the Trimeric Virion-Associated Structure. J. Virol. *74*, 627–643.

Binley, J.M., Sanders, R.W., Master, A., Cayanan, C.S., Wiley, C.L., Schiffner, L., Travis, B., Kuhmann, S., Burton, D.R., Hu, S.-L., et al. (2002). Enhancing the Proteolytic Maturation of Human Immunodeficiency Virus Type 1 Envelope Glycoproteins. J. Virol. *76*, 2606–2616.

Bonsignori, M., Hwang, K.-K., Chen, X., Tsao, C.-Y., Morris, L., Gray, E., Marshall, D.J., Crump, J.A., Kapiga, S.H., Sam, N.E., et al. (2011). Analysis of a Clonal Lineage of HIV-1 Envelope V2/V3 Conformational Epitope-Specific Broadly Neutralizing Antibodies and Their Inferred Unmutated Common Ancestors. J. Virol. *85*, 9998–10009.

Bonsignori, M., Zhou, T., Sheng, Z., Chen, L., Gao, F., Joyce, M.G., Ozorowski, G., Chuang, G.-Y., Schramm, C.A., Wiehe, K., et al. (2016). Maturation Pathway from Germline to Broad HIV-1 Neutralizer of a CD4-Mimic Antibody. Cell *165*, 449–463.

Bonsignori, M., Scott, E., Wiehe, K., Easterhoff, D., Alam, S.M., Hwang, K.-K., Cooper, M., Xia, S.-M., Zhang, R., Montefiori, D.C., et al. (2018). Inference of the HIV-1 VRC01 Antibody Lineage Unmutated Common Ancestor Reveals Alternative Pathways to Overcome a Key Glycan Barrier. Immunity *49*, 1162-1174.e8.

Borst, A.J., Weidle, C.E., Gray, M.D., Frenz, B., Snijder, J., Joyce, M.G., Georgiev, I.S., Stewart-Jones, G.B.E., Kwong, P.D., McGuire, A.T., et al. (2018). Germline VRC01 antibody recognition of a modified clade C HIV-1 envelope trimer and a glycosylated HIV-1 gp120 core. Elife *7*, e37688.

Bradley, T., Fera, D., Bhiman, J., Eslamizar, L., Lu, X., Anasti, K., Zhang, R., Sutherland, L.L., Scearce, R.M., Bowman, C.M., et al. (2016). Structural Constraints of Vaccine-Induced Tier-2 Autologous HIV Neutralizing Antibodies Targeting the Receptor-Binding Site. Cell Rep. *14*, 43–54.

Bricault, C.A., Yusim, K., Seaman, M.S., Yoon, H., Theiler, J., Giorgi, E.E., Wagh, K., Theiler, M., Hraber, P., Macke, J.P., et al. (2019). HIV-1 Neutralizing Antibody Signatures and Application to Epitope-Targeted Vaccine Design. Cell Host Microbe *25*, 59-72.e8.

Briney, B., Sok, D., Jardine, J.G., Kulp, D.W., Skog, P., Menis, S., Jacak, R.,

Kalyuzhniy, O., de Val, N., Sesterhenn, F., et al. (2016). Tailored Immunogens Direct Affinity Maturation toward HIV Neutralizing Antibodies. Cell *166*, 1459-1470.e11.

Burton, D.R. (2019). Advancing an HIV vaccine; advancing vaccinology. Nat. Rev. Immunol. *19*, 77–78.

Burton, D.R., and Hangartner, L. (2016). Broadly Neutralizing Antibodies to HIV and Their Role in Vaccine Design. Annu. Rev. Immunol. *34*, 635–659.

Burton, D.R., and Parren, P.W.H.I. (2000). Vaccines and the induction of functional antibodies: Time to look beyond the molecules of natural infection? Nat. Med. *6*, 123–125.

Campbell, E.M., and Hope, T.J. (2015). HIV-1 capsid: the multifaceted key player in HIV-1 infection. Nat. Rev. Microbiol. *13*, 471–483.

Carragher, B., Kisseberth, N., Kriegman, D., Milligan, R.A., Potter, C.S., Pulokas, J., and Reilein, A. (2000). Leginon: an automated system for acquisition of images from vitreous ice specimens. J. Struct. Biol. *132*, 33–45.

Case, K. (1986). Nomenclature: human immunodeficiency virus. Ann. Intern. Med. *105*, 133.

Centers for Disease Control and Prevention (CDC) (1996). Pneumocystis pneumonia--Los Angeles. 1981. MMWR. Morb. Mortal. Wkly. Rep. *45*, 729–733.

Chakrabarti, B.K., Feng, Y., Sharma, S.K., McKee, K., Karlsson Hedestam, G.B., Labranche, C.C., Montefiori, D.C., Mascola, J.R., and Wyatt, R.T. (2013). Robust neutralizing antibodies elicited by HIV-1 JRFL envelope glycoprotein trimers in nonhuman primates. J. Virol. *87*, 13239–13251.

Chen, W.-T., Shiu, C.-S., Yang, J.P., Simoni, J.M., Fredriksen-Goldsen, K.I., Lee, T.S.-H., and Zhao, H. (2013). Antiretroviral Therapy (ART) Side Effect Impacted on Quality of Life, and Depressive Symptomatology: A Mixed-Method Study. J. AIDS Clin. Res. *4*, 218.

Corcoran, M.M., Phad, G.E., Bernat, N.V., Stahl-Hennig, C., Sumida, N., Persson, M.A.A., Martin, M., and Hedestam, G.B.K.K. (2016). Production of individualized V gene databases reveals high levels of immunoglobulin genetic diversity. Nat. Commun. *7*, 13642.

Crooks, E.T., Tong, T., Chakrabarti, B., Narayan, K., Georgiev, I.S., Menis, S., Huang, X., Kulp, D., Osawa, K., Muranaka, J., et al. (2015). Vaccine-Elicited Tier 2 HIV-1 Neutralizing Antibodies Bind to Quaternary Epitopes Involving Glycan-Deficient Patches Proximal to the CD4 Binding Site. PLOS Pathog. *11*, e1004932.

Dal Porto, J.M., Haberman, A.M., Shlomchik, M.J., and Kelsoe, G. (1998). Antigen drives very low affinity B cells to become plasmacytes and enter germinal centers. J. Immunol. *161*, 5373–5381.

Derking, R., Ozorowski, G., Sliepen, K., Yasmeen, A., Cupo, A., Torres, J.L., Julien, J.P., Lee, J.H., van Montfort, T., de Taeye, S.W., et al. (2015). Comprehensive Antigenic

Map of a Cleaved Soluble HIV-1 Envelope Trimer. PLoS Pathog. *11*, 1–22.

Diskin, R., Scheid, J.F., Marcovecchio, P.M., West, A.P., Klein, F., Gao, H., Gnanapragasam, P.N.P.P., Abadir, A., Seaman, M.S., Nussenzweig, M.C., et al. (2011). Increasing the potency and breadth of an HIV antibody by using structure-based rational design. Science *334*, 1289–1293.

Doria-Rose, N.A., and Joyce, M.G. (2015). Strategies to guide the antibody affinity maturation process. Curr. Opin. Virol. *11*, 137–147.

Doria-Rose, N.A., Klein, R.M., Manion, M.M., O'Dell, S., Phogat, A., Chakrabarti, B., Hallahan, C.W., Migueles, S.A., Wrammert, J., Ahmed, R., et al. (2009). Frequency and Phenotype of Human Immunodeficiency Virus Envelope-Specific B Cells from Patients with Broadly Cross-Neutralizing Antibodies. J. Virol. *83*, 188–199.

Doria-Rose, N.A., Schramm, C.A., Gorman, J., Moore, P.L., Bhiman, J.N., DeKosky, B.J., Ernandes, M.J., Georgiev, I.S., Kim, H.J., Pancera, M., et al. (2014). Developmental pathway for potent V1V2-directed HIV-neutralizing antibodies. Nature *509*, 55–62.

Dosenovic, P., Von Boehmer, L., Escolano, A., Jardine, J., Freund, N.T., Gitlin, A.D., McGuire, A.T., Kulp, D.W., Oliveira, T., Scharf, L., et al. (2015). Immunization for HIV-1 Broadly Neutralizing Antibodies in Human Ig Knockin Mice. Cell *161*, 1505–1515.

Duan, H., Chen, X., Boyington, J.C., Cheng, C., Zhang, Y., Jafari, A.J., Stephens, T., Tsybovsky, Y., Kalyuzhniy, O., Zhao, P., et al. (2018). Glycan Masking Focuses Immune Responses to the HIV-1 CD4-Binding Site and Enhances Elicitation of VRC01-Class Precursor Antibodies. Immunity *49*, 301-311.e5.

Dubrovskaya, V., Tran, K., Ozorowski, G., Guenaga, J., Wilson, R., Bale, S., Cottrell, C.A., Turner, H.L., Seabright, G., O'Dell, S., et al. (2019). Vaccination with Glycan-Modified HIV NFL Envelope Trimer-Liposomes Elicits Broadly Neutralizing Antibodies to Multiple Sites of Vulnerability. Immunity *51*, 915-929.e7.

Earl, P.L., Koenig, S., and Moss, B. (1991). Biological and immunological properties of human immunodeficiency virus type 1 envelope glycoprotein: analysis of proteins with truncations and deletions expressed by recombinant vaccinia viruses. J. Virol. *65*, 31–41.

Earl, P.L., Broder, C.C., Long, D., Lee, S.A., Peterson, J., Chakrabarti, S., Doms, R.W., and Moss, B. (1994). Native oligomeric human immunodeficiency virus type 1 envelope glycoprotein elicits diverse monoclonal antibody reactivities. J. Virol. *68*, 3015–3026.

Elsheikh, M.M., Tang, Y., Li, D., and Jiang, G. (2019). Deep latency: A new insight into a functional HIV cure. EBioMedicine *45*, 624–629.

Engelman, A., and Cherepanov, P. (2012). The structural biology of HIV-1: mechanistic and therapeutic insights. Nat. Rev. Microbiol. *10*, 279–290.

Escolano, A., Steichen, J.M., Dosenovic, P., Kulp, D.W., Golijanin, J., Sok, D., Freund, N.T., Gitlin, A.D., Oliveira, T., Araki, T., et al. (2016). Sequential Immunization Elicits Broadly Neutralizing Anti-HIV-1 Antibodies in Ig Knockin Mice. Cell *166*, 1445-1458.e12.

Esparza, J. (2013). A brief history of the global effort to develop a preventive HIV vaccine. Vaccine *31*, 3502–3518.

Fauci, A.S. (2003). HIV and AIDS: 20 years of science. Nat. Med. *9*, 839–843.

Fauci, A.S., Folkers, G.K., and Marston, H.D. (2014). Ending the Global HIV/AIDS Pandemic: The Critical Role of an HIV Vaccine. Clin. Infect. Dis. *59*, S80–S84.

Feng, Y., McKee, K., Tran, K., O'Dell, S., Schmidt, S.D., Phogat, A., Forsell, M.N., Karlsson Hedestam, G.B., Mascola, J.R., and Wyatt, R.T. (2012). Biochemically Defined HIV-1 Envelope Glycoprotein Variant Immunogens Display Differential Binding and Neutralizing Specificities to the CD4-binding Site. J. Biol. Chem. *287*, 5673–5686.

Feng, Y., Tran, K., Bale, S., Kumar, S., Guenaga, J., Wilson, R., de Val, N., Arendt, H., DeStefano, J., Ward, A.B., et al. (2016). Thermostability of Well-Ordered HIV Spikes Correlates with the Elicitation of Autologous Tier 2 Neutralizing Antibodies. PLoS Pathog. *12*, 1–26.

Flynn, N.M., Forthal, D.N., Harro, C.D., Judson, F.N., Mayer, K.H., Para, M.F., and rgp120 HIV Vaccine Study Group (2005). Placebo-controlled phase 3 trial of a recombinant glycoprotein 120 vaccine to prevent HIV-1 infection. J. Infect. Dis. *191*, 654–665.

Food and Drug Administration (FDA) (2018). Antiretroviral drugs used in the treatment of HIV infection. Https://Www.Fda.Gov/Patients/Hiv-Treatment/Antiretroviral-Drugs-Used-Treatment-Hiv-Infection 9–12.

Frankel, A.D., and Young, J.A.T. (1998). HIV-1: Fifteen Proteins and an RNA. Annu. Rev. Biochem. *67*, 1–25.

Freed, E.O. (2015). HIV-1 assembly, release and maturation. Nat. Rev. Microbiol. *13*, 484–496.

Gallo, R.C. (2002). Historical essay. The early years of HIV/AIDS. Science *298*, 1728–1730.

Georgiev, I.S., Joyce, M.G., Yang, Y., Sastry, M., Zhang, B., Baxa, U., Chen, R.E., Druz, A., Lees, C.R., Narpala, S., et al. (2015). Single-Chain Soluble BG505.SOSIP gp140 Trimers as Structural and Antigenic Mimics of Mature Closed HIV-1 Env. J. Virol. *89*, 5318–5329.

Georgiou, G., Ippolito, G.C., Beausang, J., Busse, C.E., Wardemann, H., and Quake, S.R. (2014). The promise and challenge of high-throughput sequencing of the antibody repertoire. Nat. Biotechnol. *32*, 158–168.

Gilbert, P., Wang, M., Wrin, T., Petropoulos, C., Gurwith, M., Sinangil, F., D'Souza, P., Rodriguez-Chavez, I.R., DeCamp, A., Giganti, M., et al. (2010). Magnitude and Breadth of a Nonprotective Neutralizing Antibody Response in an Efficacy Trial of a Candidate HIV-1 gp120 Vaccine. J. Infect. Dis. *202*, 595–605.

Go, E.P., Zhang, Y., Menon, S., and Desaire, H. (2011). Analysis of the disulfide bond arrangement of the HIV-1 envelope protein CON-S gp140 ΔCFI shows variability in the

V1 and V2 regions. J. Proteome Res. *10*, 578–591.

Go, E.P., Hua, D., and Desaire, H. (2014). Glycosylation and Disulfide Bond Analysis of Transiently and Stably Expressed Clade C HIV-1 gp140 Trimers in 293T Cells Identifies Disulfide Heterogeneity Present in Both Proteins and Differences in O -Linked Glycosylation. J. Proteome Res. *13*, 4012–4027.

Go, E.P., Cupo, A., Ringe, R., Pugach, P., Moore, J.P., and Desaire, H. (2016). Native Conformation and Canonical Disulfide Bond Formation Are Interlinked Properties of HIV-1 Env Glycoproteins. J. Virol. *90*, 2884–2894.

Goo, L., Chohan, V., Nduati, R., and Overbaugh, J. (2014). Early development of broadly neutralizing antibodies in HIV-1-infected infants. Nat. Med. *20*, 655–658.

Gorman, J., Soto, C., Yang, M.M., Davenport, T.M., Guttman, M., Bailer, R.T., Chambers, M., Chuang, G.-Y., DeKosky, B.J., Doria-Rose, N.A., et al. (2015). Structures of HIV-1 Env V1V2 with broadly neutralizing antibodies reveal commonalities that enable vaccine design. Nat. Struct. Mol. Biol. *23*, 81–90.

Gorny, M.K., Stamatatos, L., Volsky, B., Revesz, K., Williams, C., Wang, X.-H., Cohen, S., Staudinger, R., and Zolla-Pazner, S. (2005). Identification of a New Quaternary Neutralizing Epitope on Human Immunodeficiency Virus Type 1 Virus Particles. J. Virol. *79*, 5232–5237.

Gottlieb, M.S., Schroff, R., Schanker, H.M., Weisman, J.D., Fan, P.T., Wolf, R.A., and Saxon, A. (1981). Pneumocystis carinii Pneumonia and Mucosal Candidiasis in Previously Healthy Homosexual Men. N. Engl. J. Med. *305*, 1425–1431.

Graham, B.S. (2013). Advances in antiviral vaccine development. Immunol. Rev. *255*, 230–242.

Gray, G.E., Huang, Y., Grunenberg, N., Laher, F., Roux, S., Andersen-Nissen, E., De Rosa, S.C., Flach, B., Randhawa, A.K., Jensen, R., et al. (2019). Immune correlates of the Thai RV144 HIV vaccine regimen in South Africa. Sci. Transl. Med. *11*, eaax1880.

Greene, W.C., and Peterlin, B.M. (2002). Charting HIV's remarkable voyage through the cell: Basic science as a passport to future therapy. Nat. Med. *8*, 673–680.

Gristick, H.B., von Boehmer, L., West Jr, A.P., Schamber, M., Gazumyan, A., Golijanin, J., Seaman, M.S., Fätkenheuer, G., Klein, F., Nussenzweig, M.C., et al. (2016). Natively glycosylated HIV-1 Env structure reveals new mode for antibody recognition of the CD4-binding site. Nat. Struct. Mol. Biol. *23*, 906–915.

Guenaga, J., de Val, N., Tran, K., Feng, Y., Satchwell, K., Ward, A.B., and Wyatt, R.T. (2015). Well-Ordered Trimeric HIV-1 Subtype B and C Soluble Spike Mimetics Generated by Negative Selection Display Native-like Properties. PLoS Pathog. *11*, e1004570.

Guenaga, J., Dubrovskaya, V., de Val, N., Sharma, S.K., Carrette, B., Ward, A.B., and Wyatt, R.T. (2016). Structure-Guided Redesign Increases the Propensity of HIV Env To Generate Highly Stable Soluble Trimers. J. Virol. *90*, 2806–2817.

Gulick, R.M., and Flexner, C. (2019). Long-Acting HIV Drugs for Treatment and Prevention. Annu. Rev. Med. *70*, 137–150.

Guo, Y., Bao, Y., Meng, Q.Q., Hu, X., Meng, Q.Q., Ren, L., Li, N., and Zhao, Y. (2012). Immunoglobulin genomics in the guinea pig (Cavia porcellus). PLoS One *7*, 1–18.

van Haaren, M.M., van den Kerkhof, T.L.G.M., and van Gils, M.J. (2017). Natural infection as a blueprint for rational HIV vaccine design. Hum. Vaccines Immunother. *13*, 229–236.

Halper-Stromberg, A., and Nussenzweig, M.C. (2016). Towards HIV-1 remission: potential roles for broadly neutralizing antibodies. J. Clin. Invest. *126*, 415–423.

Havenar-Daughton, C., Lee, J.H., and Crotty, S. (2017). Tfh cells and HIV bnAbs, an immunodominance model of the HIV neutralizing antibody generation problem. Immunol. Rev. *275*, 49–61.

Havenar-Daughton, C., Sarkar, A., Kulp, D.W., Toy, L., Hu, X., Deresa, I., Kalyuzhniy, O., Kaushik, K., Upadhyay, A.A., Menis, S., et al. (2018). The human naive B cell repertoire contains distinct subclasses for a germline-targeting HIV-1 vaccine immunogen. Sci. Transl. Med. *10*, eaat0381.

Haynes, B.F., and Burton, D.R. (2017). Developing an HIV vaccine. Science *355*, 1129–1130.

He, L., Kumar, S., Allen, J.D., Huang, D., Lin, X., Mann, C.J., Saye-Francisco, K.L., Copps, J., Sarkar, A., Blizard, G.S., et al. (2018). HIV-1 vaccine design through minimizing envelope metastability. Sci. Adv. *4*, eaau6769.

Hessell, A.J., Malherbe, D.C., Pissani, F., McBurney, S., Krebs, S.J., Gomes, M., Pandey, S., Sutton, W.F., Burwitz, B.J., Gray, M., et al. (2016). Achieving Potent Autologous Neutralizing Antibody Responses against Tier 2 HIV-1 Viruses by Strategic Selection of Envelope Immunogens. J. Immunol. *196*, 3064–3078.

Hoffenberg, S., Powell, R., Carpov, A., Wagner, D., Wilson, A., Kosakovsky Pond, S., Lindsay, R., Arendt, H., DeStefano, J., Phogat, S., et al. (2013). Identification of an HIV-1 Clade A Envelope That Exhibits Broad Antigenicity and Neutralization Sensitivity and Elicits Antibodies Targeting Three Distinct Epitopes. J. Virol. *87*, 5372–5383.

Hoot, S., McGuire, A.T., Cohen, K.W., Strong, R.K., Hangartner, L., Klein, F., Diskin, R., Scheid, J.F., Sather, D.N., Burton, D.R., et al. (2013). Recombinant HIV Envelope Proteins Fail to Engage Germline Versions of Anti-CD4bs bNAbs. PLoS Pathog. *9*, e1003106.

Hu, J.K., Crampton, J.C., Cupo, A., Ketas, T., van Gils, M.J., Sliepen, K., de Taeye, S.W., Sok, D., Ozorowski, G., Deresa, I., et al. (2015). Murine Antibody Responses to Cleaved Soluble HIV-1 Envelope Trimers Are Highly Restricted in Specificity. J. Virol. *89*, 10383–10398.

Huang, C.-C., Lam, S.N., Acharya, P., Tang, M., Xiang, S.-H., Hussan, S.S.-U., Stanfield, R.L., Robinson, J., Sodroski, J., Wilson, I.A., et al. (2007). Structures of the CCR5 N terminus and of a tyrosine-sulfated antibody with HIV-1 gp120 and CD4.

Science *317*, 1930–1934.

Huang, J., Kang, B.H., Ishida, E., Zhou, T., Griesman, T., Sheng, Z., Wu, F., Doria-Rose, N.A., Zhang, B., McKee, K., et al. (2016). Identification of a CD4-Binding-Site Antibody to HIV that Evolved Near-Pan Neutralization Breadth. Immunity *45*, 1108–1121.

Hwang, J.K., Wang, C., Du, Z., Meyers, R.M., Kepler, T.B., Neuberg, D., Kwong, P.D., Mascola, J.R., Joyce, M.G., Bonsignori, M., et al. (2017). Sequence intrinsic somatic mutation mechanisms contribute to affinity maturation of VRC01-class HIV-1 broadly neutralizing antibodies. Proc. Natl. Acad. Sci. *114*, 8614–8619.

Institute of Medicine (US) Committee on a National Strategy for AIDS. (1986). Confronting AIDS: Directions for Public Health, Health Care, and Research (Washington, D.C.: National Academies Press).

Iyer, S.P.N., Franti, M., Krauchuk, A.A., Fisch, D.N., Ouattara, A.A., Roux, K.H., Krawiec, L., Dey, A.K., Beddows, S., Maddon, P.J., et al. (2007). Purified, proteolytically mature HIV type 1 SOSIP gp140 envelope trimers. AIDS Res. Hum. Retroviruses.

Jardine, J., Julien, J.-P., Menis, S., Ota, T., Kalyuzhniy, O., McGuire, A., Sok, D., Huang, P.-S., MacPherson, S., Jones, M., et al. (2013). Rational HIV immunogen design to target specific germline B cell receptors. Science *340*, 711–716.

Jardine, J.G., Ota, T., Sok, D., Pauthner, M., Kulp, D.W., Kalyuzhniy, O., Skog, P.D., Thinnes, T.C., Bhullar, D., Briney, B., et al. (2015). Priming a broadly neutralizing antibody response to HIV-1 using a germline-targeting immunogen. Science *349*, 156–161.

Jardine, J.G., Kulp, D.W., Havenar-Daughton, C., Sarkar, A., Briney, B., Sok, D., Sesterhenn, F., Ereño-Orbea, J., Kalyuzhniy, O., Deresa, I., et al. (2016a). HIV-1 broadly neutralizing antibody precursor B cells revealed by germline-targeting immunogen. Science *351*, 1458–1463.

Jardine, J.G., Sok, D., Julien, J.-P.P., Briney, B., Sarkar, A., Liang, C.-H.H., Scherer, E.A., Henry Dunand, C.J., Adachi, Y., Diwanji, D., et al. (2016b). Minimally Mutated HIV-1 Broadly Neutralizing Antibodies to Guide Reductionist Vaccine Design. PLoS Pathog. *12*, 1–33.

Jeffs, S.A., Goriup, S., Kebble, B., Crane, D., Bolgiano, B., Sattentau, Q., Jones, S., and Holmes, H. (2004). Expression and characterisation of recombinant oligomeric envelope glycoproteins derived from primary isolates of HIV-1. Vaccine *22*, 1032–1046.

Johnston, M.I., and Fauci, A.S. (2008). An HIV Vaccine — Challenges and Prospects. N. Engl. J. Med. *359*, 888–890.

Jorgolli, M., Nevill, T., Winters, A., Chen, I., Chong, S., Lin, F., Mock, M., Chen, C., Le, K., Tan, C., et al. (2019). Nanoscale integration of single cell biologics discovery processes using optofluidic manipulation and monitoring. Biotechnol. Bioeng. *116*, 2393–2411.

Julien, J.-P.J.-P., Cupo, A., Sok, D., Stanfield, R.L., Lyumkis, D., Deller, M.C., Klasse,

P.-J.P.-J., Burton, D.R., Sanders, R.W., Moore, J.P., et al. (2013). Crystal structure of a soluble cleaved HIV-1 envelope trimer. Science *342*, 1477–1483.

Kanekiyo, M., Bu, W., Gordon, M., Graham, B.S., Jeffrey, I., Nabel, G.J., Kanekiyo, M., Bu, W., Joyce, M.G., Meng, G., et al. (2015). Rational Design of an Epstein-Barr Virus Vaccine Targeting the Receptor-Binding Site Article Rational Design of an Epstein-Barr Virus Vaccine Targeting the Receptor-Binding Site. Cell *162*, 1090–1100.

Kelsoe, G., Verkoczy, L., and Haynes, B. (2013). Immune System Regulation in the Induction of Broadly Neutralizing HIV-1 Antibodies. Vaccines *2*, 1–14.

Kepler, T.B., and Wiehe, K. (2017). Genetic and structural analyses of affinity maturation in the humoral response to HIV-1. Immunol. Rev. *275*, 129–144.

Kinch, M.S., and Patridge, E. (2014). An analysis of FDA-approved drugs for infectious disease: HIV/AIDS drugs. Drug Discov. Today *19*, 1510–1513.

Klasse, P.J. (2014). Neutralization of Virus Infectivity by Antibodies: Old Problems in New Perspectives. Adv. Biol. *2014*, 1–24.

Klasse, P.J., Ketas, T.J., Cottrell, C.A., Ozorowski, G., Debnath, G., Camara, D., Francomano, E., Pugach, P., Ringe, R.P., LaBranche, C.C., et al. (2018). Epitopes for neutralizing antibodies induced by HIV-1 envelope glycoprotein BG505 SOSIP trimers in rabbits and macaques. PLoS Pathog. *14*, e1006913.

Klein, U., and Dalla-Favera, R. (2008). Germinal centres: role in B-cell physiology and malignancy. Nat. Rev. Immunol. *8*, 22–33.

Klein, F., Gaebler, C., Mouquet, H., Sather, D.N., Lehmann, C., Scheid, J.F., Kraft, Z., Liu, Y., Pietzsch, J., Hurley, A., et al. (2012). Broad neutralization by a combination of antibodies recognizing the CD4 binding site and a new conformational epitope on the HIV-1 envelope protein. J. Exp. Med. *209*, 1469–1479.

Kong, L., He, L., de Val, N., Vora, N., Morris, C.D., Azadnia, P., Sok, D., Zhou, B., Burton, D.R., Ward, A.B., et al. (2016a). Uncleaved prefusion-optimized gp140 trimers derived from analysis of HIV-1 envelope metastability. Nat. Commun. *7*, 12040.

Kong, L., Ju, B., Chen, Y.Y., He, L., Ren, L., Liu, J., Hong, K., Su, B., Wang, Z., Ozorowski, G., et al. (2016b). Key gp120 Glycans Pose Roadblocks to the Rapid Development of VRC01-Class Antibodies in an HIV-1-Infected Chinese Donor. Immunity *44*, 939–950.

Kovacs, J.M., Nkolola, J.P., Peng, H., Cheung, A., Perry, J., Miller, C.A., Seaman, M.S., Barouch, D.H., and Chen, B. (2012). HIV-1 envelope trimer elicits more potent neutralizing antibody responses than monomeric gp120. Proc. Natl. Acad. Sci. *109*, 12111–12116.

Kulp, D.W., and Schief, W.R. (2013). Advances in structure-based vaccine design. Curr. Opin. Virol. *3*, 322–331.

Kulp, D.W., Steichen, J.M., Pauthner, M., Hu, X., Schiffner, T., Liguori, A., Cottrell, C.A., Havenar-Daughton, C., Ozorowski, G., Georgeson, E., et al. (2017). Structure-

based design of native-like HIV-1 envelope trimers to silence non-neutralizing epitopes and eliminate CD4 binding. Nat. Commun. *8*, 1655.

Kurosaki, T., Kometani, K., and Ise, W. (2015). Memory B cells. Nat. Rev. Immunol. *15*, 149–159.

Kurosawa, N., Yoshioka, M., Fujimoto, R., Yamagishi, F., and Isobe, M. (2012). Rapid production of antigen-specific monoclonal antibodies from a variety of animals. BMC Biol. *10*, 80.

Do Kwon, Y., Pancera, M., Acharya, P., Georgiev, I.S., Crooks, E.T., Gorman, J., Joyce, M.G., Guttman, M., Ma, X., Narpala, S., et al. (2015). Crystal structure, conformational fixation and entry-related interactions of mature ligand-free HIV-1 Env. Nat. Struct. Mol. Biol. *22*, 522–531.

LaBranche, C.C., McGuire, A.T., Gray, M.D., Behrens, S., Zhou, T., Sattentau, Q.J., Peacock, J., Eaton, A., Greene, K., Gao, H., et al. (2018). HIV-1 envelope glycan modifications that permit neutralization by germline-reverted VRC01-class broadly neutralizing antibodies. PLOS Pathog. *14*, e1007431.

Landais, E., and Moore, P.L. (2018). Development of broadly neutralizing antibodies in HIV-1 infected elite neutralizers. Retrovirology *15*, 61.

Lander, G.C., Stagg, S.M., Voss, N.R., Cheng, A., Fellmann, D., Pulokas, J., Yoshioka, C., Irving, C., Mulder, A., Lau, P.-W., et al. (2009). Appion: an integrated, database-driven pipeline to facilitate EM image processing. J. Struct. Biol. *166*, 95–102.

Lanzavecchia, A., and Sallusto, F. (2009). Human B cell memory. Curr. Opin. Immunol. *21*, 298–304.

Lee, E.-C., Liang, Q., Ali, H., Bayliss, L., Beasley, A., Bloomfield-Gerdes, T., Bonoli, L., Brown, R., Campbell, J., Carpenter, A., et al. (2014). Complete humanization of the mouse immunoglobulin loci enables efficient therapeutic antibody discovery. Nat. Biotechnol. *32*, 356–363.

Lei, L., Tran, K., Wang, Y., Steinhardt, J.J., Xiao, Y., Chiang, C.-I., Wyatt, R.T., and Li, Y. (2019a). Antigen-Specific Single B Cell Sorting and Monoclonal Antibody Cloning in Guinea Pigs. Front. Microbiol. *10*, 672.

Lei, L., Yang, Y.R., Tran, K., Wang, Y., Chiang, C.-I., Ozorowski, G., Xiao, Y., Ward, A.B., Wyatt, R.T., and Li, Y. (2019b). The HIV-1 Envelope Glycoprotein C3/V4 Region Defines a Prevalent Neutralization Epitope following Immunization. Cell Rep. *27*, 586-598.e6.

Li, G., and De Clercq, E. (2016). HIV Genome-Wide Protein Associations: a Review of 30 Years of Research. Microbiol. Mol. Biol. Rev. *80*, 679–731.

Li, M., Gao, F., Mascola, J.R., Stamatatos, L., Polonis, V.R., Koutsoukos, M., Voss, G., Goepfert, P., Gilbert, P., Greene, K.M., et al. (2005). Human Immunodeficiency Virus Type 1 env Clones from Acute and Early Subtype B Infections for Standardized Assessments of Vaccine-Elicited Neutralizing Antibodies Human Immunodeficiency Virus Type 1 env Clones from Acute and Early Subtype B Infections for. J. Virol. *79*,

10108–10125.

Li, Y., Migueles, S.A., Welcher, B., Svehla, K., Phogat, A., Louder, M.K., Wu, X., Shaw, G.M., Connors, M., Wyatt, R.T., et al. (2007). Broad HIV-1 neutralization mediated by CD4-binding site antibodies. Nat. Med. *13*, 1032–1034.

Li, Y., O'Dell, S., Walker, L.M., Wu, X., Guenaga, J., Feng, Y., Schmidt, S.D., McKee, K., Louder, M.K., Ledgerwood, J.E., et al. (2011). Mechanism of Neutralization by the Broadly Neutralizing HIV-1 Monoclonal Antibody VRC01. J. Virol. *85*, 8954–8967.

Li, Z., Woo, C.J., Iglesias-Ussel, M.D., Ronai, D., and Scharff, M.D. (2004). The generation of antibody diversity through somatic hypermutation and class switch recombination. Genes Dev. *18*, 1–11.

Liao, H.-X., Bonsignori, M., Alam, S.M., McLellan, J.S., Tomaras, G.D., Moody, M.A., Kozink, D.M., Hwang, K.-K., Chen, X., Tsao, C.-Y., et al. (2013a). Vaccine Induction of Antibodies against a Structurally Heterogeneous Site of Immune Pressure within HIV-1 Envelope Protein Variable Regions 1 and 2. Immunity *38*, 176–186.

Liao, H.-X., Bonsignori, M., Alam, S.M., McLellan, J.S., Tomaras, G.D., Moody, M.A., Kozink, D.M., Hwang, K.-K., Chen, X., Tsao, C.-Y., et al. (2013b). Vaccine Induction of Antibodies against a Structurally Heterogeneous Site of Immune Pressure within HIV-1 Envelope Protein Variable Regions 1 and 2. Immunity *38*, 176–186.

Lloyd, S.B., Kent, S.J., and Winnall, W.R. (2014). The High Cost of Fidelity. AIDS Res. Hum. Retroviruses *30*, 8–16.

Lynch, R.M., Wong, P., Tran, L., O'Dell, S., Nason, M.C., Li, Y., Wu, X., and Mascola, J.R. (2015). HIV-1 Fitness Cost Associated with Escape from the VRC01 Class of CD4 Binding Site Neutralizing Antibodies. J. Virol. *89*, 4201–4213.

Lyumkis, D., Julien, J.-P., de Val, N., Cupo, A., Potter, C.S., Klasse, P.-J., Burton, D.R., Sanders, R.W., Moore, J.P., Carragher, B., et al. (2013). Cryo-EM structure of a fully glycosylated soluble cleaved HIV-1 envelope trimer. Science *342*, 1484–1490.

Ma, B., Osborn, M.J., Avis, S., Ouisse, L.-H., Ménoret, S., Anegon, I., Buelow, R., and Brüggemann, M. (2013). Human antibody expression in transgenic rats: Comparison of chimeric IgH loci with human VH, D and JH but bearing different rat C-gene regions. J. Immunol. Methods *400–401*, 78–86.

Martinez-Murillo, P., Tran, K., Guenaga, J., Lindgren, G., Àdori, M., Feng, Y., Phad, G.E., Vázquez Bernat, N., Bale, S., Ingale, J., et al. (2017). Particulate Array of Well-Ordered HIV Clade C Env Trimers Elicits Neutralizing Antibodies that Display a Unique V2 Cap Approach. Immunity *46*, 804-817.e7.

Mascola, J.R., and Montefiori, D.C. (2003). HIV-1: nature's master of disguise. Nat. Med. *9*, 393–394.

Masur, H., Michelis, M.A., Greene, J.B., Onorato, I., Vande Stouwe, R.A., Holzman, R.S., Wormser, G., Brettman, L., Lange, M., Murray, H.W., et al. (1981). An Outbreak of Community-Acquired Pneumocystis carinii Pneumonia. N. Engl. J. Med. *305*, 1431–1438.

McCoy, L.E. (2018). The expanding array of HIV broadly neutralizing antibodies. Retrovirology *15*, 70.

McCoy, L.E., and Burton, D.R. (2017). Identification and specificity of broadly neutralizing antibodies against HIV. Immunol. Rev. *275*, 11–20.

McCoy, L.E., van Gils, M.J., Ozorowski, G., Messmer, T., Briney, B., Voss, J.E., Kulp, D.W., Macauley, M.S., Sok, D., Pauthner, M., et al. (2016). Holes in the Glycan Shield of the Native HIV Envelope Are a Target of Trimer-Elicited Neutralizing Antibodies. Cell Rep. *16*, 2327–2338.

McGuire, A.T., Hoot, S., Dreyer, A.M., Lippy, A., Stuart, A., Cohen, K.W., Jardine, J., Menis, S., Scheid, J.F., West, A.P., et al. (2013). Engineering HIV envelope protein to activate germline B cell receptors of broadly neutralizing anti-CD4 binding site antibodies. J. Exp. Med. *210*, 655–663.

McGuire, A.T., Dreyer, A.M., Carbonetti, S., Lippy, A., Glenn, J., Scheid, J.F., Mouquet, H., and Stamatatos, L. (2014). HIV antibodies. Antigen modification regulates competition of broad and narrow neutralizing HIV antibodies. Science *346*, 1380–1383.

McGuire, A.T., Gray, M.D., Dosenovic, P., Gitlin, A.D., Freund, N.T., Petersen, J., Correnti, C., Johnsen, W., Kegel, R., Stuart, A.B., et al. (2016). Specifically modified Env immunogens activate B-cell precursors of broadly neutralizing HIV-1 antibodies in transgenic mice. Nat. Commun. *7*, 10618.

Medina-Ramírez, M., Garces, F., Escolano, A., Skog, P., de Taeye, S.W., Del Moral-Sanchez, I., McGuire, A.T., Yasmeen, A., Behrens, A.-J., Ozorowski, G., et al. (2017). Design and crystal structure of a native-like HIV-1 envelope trimer that engages multiple broadly neutralizing antibody precursors in vivo. J. Exp. Med. *214*, 2573–2590.

Montagnier, L. (2002). Historical essay. A history of HIV discovery. Science *298*, 1727–1728.

Montaner, J.S.G., Montessori, V., Harrigan, R., O'Shaughnessy, M., and Hogg, R. (1999). Antiretroviral therapy: 'the state of the art.' Biomed. Pharmacother. *53*, 63–72.

Montefiori, D.C., Roederer, M., Morris, L., and Seaman, M.S. (2018). Neutralization tiers of HIV-1. Curr. Opin. HIV AIDS *13*, 128–136.

Moore, P.L. (2018). The Neutralizing Antibody Response to the HIV-1 Env Protein. Curr. HIV Res. *16*, 21–28.

Moore, P.L., Gray, E.S., Choge, I.A., Ranchobe, N., Mlisana, K., Abdool Karim, S.S., Williamson, C., and Morris, L. (2008). The c3-v4 region is a major target of autologous neutralizing antibodies in human immunodeficiency virus type 1 subtype C infection. J. Virol. *82*, 1860–1869.

Moore, P.L., Ranchobe, N., Lambson, B.E., Gray, E.S., Cave, E., Abrahams, M.-R.R., Bandawe, G., Mlisana, K., Abdool Karim, S.S., Williamson, C., et al. (2009). Limited neutralizing antibody specificities drive neutralization escape in early HIV-1 subtype C infection. PLoS Pathog. *5*, e1000598.

Murphy, A.J., Macdonald, L.E., Stevens, S., Karow, M., Dore, A.T., Pobursky, K., Huang, T.T., Poueymirou, W.T., Esau, L., Meola, M., et al. (2014). Mice with megabase humanization of their immunoglobulin genes generate antibodies as efficiently as normal mice. Proc. Natl. Acad. Sci. U. S. A. *111*, 5153–5158.

Murray, A.J., Kwon, K.J., Farber, D.L., and Siliciano, R.F. (2016). The Latent Reservoir for HIV-1: How Immunologic Memory and Clonal Expansion Contribute to HIV-1 Persistence. J. Immunol. *197*, 407–417.

Nkolola, J.P., Peng, H., Settembre, E.C., Freeman, M., Grandpre, L.E., Devoy, C., Lynch, D.M., La Porte, A., Simmons, N.L., Bradley, R., et al. (2010). Breadth of Neutralizing Antibodies Elicited by Stable, Homogeneous Clade A and Clade C HIV-1 gp140 Envelope Trimers in Guinea Pigs. J. Virol. *84*, 3270–3279.

Padilla-Carlin, D.J., McMurray, D.N., and Hickey, A.J. (2008). The guinea pig as a model of infectious diseases. Comp. Med. *58*, 324–340.

Parks, K.R., MacCamy, A.J., Trichka, J., Gray, M., Weidle, C., Borst, A.J., Khechaduri, A., Takushi, B., Agrawal, P., Guenaga, J., et al. (2019). Overcoming Steric Restrictions of VRC01 HIV-1 Neutralizing Antibodies through Immunization. Cell Rep. *29*, 3060-3072.e7.

Parren, P.W.H.I., Burton, D.R., and Sattentau, Q.J. (1997). HIV-1 antibody — debris or virion? Nat. Med. *3*, 366–367.

Pauthner, M., Havenar-Daughton, C., Sok, D., Nkolola, J.P., Bastidas, R., Boopathy, A. V., Carnathan, D.G., Chandrashekar, A., Cirelli, K.M., Cottrell, C.A., et al. (2017). Elicitation of Robust Tier 2 Neutralizing Antibody Responses in Nonhuman Primates by HIV Envelope Trimer Immunization Using Optimized Approaches. Immunity *46*, 1073-1088.e6.

Phad, G.E., Vázquez Bernat, N., Feng, Y., Ingale, J., Martinez Murillo, P.A., O'Dell, S., Li, Y., Mascola, J.R., Sundling, C., Wyatt, R.T., et al. (2015). Diverse Antibody Genetic and Recognition Properties Revealed following HIV-1 Envelope Glycoprotein Immunization. J. Immunol. *194*, 5903–5914.

Pitisuttithum, P., Gilbert, P., Gurwith, M., Heyward, W., Martin, M., van Griensven, F., Hu, D., Tappero, J.W., and Choopanya, K. (2006). Randomized, Double-Blind, Placebo-Controlled Efficacy Trial of a Bivalent Recombinant Glycoprotein 120 HIV-1 Vaccine among Injection Drug Users in Bangkok, Thailand. J. Infect. Dis. *194*, 1661–1671.

Rantalainen, K., Berndsen, Z.T., Murrell, S., Cao, L., Omorodion, O., Torres, J.L., Wu, M., Umotoy, J., Copps, J., Poignard, P., et al. (2018). Co-evolution of HIV Envelope and Apex-Targeting Neutralizing Antibody Lineage Provides Benchmarks for Vaccine Design. Cell Rep. *23*, 3249–3261.

Rerks-Ngarm, S., Pitisuttithum, P., Nitayaphan, S., Kaewkungwal, J., Chiu, J., Paris, R., Premsri, N., Namwat, C., de Souza, M., Adams, E., et al. (2009). Vaccination with ALVAC and AIDSVAX to Prevent HIV-1 Infection in Thailand. N. Engl. J. Med. *361*, 2209–2220.

Ringe, R.P., Sanders, R.W., Yasmeen, A., Kim, H.J., Lee, J.H., Cupo, A., Korzun, J., Derking, R., van Montfort, T., Julien, J.-P., et al. (2013). Cleavage strongly influences whether soluble HIV-1 envelope glycoprotein trimers adopt a native-like conformation. Proc. Natl. Acad. Sci. *110*, 18256–18261.

Ringe, R.P., Yasmeen, A., Ozorowski, G., Go, E.P., Pritchard, L.K., Guttman, M., Ketas, T.A., Cottrell, C.A., Wilson, I.A., Sanders, R.W., et al. (2015). Influences on the Design and Purification of Soluble, Recombinant Native-Like HIV-1 Envelope Glycoprotein Trimers. J. Virol. *89*, 12189–12210.

Robinson, H.L. (2018). HIV/AIDS Vaccines: 2018. Clin. Pharmacol. Ther. *104*, 1062–1073.

Rutten, L., Lai, Y.-T.T., Blokland, S., Truan, D., Bisschop, I.J.M., Strokappe, N.M., Koornneef, A., van Manen, D., Chuang, G.-Y.Y., Farney, S.K., et al. (2018). A Universal Approach to Optimize the Folding and Stability of Prefusion-Closed HIV-1 Envelope Trimers. Cell Rep. *23*, 584–595.

Saag, M.S., Benson, C.A., Gandhi, R.T., Hoy, J.F., Landovitz, R.J., Mugavero, M.J., Sax, P.E., Smith, D.M., Thompson, M.A., Buchbinder, S.P., et al. (2018). Antiretroviral Drugs for Treatment and Prevention of HIV Infection in Adults. JAMA *320*, 379.

Sadanand, S., Suscovich, T.J., and Alter, G. (2016). Broadly Neutralizing Antibodies Against HIV: New Insights to Inform Vaccine Design. Annu. Rev. Med. *67*, 185–200.

Sanders, R.W., and Moore, J.P. (2017). Native-like Env trimers as a platform for HIV-1 vaccine design. Immunol. Rev. *275*, 161–182.

Sanders, R.W., Vesanen, M., Schuelke, N., Master, A., Schiffner, L., Kalyanaraman, R., Paluch, M., Berkhout, B., Maddon, P.J., Olson, W.C., et al. (2002). Stabilization of the soluble, cleaved, trimeric form of the envelope glycoprotein complex of human immunodeficiency virus type 1. J. Virol. *76*, 8875–8889.

Sanders, R.W., Derking, R., Cupo, A., Julien, J.-P., Yasmeen, A., de Val, N., Kim, H.J., Blattner, C., de la Peña, A.T., Korzun, J., et al. (2013). A Next-Generation Cleaved, Soluble HIV-1 Env Trimer, BG505 SOSIP.664 gp140, Expresses Multiple Epitopes for Broadly Neutralizing but Not Non-Neutralizing Antibodies. PLoS Pathog. *9*, e1003618.

Sanders, R.W., van Gils, M.J., Derking, R., Sok, D., Ketas, T.J., Burger, J.A., Ozorowski, G., Cupo, A., Simonich, C., Goo, L., et al. (2015). HIV-1 VACCINES. HIV-1 neutralizing antibodies induced by native-like envelope trimers. Science *349*, aac4223.

Sarkar, A., Bale, S., Behrens, A.-J., Kumar, S., Sharma, S.K., de Val, N., Pallesen, J., Irimia, A., Diwanji, D.C., Stanfield, R.L., et al. (2018). Structure of a cleavage-independent HIV Env recapitulates the glycoprotein architecture of the native cleaved trimer. Nat. Commun. *9*, 1956.

Sather, D.N., Carbonetti, S., Malherbe, D.C., Pissani, F., Stuart, A.B., Hessell, A.J., Gray, M.D., Mikell, I., Kalams, S.A., Haigwood, N.L., et al. (2014). Emergence of broadly neutralizing antibodies and viral coevolution in two subjects during the early stages of infection with human immunodeficiency virus type 1. J. Virol. *88*, 12968–12981.

Sattentau, Q.J., and Moore, J.P. (1995). Human immunodeficiency virus type 1 neutralization is determined by epitope exposure on the gp120 oligomer. J. Exp. Med. *182*, 185–196.

Saunders, K.O., Nicely, N.I., Wiehe, K., Bonsignori, M., Meyerhoff, R.R., Parks, R., Walkowicz, W.E., Aussedat, B., Wu, N.R., Cai, F., et al. (2017). Vaccine Elicitation of High Mannose-Dependent Neutralizing Antibodies against the V3-Glycan Broadly Neutralizing Epitope in Nonhuman Primates. Cell Rep. *18*, 2175–2188.

Saunders, K.O., Wiehe, K., Tian, M., Acharya, P., Bradley, T., Alam, S.M., Go, E.P., Scearce, R., Sutherland, L., Henderson, R., et al. (2019). Targeted selection of HIV-specific antibody mutations by engineering B cell maturation. Science *366*, eaay7199.

Scharf, L., West, A.P., Sievers, S.A., Chen, C., Jiang, S., Gao, H., Gray, M.D., McGuire, A.T., Scheid, J.F., Nussenzweig, M.C., et al. (2016). Structural basis for germline antibody recognition of HIV-1 immunogens. Elife *5*.

Scheid, J.F., Mouquet, H., Ueberheide, B., Diskin, R., Klein, F., Oliveira, T.Y.K., Pietzsch, J., Fenyo, D., Abadir, A., Velinzon, K., et al. (2011). Sequence and structural convergence of broad and potent HIV antibodies that mimic CD4 binding. Science *333*, 1633–1637.

Scheres, S.H.W. (2012). RELION: Implementation of a Bayesian approach to cryo-EM structure determination. J. Struct. Biol. *180*, 519–530.

van Schooten, J., and van Gils, M.J. (2018). HIV-1 immunogens and strategies to drive antibody responses towards neutralization breadth. Retrovirology *15*, 74.

Schwickert, T.A., Victora, G.D., Fooksman, D.R., Kamphorst, A.O., Mugnier, M.R., Gitlin, A.D., Dustin, M.L., and Nussenzweig, M.C. (2011). A dynamic T cell–limited checkpoint regulates affinity-dependent B cell entry into the germinal center. J. Exp. Med. *208*, 1243–1252.

Seelamgari, A. (2004). Role of viral regulatory and accessory proteins in HIV-1 replication. Front. Biosci. *9*, 2388.

Sekaly, R.-P. (2008). The failed HIV Merck vaccine study: a step back or a launching point for future vaccine development? J. Exp. Med. *205*, 7–12.

Sharma, S.K., deVal, N., Bale, S., Guenaga, J., Tran, K., Feng, Y., Dubrovskaya, V., Ward, A.B., and Wyatt, R.T. (2015). Cleavage-Independent HIV-1 Env Trimers Engineered as Soluble Native Spike Mimetics for Vaccine Design. Cell Rep. *11*, 539–550.

Shih, T.-A.Y., Meffre, E., Roederer, M., and Nussenzweig, M.C. (2002). Role of BCR affinity in T cell dependent antibody responses in vivo. Nat. Immunol. *3*, 570–575.

Silva, M., Nguyen, T.H., Philbrook, P., Chu, M., Sears, O., Hatfield, S., Abbott, R.K., Kelsoe, G., and Sitkovsky, M. V. (2017). Targeted Elimination of Immunodominant B Cells Drives the Germinal Center Reaction toward Subdominant Epitopes. Cell Rep. *21*, 3672–3680.

Sliepen, K., Ozorowski, G., Burger, J.A., van Montfort, T., Stunnenberg, M., LaBranche, C., Montefiori, D.C., Moore, J.P., Ward, A.B., and Sanders, R.W. (2015). Presenting native-like HIV-1 envelope trimers on ferritin nanoparticles improves their immunogenicity. Retrovirology *12*, 82.

Sliepen, K., Han, B.W., Bontjer, I., Mooij, P., Garces, F., Behrens, A.-J.J., Rantalainen, K., Kumar, S., Sarkar, A., Brouwer, P.J.M.M., et al. (2019). Structure and immunogenicity of a stabilized HIV-1 envelope trimer based on a group-M consensus sequence. Nat. Commun. *10*, 2355.

Sok, D., and Burton, D.R. (2018). Recent progress in broadly neutralizing antibodies to HIV. Nat. Immunol. *19*, 1179–1188.

Sok, D., van Gils, M.J., Pauthner, M., Julien, J.-P., Saye-Francisco, K.L., Hsueh, J., Briney, B., Lee, J.H., Le, K.M., Lee, P.S., et al. (2014). Recombinant HIV envelope trimer selects for quaternary-dependent antibodies targeting the trimer apex. Proc. Natl. Acad. Sci. U. S. A. *111*, 17624–17629.

Sok, D., Briney, B., Jardine, J.G., Kulp, D.W., Menis, S., Pauthner, M., Wood, A., Lee, E.-C., Le, K.M., Jones, M., et al. (2016). Priming HIV-1 broadly neutralizing antibody precursors in human Ig loci transgenic mice. Science *353*, 1557–1560.

Sok, D., Le, K.M., Vadnais, M., Saye-Francisco, K.L., Jardine, J.G., Torres, J.L., Berndsen, Z.T., Kong, L., Stanfield, R., Ruiz, J., et al. (2017). Rapid elicitation of broadly neutralizing antibodies to HIV by immunization in cows. Nature *548*, 108–111.

Stamatatos, L., Morris, L., Burton, D.R., and Mascola, J.R. (2009). Neutralizing antibodies generated during natural HIV-1 infection: good news for an HIV-1 vaccine? Nat. Med. *15*, 866–870.

Stamatatos, L., Pancera, M., and McGuire, A.T. (2017). Germline-targeting immunogens. Immunol. Rev. *275*, 203–216.

Starkie, D.O., Compson, J.E., Rapecki, S., and Lightwood, D.J. (2016). Generation of Recombinant Monoclonal Antibodies from Immunised Mice and Rabbits via Flow Cytometry and Sorting of Antigen-Specific IgG+ Memory B Cells. PLoS One *11*, e0152282.

Steichen, J.M., Kulp, D.W., Tokatlian, T., Escolano, A., Dosenovic, P., Stanfield, R.L., McCoy, L.E., Ozorowski, G., Hu, X., Kalyuzhniy, O., et al. (2016). HIV Vaccine Design to Target Germline Precursors of Glycan-Dependent Broadly Neutralizing Antibodies. Immunity *45*, 483–496.

Stewart-Jones, G.B.E.E., Soto, C., Lemmin, T., Chuang, G.-Y.Y., Druz, A., Kong, R., Thomas, P. V., Wagh, K., Zhou, T., Behrens, A.-J.J., et al. (2016). Trimeric HIV-1-Env Structures Define Glycan Shields from Clades A, B, and G. Cell *165*, 813–826.

Sundling, C., Phad, G., Douagi, I., Navis, M., and Karlsson Hedestam, G.B. (2012a). Isolation of antibody V(D)J sequences from single cell sorted rhesus macaque B cells. J. Immunol. Methods *386*, 85–93.

Sundling, C., Li, Y., Huynh, N., Poulsen, C., Wilson, R., O'Dell, S., Feng, Y., Mascola,

J.R., Wyatt, R.T., and Karlsson Hedestam, G.B. (2012b). High-Resolution Definition of Vaccine-Elicited B Cell Responses Against the HIV Primary Receptor Binding Site. Sci. Transl. Med. *4*, 142ra96-142ra96.

Swanson, C.M., and Malim, M.H. (2008). SnapShot: HIV-1 Proteins. Cell *133*, 742-742.e1.

Takata, H., Kessing, C., Sy, A., Lima, N., Sciumbata, J., Mori, L., Jones, R.B., Chomont, N., Michael, N.L., Valente, S., et al. (2019). Modeling HIV-1 Latency Using Primary CD4+ T Cells from Virally Suppressed HIV-1-Infected Individuals on Antiretroviral Therapy. J. Virol. *93*.

Tas, J.M.J.J., Mesin, L., Pasqual, G., Targ, S., Jacobsen, J.T., Mano, Y.M., Chen, C.S., Weill, J.-C., Reynaud, C.-A., Browne, E.P., et al. (2016). Visualizing antibody affinity maturation in germinal centers. Science *351*, 1048–1054.

Tetteh, R.A., Yankey, B.A., Nartey, E.T., Lartey, M., Leufkens, H.G.M., and Dodoo, A.N.O. (2017). Pre-Exposure Prophylaxis for HIV Prevention: Safety Concerns. Drug Saf. *40*, 273–283.

Tian, M., Cheng, C., Chen, X., Duan, H., Cheng, H.L., Dao, M., Sheng, Z., Kimble, M., Wang, L., Lin, S., et al. (2016). Induction of HIV Neutralizing Antibody Lineages in Mice with Diverse Precursor Repertoires. Cell *166*, 1471-1484.e18.

Tiller, T., Meffre, E., Yurasov, S., Tsuiji, M., Nussenzweig, M.C., and Wardemann, H. (2008). Efficient generation of monoclonal antibodies from single human B cells by single cell RT-PCR and expression vector cloning. J. Immunol. Methods *329*, 112–124.

Tiller, T., Busse, C.E., and Wardemann, H. (2009). Cloning and expression of murine Ig genes from single B cells. J. Immunol. Methods *350*, 183–193.

Tomaras, G., and Haynes, B. (2013). Advancing Toward HIV-1 Vaccine Efficacy through the Intersections of Immune Correlates. Vaccines *2*, 15–35.

Torrents de la Peña, A., and Sanders, R.W. (2018). Stabilizing HIV-1 envelope glycoprotein trimers to induce neutralizing antibodies. Retrovirology *15*, 63.

Torres, A.G., Gregory, A.E., Hatcher, C.L., Vinet-Oliphant, H., Morici, L.A., Titball, R.W., and Roy, C.J. (2015). Protection of non-human primates against glanders with a gold nanoparticle glycoconjugate vaccine. Vaccine *33*, 686–692.

Tran, K., Poulsen, C., Guenaga, J., de Val, N., Wilson, R., Sundling, C., Li, Y., Stanfield, R.L., Wilson, I.A., Ward, A.B., et al. (2014). Vaccine-elicited primate antibodies use a distinct approach to the HIV-1 primary receptor binding site informing vaccine redesign. Proc. Natl. Acad. Sci. *111*, E738–E747.

Tree, J.A., Elmore, M.J., Javed, S., Williams, A., and Marsh, P.D. (2006). Development of a guinea pig immune response-related microarray and its use to define the host response following Mycobacterium bovis BCG vaccination. Infect. Immun. *74*, 1436–1441.

Umotoy, J., Bagaya, B.S., Joyce, C., Schiffner, T., Menis, S., Saye-Francisco, K.L.,

Biddle, T., Mohan, S., Vollbrecht, T., Kalyuzhniy, O., et al. (2019). Rapid and Focused Maturation of a VRC01-Class HIV Broadly Neutralizing Antibody Lineage Involves Both Binding and Accommodation of the N276-Glycan. Immunity *51*, 141-154.e6.

UNAIDS (2019). Global HIV & AIDS statistics — 2019 fact sheet.

Valihrach, L., Androvic, P., and Kubista, M. (2018). Platforms for Single-Cell Collection and Analysis. Int. J. Mol. Sci. *19*, 807.

VanCott, T.C., Veit, S.C.D., Kalyanaraman, V., Earl, P., and Birx, D.L. (1995). Characterization of a soluble, oligomeric HIV-1 gp160 protein as a potential immunogen. J. Immunol. Methods *183*, 103–117.

Verkoczy, L. (2017). Humanized Immunoglobulin Mice. In Advances in Immunology, pp. 235–352.

Verkoczy, L., Alt, F.W., and Tian, M. (2017). Human Ig knockin mice to study the development and regulation of HIV-1 broadly neutralizing antibodies. Immunol. Rev. *275*, 89–107.

Victora, G.D., and Nussenzweig, M.C. (2012). Germinal centers. Annu. Rev. Immunol. *30*, 429–457.

Vigdorovich, V., Oliver, B.G., Carbonetti, S., Dambrauskas, N., Lange, M.D., Yacoob, C., Leahy, W., Callahan, J., Stamatatos, L., and Sather, D.N. (2016). Repertoire comparison of the B-cell receptor-encoding loci in humans and rhesus macaques by next-generation sequencing. Clin. Transl. Immunol. *5*, e93.

Wang, Y., Sundling, C., Wilson, R., O'Dell, S., Chen, Y., Dai, K., Phad, G.E., Zhu, J., Xiao, Y., Mascola, J.R., et al. (2016). High-Resolution Longitudinal Study of HIV-1 Env Vaccine-Elicited B Cell Responses to the Virus Primary Receptor Binding Site Reveals Affinity Maturation and Clonal Persistence. J. Immunol. *196*, 3729–3743.

Wang, Y., O'Dell, S., Turner, H.L., Chiang, C.-I., Lei, L., Guenaga, J., Wilson, R., Martinez-Murillo, P., Doria-Rose, N., Ward, A.B., et al. (2017). HIV-1 Cross-Reactive Primary Virus Neutralizing Antibody Response Elicited by Immunization in Nonhuman Primates. J. Virol. *91*.

Ward, A.B., and Wilson, I.A. (2015). Insights into the trimeric HIV-1 envelope glycoprotein structure. Trends Biochem. Sci. *40*, 101–107.

Ward, A.B., and Wilson, I.A. (2017). The HIV-1 envelope glycoprotein structure: nailing down a moving target. Immunol. Rev. *275*, 21–32.

West, A.P., Diskin, R., Nussenzweig, M.C., and Bjorkman, P.J. (2012). Structural basis for germ-line gene usage of a potent class of antibodies targeting the CD4-binding site of HIV-1 gp120. Proc. Natl. Acad. Sci. *109*, E2083–E2090.

Wibmer, C.K., Moore, P.L., and Morris, L. (2015). HIV broadly neutralizing antibody targets. Curr. Opin. HIV AIDS *10*, 135–143.

Wibmer, C.K., Gorman, J., Anthony, C.S., Mkhize, N.N., Druz, A., York, T., Schmidt,

S.D., Labuschagne, P., Louder, M.K., Bailer, R.T., et al. (2016). Structure of an N276-Dependent HIV-1 Neutralizing Antibody Targeting a Rare V5 Glycan Hole Adjacent to the CD4 Binding Site. J. Virol. *90*, 10220–10235.

Wiehe, K., Nicely, N.I., Lockwood, B., Kuraoka, M., Anasti, K., Arora, S., Bowman, C.M., Stolarchuk, C., Parks, R., Lloyd, K.E., et al. (2017). Immunodominance of Antibody Recognition of the HIV Envelope V2 Region in Ig-Humanized Mice. J. Immunol. *198*, 1047–1055.

Wilen, C.B., Tilton, J.C., and Doms, R.W. (2012). HIV: Cell Binding and Entry. Cold Spring Harb. Perspect. Med. *2*, a006866–a006866.

Winters, A., McFadden, K., Bergen, J., Landas, J., Berry, K.A., Gonzalez, A., Salimi-Moosavi, H., Murawsky, C.M., Tagari, P., and King, C.T. (2019). Rapid single B cell antibody discovery using nanopens and structured light. MAbs *11*, 1025–1035.

Worobey, M., Watts, T.D., McKay, R.A., Suchard, M.A., Granade, T., Teuwen, D.E., Koblin, B.A., Heneine, W., Lemey, P., and Jaffe, H.W. (2016). 1970s and 'Patient 0' HIV-1 genomes illuminate early HIV/AIDS history in North America. Nature *539*, 98–101.

Wu, X., Parast, A.B., Richardson, B. a, Nduati, R., John-stewart, G., Mbori-ngacha, D., Rainwater, S.M.J., and Overbaugh, J. (2006). Neutralization escape variants of human immunodeficiency virus type 1 are transmitted frommother to infant. J. Virol. *80*, 835–844.

Wu, X., Yang, Z.-Y., Li, Y., Hogerkorp, C.-M., Schief, W.R., Seaman, M.S., Zhou, T., Schmidt, S.D., Wu, L., Xu, L., et al. (2010). Rational design of envelope identifies broadly neutralizing human monoclonal antibodies to HIV-1. Science *329*, 856–861.

Wu, X., Zhang, Z., Schramm, C.A., Joyce, M.G., Do Kwon, Y., Zhou, T., Sheng, Z., Zhang, B., O'Dell, S., McKee, K., et al. (2015). Maturation and diversity of the VRC01-antibody lineage over 15 years of chronic HIV-1 infection. Cell *161*, 480–485.

Wyatt, R., and Sodroski, J. (1998). The HIV-1 envelope glycoproteins: fusogens, antigens, and immunogens. Science *280*, 1884–1888.

Wyatt Shields IV, C., Reyes, C.D., and López, G.P. (2015). Microfluidic cell sorting: a review of the advances in the separation of cells from debulking to rare cell isolation. Lab Chip *15*, 1230–1249.

Xiao, Q., Guo, D., and Chen, S. (2019). Application of CRISPR/Cas9-Based Gene Editing in HIV-1/AIDS Therapy. Front. Cell. Infect. Microbiol. *9*, 69.

Xu, K., Acharya, P., Kong, R., Cheng, C., Chuang, G.-Y., Liu, K., Louder, M.K., O'Dell, S., Rawi, R., Sastry, M., et al. (2018). Epitope-based vaccine design yields fusion peptide-directed antibodies that neutralize diverse strains of HIV-1. Nat. Med. *24*, 857–867.

Yang, L., Sharma, S.K., Cottrell, C., Guenaga, J., Tran, K., Wilson, R., Behrens, A.-J., Crispin, M., de Val, N., and Wyatt, R.T. (2018). Structure-Guided Redesign Improves NFL HIV Env Trimer Integrity and Identifies an Inter-Protomer Disulfide Permitting

Post-Expression Cleavage. Front. Immunol. *9*, 1631.

Yang, X., Wyatt, R., and Sodroski, J. (2001). Improved Elicitation of Neutralizing Antibodies against Primary Human Immunodeficiency Viruses by Soluble Stabilized Envelope Glycoprotein Trimers. J. Virol. *75*, 1165–1171.

Yang, X., Lee, J., Mahony, E.M., Kwong, P.D., Wyatt, R., and Sodroski, J. (2002). Highly stable trimers formed by human immunodeficiency virus type 1 envelope glycoproteins fused with the trimeric motif of T4 bacteriophage fibritin. J. Virol. *76*, 4634–4642.

Ye, J., Ma, N., Madden, T.L., and Ostell, J.M. (2013). IgBLAST: an immunoglobulin variable domain sequence analysis tool. Nucleic Acids Res. *41*, W34–W40.

Zaunders, J., Dyer, W.B., and Churchill, M. (2011). The Sydney Blood Bank Cohort: implications for viral fitness as a cause of elite control. Curr. Opin. HIV AIDS *6*, 151–156.

Zhao, X., Howell, K.A., He, S., Brannan, J.M., Wec, A.Z., Davidson, E., Turner, H.L., Chiang, C.I., Lei, L., Fels, J.M., et al. (2017). Immunization-Elicited Broadly Protective Antibody Reveals Ebolavirus Fusion Loop as a Site of Vulnerability. Cell *169*, 891-904.e15.

Zhou, T., Georgiev, I., Wu, X., Yang, Z.-Y., Dai, K., Finzi, A., Kwon, Y. Do, Scheid, J.F., Shi, W., Xu, L., et al. (2010). Structural basis for broad and potent neutralization of HIV-1 by antibody VRC01. Science *329*, 811–817.

Zhou, T., Zhu, J., Wu, X., Moquin, S., Zhang, B., Acharya, P., Georgiev, I.S., Altae-Tran, H.R., Chuang, G.-Y., Joyce, M.G., et al. (2013). Multidonor Analysis Reveals Structural Elements, Genetic Determinants, and Maturation Pathway for HIV-1 Neutralization by VRC01-Class Antibodies. Immunity *39*, 245–258.

Zhou, T., Lynch, R.M., Chen, L., Acharya, P., Wu, X., Doria-Rose, N.A., Joyce, M.G., Lingwood, D., Soto, C., Bailer, R.T., et al. (2015). Structural repertoire of HIV-1-neutralizing antibodies targeting the CD4 supersite in 14 donors. Cell *161*, 1280–1292.

Zhou, T., Doria-Rose, N.A., Cheng, C., Stewart-Jones, G.B.E., Chuang, G.-Y.Y., Chambers, M., Druz, A., Geng, H., McKee, K., Kwon, Y. Do, et al. (2017). Quantification of the Impact of the HIV-1-Glycan Shield on Antibody Elicitation. Cell Rep. *19*, 719–732.

Zhu, C., Dukhovlinova, E., Council, O., Ping, L., Faison, E.M., Prabhu, S.S., Potter, E.L., Upton, S.L., Yin, G., Fay, J.M., et al. (2019). Rationally designed carbohydrate-occluded epitopes elicit HIV-1 Env-specific antibodies. Nat. Commun. *10*, 948.

Zhu, J., Wu, X., Zhang, B., McKee, K., O'Dell, S., Soto, C., Zhou, T., Casazza, J.P., Mullikin, J.C., Kwong, P.D., et al. (2013). De novo identification of VRC01 class HIV-1-neutralizing antibodies by next-generation sequencing of B-cell transcripts. Proc. Natl. Acad. Sci. *110*, E4088–E4097.

Zolla-Pazner, S., Cohen, S.S., Boyd, D., Kong, X.-P., Seaman, M., Nussenzweig, M., Klein, F., Overbaugh, J., and Totrov, M. (2016). Structure/Function Studies Involving the

V3 Region of the HIV-1 Envelope Delineate Multiple Factors That Affect Neutralization Sensitivity. J. Virol. *90*, 636–649.